Causes and Impacts of northern North Atlantic Freshening

Dissertation

zur Erlangung des Doktorgrades

der Christian-Albrechts-Universität

zu Kiel

vorgelegt von

Markus Scheinert

Kiel

2008

Referent:	Prof. Claus Böning
Korreferent:	Prof. Peter Brandt
Tag der mündlichen Prüfung:	15.7.2008
Zum Druck genehmigt:	Kiel, 19.12.2008

Der Dekan

Humans can forget but not so the ocean.
In remembrance of my father.

Abstract

The main focus of this study is on the variability of the freshwater budget in the subpolar North Atlantic. This region plays a crucial role in the large scale ocean circulation since the North Atlantic Deep Water (NADW) is formed here, which is an important part of the Meridional Overturning Circulation (MOC). Repeatedly appearing freshening events in the upper layer, known as 'Great Salinity Anomalies' during the 1970s, 80s and 90s, are hereby suspected to weaken the processes of deep water formation. Besides an increase of freshwater in the upper NADW, which is mainly fed by the Deep Convection in the Labrador Sea, there is also observational evidence for a freshening of the lower NADW. In this context, a large increase of the freshwater content in the subpolar basin and in the Nordic Seas has been found in observations between 1970 and 1995. However, the mechanisms that drive this freshening are still unclear. Numerous studies have investigated the variability of freshwater exports out of the Arctic, but only little is known about the exchange with the Atlantic south of the Subpolar Gyre. This study tries to close the gap for a better understanding of the deep water formation variability and the associated changes in the Meridional Overturning Circulation (MOC).

For this purpose, a set of sensitivity experiments with a global ocean circulation model (including sea ice) is used to examine the freshwater budget for the Arctic Ocean and and the subpolar North Atlantic. The main focus hereby is on the variability of the freshwater content and the related flux anomalies.

The results of this study suggest that the largest contribution to the subpolar freshening is accomplished by the freshwater and salt exchange with the Subtropical Gyre, while freshening signals originating from the Arctic or from surface fluxes only play a minor role. Furthermore, the sensitivity experiments reveal that the variability of the exchange is mainly wind-driven and affects the whole North Atlantic Ocean. The long-term change of the MOC, associated with the observed freshening, is,however, relatively small in the model simulation and appears as a minor modification of the MOC anomalies related to changes in deep convection caused by the strong variability of winter heat loss in the Labrador Sea.

Zusammenfassung

Gegenstand dieser Studie ist die Variabilität des Süßwasserhaushaltes im subpolaren Nordatlantik, welchem durch die dort stattfindende Tiefenwasserbildung eine besondere Rolle in der meridionalen Umwälzbewegung des Ozeans zukommt. Dabei stehen immer wieder auftretende Süßwassersignale in der obersten Schicht des Nordatlantiks, die sog. großen Salzgehaltsanomalien der 1970er, 80er und 90er, im Verdacht, die Bildungsprozesse für das Tiefenwasser zu behindern. Neben einer Zunahme des Süßwassergehaltes im oberen Nordatlantischen Tiefenwasser (NADW), welches von Tiefenkonvektion in der Labradorsee gespeist wird, gibt es auch Hinweise aus Beobachtungen, dass der Salzgehalt des tiefen NADW ebenfalls abnimmt. In diesem Zusammenhang konnte für das subpolare Becken und die Nordmeere aus Beobachtungen eine generelle Zunahme des Süßwassergehaltes von enormen Ausmaß zwischen 1970 und 1995 festgestellt werden. Die Prozesse und Mechanismen, die hinter diesen multi-dekadischen Veränderungen stehen, sind jedoch noch nicht vollständig verstanden. Zwar gibt es mittlerweile zahlreiche Studien, die sich mit dem Süßwasserexport aus der Arktis beschäftigen, aber der Austausch mit dem restlichen Atlantik ist noch völlig unklar. Diese Lücke soll mit Hilfe der hier vorgelegten Studie geschlossen werden, um so die Variabilität der Tiefenwasserbildung und der meridionalen Umwälzung besser verstehen zu können.

Zu diesem Zweck wird mit Hilfe eines numerischen, globalen Ozeanzirkulationsmodells, welches auch Meereis berücksichtigt, eine Süßwasserbilanz für die arktischen und subarktischen Becken aufgestellt. Dabei steht die Variabilität des Süßwassergehaltes und die damit verbundenen Schwankungen in den Süßwasserflüssen im Vordergrund.

Die Ergebnisse dieser Studie legen einen enormen Einfluss des Süßwasseraustauschs zwischen dem subpolaren und subtropischen Wirbel nahe, da hiermit der Großteil der Änderung des subpolaren Süßwassergehaltes im Modell und Beobachtung erklärt werden kann, während Süßwasseranomalien arktischen Ursprungs und Veränderngen der Oberflächeneinträge nur wenig zu subpolaren Süßwasserschwankungen beitragen. Es zeigt sich ferner, dass der Austausch mit dem Subtropenwirbel stark von Schwankungen im Windantrieb abhängt und sich auf den Salzgehalt der gesamten Wassersäule des Nordatlantiks auswirkt. Die

damit verbundene Änderung der meridionalen Umwälzbewegung über eine veränderte Tiefenwasserbildung ist in der Simulation jedoch vergleichsweise klein und trägt eher zu geringfügigen Modifikationen der MOC Schwankungen bei, welche der Tiefenkonvektion, hervorgerufen durch einen stark schwankenden winterlichen Wärmeverlust in der Labradorsee, zugeschrieben werden kann.

Contents

1 Introduction

Recent observations show evidence for a substantial freshening of the Subpolar Gyre and the Nordic Seas between the 1960s and the mid-1990s. These regions are known as key regions for deep water production. A freshening of subpolar waters can potentially affect the renewal of North Atlantic Deep Water (NADW) in mainly two ways: by weakening or even inhibiting deep winter convection, e.g. in the Labrador Sea and by a buoyancy gain in the intermediate waters comprising the overflows from the Nordic Seas. As a consequence of reduced transformation of warm surface waters from the south into dense deep water the strength of the Meridional Overturning Circulation in the North Atlantic would be retarded, implying a weakening of the poleward heat transport which is of critical importance for the climate in this part of the world ocean.

An overview of past and present studies on the freshening issue in the north polar and subpolar region will be given in the following chapter. The proposed mechanisms behind the freshwater variability will be discussed and the unspecified connections and open questions that motivate this study will be outlined. Special attention will be given on the processes which govern the deep water production in the North Atlantic, impacting on the Meridional Overturning Circulation. Finally the scientific objectives of this work will be specified.

The subpolar North Atlantic plays an important role in the large scale ocean circulation due to the formation of North Atlantic Deep Water (NADW). This water mass and its formation processes connect the upper layer with the deep ocean, closing the Meridional Overturning Circulation (MOC), which is of special importance for the poleward heat transport in the Atlantic Ocean. As a consequence of the interhemispheric, southward transport of cold NADW below $\sim$ 1000m, and the compensatory flow of warm water in the upper layer, the Atlantic Ocean stands out in comparisons of oceanic heat budgets (Trenberth and Solomon, 1994; Trenberth and Caron, 2001; Ganachaud and Wunsch, 2000, 2003), because it carries heat northward in both hemispheres (see Fig. 1).

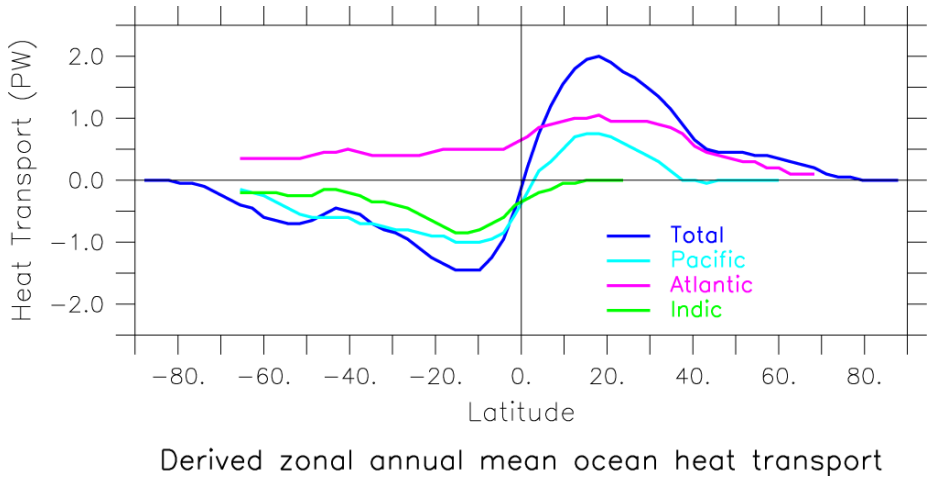

Figure 1 Zonal mean of annual oceanic northward heat transport for global ocean and single basins, derived from Trenberth and Caron (2001), based on NCEP/NCAR and ECMWF reanalysis data.

Recently, the interest in the MOC has further increased due to its possible weakening under global warming scenarios (Bindoff et al., 2007), associated with a decrease in NADW formation due to changes in hydrography in the northern and subpolar North Atlantic (e.g. Johnson and Marshall, 2002). The sensitivity arises from the two key processes, that govern the NADW production: The Overflows from the Nordic Seas, supporting the lower NADW, and the Labrador Sea Deep Convection, which feeds the upper branch.

The overflow waters originate from the pool of dense water in the Nordic Seas entering the North Atlantic through Denmark Strait, the Faroe Bank Channel and across the Iceland-Scotland Ridge (Talley, 1996; Hansen and Osterhus, 2000; Macrander et al., 2005; Jonsson and Valdimarsson, 2004). The sources of the overflows are mixing products of Arctic Water in the East Greenland Current

(Carmack, 1990; Aargaard et al., 1991), convective deep water from the Greenland Sea south of Spitsbergen (Rudels, 1993), recirculated North Atlantic water (McCartney and Talley, 1984; Quadfasel et al., 1987) and very cold water from the Icelandic Sea (Jonsson and Valdimarsson, 2004). The density of the overflows depends thus on the hydrography in the Nordic Seas while the transport across the sills appears hydraulically controlled (Whitehead, 1998; Käse and Oschlies, 2000), and thus relates to the meridional density gradient and the reservoir height of dense water, superimposed by wind-driven variability (Macrander, 2004).

Deep convection in the Labrador Sea occurs due to strong buoyancy loss at the surface, associated with strong winterly cooling conditions (The Lab Sea Group, 1998). This destabilizes the water column and leads to turbulent vertical mixing down to depths of, in general more than 1000m, e.g. in the Greenland Sea and Labrador Sea (Killworth, 1983; The Lab Sea Group, 1998). The deep convection in the Labrador Sea[1] generates the Labrador Sea Water (LSW) which feeds the upper NADW (Marshall and Schott, 1999), and can be tracked due to its temperature/salinity (and potential vorticity) signature (Worthington, 1976; Talley and McCartney, 1982) throughout the North Atlantic. As shown by records of the hydrographic conditions in the Labrador Sea (e.g. Lazier (1980); Avsic et al. (2006)) and the CFC inventory[2] of LSW (Rhein et al., 2002; Kieke et al., 2006), the intensity of deep winter convection has been highly variable during the last decades. Inferences of the formation rate of LSW have especially been obtained from the thickness of the LSW density layer, e.g. at Ocean Weather Ship Bravo (OWS-B) in the southern central Labrador Sea, as shown by Lazier (1980) and Curry et al. (1998) (see Fig. 2). As a result of such estimates it has also been shown (Curry et al., 1998; Latif et al., 2006), that the convection variability can be partly linked to the North Atlantic Oscillation (NAO), a sea level pressure pattern over the North Atlantic which accounts for the dominant climate signals in this region (Hurrell, 1995; Marshall et al., 2001). When the NAO is positive (negative), convection activity and layer thickness increase (decrease). See Haine et al. (2008) for a recent review of LSW formation variability.

[1] The Irminger Sea, as a secondary region of deep water formation with similar characteristics as in the Labrador Sea, is still under discussion (Pickart et al., 2003a,b; Falina et al., 2007).

[2] CFC (chlorofluorocarbon): its components CFC-11 and CFC-12, which have no natural sources, are taken up by air-sea gas-exchange. Its atmospheric increase since 1930 is well known and with its very long lifetimes the inventory in the ocean thus allows an inference on the intensity of the uptake processes (Orsi et al., 1999) which is the deep convection in the North Atlantic.

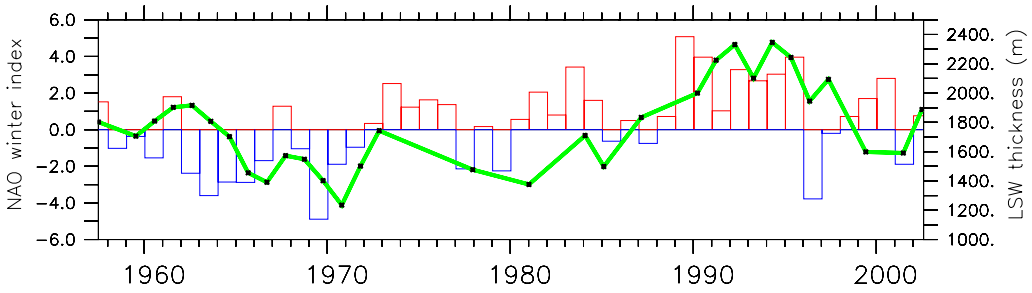

Figure 2 NAO winter index as bar plot (following Hurrell (1995); left axis) and observed layer thickness of Labrador Sea Water (LSW) at OWS Bravo following Curry et al. (1998); adapted from Latif et al. (2006)(right axis; black stars indicate observations while the green line interpolates linearly between them).

However, periods with a weaker linkage between LSW thickness and NAO during the 1970s and 1980s seems to exist. Lazier (1980), who reported on the declining Labrador Sea convection in the 70s, found a large hydrographic signal in the salinity records, which revealed a freshening of the North Atlantic, especially in the Labrador Sea during the late 1960ies and early 1970ies. Later on, a systematic salinity offset between 1962 and 1981 was observed by Brewer et al. (1983) within the LSW layer in the Subpolar Gyre. An in-depth characterization of the observed freshening, especially near the surface, was then presented by Dickson et al. (1988) who called the phenomenon the 'Great Salinity Anomaly' (GSA). They also tried to track the signal as it propagates following the Subpolar Gyre and dated the re-entrance into the Nordic Seas to 10-12 years later. Further freshening events have been reported for the 1980ies (Read and Gould, 1992; Belkin et al., 1998) and 1990ies (Belkin, 2004). But not only the upper and mid-depth North Atlantic seemed to be affected by the freshening but also the deep ocean beneath the LSW (Dickson et al., 2002) and its source region, the Nordic Seas (Blindheim et al., 2000). As already conducted by Brewer et al. (1983), a freshening of deep water, including LSW, reflects changes in the formation regions and must be linked to the surface freshwater fluxes and the advective supply.

The net surface freshwater flux in the ocean is dominated by evaporation in the subtropics and precipitation at high latitudes and the tropics (Fig. 3 and Fig. 4). With the exception of the equatorial region, the atmospheric circulation accounts for the poleward freshwater transport (Fig. 5), while the divergence of the resulting net surface freshwater flux implies an oceanic freshwater transport from the poles to the evaporative areas (Wijffels et al., 1992). In the North Atlantic, where the ocean gains freshwater not only by precipitation but also from the Arctic ocean with its accumulating river runoffs and the inflow from the Pacific

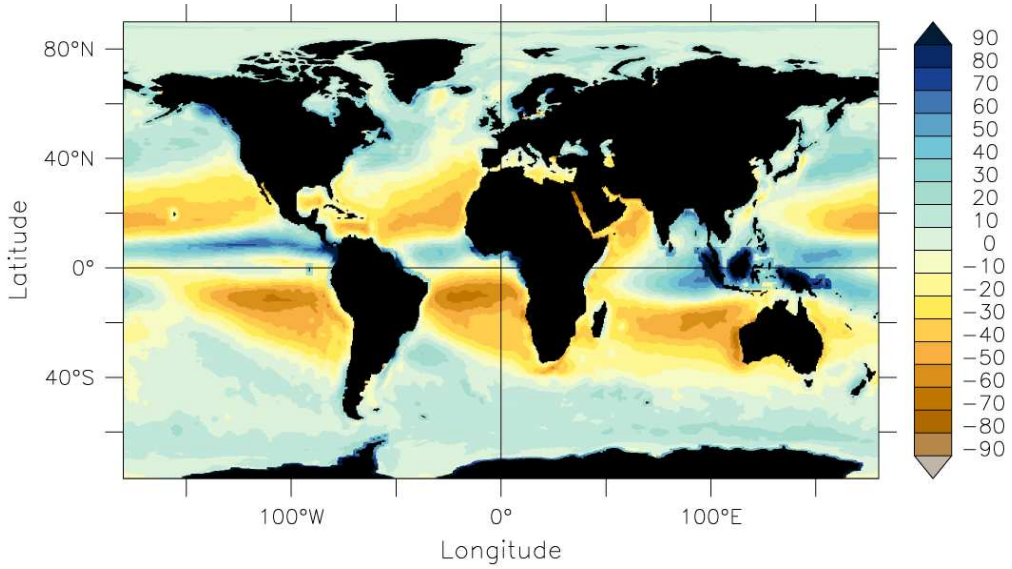

Figure 3 Net surface freshwater flux Precipitation-Evaporation+Runoff ($mg/m^2/s$) over ocean as realized in a model simulation (the REFERENCE experiment, see chapter 2.2.4) using freshwater flux forcing by Large and Yeager (2004), based on NCEP/NCAR reanalysis products. Fluxes are positive into the ocean.

through the Bering Strait, which provides an additional freshwater source, there is a mean northward salt transport in the upper ocean layer accompanied by a southward export of relatively fresh water in the deep. Since a large amount of multi-year sea ice resides in the Arctic, which stores a huge mass of pure freshwater, melting as well as ice export out of the Arctic provide another freshwater source for the North Atlantic.

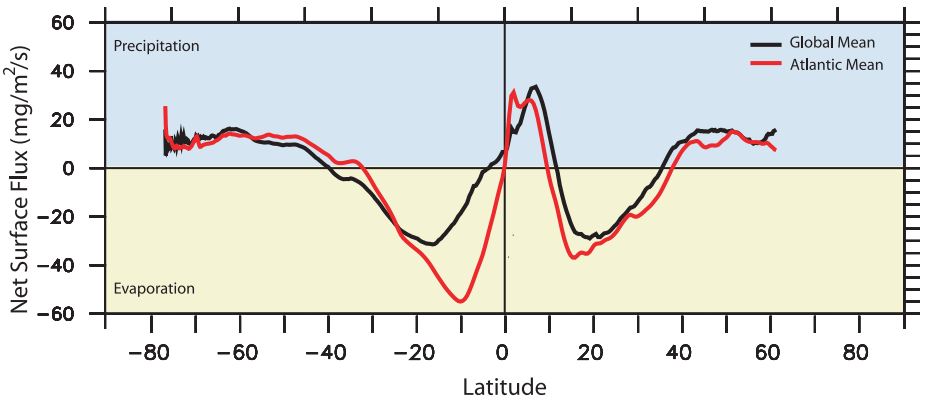

Figure 4 Zonal averaged net surface freshwater flux over ocean globally (black) and for the Atlantic Ocean only (red) derived from the same simulation as used for Fig.3.

Concerning the causes of the observed freshening in the subpolar North Atlantic, the first hypothesis put forward involved anomalous additive freshwater fluxes from further north. This idea was originally proposed by Brewer et al. (1983) and supported by Dickson et al. (1988) who located the origin of the GSA during the 1970s within the Nordic Seas and related it to changes in the wind-driven oceanic circulation. A direct link between the Arctic and the freshening in the Nordic Seas then was found by Aargaard and Carmack (1989), by showing that the GSA was initiated by an anomalously large ice export through Fram Strait as observed in 1968. Model simulations by Häkkinen (1993) revealed similar results. The following GSA in the 80s however, could not be associated with fluctuations in the Fram Strait ice export. Instead, Belkin et al. (1998) suggested that it either originated in the Canadian Archipelago or was formed locally in the Labrador Sea. Houghton and Visbeck (2002) specified this and found a strong relation between the Davis Strait freshwater export and the freshwater in the Labrador Sea. The most recent GSA in the 1990ies (Belkin, 2004), seems to be induced by Arctic export anomalies through Fram Strait again, but now involving a release of a large amount of liquid freshwater into subpolar water masses instead of large sea ice exports (c.f., Karcher et al. (2005) for observation and model simulations).

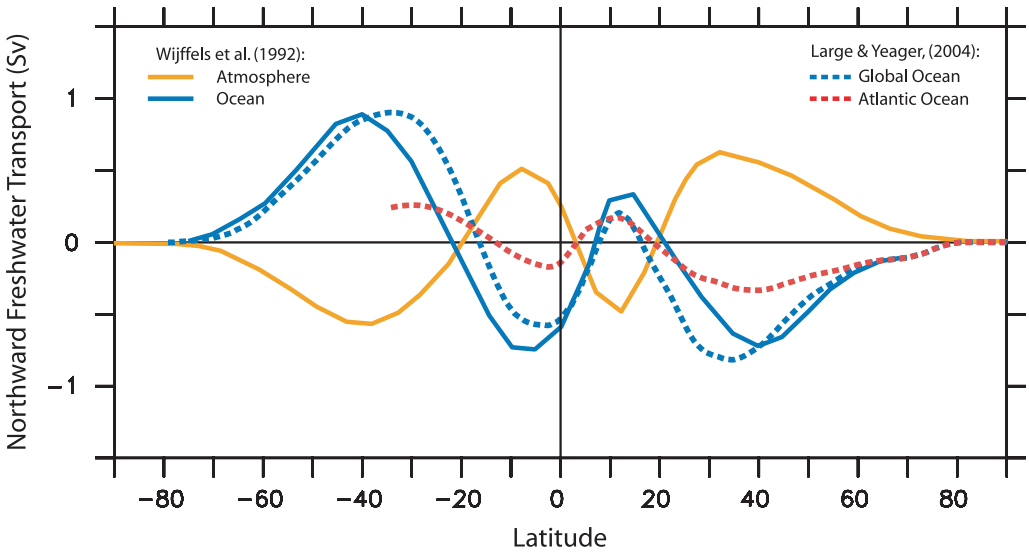

Figure 5 Global freshwater transport ($Sv = 10^6 m^3 s^{-1}$) according to Wijffels et al. (1992) for atmosphere (orange) and ocean (blue solid line). Dotted lines denote results from Large and Yeager (2004) for the world ocean (blue dotted) and Atlantic Ocean only (red dotted).

While the GSA events are useful to explain the freshening in the upper-layer western subpolar North Atlantic, the causes for the salinity decrease over its eastern portions are still under discussion (Josey and Marsh, 2005). Read and Gould (1992) connected the LSW salinity changes in the formation region during the freshening periods 1971-76 and 1986-90 with those in the eastern North Atlantic. They estimated an advective time scale of 18-19 years for the LSW spread into the east, which is much longer than that proposed by Dickson et al. (1988) for the surface signal (10-12 years). However, in their analysis of the freshening in the northeastern Atlantic, Reverdin et al. (2002) disputed its dependence on the advective GSA signal above the LSW layer because of a lack of correlation between salinity and temperature records. Josey and Marsh (2005) tried to close the gap using air-sea fluxes of freshwater (precipitation-evaporation) based on ERA-40 reanalysis data (Uppala et al., 2005) and suggested that the observed freshening could be explained by an increase in those surface fluxes. As another explanation for the decrease of Sea Surface Salinity (SSS) in the Labrador Sea during 1951-2001, Häkkinen (2002a) invoked an advective signal from the south, associated with a weakening of the MOC and its northward transport of high salinity Atlantic water. Based on model simulations Häkkinen (2002b) concluded, that sea ice export variability has an impact on the subpolar SSS on interannual time scales, while SSS changes on longer time scales can be associated with variations in the AMOC.

In addition to the freshening of the upper North Atlantic which has been rationalized in terms of advective GSA signals from further north, MOC-related salinity signals from the south and by an increase of surface freshwater flux into the ocean, there are also indications for a wide-spread freshening of the deep Subpolar Gyre during the last decade of the 20th century. The causes for this signal which is manifested in salinity data from various sites, particularly at OWS Bravo in the southern Labrador Sea (Fig. 6), are however still unclear. Dickson et al. (2002) argued that the salinity decrease was generally caused by a freshening of the source water masses, namely the overflows in conjunction with less saline surrounding waters, however, there is little quantitative information known about the signals in the overflows and their entrained waters.

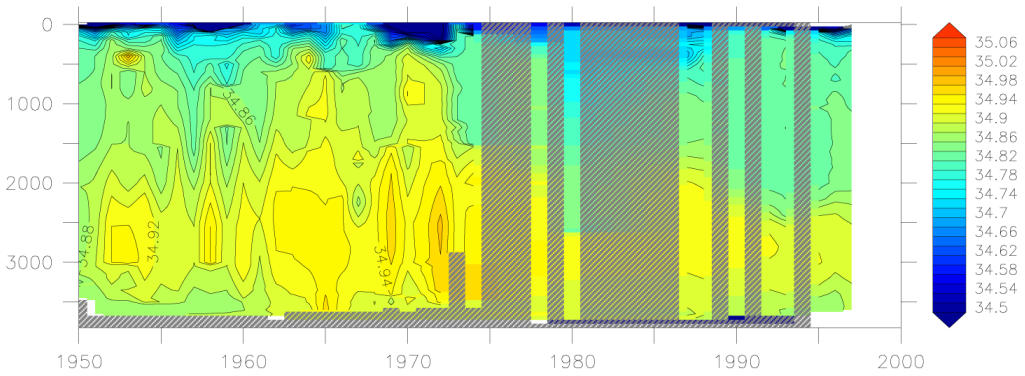

Figure 6 Hovmøller diagram of salinity profiles observed next to Ocean Weather Ship Bravo (data from ICES, 2007). Grey shaded areas denote missing data in time and depth.

A quantification of the total equivalent freshwater content change (FWC change), that is, the equivalent amount of freshwater that would have needed to be added to the subpolar North Atlantic to produce the observed decrease in salinity, over the last decades was recently provided by Curry and Mauritzen (2005). They analyzed the collection of hydrographic records available for the last 50 years and found, analogous to the previous findings for the upper and LSW layers, a general freshening of the ocean since 1965 in the basins of the Subpolar Gyre and the Nordic Seas. Their data provide an estimation for the rate of change in total, which they attempted to explain (updated by Peterson et al. (2006)) in terms of the freshwater contributions by the GSAs (Dickson et al., 1988; Belkin, 2004) and the surface fluxes by Josey and Marsh (2005).

But their results are somehow contradictory to the study by Hátún et al. (2005), who discussed a more 'dynamical' point of view of recent (after 1993) trends, especially in the east, using a numerical Ocean General Circulation Model (OGCM). They found that anomalously fresh inflow from the south into the Nordic Seas during the period 1993-1998 could not be explained by changes in the surface freshwater fluxes (here originating from NCEP/NCAR) over the eastern subpolar gyre. Instead, they were able to correlate the subpolar freshwater anomaly with a SSH-based gyre index as proposed by Häkkinen and Rhines (2004): under strong NAO conditions, when the gyre transport is high, less saline waters enters the gyre from the south, while freshwater export from the Arctic increases and accumulates within the gyre. Deep convection events during that NAO phase mix it vertically. During weak NAO periods the subpolar gyre weakens, the subarctic front tilts in a more northward direction, permitting an increase of the inflow of saline Atlantic waters to the Nordic Seas. The model results are corroborated by

a recent study of Sundby and Drinkwater (2007), who also point to the impact of the subpolar front between the Subpolar and Subtropical Gyre on the subpolar freshwater content. In addition, they classified the GSA events in the 1970ies, 80ies and 90ies as low salinity anomalies and propose the existence of larger freshwater signals, caused by varying volume fluxes in and out of the Arctic basin. An extension of the model-based work of Hátún et al. (2005) was recently provided by a detailed analysis of salinity records in the eastern subpolar North Atlantic by Holliday et al. (2008). They found the reversal of the freshening trend (after 1993) to be governed by a northward signal propagation, i.e., from the subpolar North Atlantic into the Nordic Seas.

As already mentioned above, the freshening of the North Atlantic is assumed to have the capability to weaken the NADW production. For the Labrador Sea Deep Convection, Lazier (1980) linked the observed SSS decrease to a reduction of the mixing depth. Dickson et al. (1988), Belkin et al. (1998) and Belkin (2004) had drawn similar conclusions, whereas Houghton and Visbeck (2002) focused on the mixing effect of the convection itself and relativized the effect of surface freshening on LSW production: They concluded that during low NAO phases the accumulation of freshwater is initiated due to shallower convection and is terminated by deep convection due to increased cooling in the presence of stronger winds, related to high NAO phases. This is supported by findings from Lazier et al. (2002), who reported on a significant reduction of Labrador Sea convection during the second half of the 1990ies, which was mainly associated with profound changes in the heat loss at the surface due to weaker NAO conditions and less to lower SSS.
A potentially stronger impact of freshwater anomalies on the NADW production could be associated with the overflows, communicating variations in the freshwater budget of the Nordic Seas (Gerdes et al., 2005) to the Atlantic proper. A critical finding in this context is the decrease in the overflow salinity since the late 1960s noted by Dickson et al. (2002).

The effect of changes in the water mass properties and deep water formation processes has been addressed in several model studies. Johnson and Marshall (2002) have shown in climate change scenarios that the source for decadal and higher frequency changes of the North Atlantic overturning can be located generally in the North Atlantic itself. In this context, the most recent set of climate projections for the fourth Assessment Report (AR4), composed by the Intergovernmental Panel of Climate Change (IPCC), predict a Meridional Overturning decline of

about 30% until 2100 as discussed by Schmittner et al. (2005). In ocean model sensitivity experiments, the IPCC MOC predictions could be linked to the hydrographic conditions in the Nordic Seas north of the Greenland-Scotland ridge (Schweckendiek and Willebrand, 2005), downgrading the relative importance of Labrador Sea convection for long term trends of the MOC.
The role of anomalies in the nordic freshwater budget, particularly the effect of melting ice on land and glaciers, which are not included in the IPCC scenario runs, has been considered in various climate model studies. Jungclaus et al. (2006) repeated an IPCC climate projection by taking melting water from the Greenland Ice Sheet into account and found a larger decrease of the MOC of about 40%. To extract the effects and to enlighten the mechanisms of such an additional freshwater flux around Greenland, some 'hosing' experiments have been established and discussed, where a large amount of extra freshwater is distributed over a distinct region (Stouffer et al., 2006; Gerdes et al., 2006). Those experiments revealed a strong dependence on where the additional freshwater is released. Within the boundary current it is exported quickly without affecting the convection region (Gerdes et al., 2005) whereas a more wide-spread distribution across the surface leads to a buoyancy gain limiting convection. Correspondingly, the effect of the GSAs on the MOC is still under discussion due to some contradictory model studies: Mauritzen and Häkkinen (1997) proposed that variations in the sea ice export can affect the MOC; this was supported by Häkkinen (1999), who noted a strong decline of the MOC upon an idealized GSA. However, more recent studies do not support such an influence (Haak et al., 2003; Curry and Mauritzen, 2005).

The Scientific Objectives

The observed multi-decadal changes in the freshwater content in the subpolar North Atlantic thus raise a number of questions which in this study will be addressed by a sequence of experiments with a global ocean-ice model (chapter 2). The focus is on these main areas of interest:

- The variability in the components of the freshwater budget of the subpolar North Atlantic: i.e., what determines this variability in aspects of amplitude and phase? What is the relative importance of each contribution?
- The multi-decadal freshening trend and its recent reversal in the subpolar

North Atlantic: i.e., what are the mechanisms that account for the basin-scale changes in salinity and on which time scales do they act?

- The effect of the subpolar freshening on the MOC: i.e. can the observed Subpolar Gyre freshening have already weakened the MOC and how large might have been the effect?

The outline of the thesis is as follows: After an introduction into the methodology used for this study, where the components of the freshwater balance are identified (chapter 3), the representation of simulated sea ice and the freshwater budget in the Arctic is discussed with respect to the mean state and temporal variability (chapter 4). Afterwards, the freshwater content variablity in the subpolar basin and the lateral freshwater exchange with the neighboring basins is investigated (chapter 5). The simulated variability is compared with observational studies where it is possible, especially, the ice extent and transport, the liquid freshwater transport and the convection activity. A host of sensitivity experiments with different surface flux variabilities is then used to investigate the various thermohaline and wind driven mechanisms, contributing to the variability and, in particular, to identify the causes of the multi-decadal freshening trend (chapter 4 and 5). Finally, the influence of subpolar freshwater anomalies on the deep water formation and on the Meridional Overturning Circulation is examined by artificially perturbing surface components of the freshwater budget in the polar and subpolar regions (chapter 6).

2 The Model Framework

In this study, simulated data from the global ocean+sea-ice model framework NEMO are analyzed. The model is based on the primitive equations, which are solved on a tri-polar grid to avoid problems with the singularity at the north pole which would arise in a common Mercator grid. With a nominal horizontal resolution of $1/2$ degree, this model does not resolve mesoscale eddies but an eddy-parameterization is used to include their mixing effects.

The sea ice characteristics are determined using a simple thermodynamic-dynamic sea ice model with a viscous-plastic rheology for dynamics. Only one ice class with two layers and snow atop is considered. Since the sea ice model strongly depends on certain key parameters, some sensitivity tests have been performed to determine the most judicious combination.

The model is forced at the ocean surface using the CORE flux formulation and data, which provides two different sets: One with seasonal variability consisting of a climatological year and the other with interannual fluctuations covering the time range 1958-2001. The experiments used for the analysis in this study are based on varying combinations of these two types of variability for different forcing components.

The numerical model in this study is based on the NEMO ocean modeling framework and makes use of its ocean component OPA9 (Madec et al., 1998; Madec, 2007) and the Louvain-la-Neuve sea ice ice model LIM-2 (Fichefet and Morales Maqueda, 1997). A brief description of the model architecture is given in the following sections.

2.1 Ocean

OPA is a global Ocean General Circulation Model (OGCM) using primitive equations for tracers and velocities which are solved on an ARAKAWA-C type grid (Arakawa and Lamb, 1977; see Fig. 7a) where the tracer point T resides in the middle of the grid box and velocities are computed on the side faces.

2.1.1 Grid and Resolution

The vertical water column is divided into 46 z-levels and the horizontal grid has a nominal resolution of $\frac{1}{2}^\circ$ ($\Delta x \approx 55km$) at the equator (the so called ORCA05 configuration) with a slight refinement at higher latitudes ($\Delta x \approx 35\,km$ at 60°N). To avoid singularity problems in the central Arctic, the north pole is split into two poles on North America and Eurasia resulting in a tri-polar grid following Madec and Imbard (1996) (Fig. 7a).

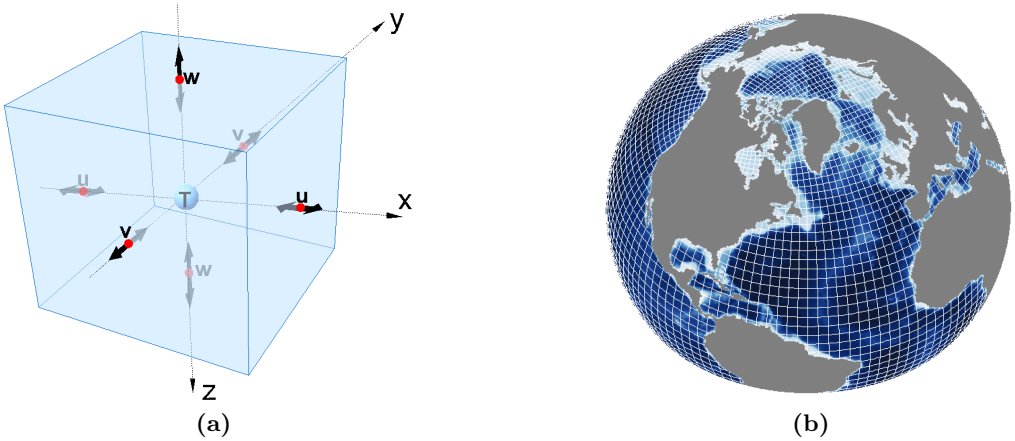

Figure 7 **(a)** A cell in an Arakawa-C Grid with a tracer grid point (T; blue) in the middle and velocity points ($\vec{u}, \vec{v}, \vec{w}$; red with black arrows) on each side. **(b)** Orthographic view on the tripolar grid (no singularity at the North Pole) of the ORCA05 configuration as used for this study.

The bathymetry is derived from ETOPO5 (1988) and is interpolated onto the model grid. The vertical grid spacing varies from 10m near the surface to 250m in the depth (Fig. 8). As this coarser resolution of the deep ocean can lead to a worse representation of steep and narrow topography in the classical full step approach (see grid boxes in Fig. 8a covered by the red line) the model uses partial step (or partial cell) (Adcroft et al., 1997), thus the bottom ocean cell is partially filled (green line) which improves the representation of bottom-near flow significantly (Barnier et al., 2006).

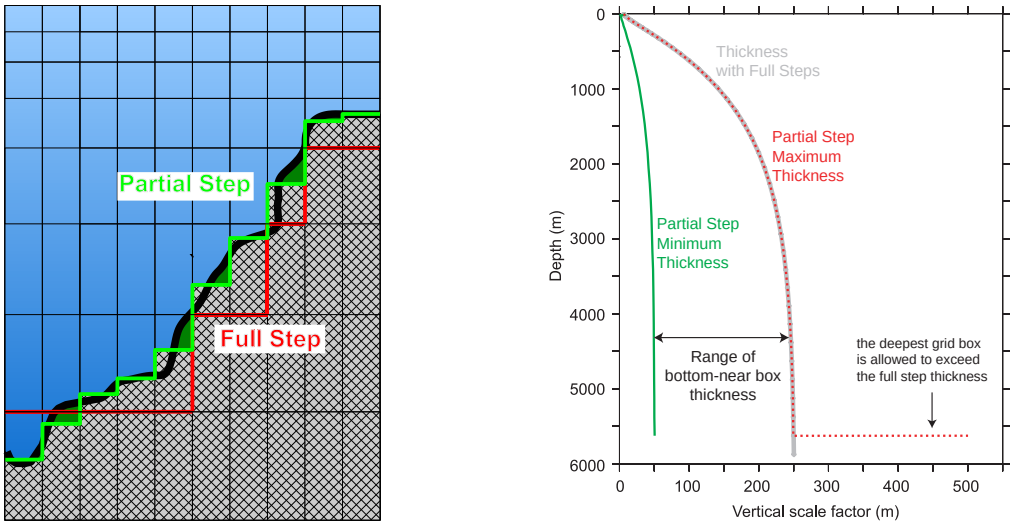

Figure 8 **(a)** Representation of the real bathymetry (black) by the model in the 'Full Step' case (red) and the used 'Partial Step' case (green). **(b)** Vertical grid space in ORCA05: 46 levels from 10m cell thickness at the top to 250m near the bottom with full step (grey) and partial step (domain-wide minima (green) and maxima (red).

Though the bottom ocean box with partial cell is less thick than it is with full step (Fig. 8), apart from the abyssal ocean, where the deepest ocean box can be thicker than 250m to allow for a notably deep bathymetry in some places.

The thickness of the upper-most ocean layer can vary since an implicit free surface (Madec, 2007) is implemented which takes real freshwater fluxes into account. This allows slow barotropic Rossby waves while faster external gravity waves are filtered out and appear only as high frequency noise.

2.1.2 Ocean Physics

Since the horizontal resolution is a half degree, this configuration does not resolve small mesoscale eddies (scales: 50-500 km, 10-100 days). Instead, an eddy induced tracer advection is considered by using the Gent and McWilliams (1990) eddy parameterization ($A_{eiv} = 1000 m^2/s$).

Lateral mixing is accomplished by a lateral diffusion for tracers along isopycnals (using a harmonic operator $A_{ht} = 1000 m^2/s$, scaled by Δx and Δy) similar to Cox (1987), except for their background horizontal diffusion which is neglected here ($A_{htb} = 0$). For momentum, diffusion acts along geopotential surfaces (using a biharmonic viscous operator, $A_{hm} = -8.5 \times 10^{11} m^4/s$).

Vertical sub grid scale mixing is implemented by a vertical viscosity for momentum ($A_{vm} = 1.2 \times 10^{-4} m^2/s$) and a vertical diffusivity for tracers ($A_{vt} = 1.2 \times 10^{-5} m^2/s$). Within the surface mixed layer, where the wind induced diffusivity can become large, a TKE turbulent closure scheme (Madec et al., 1998) is used to get more reliable values for A_{vm} and A_{vt}. Additionally, to ensure a reasonable deep convection an enhanced vertical diffusion scheme on tracers following Lazar (1997) is implemented.

Tracer advection is computed by the 3D-MUSCL scheme (Monotone Upstream-centered Scheme for Conservation Laws) by Hourdin and Armengaud (1999).

There is no lateral friction (free-slip) but a non-linear friction at the bottom (drag coefficient $C_D = 1.0 \times 10^{-3}$) taking into account the effect of tides, internal wave breaking and other short timescale currents (bottom turbulent kinetic energy: $e_b = 2.5 \times 10^{-3} m^2/s$).

2.2 Sea Ice

The global view on the ocean's role in the earth climate system makes it necessary to take other processes into account besides ocean physics. One issue that can influence the ocean's behavior is sea ice. The arctic and antarctic regions store and buffer large amounts of freshwater and release extremely salty and dense or very fresh and light waters in a seasonal and interannual cycle (McBean et al., 2005; Lippsett, 2005). Because of its physical complexity, sea ice is not easy to model, although some sea ice models have been evolved that are useful for ocean modeling in a global context.

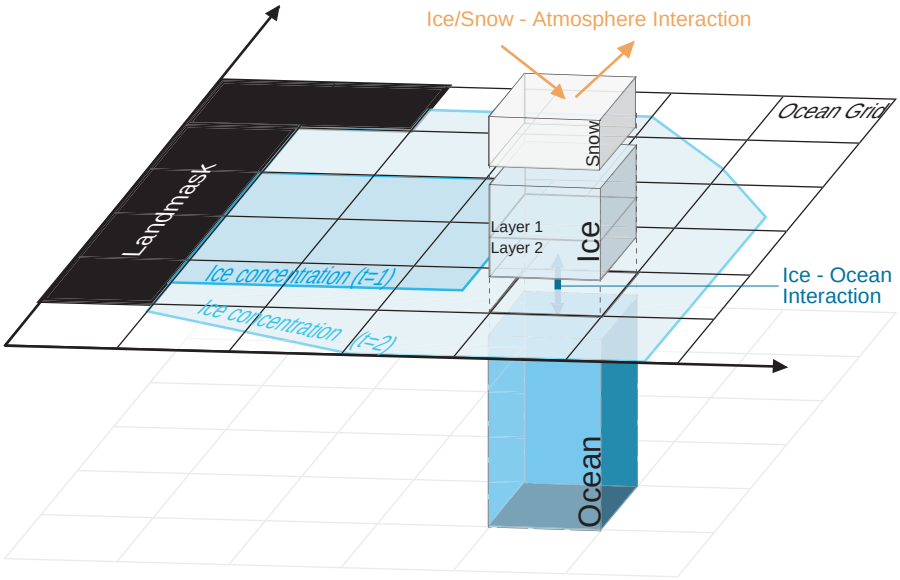

Figure 9 Illustration of the sea ice model grid boxes atop the ocean grid: two ice layers and one for snow. Ice concentration is shown for two consecutive time steps as green-blue contoured partial coverage in the horizontal plane. Black areas indicate grid boxes on land.

The ocean model in this study is coupled with the Louvain-la-Neuve sea ice model (LIM) as described by Fichefet and Morales Maqueda (1997) and Goosse et al. (1999). The ice model has to be configured properly to get a reliable representation of sea ice under the given forcing fields and ocean model set-up. For this purpose, the key parameters, governing the sea ice physics, have to be elucidated and the ice sensitivity on them has to be investigated. Thus, a short discussion on the ice model and its key parameters is given in the following section.

As illustrated in Fig. 9, LIM is based on a thermodynamic-dynamic sea ice model with three layers (two for ice, one for snow) to deal with the thermodynamic processes on the one hand and with the dynamic characteristics of an two-dimensional viscous-plastic continuum on the other hand.

Aspects of sea ice evolution that are determined by thermodynamic processes are storage of sensible heat and vertical heat conduction, whereas effects of sub grid-scale snow and ice thickness are picked up by an effective thermal conductivity.

Other aspects are storage of latent heat by trapping short-wave radiation within brine pockets, the presence of leads and vertical/lateral growth/decay of ice.

Dynamical processes are represented by a momentum balance in dynamical interaction with atmosphere and ocean. Internal forces and ice strength as function of ice thickness and compactness are taken into account, too. Leads can be opened by shearing deformation and the closure of leads by frazil ice is parameterized by the collection thickness. Fields of ice and snow concentration/volume are advected as well as snow/ice enthalpy and brine reservoir; each field per unit area.

As the sea ice model is defined on an ARAKAWA-B-grid (tracer and velocity grid points are both located in the center of the grid box; c.f. Arakawa and Lamb (1977)) ice variables, interacting with the ocean, have to be interpolated onto the C-grid of the ocean.

2.2.1 Thermodynamics

There are four thermodynamic mechanisms to produce or reduce sea ice in thickness or lateral extent, respectively:

1. At the ice surface, the snow cover is transformed into new ice or existing ice is melting.
2. At the bottom, new ice is formed by freezing ocean surface water or existing ice is melting at the ocean-ice boundary.
3. Lateral freezing accretes existing ice or melting ablates.
4. Open ocean freezing

To simulate these processes, the LIM sea ice model affects the internal and interface temperature as well as surface and conductive fluxes for each grid cell (see figure 10).

2.2.1.1 Internal Temperature

Each layer has its own internal Temperature $T_c = \{T_i, T_s\}$. Its evolution is determined by the heat conduction within the snow-ice-system and can be described by the following one-dimensional heat-diffusion equation:

$$\frac{\partial T_c}{\partial t} = G(h_e) * \frac{k_c}{\rho_c c_p} * \frac{\partial^2 T_c}{\partial z^2} \tag{1}$$

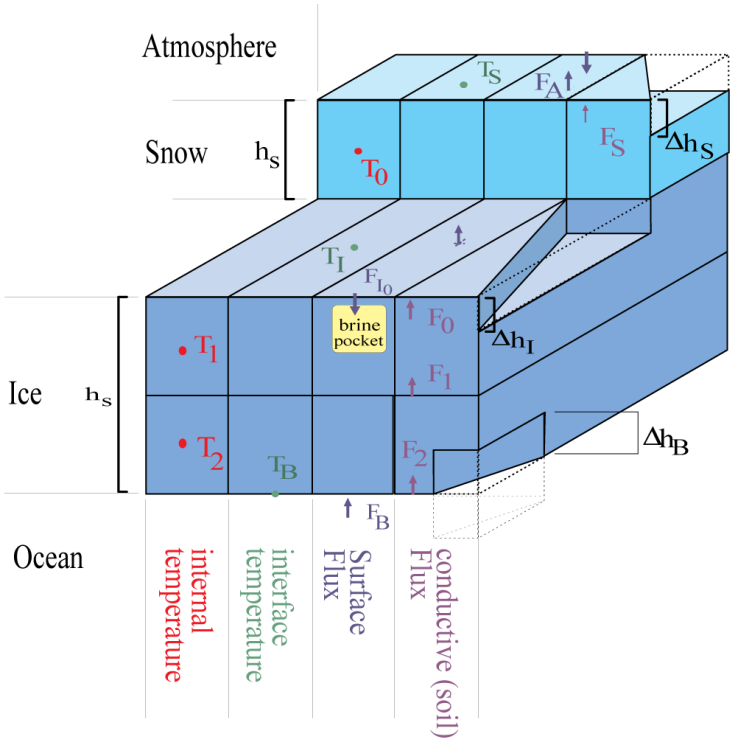

Figure 10 Scheme of the thermodynamic model with its two layers for sea ice and one for snow according to Semtner (1976). The location of internal temperature points ($T_{0,1,2}$; red) as well as those at interfaces ($T_{S,I,B}$for surface, interface and Bottom; green) and the conceptional location of surface fluxes ($F_{B,IO,A}$ for bottom, ice-ocean interface, atmosphere; blue) and internal conductive fluxes (F_S for snow and $F_{0,1,2}$ for ice layers; purple) on and within a grid box are shown. Partial filled grid boxes indicate the ice concentration per box while $\Delta h_{S,I,B}$ mark changes of thickness for the snow layer, the upper snow-free ice layer and at the bottom of the second ice layer in contact with the ocean. The yellow box denote brine pockets of highly saline water which is used for the energy balance.

with a correction factor

$$G(h_e) = \begin{cases} 1 & \text{for } h_e < \frac{e}{2}\epsilon \\ 1 + \frac{1}{2}\ln\left(\frac{2}{e}\frac{h_e}{\epsilon}\right) & \text{otherwise} \end{cases} \tag{2}$$

which accounts for the fact that the unresolved ice floes of varying thickness contribute differently to the average heat conduction Mellor and Kantha (1989). It can be shown that under horizontally homogeneous atmospheric and oceanic forcing conditions, the surface temperature is nearly the same for all thicknesses as long as the effective thicknesses for heat conduction (h_e) are greater than a certain threshold thickness ϵ [thth[1]] (Fichefet and Morales Maqueda, 1997). In the range

[1] variable name in LIM/OPA Code.

of $0 \leq h_e \leq \epsilon$ the surface temperature varies linearly with h_e between the bottom temperature and the surface temperature of thick ice/snow ($h_e > \epsilon$).

The left panel of figure 11 shows the effective thickness h_e under different conditions for ice thickness h_i and snow depth h_s. Additionally, the "threshold thickness boundary" $\frac{e}{2}\epsilon$ (see definition of G) is plotted. The right panel in figure 11 presents the resulting correction factor G. The thinner the threshold thickness ϵ the greater the correction factor G (figure 12).

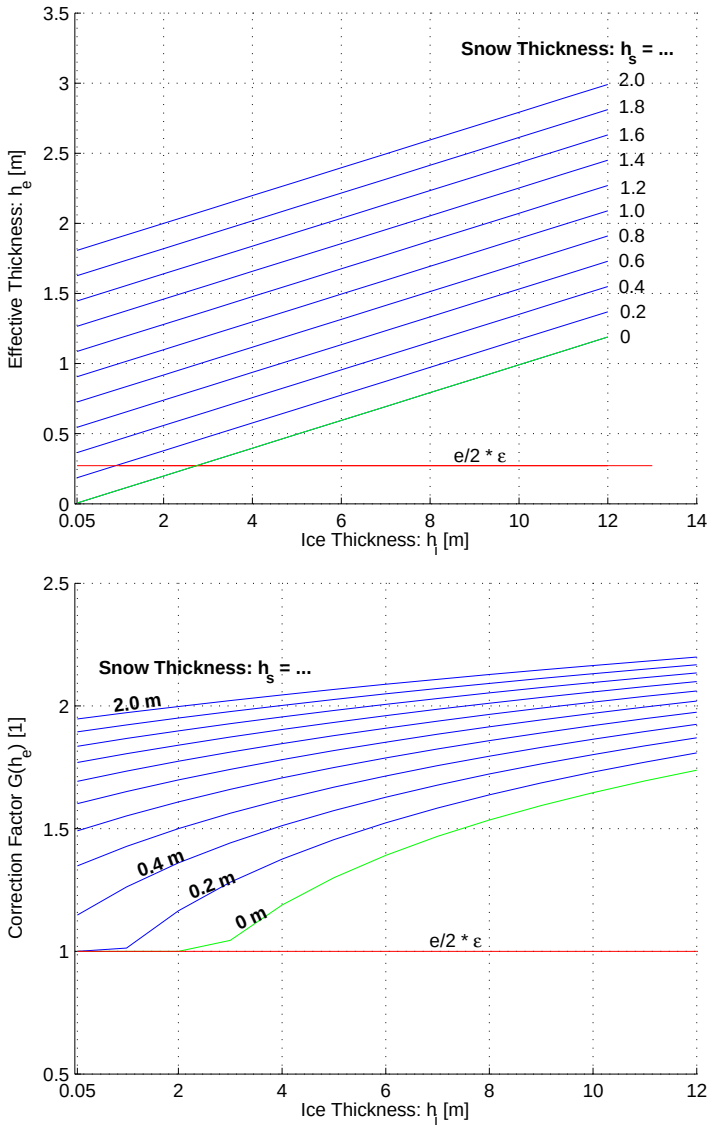

Figure 11 Effective Thickness h_e (upper) and Correction Factor $G(h_{e)}$ (lower) depending on ice thickness (on the abscissa) and on snow thickness (green and blue lines). The red line indicates the condition, when h_e has reached the threshold thickness boundary.

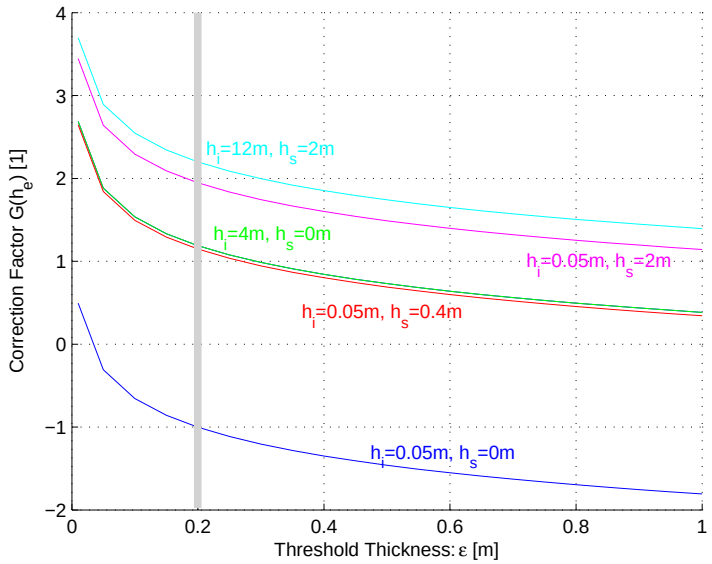

Figure 12 Correction Factor $G(h_e)$ vs. Threshold Thickness ϵ for different combinations of ice and snow thickness (h_i, h_s).

Estimations from ice distribution measurements can help to get the most suitable ϵ. Assuming winter ice/snow thickness in central arctic reaches 3.0m/0.3m for example, observations suggest $G(h_e) = 1.8$ for correction factor which can be obtained by using $\epsilon = 0.1$. The default value ($\epsilon = 0.2$) underestimates this slightly but has remarkable effects on ice evolution. Thus the most important parameter in equation (1) is the threshold thickness ϵ of the correction factor G.

2.2.1.2 Interfaces

Surface The surface temperature (snow or ice) can be determined by the heat budget of a thin layer at top surface using a surface layer thickness h_{su} [hnzst].

$$
\begin{aligned}
B(T)_{su} = h_{su}(\rho c_p)_{su}\frac{\partial T_{su}}{\partial t} = \; & (1-i_0)Q_I && \text{fraction of } Q_I \text{ that is not absorbed and penetrates inside ice.} \\
& +\epsilon_{su}Q_A && \text{absorbed downward longwave radiation} \\
& -\epsilon_{su}\sigma_{SB}T_{su}^4 && \text{'grey-body' (Lambert) radiation} \\
& +Q_s && \text{sensible turbulent heat flux} \\
& +Q_l && \text{latent turbulent heat flux} \\
& +F_{cs} && \text{conductive heatflux from below}
\end{aligned}
\tag{3}
$$

The heat capacity of the surface layer is usually negligible ($h_{su} = 0$), because this is a very small element of the budget but it helps to stabilize the system. Thus h_{su} has a very small non-zero value (Goosse et al., 1999).

In the case of surface melting, i.e. the surface temperature T_{su} in Eq. (3) is above the melting point, T_{su} is held at that point and and reducing ice thickness h_i against snow depth h_s occurs:

$$\begin{aligned} \left(\frac{\partial h_s}{\partial t}\right) &= -\frac{B_{su}T_{su}}{L_s} \qquad \text{for } h_s > 0 \\ \left(\frac{\partial h_i}{\partial t}\right) &= -\frac{B_{su}T_{su}}{L_i} \qquad \text{for } h_s = 0 \end{aligned} \tag{4}$$

Bottom At the bottom of the ice shield, new ice can be formed by freezing sea water or melting can occur, both changing the ice thickness. These processes can be described by the balance between conductive heat flux within ice F_{cb}, heat flux from ocean F_w and ice accretion/ablation:

$$\frac{\partial h_i}{\partial t} = \frac{F_{cb} - F_w}{L_i} \tag{5}$$

2.2.1.3 Brine Pockets/Energy Reservoir in upper Ice Layer

Part of solar radiation that is absorbed within ice:

$$F_{si} = i_o * \ (1 - \alpha_{su}) \ * [\, 1 - \underbrace{e^{-1.5(h_i - h_{su})}}_{[zexp]} \,] \, Q_I \tag{6}$$

Energy from this reservoir is used to increase the volume of brine pockets in summer, whereas in autumn this latent heat is released through the re-freezing of the brine pockets. It keeps the temperature of the upper ice layer from dropping below the freezing point as long as the reservoir is not empty. This mechanism is known as “brine damping” (Semtner, 1976).

2.2.1.4 Submerged Snow forming Snow-Ice

The snow-ice boundary can be depressed under the water level when the load of snow is large enough. In this case, sea water infiltrates the underwater snow and freezes there.

The change of ice layer thickness is computed after snow-ice formation:

$$(\Delta h_i)_{si} = \frac{(\Delta h_s)_{si}}{\beta_{si}} = \frac{\rho_s h_s - (\rho_0 - \rho_i)_{hi}}{\beta_{si}\rho_s + \rho_0 - \rho_i} \tag{7}$$

The parameter β_{si} [alphs] is equal to 1 (empirical). No need to change this.

2.2.1.5 Ice Concentration

The sea ice concentration A_i quantifies the fraction of ice that fills a model grid box. It is often used as a reciprocal concentration $A = (1 - A_i)$, the lead fraction of open ocean water.

Accretion Lateral accretion in leads is the most important thermodynamic process to produce ice during winter time, whenever the heat budget of open water becomes negative ($B_l < 0$), the change of lead fraction A is determined by

$$(\frac{\partial A}{\partial t})_{acc} = \frac{\sqrt[\gamma]{(1 - a^\gamma)}}{h_0} * \frac{B_l}{L_i} \tag{8}$$

with a leads closure rate γ [exld], usually quadratic. The relative ice concentration a with its minimum fraction of open water (A_{crit} [acrit]) is used to prevent the sea ice from filling up the grid box completely, which would neglect any further lateral change otherwise:

$$a = \min\left(1, \frac{(1 - A)}{(1 - A_{crit})}\right)$$

The multiplicand on the right side of equation (8) is the amount of ice created in leads using the *volumetric heat of fusion* of ice L_i, which is the amount of energy that is needed to transform sea water from liquid to solid state by freezing. The multiplicator describes the dependency on existing ice concentration and characteristic thickness of the ice (h_0 [hiccrit]) created in leads. Since the latter defines

whether thick ice is newly formed, without changing much the ice concentration, or thin ice closes the grid box quickly, h_0 is the most important parameter for thermodynamics with a high sensitivity on existing ice concentrations.

Ablation Since lateral melting has only little effect on reducing ice volume, vertical melting of thin ice is the most important process to enlarge open ocean areas. Thus for a positive heat budget of open water, ($B_l > 0$) total vertical melting decreases ice concentration, which is described by:

$$\left(\frac{\partial A}{\partial t}\right)_{abl} = \frac{A}{2h_i} * \Gamma\left[-\frac{\partial h_i}{\partial t}\right] \qquad \text{for } B_l > 0 \tag{9}$$

The Heaviside function $\Gamma[x] = \{0, 1\}$ only prevents function 9 from reaching results less than zero in absence of ice ($h_i = 0$).

2.2.2 Dynamics

Given a volume of ice, forming a body, it can be moved, rotated and deformated due to the acting forces It can behave hereby as a solid medium as well as a fluid. The conservation of momentum is given by

$$m_{si}\frac{\partial \vec{u}_i}{\partial t} = \underbrace{\vec{\tau}_{ai} + \vec{\tau}_{wi}}_{drag} - \underbrace{mf\vec{e}_z \times \vec{u}_i}_{Coriolis} - \underbrace{mg\nabla\eta}_{Gravity} + \underbrace{F_i}_{\substack{Internal \\ Forces}} \tag{10}$$

where a change of momentum must be caused by changes either in the ocean and air drag, the sea surface tilt and Coriolis effect or internal forces due to deformation. Any advection of momentum is hereby neglected due to a scale analysis (Fichefet and Morales Maqueda, 1997).

2.2.2.1 Internal Forces

The internal force F_i comprises inner and outer forces and the deformation of the ice volume. According to Green's theorem, it can be defined as the divergence of a two-dimensional, symmetric Cauchy stress tensor σ

$$F_i = \nabla \cdot \tilde{\sigma} \qquad \text{where } \tilde{\sigma} = \begin{pmatrix} \sigma_{xx} & \sigma_{xy} \\ \sigma_{yx} & \sigma_{yy} \end{pmatrix} \tag{11}$$

The normal stress σ_{xx}, σ_{yy} acts perpendicular on each side and is equal to the hydrostatic pressure ($\sigma_{xx} = \sigma_{yy} = P_{hydro}$) if present,. while the shear stress σ_{yx}, σ_{xy} acts alongside (see Fig. 13).

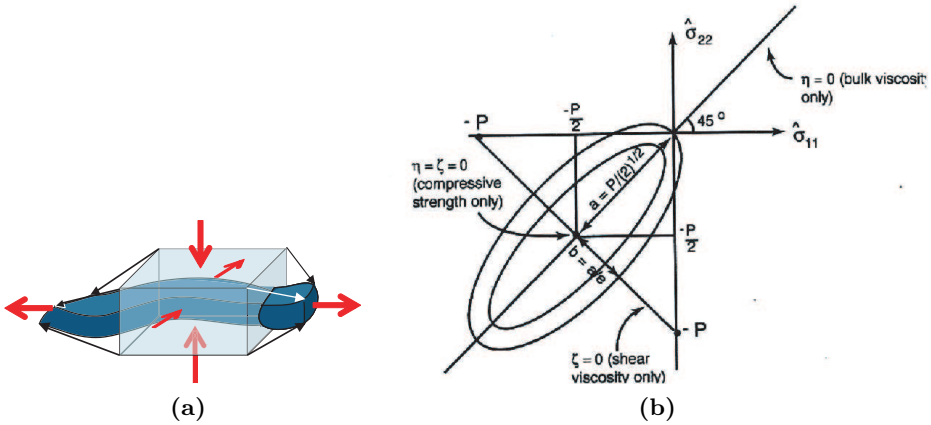

Figure 13 Inner and outer forces acting perpendicular or along on each side (a) can deformate an sea ice volume which is described by the viscous-plastic rheology by Hibler (1979) as illustrated in the stress space (b).

The associated deformation of the body, which means the displacement of each particle within the volume, can be described by a second tensor, the strain tensor ϵ. According to Hooke's law, the stress tensor can be expressed as a product of elasticity constants and the strain tensor. For continuous matter, that can behave concurrently as non-Newtonian fluid as well as plastic solid, which is the general assumption for sea ice, the connection between stress and strain is given by the so called rheology. The LIM sea ice model here makes use of the viscous-plastic formulation by Hibler (1979), who assumed that, based on the out comings from field experiments during AIDJEX (Arctic Dynamics Joint Experiment), the sea ice can be treated as such a two-dimensional, isotropic continuum with two material states due to the deformation rate ($\dot{\epsilon}$) and stated therfore:

$$\sigma = 2\mu\dot{\epsilon} + \left[(\zeta - \mu)\underline{\dot{T}}(\dot{\epsilon}) - \frac{P}{2}\right]\underline{I} \tag{12}$$

with $\underline{\dot{T}}(\dot{\epsilon})$ being the trace of the strain rate tensor and $\underline{I}$ the unit tensor.

The first term on the right side of Eq. (12) gives the acting stress by shear strain, the second the volume change without shear and the third the static pressure. The variable viscosity of the fluid (as it is assumed to be a non-Newtonian fluid) is given as a non-linear shear viscosity ζ, which describes the lateral shear defor-

mation, and the non-linear bulk viscosity μ that acts normal on the ice volume surfaces:

$$\zeta = \frac{P}{2\Delta} \qquad \text{and} \qquad \mu = \frac{\zeta}{e_c^2} \tag{13}$$

The definition of ζ includes a 'creep-limit' $\dot{\epsilon_0}$ [creepl] that inhibits the shear viscosity, and consequently the bulk viscosity, from exceeding a maximum value:

$$\Delta = \max\{\dot{\epsilon_0}, f(\dot{\epsilon}, e_c)\} \tag{14}$$

The function $f(\dot{\epsilon}, e_c)$ in equation 14 is responsible for the elliptical yield curve in the 2-dimensional stress space (see figure 13b) with eccentricity e_c [ecc].

With this formulation sea ice is treated as a 2-dimensional, linear-viscous, compressible fluid for a small deformation rate $\dot{\epsilon}$ until a yield strength is reached. For larger $\dot{\epsilon}$ it then behaves as plastic material that can burst.

To close the system in eq. 12, an equation of state is included. It couples the ice strength to the ice thickness characteristics:

$$P = P^*(1 - A)h_i \mathrm{e}^{(-CA)} \tag{15}$$

Equation 15 was originally postulated by Hibler (1979) and was modified by Fichefet and Morales Maqueda (1997), who added a linear lead fraction dependency. Thus, depending on the ice thickness (h_i) and lead fraction (A), the internal pressure is determined by the yield pressure P^*[pstar], which is responsible for the change-over from a viscous fluid to a plastic material. This formulation also takes into account, that the internal forces are only important for densely packed ice floe fields ($A < 0.2$) (Beckmann and Birnbaum, 2001).

Since its introduction by Hibler (1979), the ice pressure P has been used to tune sea ice models in aspects of thickness distribution and ice drift (Hibler, 1980). Using numerical models, Overland and Pease (1988) found a grid dependency for P with values starting with $10^5 N/m$ for coarse resolution models ($\mathcal{O}$(100km) up to $10^4 N/m$ for higher resolutions ($\mathcal{O}$(1km)). And as observations of in situ stress and strain are rare, Steele et al. (1997) examined the dependency of sea ice dynamics on the ice strength P in a numerical model of the Arctic Ocean to find reliable values for P^*. They stated that their range of values for $P^* =$

$(5.5 \times 10^3 - 1.375 \times 10^5 N/m^2)$ resulted in a too low ($P = 8 \times 10^3 N/m$) and too large ($2 \times 10^5 N/m$) ice strength which lead to an unrealistic sea ice thickness distribution and ice drift.

As the formulation of the ice strength here differs slightly from that one used by Steele et al. (1997), some sensitivity experiments has been done (not shown), to discover the most useful rheology parameter set for the model configuration in this study . But contrary to Steele et al. (1997) not only P^* is diversified here but also the second bulk parameter C [c_rhg]. The impact on the ice strength P is discussed for different lead fractions and ice thicknesses.

Sensitivity on P* The first bulk parameter, P^*, is the dominant factor in eq. 15. It prescribes the maximum ice strength under given ice concentrations.

Fig. 14 shows the relation of P to P^* for different lead fractions A. The valid range of P for mean sea ice characteristics using Hiblers original rheology is shaded as grey box, using the limits for P^* (between the 'S97' labels at the upper bound) as proposed by Steele et al. (1997). Taken $P^* = 2.5 \times 10^4$ (vertical, grey line), which was suggested by Hibler and Walsh (1980), the ice strength gets larger than 1.0 only with lead fractions lower than 50% (blue line in left panel of Fig.14) and reaches the scope by Overland and Pease (1988) only with high sea ice concentrations.

Taken additionally the ice thickness into account, the strength is amplified linearly (in Fig.14 thin solid lines represent an ice thickness of $h_i = 1m$, while thick solid lines indicate $h_i = 3m$). Since multi-year ice floes can reach a thickness of more than $10m$ in front of the Canadian Archipelago (McBean et al., 2005), only a small band of equitable P^*around 2.5×10^4 arises from this analysis.

Sensitivity on C The default value of the second bulk parameter is $C = 20$ (Hibler, 1979). Figure 15 shows ice strength P as function of C, normalized by $P*$, for distinct open ocean fractions A and for a mean ice thicknesses of $h_i = 3m$. While h_i only scales the ice strength (left axis), the impact of the ice concentration on the yield pressure is strongly determined by the chosen value for C. This parameter governs for which magnitude of ice concentration the ice strength and thus the internal forces in (10) get important for the sea ice dynamics. For the default value $C = 20$ only lead fractions of less than 20% ($A = 0.2$) induces internal forces (Fig.15 and Fig.14). Lower values (e.g. $C = 2$)

also allow for larger open ocean fractions, as can be clearly retrieved from Fig.15 and the relation between P and P^* in Fig. 14, where the ice strength increases for low sea ice concentrations.

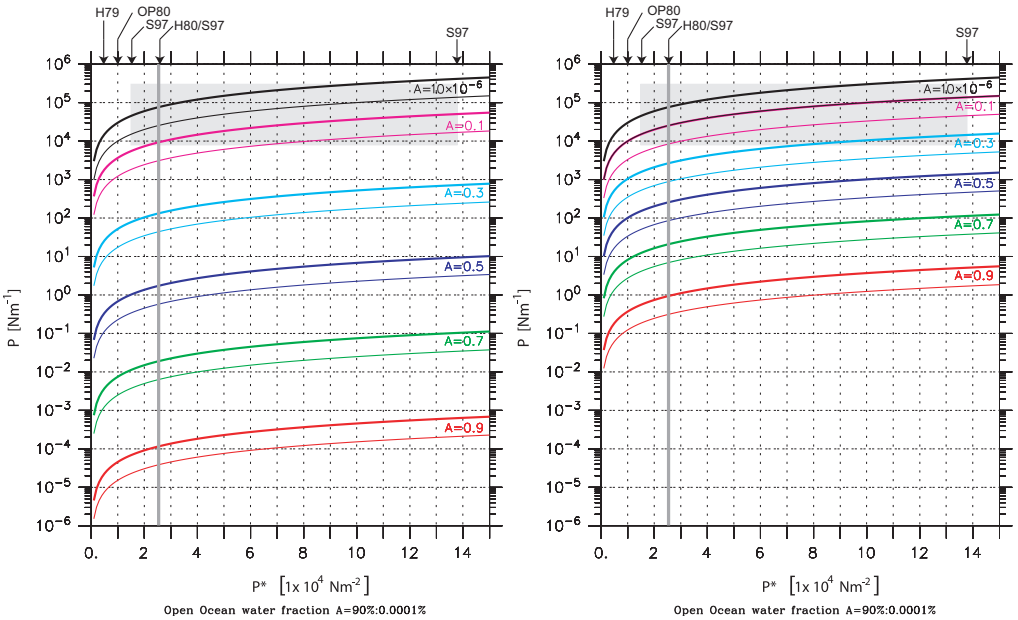

Figure 14 Ice strength P as function of yield pressure $P*$ under varying leads fraction conditions $A = \{0.9 - 0.1, A_{crit} = 1 \times 10^{-6}\}$ for ice thickness $h = 1m$ (thick solid curves) and $3m$ (thin curves). Labels at the upper bound denote suggested values by Hibler (1979, H79),Steele et al. (1997, S97),Hibler and Walsh (1980, H80) and Overland and Pease (1988, OP98). **left** with second bulk parameter $C = 20$, **right** $C = 2$.

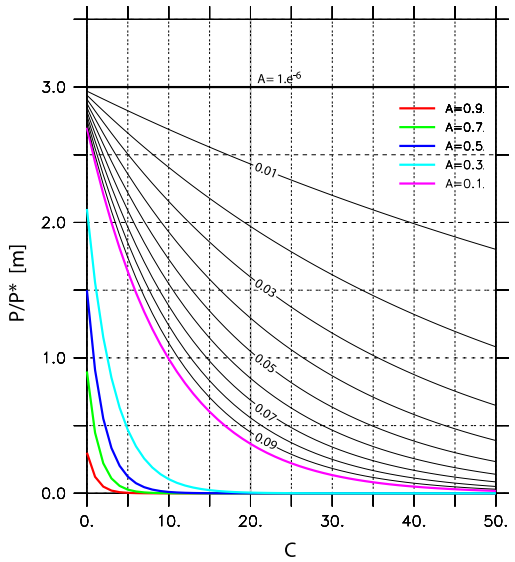

Figure 15 Ice strength P as function of the second bulk parameter $C = [0 : 10 : 50]$ using varying lead fractions $A = [0 : .1 : 1]$; see equation 15. P is normalized by $P*$.

2.2.2.2 Horizontal Transport

The LIM sea ice model knows six different fields Ψ that can be transported horizontally: Lead fraction (A), snow and ice volume per unit area (h_s, h_i), sensible heat content per unit area for snow and ice (Q_s, Q_i) and latent heat content in brine pockets (Q). The transport is affected by the general conservation law:

$$\frac{\partial \Psi}{\partial t} = -\nabla \cdot (\vec{u}_i \Psi) + D\nabla^2 \Psi + S_\Psi \tag{16}$$

with a horizontal difussivity $D = \begin{cases} const. & \text{inside ice pack} \\ 0 & \text{at ice edge} \end{cases}$ (due to non linear instabilities arising from coupling between ice dynamics and transport) and the rate of change of Ψ (by virtue of thermodynamic effects).

2.2.3 Coupling

2.2.3.1 Ocean

There is an exchange of momentum, heat and mass between the sea ice and the ocean model. Conceptually, the boundary layer of rough surfaces such as sea ice can be divided into various sub-layers (McPhee et al., 1987), each with different viscous and turbulent effects: A molecular sub-layer (L1), a transition region (L2), a surface sub-layer (L3) and an Ekman layer (L4) as shown in figure 16.

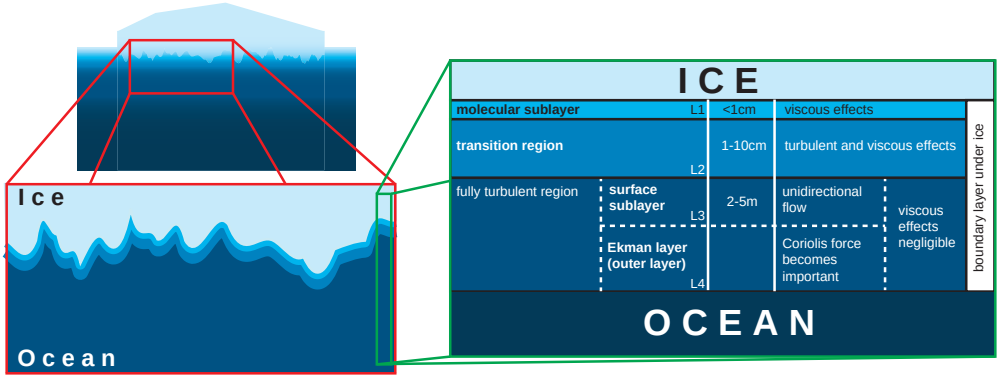

Figure 16 Conceptional layers at the ice-ocean boundary following McPhee et al. (1987). Nomenclature, thickness and viscous effects are indicated for each layer.

Heat The Heat flux at ice-ocean interface is expressed as a function of Sea Surface Temperature at ice-ocean interface, SST_{io}, the freezing point of sea water (references to 34.0) T_{freeze} and turbulent mixing:

$$Q_w = \rho_o c_{pw} c_h \left(T_{io} - T_{freeze}\right) u^*_{io} \tag{17}$$

This heat flux between the ocean and the ice is part of the non solar heat budget of the ice/ocean-atmosphere coupling and the forcing respectively (see also section 2.2.3.2). The friction velocity u^*_{io} is restricted to the range of $5 \times 10^{-3} \leq u^*_{io} \leq 2 \times 10^{-2} \frac{m}{s}$ to avoid too extreme values of the flux during one time step. The coefficient $c_h = 0.006$ is empirical (McPhee, 1992).

Momentum McPhee et al. (1987) have argued that for rough surfaces such as sea ice, the molecular viscosity (L1 in figure 16) plays no role in determining the mean velocity profile below the transition layer and thus only the surface and Ekman layer (L3 and L4) have to be taken into account. The surface integral of the pressure acting on under-ice pertrusions yields the ice-ocean stress (with τ_{wi} as stress of the water on the ice):

$$\tau_{wi} = -\tau_{iw} = \rho_0 c_w \left|\vec{u_w}(z) - \vec{u}_i\right| \left[\left(\vec{u}_w(z) - \vec{u}_i\right)\cos\theta + \vec{k} \times \left(\vec{u}_w(z) - \vec{u}_i\right)\sin\theta\right] \tag{18}$$

The drag coefficient c_w [cw], used in this formulation, depends on the depth of $\vec{u}_w(z)$. As the upper ocean layer in the model is about 5m thick and accordingly, the upper most velocity point in ocean lies in the range of the surface sub-layer (L3), there is no need to consider velocity turning in Ekman layer; with a turning angle of $\theta = 0$ [angvg] equation 18 reduces to:

$$\tau_{wi} = -\tau_{iw} = \rho_0 c_w \left|\vec{u}(z) - \vec{u}_i\right| \left(\vec{u}(z) - \vec{u}_i\right) \tag{19}$$

Mass The exchange of mass between the ice and the ocean is accomplished by a realistic freshwater flux (Tartinville et al., 2001) due to change of salt content of ocean and ice

$$F_{salt} = (S_{oce} - S_{ice})\frac{\partial m_i}{\partial t} \tag{20}$$

and the melting of snow in the upper layer ocean in the case of ice ablation or snow-ice transformation:

$$F_{snow} = -\frac{1}{\rho_s}\left(\frac{\partial m_s}{\partial t}\right)_{abl+si} \tag{21}$$

The freshwater flux strongly depends on precipitation as rain or snow: While snow accumulates in the snow layer on the ice covered part of the grid cell, the rain is passed directly into the ocean. The mass flux out of the ocean due to freshwater exchange can be written as:

$$F_{mass} = E_o - (P - P_s) - \rho_s F_{snow} \tag{22}$$

2.2.3.2 Atmosphere

The exchange between sea ice model and atmosphere is determined by the forcing fields and concerns solar and long-wave radiative fluxes, turbulent fluxes of heat (sensible and latent). and momentum as well as the flux of freshwater, which are described for ocean and ice in the following forcing section section 2.3.

Since the flux of momentum and the treating of freshwater differs slightly for sea ice from that for the ocean some additional comments are given in the following:

Momentum There is a flux of momentum on ice/ocean surface by wind stress. In respect of surface conditions, wind has varying effects on ice. As CORE makes use of wind stress fields there is no need to take an angle of deflection into account as used with geostrophic wind velocities, but different drag coefficients are necessary for different types of ice roughness.

Freshwater As liquid precipitation is directly passed through the ice into the ocean (see paragraph 2.2.3.1) solid precipitation (snow) is used to increase snow thickness and hence snow mass:

$$\frac{\partial m_s}{\partial t} = P_s + \left(\frac{\partial m_s}{\partial t}\right)_{melt} \tag{23}$$

The ice mass is then effected by snow-ice transformation hereafter.

2.3 Initialization and Forcing

Temperature and salinity fields are initialized using the World Ocean Database 2001 (WOA01 by Conkright et al., 2002) for all basins except for the Arctic where the advanced PHC-3.0 climatology (updated from Steele et al., 2001) is applied, which merges the World Ocean Atlas (WOA98, e.g. Antonov et al., 1998; Boyer et al., 1998) with more reliable data sets from the regional Arctic Ocean Atlas (Arctic Climatology Project, 1997, 1998). Dynamics are started globally from zero velocities.

As the model in this study is an ocean-only model (including sea-ice), atmospheric surface conditions have to be prescribed. Here, the CORE forcing by Large and Yeager (2004) is used, which provides the atmospheric state at 10m (temperature, humidity and wind), downwelling radiation (long-wave and short-wave), precipitation (rain and snow) as well as continental runoff. All required atmosphere-ocean and atmosphere-sea ice fluxes are then computed via bulk formulae (Kara et al., 2000) taking the prognostic ocean state (sea surface temperature and ocean velocity) into account. The fields comprise different kinds of variability: seasonal/climatological for one normal year or interannual (including seasonal variations) for the period 1958-2000[2].

Since the model is initialized from rest with the present ocean state (e.g. Levitus climatology; World Ocean Data), the model has to be integrated first until it adjusts dynamically under a given surface-forcing to its initial state or, with other words, until the circulation is consistent with the prescribed water mass structure. As the deep ocean would require hundreds of years to adjust while the upper ocean only requires a few decades (Kantha and Clayson, 2000), the following assumption is used: The spin-up time is related to the time needed for the large-scale planetary waves to cross an ocean basin, where they affect currents and water mass properties. For the largest basin, the Pacific, this time is ~ 11 years in mid-latitudes. During that time and away from strong currents and convection regions, the deep ocean will not evolve far from the initial state, which is imperfect due to the sparseness of the data at depth. And because a too long spin-up moreover would be too expensive in terms of computing time (compared to the actual period of interest, which is about 50 years of forward integration), 20 annual loops applying the climatological forcing fields seems to

[2]It has to be noted that some of the forcing components only provide interannual variability for the second half of the simulated period (see Large and Yeager (2004, their Fig. 2) due to lacks of trustworthy historical data, such as for precipitation (see section 2.3.1.1).

be reasonable.

The required forcing fields and their associated Bulk formulae are discussed briefly in the following as they are interesting for the freshwater budget (for further details see Large and Yeager (2004)):

2.3.1 Freshwater flux

The CORE forcing provides datasets for Precipitation by rain (P_R) and snow (P_S), River+Coastal Runoff (RNF), whereas evaporation is computed by the model using bulk formulae. Additionally, a weak global surface salinity restoring (ERP) and a weak Nowtonian damping for tracers is applied.

2.3.1.1 Precipitation

For climate studies, long-term (longer than 20 years) records of precipitation (hereafter P) are desirable to investigate interannual and decadal variability successfully. Unfortunately, observations of P are very sparse in time and space, although large improvements have been made since the introduction of remote sensing by the modern generation of satellite techniques in 1978 (Kalnay et al., 1996; Huesmann and Hitchman, 2003; Hernandez et al., 2004; Uppala et al., 2005). But global coverage by satellite observation is restricted to lower and mid-latitudes while it fails in high-latitude bands due to problems that arise from the presence of land- and sea-ice and solid precipitation in these regions. Thus the best data quality can be reached in conjunction with records of direct measurements, e.g. by rain gauges, which exist mainly on land (GHCN v2; Peterson and Vose, 1997; Chen et al., 2002). Since such observations are highly infrequent over ocean, e.g. by ship weather observations, several methods have been established to extrapolate measurements along coast lines and from islands to close the gaps over ocean, for instance by using EOF patterns or cross correlations with climate indices such as the North Atlantic Oscillation (NAO) (Efthymiadis et al., 2005; Mariotti and Arkin, 2007). Using a projection of historical records from the period before 1978, this can also be used to reconstruct global precipitation data sets for the pre-satellite era for both, over land and over sea (PREC project by NOAA-CPC; Chen et al., 2002).

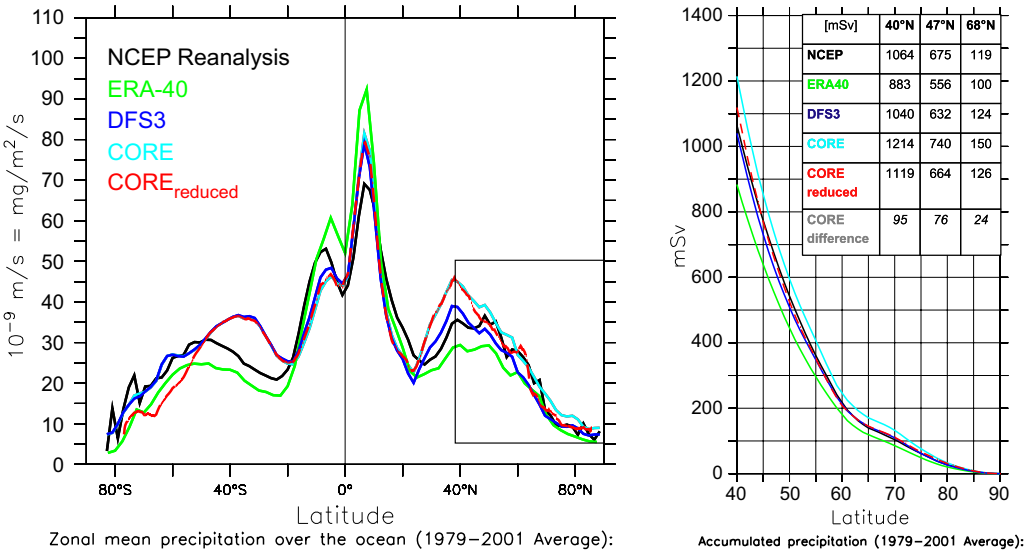

Figure 17 **Left**: Zonally averaged total precipitation (rain+snow) into ocean from different datasets. **Right**: Total precipitation accumulated southward from the north pole to 40°N. See text for referencing the different products.

Another data set covering a satisfying temporal and spatial resolution is provided by reanalysis-projects, such as the NCEP/NCAR reanalysis or ECMWF ERA-40 (Kalnay et al., 1996; Uppala et al., 2005) for the second half of the 20th century. They use observations to assimilate time step-wise predictions from forecast models. But the output fields have to be handled with care: rain observations are not taken into account by the assimilation process and thus P fields only depend on the forecast models (Kalnay et al., 1996; Poccard et al., 2000; Efthymiadis et al., 2005). However, they are not completely independent from the progress in satellite observations after 1978 as the latter caused a significant shift in the quality of the atmospheric state (Huesmann and Hitchman, 2003; Dell'Aquila et al., 2005), governing the precipitation at least.

Long-term forcing datasets are required for this study, encompassing the period 1958-2000. Due to the difficulties with single products as discussed above, the CORE dataset for precipitation is composed of different sources (Large and Yeager, 2004), including satellite data as well as rain gauge observations. It consists of GPCP (v1; satellite), merged data set by Xie and Arkin (1996) (based on GPCP gauge analysis, three different satellite products and predictions produced by the ECMWF; precursor for the CMAP data set, Xie and Arkin, 1997) and a climatology by Serreze and Hurst 2000 for the Arctic region. Since these datasets only start in 1978 along with the satellite era, the model forcing in this study only provides interannual variability for precipitation since then. For the period

before 1978, a climatology (based on the described datasets) is used instead.

In comparison with other products, like NCEP Reanalysis (Kalnay et al., 1996), ERA40 (Uppala et al., 2005) or DFS3 (Molines et al., 2006; Brodeau and Barnier, 2006, Brodeau and Barnier, in prep.) the mean CORE precipitation appears excessively large in the subtropics and the north polar region (Fig. 17). As the freshwater budget in the (sub-) polar basin is a main subject in this study, precipitation is reduced to more reasonable values (red curve).

2.3.1.2 Evaporation

Following (Large and Yeager, 2004) the evaporation E over the ocean is defined as a function of the humidity of saturation q_{sat}, depending on the sea surface temperature SST (prognosted by the ocean model), the air humidity q_{10} (taken from forcing fields) and velocity difference $\Delta\vec{U}$ between wind speed and surface velocity. Interannual variability in the evaporation is accomplished by fluctuations in the wind field and air humidity.

$$E = \rho_a C_E (q_{sat}(SST) - q_{10}) |\Delta\vec{U}| \tag{24}$$

2.3.1.3 Runoff

Large and Yeager (2004) used an estimated climatological freshwater runoff from continental imbalances (Baumgartner and Reichel, 1975) between precipitation, evaporation and storage, based on NCEP/NCAR reanalysis data. For the contribution by rivers they computed a freshwater flux using the 275 most important rivers, whereas the runoff was smoothed around the river mouths by a Gaussian distribution (an example for the northern hemisphere is given in Fig. 18a). To globally balance the obtained freshwater input and the retrieved continental imbalance a 'coastal runoff ' was distributed evenly along the coast.
However, in comparison with observational estimates of volume flux, collected by the Global Runoff Data Center (GRDC) and reviewed e.g. by Dai and Trenberth (2002), the CORE runoff appears to be too large, especially north of 70°N (Fig. 18b) and is therefore modified, ensuring the following constraints: The arctic region receives $0.11 \times 10^6 m^3/s$ north of 65°N (GRDC, 2004b) while the world discharge into the ocean is assumed to be $1.29 \times 10^6 m^3/s$ which compares better to other studies (GRDC, 2004a).

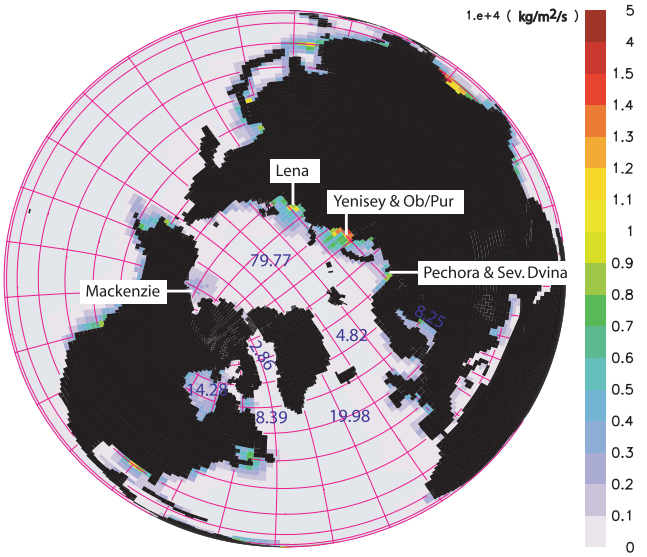

(a) Annual Mean

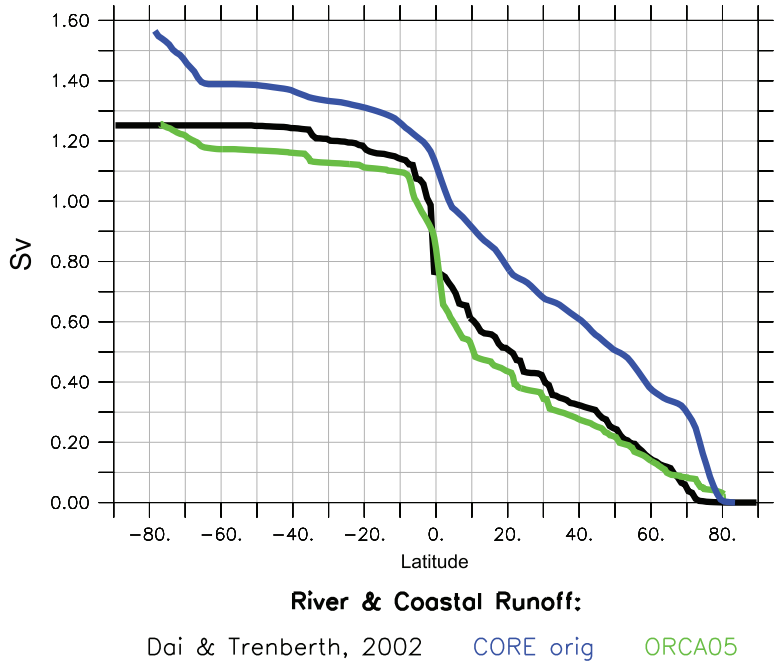

(b) Zonal integral of the global runoff.

Figure 18 (**a**) River and coastal runoff in northern hemisphere as used for simulation. Some of the most important rivers are labeled, numbers indicate the related basin-wide annual fluxes. (**b**) The zonally integrated global runoff for the modified dataset used in this study (green) in comparison with the original CORE-Runoff (blue) and the dataset by (Dai and Trenberth, 2002).

2.3.1.4 Surface Restoring

To avoid a drift in the surface layer due to missing coupled effects with the atmosphere the surface salinity restoring (or evaporation damping) ERP is defined as a relaxation of sea surface salinity SSS towards the initial condition S_{init} (Boyer et al., 1998) on given timescales $cdmp2D$ (in days) as real freshwater flux for pure water with density ρ_{water}:

$$ERP = \frac{cdmp2D}{86400s}(SSS - S_{init})/SSS \times \rho_{water} \tag{25}$$

Throughout all experiments a long timescale (weak restoring) of 180 days is used.

2.3.1.5 3D-Damping

Marginal seas tend to drift faster toward unreliable ocean states not only at the surface but also in the deep, because the water mass exchange with the world ocean is mostly accomplished only through narrow and shallow passages. To reduce these tracer trends, a weak Newtonian damping (γ=180 days)

$$\frac{\partial T}{\partial t} = ... - \gamma(T - T_{init}) \tag{26a}$$

$$\frac{\partial S}{\partial t} = ... - \gamma(S - S_{init}) \tag{26b}$$

toward initial conditions (T_{init}, S_{init}) is applied to salinity S and temperature T in the whole water column in some marginal seas (e.g. Mediterranean and Red Sea). It is also applied to the Arctic Ocean and the Nordic Seas north of 70°N to avoid too unreliable values in these regions as they can have a large effect on the global ocean circulation.

2.3.2 Heat flux

Ocean Surface fluxes are calculated by the model using the following budget

$$Q_{as} = Q_S + Q_L + Q_E + Q_H + Q_P \tag{27a}$$

with the radiative fluxes for short and long waves

$$Q_S = (1 - \alpha_{oce}) * Q_I \tag{27b}$$
$$Q_L = Q_A - \sigma_{SB}(SST)^4$$

and the turbulent fluxes for the latent and sensible heat

$$Q_E = \Lambda_v E \tag{27c}$$
$$Q_H = \rho_a c_p C_H (\Theta_{10} - SST)|\Delta\vec{U}|$$

and the precipitation heat flux by melting snow

$$Q_P = -\Lambda_f P_S \tag{27d}$$

where α_{oce} is the albedo of open ocean, Q_I the forced solar insolation, Q_A the long-wave energy from the atmosphere, σ_{SB} the Stefan-Boltzmann constant. Λ_v is the latent heat of vaporization, ρ_a is the near surface air density, c_p defines the specific heat of the air and Θ_{10} is the given air temperature. Finally, Λ_f is the heat of fusion and $P_S$is the precipitation by snow.

The turbulent transfer coefficients for sensible (C_H) and latent (C_E) heat fluxes between atmosphere and ocean are calculated by using NCAR bulk formulae as supposed by Large and Yeager (2004).

Ice As the ice/snow surface has a different albedo from the ocean, fluxes are calculated separately:

$$Q_S^* = (1 - \alpha_{ice/snow})Q_I \tag{28a}$$
$$Q_L^* = \epsilon_i \left(Q_A - \sigma_{SB}(T_{ice/snow})^4\right) \tag{28b}$$

For the ice/snow-system the turbulent fluxes are computed accordingly to (27c) but all transfer coefficients are kept equal and constant ($C_E^* = C_H^* = C_D^* = 1.63 \times 10^{-3}$).

2.3.3 Momentum flux

Momentum is put into the ocean/ice system by wind stress which is computed for ocean ($\vec{\tau}_{ao}$) and sea ice ($\vec{\tau}_{ai}$) separately using

$$\vec{\tau}_{ao} = \rho_a C_D |\Delta\vec{U}| \Delta\vec{U} \quad (29)$$

$$\vec{\tau}_{ai} = \rho_a C_D^* |\vec{U}_{10}| \vec{U_{10}} \quad (30)$$

$\Delta\vec{U} = \vec{U}_{10} - \vec{U}_0$ vector difference between wind at height z_u and the surface ocean current $\vec{U_o}$. The sea ice drift velocity is assumed to be much smaller than wind speed and is thus neglected. The transfer coefficient C_D is computed by bulk formulae similar to the turbulent heat fluxes. For sea ice, C_D^* remains constant (see 2.3.2)

2.4 Experiments overview

To examine the influence of interannual forcing variability on the ocean currents and water mass properties, climatological forcing fields for the three components heat, freshwater and wind are combined with interannual varying fields in different ways. Tabular 1 shows the experiments and their forcing components

REFERENCE This experiment is forced including interannual as well as seasonal variability in each forcing component. It reflects most of the features that can be observed in the real ocean and is thus used as reference run.

THERMHAL The interannual thermohaline forcing, which is applied to the ocean while wind stress is kept climatological, neglects any wind stress induced ocean variability on timescales longer than seasonal.

HEAT Like THERMHAL but no interannual freshwater variability in Precipitation and Evaporation but with still interannual varying latent heat fluxes $Q_E(E)$.

WIND Only the wind stress field is allowed to vary interannually to extract the dynamic effect without any thermohaline driven changes in the ocean circulation.

NONARCTIC This is a regional sensitivity experiment since only the arctic region north of the arctic circle (˜67°N) is forced climatological while the forcing field for the rest of the model domain is fully interannual (see mask shown in Fig. 19). In comparison to REF any locally induced variability in the Arctic and its effect on the northern subpolar region is suppressed.

FRESH This experiment is similar to the reference run, because all forcing fields are interannual, too. But here, the original (larger) CORE precipitation field is used. The difference to the REFERENCE run can be interpreted as additional freshwater input in a kind of 'hosing experiment'.

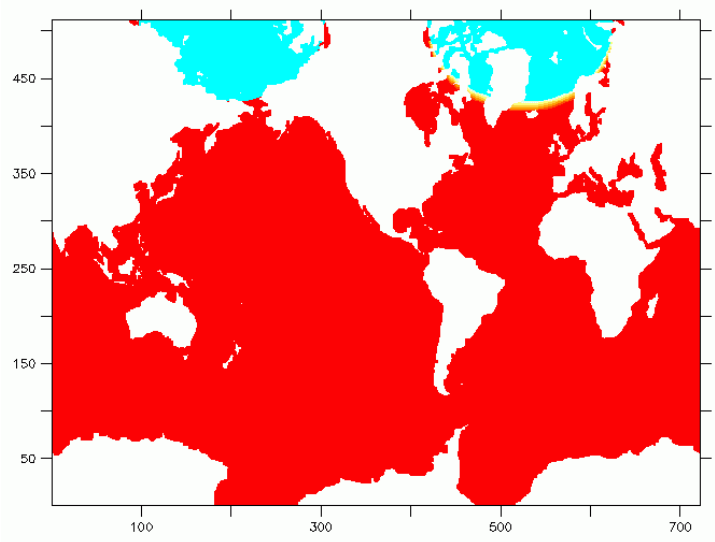

Figure 19 Horizontal map of the weighting mask on the ocean model grid for experiment NONARCTIC . Red areas indicate the usage of interannual varying data sets while a climatological forcing is applied to the blue shaded region within the arctic circle. The yellow transition region in-between indicates the linear interpolation between both kinds of forcing.

	Heatfluxes				Freshwater		Wind
	Q_S	Q_L	Q_H	Q_E	E	P	τ
REF	ia	ia	ia	ia	ia	ia	ia
THERMHAL	ia	ia	ia	ia	ia	ia	ny
HEAT	ia	ia	ia	ia	ny	ny	ny
WIND	ny	ny	ny	ny	ny	ny	ia
NONARCTIC	ia / ny	ia / ny	ia / ny	ia / ny	ia / ny	ia / ny	ia / ny
FRESH	ia	ia	ia	ia	ia	ia ++	ia

Table 1 ORCA05 Experiments overview and the nomenclature: forcing components with interannual variability (ia) or climatological as 'normal year' (ny). For experiment FRESH ia++ indicates an interannual varying increased precipitation field.

3 Methods of Freshwater Budget Analysis

There is no general agreement of how the term 'freshwater' is specified and how it is computed. Thus a brief overview is given in the following chapter ere a definition is provided as it is used in this study. Afterwards a formal description of the freshwater budget components is given.

3.1 Specification of equivalent Freshwater Content Change

For a discussion of the freshwater budget of an open ocean domain, first it has to be specified how the freshwater content (FWC) and the related fluxes in the ocean are defined. In general, the equivalent freshwater content change (FWCC) is introduced as a useful concept to characterize the change in mean salinity in an ocean volume; i.e., FWCC is defined as the equivalent amount of freshwater that would have to be added or subtracted in order to attain the observed salinity change (Boyer et al., 2007).

In most practical applications, as used by many studies on the Arctic freshwater budget (e.g. Aargaard and Carmack (1989); Serreze et al. (2006); Holfort et al. (2008)), the fraction of fresh water in a box is computed as volumetric equivalent freshwater relative to the mean salinity (S_0) within the box[1]. This *reference salinity* S_0 can be also chosen with regard to a distinct layer, e.g. the halocline (Tully and Barber, 1960) or to a specific water mass, e.g. the Atlantic Water inflow into the Nordic Seas (Dickson et al., 2007).

For the subarctic Atlantic, different definitions of S_0 have been chosen, e.g., Aargaard and Carmack (1989); Serreze et al. (2006) used 34.8 whilst Dickson et al. (2007) used 35.2 . Computation of freshwater budget terms and trends in the present study are calculated for a reference salinity $S_0 = 34.7$; this choice allows to capitalize on internal computations of budget terms used in the numerical model code. It is important to note, however, that the main results of the study are not dependent on the particular choice of S_0, because the content and transport anomalies, which are in the focus of this study, are less sensitive to the reference salinity than the mean (see also Appendix A on page 151 for some comments on this topic).

3.2 Budget Components

For the freshwater budget several components must be taken into account. Some are prescribed by the forcing fields while others are computed internally by the

[1] In contrast to a global freshwater budget, as e.g. constructed by Wijffels et al. (1992) based on the conservation of mass salt, formulations for limited domains or sections need to invoke a reference salinity S_0.

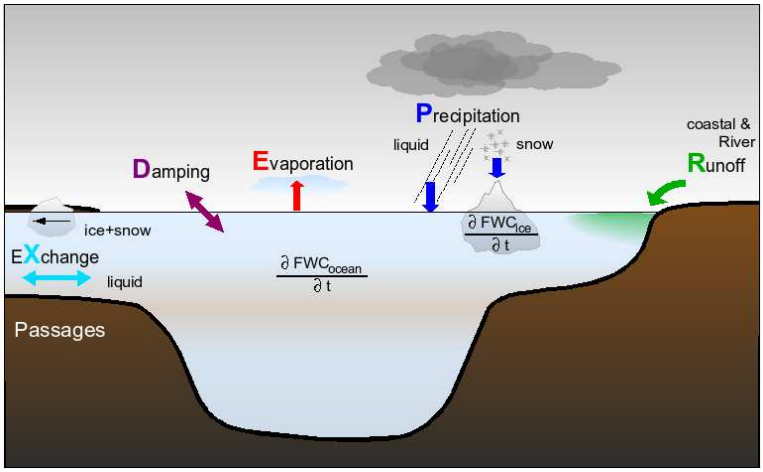

Figure 20 Freshwater budget components in a semi-closed basin with one passage. Direction of arrows indicate a positive flux direction for surface fluxes (evaporation, liquid and snow precipitation, runoff and surface damping). Snow can accumulate on top of the sea ice, while rain is transferred directly into the ocean. Passage exchange of freshwater is governed by lateral transports of liquid freshwater within the ocean and solid by sea ice.

ocean/ice model or they are diagnosed offline using the output data from the simulation. For a better understanding an overview of these contributions is given and discussed briefly.

Sinks:

E	Evaporation over open ocean
IO	ice-ocean exchange by freezing; ice storage
X	Exchange through passages (liquid, ice, snow)

Sources:

P_{liq}	Precipitation (liquid)
P_{snow}	Precipitation (snow)
R	Runoff (coastal & river)
IO	ice-ocean exchange by melting; ice storage
X	Exchange through passages (liquid, ice, snow)

Other:

D	Damping (Surface restoring and Newtonian 3D damping)
$\frac{\partial FWC}{\partial t}$	change of ocean freshwater content (FWC)

3.2.1 Surface Fluxes

Additionally to the prescribed forcing fields for the surface freshwater fluxes, namely rain and snow precipitation, runoff, restoring and evaporation (see section 2.3.1), ice-ocean interaction has to be included in the freshwater budget and is computed online by the ice/ocean model.

3.2.1.1 Equivalent Freshwater Flux from melting Snow and Ice

Melting snow from atop the sea ice is a freshwater source for the ocean. As snow has a density different from pure water, the snow water equivalent (SWE) for melting layer with thickness $h_{melting\,snow}$ is used here:

$$SWE = h_{melting\,snow} * \rho_{snow} \tag{31}$$

where ρ_{snow} is density of snow. This leads to a freshwater flux by melting snow

$$FWF_{snow} = \frac{\partial SWE}{\partial t} \tag{32}$$

According to (32) an equivalent freshwater flux into the ocean for melting ice can be defined, accounting for salinity of sea ice S_{ice}:

$$FWF_{ice,} \quad = \quad \frac{S_{oce} - S_{ice}}{SSS_{io}} \frac{\partial}{\partial t}(h_{melting\,ice} * \rho_{ice}) \tag{33}$$

3.2.1.2 Net Surface Freshwater Flux

For the simplified free surface condition as used in the ocean model in this study, the net surface freshwater flux for the ice-free ($frld$) ocean is determined by forcing fields and diagnostic terms:

$$FWF_{surface} \quad = \quad P_{rain} + frld * (P_{snow} - E) + FWF_{ice} + FWF_{snow} + RNF + ERP$$

taking precipitation P (by rain and snow), evaporation E, freshwater fluxes from ice and snow FWF, runoff RNF and Restoring ERP into account.

3.2.2 Passage Exchange

Another source or sink for freshwater in the ocean is the lateral exchange with other basins. This can be accomplished on one hand by sea ice transport and on the other hand by liquid water transport relating to a reference salinity (S_0; see above). Additionally, the freshwater content itself can vary with time.

3.2.2.1 Equivalent Freshwater Transport from advecting Ice

The sea ice volume flux F_{ice} across a section between the borders x_0, x_1 can be described by:

$$F_{ice} = \int_{x_0}^{x_1} \bar{u}_{ice}(x) h_{ice}(x) dx, \tag{34}$$

for sea ice with thickness $h_{ice}(x)$ and drift velocity $\bar{u}_{ice}$ across the section.

Following Cuny et al. (2005), the freshwater flux from melting (advected) ice is then defined by

$$FWT_{ice} = F_{ice} \frac{(S_0 - S_{ice})}{S_0} \frac{\rho_{ice}}{\rho_{water}} \tag{35}$$

The freshwater flux from advecting snow (FWT_{snow}) lying on ice is calculated accordingly using also the ice drift velocity.

3.2.2.2 Equivalent Freshwater Transport in the Ocean

The freshwater transport within the ocean depends on the difference between the ocean salinity S and the reference salinity S_0 as well as the ocean velocity $\bar{u}_{ocean}$. It is integrated over the area A spanned by the section:

$$FWT_{ocean} = \int \bar{u}_{ocean} \frac{(S_0 - S)}{S_0} dA \tag{36}$$

3.2.3 Equivalent Freshwater Content

Since the volume of the sea ice and the snow layer atop the ice sheet as well as the salinity in the ocean can change, the freshwater budget has to include the change of freshwater storage or drift in these systems.

3.2.3.1 Ice/Snow System

Depending on the different densities for snow/ice ($\rho_{snow,ice}$) and the specific salinities ($S_{ice,snow}$) the freshwater content in a ice/snow layer with thickness $h_{ice,snow}$ is computed by

$$FWC_{ice,snow} = \iint h_{ice,snow}\,\mathrm{d}x\mathrm{d}y * \frac{\rho_{ice,snow}}{\rho_{water}} * \frac{(S_0 - S_{ice,snow})}{S_0} \tag{37}$$

3.2.3.2 Ocean

Similar to the freshwater transport, the equivalent freshwater content in the ocean is a function of ocean salinity S and the reference salinity S_0 :

$$FWC = \int \frac{(S_0 - S)}{S_0} dV \tag{38}$$

3.3 Statistical Analysis of Budget Components

In a given volume where all lateral fluxes are known and the volume is conserved, a simple closed freshwater budget can be established following the Gaussian Law:

$$\frac{\partial FWC}{\partial t} = FWF_{SRF} + FWT_{NB} + FWT_{SB} \tag{39}$$

where FWF_{SRF} is the net surface flux, FWT_{NB} and FWT_{SB} are the equivalent freshwater net transports for the northern and southern sections respectively.

A statistical description of this budget can be performed using a causal model in that way, that the actual FWC change (Y hereafter) can be predicted by an estimated $\hat{Y}$ using the budget components as predictors (X), whereby $\sum(Y-\hat{Y})^2$ is a minimum. Using a multiple linear regression model, equation 39 turns to

$$\begin{aligned} Y &= \hat{Y} \\ &= b_{Y.123} + b_{Y1.23}X_1 + b_{Y2.13}X_2 + b_{Y3.12}X_3 \end{aligned} \tag{40}$$

with the criterion on the left-hand side and the sum of the intercept $b_{Y.123}$ and the products of partial regression coefficients b_{Yi} with predictors X_i on the right-

hand side. In a perfect statistical budget model the intercept would then disappear ($b_{Y.123} = 0$) and the regression coefficients would be each equal to one ($b_{Y1.23} = b_{Y2.13} = b_{Y3.12} = 1$). But in fact, the computational regression would result in slightly different constants from that due to the fact that the regression coefficients are determined under the condition of minimizing the residual $(Y - \hat{Y})^2$.

A measure of association between the criterion variable (Y) and an optimally weighted (linear) combination of predictor variables (resulting in $\hat{Y}$) is given by the multiple regression coefficient $R_{Y.123}$, which is nothing else than the correlation $r_{Y\hat{Y}}$ between Y and $\hat{Y}$. To consider the role of individual variables in predicting the criterion partial or semipartial (or part) correlations can be diagnosed. Following the formal description of Howell (1992) and Cohen et al. (2003) the partial correlation (e.g. $r_{Y1.23}$) has variable 2 and 3 partialled out of both the criterion and predictor 1. Partialled out means hereby the variable is kept constant while evaluating the correlation. The semipartial correlation ($r_{Y(i.12..(i)..k)}$ for k predictors) describes the relation between all of the variability of Y and X_i from which all other X different from X_i(that is $X_{(i)}$) has been partialled. It is a semi-partial correlation because the effects of all $X_{(i)}$ has been removed from X_i but not from Y (contrary to partial correlations).

This can be easily illustrated using Venn diagrams (c.f. Cohen et al., 2003): Assuming the variance of a variable (Y, X) is represented by a box of unit area and the overlapping area of two boxes represents their relationship as r^2 (or percentage of explained variance of Y) Fig. 21 shows the two cases. The partial correlation (shaded box in the left panel) always represents 100% of the reference variance (framed box), while the semipartial correlation typifies the percentage of explained variance of the whole budget (thick black framed box in the right panel).

In this context, it can be shown (e.g. by Howell, 1992) that the square of the multiple correlation coefficient can be expressed as sum of squared bivariate and semipartial correlations:

$$R^2_{Y.123} = r^2_{Y1} + r^2_{Y(2.1)} + r^2_{Y(3.12)}. \tag{41}$$

In the case of completely independent predictors, this reduces to

$$R^2_{Y.123} = r^2_{Y1} + r^2_{Y2} + r^2_{Y3} \tag{42}$$

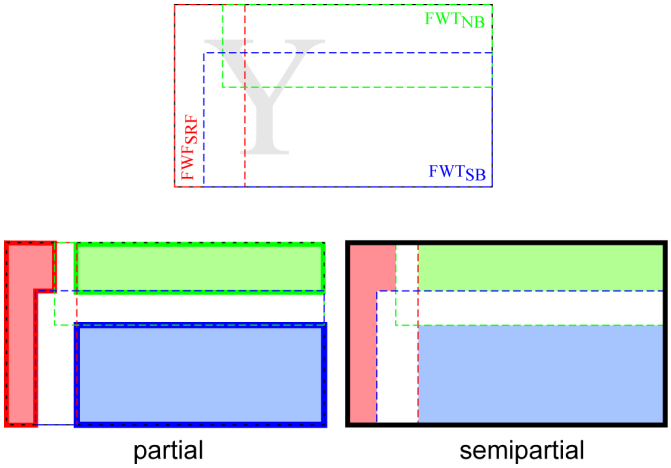

Figure 21 Venn diagrams for the statistical budget model. Box of unit area indicates the variance of the corrector (Y; thin black framed box for the complete budget) and the predictor variables (X; dashed framed boxes). Overlapping areas of two boxes represent their relationship as r^2. **Upper panel**: The model with its overlapping components for the net surface flux (red dashed framed box), northern (green) and southern (blue) transports. **Lower left**: The partial correlation represents the relation between a predictor with all other predictors partialled out (shaded box) and the residual of Y with all other predictors partialled out, too (thick framed boxes which are virtually the same in this case). **Lower right**: In the semipartial case, each correlation (shaded boxes) is related to the complete variance of Y (thick black framed box).

without overlapping areas in the Venn diagram. Since the components in a freshwater budget are usually not independent from each other the sum of all squared semipartial correlation coefficients will not result in 100% explained variance but in a residual representing the joint effects of the budget components (surface flux changes may appear in the section transports or variations at the southern boundary are transported through the basin affecting the northern transport).

4 Arctic Ocean

The climate in the arctic region is dominated by a low solar insolation and a general heat loss of the ocean and atmosphere. The most prominent feature is the cryosphere which consists of ice sheets, glaciers, snow and permafrost on land and sea ice in the ocean. As the latter can modify the sea surface heat flux significantly and is responsible for the storage and the export of pure freshwater out of the polar region, it is a key feature for freshwater budgets in global ice-ocean models. Since it is essential for understanding the freshwater variability in the north polar region a brief introduction into the geographical conditions as well as the sea ice transport in the arctic region is given in the following sections.

The evaluation of the simulation using observational data reveals a reasonable representation of the sea ice extent as well as the variability in the coverage and transport on different time scales.

4.1 Geographic and Hydrographic Conditions

In this study, the Arctic Ocean (as illustrated in Fig. 22) is defined to comprise the region approximately north of the Acetic Circle (66.6°N) including three different seas: the *Arctic Sea*[1], *Baffin Bay* in the west of Greenland and *Nordic Seas* in the east respectively. The latter is often referenced as *'GIN Sea'* due to its sub-domains *Greenland Sea*, *Iceland Sea* and *Norwegian Sea*.

The inner Arctic is enclosed by the Eurasian and American continent and Greenland. It can be divided into two sub-basins: the *Amerasian* and the *Eurasian Basin* which are more than 4000m deep, separated by the *Lomonosov Ridge* in-between (McBean et al., 2005).

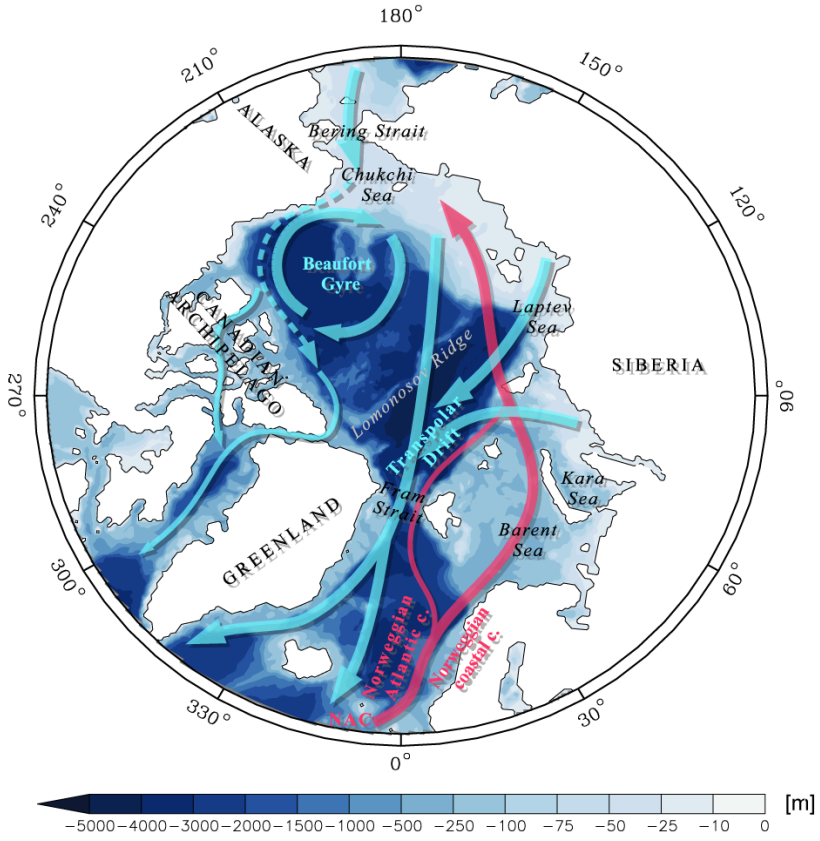

Figure 22 Arctic bathymetry (m; blue shade) and some main features of the current system (simplified) according to McBean et al. (2005).

[1] The International Hydrography Organization recognizes this basin as the 'Arctic Ocean' (IHO, 1953)

The open boundary at Bering Strait next to the Pacific Ocean is very shallow (45m) and the other passages at the Canadian Archipelago and through the Barent Sea allow an inter-oceanic transport only within the upper 220m. The only deep exchange with the world ocean is accomplished at the Fram Strait (2600m) east of Greenland. At this passage fresh and very cold surface waters are exported by the East Greenland Current while warm and salty waters enter the Arctic basin via the West Spitsbergen Current originating from the NAC (Fig. 23). In the deep, cold and relatively salty waters can exit the Arctic.

Another source of salt for the Arctic Ocean is the Norwegian Coastal current which is fed by the NAC and flows on the shelf through the Barent Sea further eastward. On its way it submerges below 200m as the warm but salty inflow is denser than the cold but very fresh water in the layer above. The latter forms the *Arctic Halocline* (Fig. 24), which is fed by the surface fluxes, coastal and river runoff and by the import of cold and relatively salty water from the Pacific through the Bering Strait. It provides a barrier that shields the sea ice cover from contact with the warm North Atlantic water and thus prevents the sea ice from melting (Lippsett, 2005). This water mass appears in the upper 300m of the western Fram Strait outflow (Fig. 23).

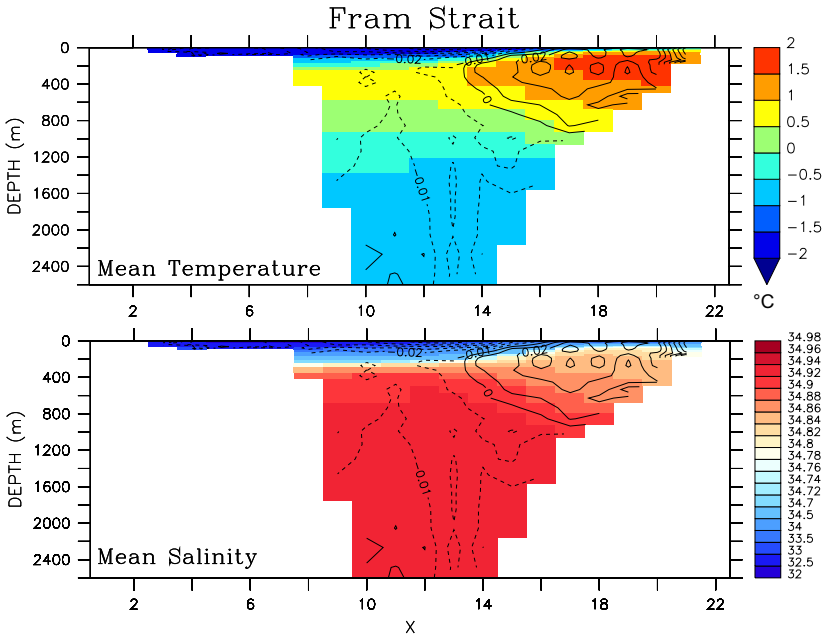

Figure 23 Fram Strait section from simulation REFERENCEfrom west to east: (**upper panel**) mean temperature and (**lower panel**) mean salinity. Contour lines indicate the long-term mean meridional velocity (m/s) for the integrations period in intervals of 0.01 m/s. The abscissae are on the model grid and indicate tracer grid boxes.

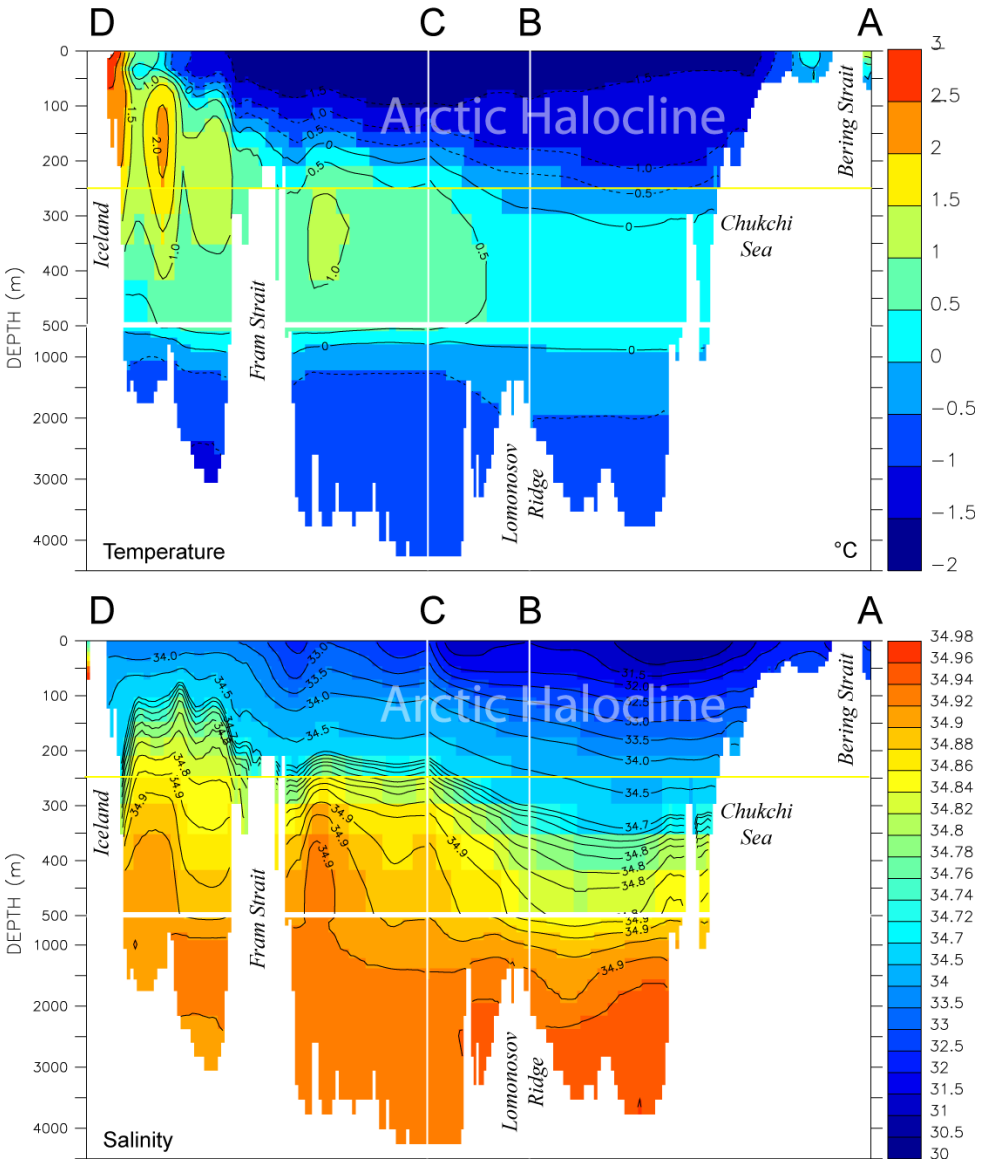

Figure 24 Composite of 4 sections crossing the Arctic (see green line in Fig. 25) showing the hydrographic conditions as long-term mean temperature (upper panel, °C) and salinity (lower panel) from the reference simulation. (The upper 500m are stretched vertically.)

The most important dynamic features in the inner Arctic Ocean are the *Beaufort Gyre* and the *Transpolar Drift* (Fig. 22). The wind-driven circular Beaufort Gyre (BG) in the Amerasian basin keeps a large amount of freshwater (Martin and Gerdes, 2006; Proshutinsky and Johnson, 2001). Two phases of the gyre

circulation have been identified, which depend on the structure of the wind field, as shown by Rigor et al. (2002): In the ocean, the very fresh and light water in the interior Beaufort Sea implies an anti-cyclonic geostrophic ocean circulation in the upper layer. During periods, when the atmospheric sea level pressure (SLP) is high, the resulting clockwise wind regime strengthens the BG. When the SLP lowers, the wind-field shifts and a more cyclonic atmospheric circulation is established. This retards the counteracting oceanic flow and the BG weakens. This seesaw can even be associated with the Sea Surface Height (SSH) in the Arctic and the Arctic Oscillation index (AO), as discussed by Häkkinen and Proshutinsky (2004). Unfortunately, these dynamic relations could not be found in this study. But the mean hydrological signature of the simulated BG is represented well in comparison with observations by the Environmental Working Group (EWG), which is reported by Steele et al. (2004) for the Arctic Ocean Model Intercomparison Project (AOMIP). Admittedly, this is not a surprising result since the Arctic ocean is initialized with the named EWG data set and a weak tracer relaxation towards these initial conditions is performed (see section 2.3.1.5). In any case, this seems to have only a minor effect, as the sea ice and freshwater export out of the arctic are nevertheless reasonable, as will be shown later.

The Transpolar Drift (TD) next to the Beaufort Gyre is a current-system that transits both arctic basins and flows towards the northern coast of Greenland and the Fram Strait (McBean et al., 2005). It transports plenty of freshwater in the upper layer and relatively salty and warm water beneath. The latter water mass is originated from the NAC inflow into the arctic while the freshwater is fed by runoffs from the Eurasian coast and the freshwater release during a weakening of the Beaufort Gyre. Since the Transpolar Drift also depends on the wind field, the two phases, which were found for the BG circulation, also affect the pathway of the TD (Mysak, 2001).
Due to its importance for the Arctic freshwater budget and its oscillating character, the BG is also called the 'Flywheel' (Proshutinsky et al., 2002) of the arctic oscillation.

The Nordic Seas encloses the *Greenland Sea* in the north, the *Iceland Sea* in the south and the *Norwegian Sea* in the east and is thus often called *GIN Sea* (according to the abbreviations). One of the most prominent features of the bathymetry is the mid-ocean ridge, which separates the eastern from the much

deeper western basin (e.g. Blindheim and Østerhus, 2005). The deepest connection with the Arctic is located in the Fram Strait (2600m), whereas the passages to the subpolar North Atlantic are much shallower, because the *Greenland Scotland Ridge* forms a sill east (˜850m) and west (˜650m) of Iceland.

Connecting the inner Arctic with the North Atlantic there is a general northward flow in the east, maintained by the *Northeast Atlantic Current* (NEAC) and the *Norwegian Atlantic Current* (NwAC) and a southward flow east of Greenland (*East Greenland Current*; EGC). A northwestward branches from the eastern currents and recirculations from the western current system makes for an interconnection in-between (e.g. Eldevik et al., 2005).

The inflow of Atlantic Water provides salty water while the import of Arctic Water makes for a reduction of salt (Dickson et al., 2007). Within the basin highly dense water masses are produced (Jonsson and Valdimarsson, 2004) which are exported as Overflows across the sills in the Denmark Strait (600m deep) and the Faroe-Scotland ridge and then appears as bottom water in the subpolar basin.

The Baffin Bay in the west of Greenland gets in contact with the inner Arctic through the Canadian Archipelago with its narrow channels and islands. Two of the largest passages are resolved in the model simulation: The Nares Strait in the northeast and the Lancaster Sound in the northwest of the Baffin Bay. The only passage in the south is the Davis Strait next to the Labrador Sea. The flow through the northern passages is generally southward while in the south there is an inflow of subpolar waters (*West Greenland Current*) in the east of Davis Strait and an southward flow in the west (*Baffin Current*).

4.2 Sea Ice

4.2.1 Production and Dynamics

Sea ice is produced during wintertime by open ocean freezing of surface waters or lateral accretion at existing ice sheets. There is a drift of the sea ice due to wind and ocean stress and it thus follows mainly the horizontal current system of the ocean (Fig. 25). Depending on its thickness and formation, it can break up and can be stacked. Especially the Chukchi Sea, in contact to the Bering Strait, is known as 'ice factory' (Lippsett, 2005): In winter frigid winds from Alaska squalls

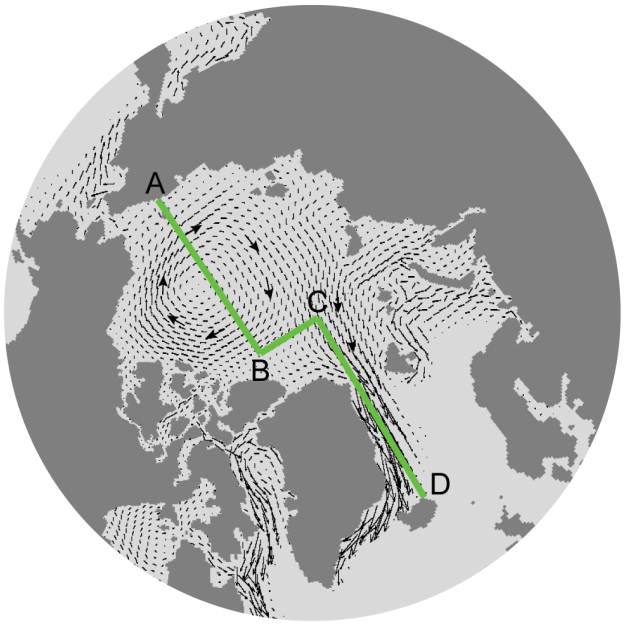

Figure 25 Qualitative illustration of simulated winter mean sea ice drift in REFERENCE. The green line indicates sections as used for Fig. 24. Vector length represents the strength of sea ice drift velocity.

over the shallow sea, sea ice is formed and is pushed by the wind further out the sea.

Like the export paths of liquid surface water (see previous chapter), there are only a few passages for the sea ice to exit the arctic basin: The Barent Sea, the Canadian Archipelago and the Fram Strait, whereas the latter gateway is the most important of all as it is located at the end of the Transpolar Drift which pushes the sea ice towards this passage.

4.2.2 Extent/Area

There are different ways to describe the sea ice coverage. The **sea ice concentration** (in %) is the ice coverage per unit area (e.g. one grid cell) whereas the **sea ice extent** is the total expanse (in m^2) that is covered by ice, including open water between the floes. It's a measurement how many grid cells are affected by sea ice and thus depends on the model resolution or satellite sampling grid. The **sea ice area** is the total area that is covered by sea ice. Open Water is not

included but all classes of ice (permanent, seasonal and marginal ice cover). Finally, the **ice volume** is the sea ice area per grid box multiplied with it's mean ice thickness per box. In addition to sea ice extent this provides an indication for the vertical scale.

A map of the sea ice extent in simulation (REFERENCE) and observation (SSMI, provided by the Goddard Space Flight Center (GSFC, 2007)) is shown in Fig. 27 for mean winter (March) and summer (September) season. Although there are some marginal differences, the simulation is in good agreement with the observation. In winter the inner arctic is completely covered by sea ice while at the southern boundaries the inflow of warm NAC water makes for indentations truthfully west of Spitsbergen and in the Barent Sea. The mean winter concentration seems to be somewhat too large off the Labrador coast and during the summer season on the Amerasian shelf. Besides this qualitative comparison the integrated sea ice area however reveals a much better accordance for the inner arctic basin (north of the Nordic Seas, Baffin Bay and Bering Strait) as well as for the north polar region (all arctic and subpolar basins). The simulated sea ice area (Fig. 26) fits pretty well into observations. In both there is a large seasonal variability while on interannual and longer timescales fluctuations appears to be small.

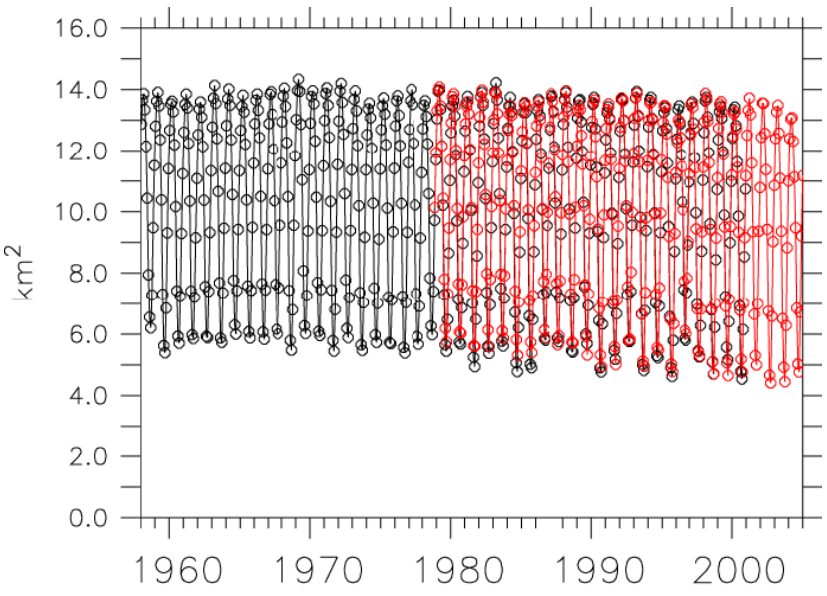

Figure 26 Monthly integrated north polar sea ice area (for coverage > 15%,whole arctic and subarctic region) in the simulation (REFERENCE, black) and observation (SSMI data (GSFC, 2007), red). Circles indicate single months.

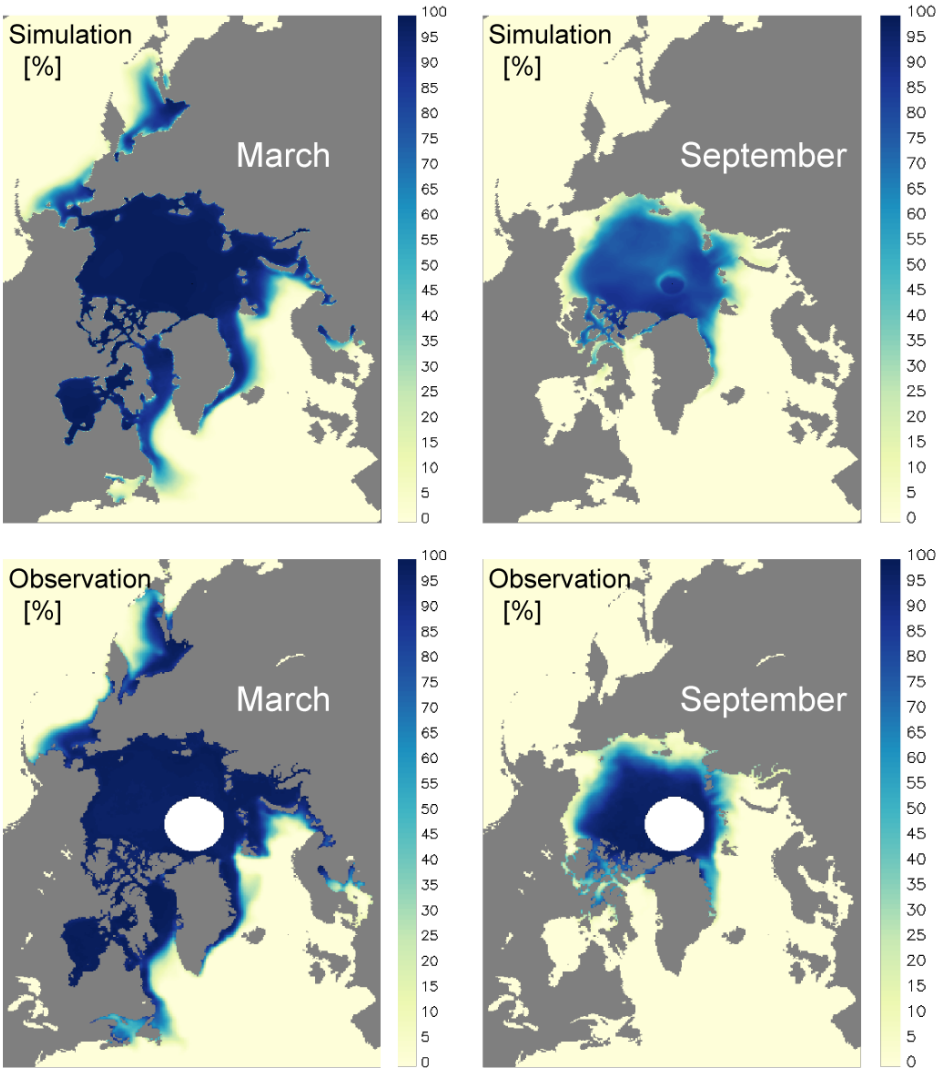

Figure 27 Maps of long-term mean sea ice concentration (percent) for winter maximum (March, left column) and summer minimum (September; right column) in REFERENCE simulation (upper row) and in SSMI observation (lower row; provided by the Goddard Space Flight Center GSFC (2007).)

Recent studies report a tremendous decline of arctic sea ice extension (Meier et al., 2007; Serreze et al., 2007; Stroeve et al., 2007). Indeed, the summer coverage in 2007 reached its lowest ratio (NSIDC, 2007). Using SSMI data the summer sea ice area (red curve in Fig. 28) reveals a negative trend (thick red line) since 1978 of about $0.05 \times 10^6 \frac{km^2}{a}$ ($\sim 8\%$ per decade) with an acceleration in the beginning of the 21st century as shown by Stroeve et al. (2007). The simulation REFERENCE (black lines) provides a similar trend only for the shorter period 1986-2000 ($0.05 \times 10^6 \frac{km^2}{a}$), while the sea ice extent since 1978 indicates a weaker simulated trend due to general smaller extents between 1978 and 1985. The reasons for these different trends in observations and modeling are not clear but, e.g. for the IPCC scenarios, this got just into discussion (Stroeve et al., 2007).

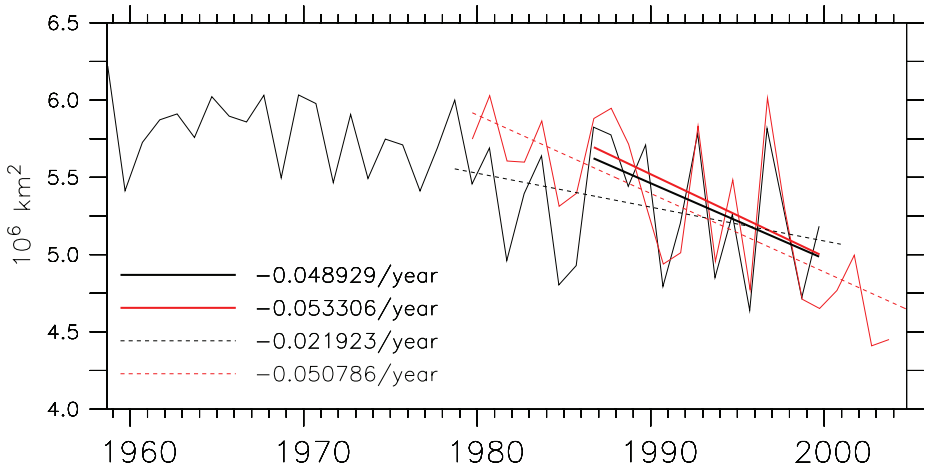

Figure 28 Summer Minimum of integrated ice area in simulation (REFERENCE, black) and observation (SSMI (GSFC, 2007), red). Trends from a linear regression are added for two overlapping periods (1979-2000 (thin dashed lines) and 1986-2000 (thick solid)).

4.2.3 Exports

The Fram Strait is the most important passage for sea ice export out of the Arctic as already mentioned above. Several observations allow a comparison with the simulated sea ice export. The Fig. 29 shows the annual sea ice area flux anomaly, which is defined as the temporal (annual) and coast-to-coast integral of the sea ice drift velocity across the strait (positive downstream). The observational estimates are taken from Kwok and Rothrock (1999) who used satellite data and drift buoys.

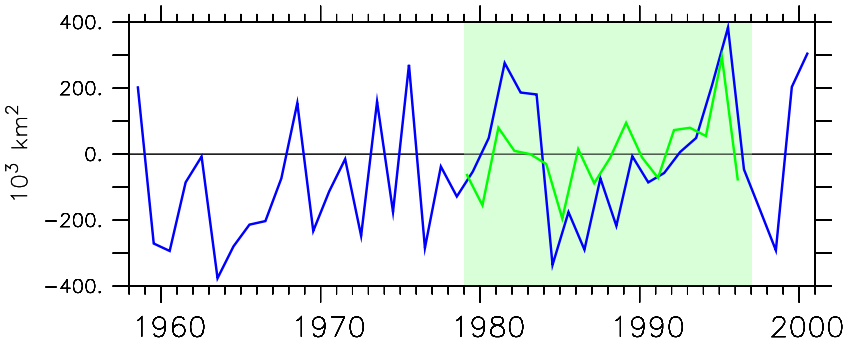

Figure 29 Fram Strait: annual sea ice area flux anomalies (km^2) in simulation (REFERENCE, blue) and observation (green, Kwok and Rothrock (1999)). Values are positive downstream. Green shaded area indicates observation period.

A better measurement for the freshwater exported by sea ice is the actual volume flux of sea ice. The simulated flux anomalies are compared with few observations by Vinje (2001) (shown in Fig. 30). In both diagnostics there is a good agreement of simulation and observational sea ice export. Not only the range of variability is represented reasonably but also the tenor of the interannual and intra-decadal fluctuations.

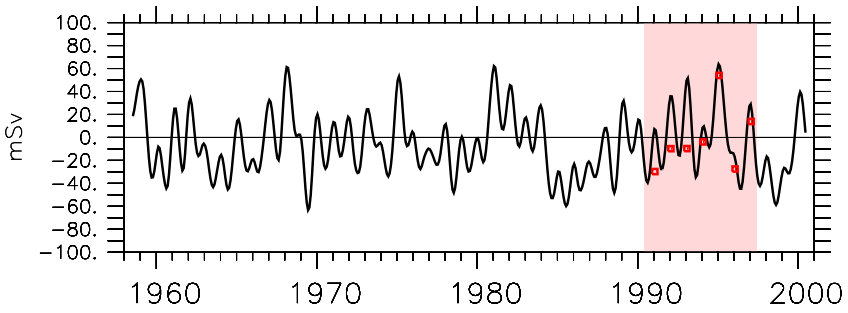

Figure 30 Fram Strait: Sea ice volume flux anomalies in simulation (REFERENCE, black) and observation (Vinje (2001), red squares). Anomalies are given in $mSv = 10^3 m^3 s^{-1}$, positive downstream. Red shaded area indicates observation period.

There are three periods of increase in the sea ice export time series during the late 1960ies, early 1980ies and between the mid-80ies and mid-90ies. The former is often discussed (e.g. Dickson et al. (1988)) in conjunction with the Great Salinity Anomaly 1970 (GSA70), an increase of freshwater within the upper layer in the Nordic Seas and the Subpolar Gyre. See section 5.2.3.3 for a further discussion of the GSAs.

Since the ice drift depends on the wind-stress several efforts have been made to correlate this ice export with climate signals (Fig. 31) such as the NAO (North Atlantic oscillation) or the AO (Arctic Oscillation). Such a correlation however seems to be only meaningful for the period after 1978. Cavalieri (2002) supposed this is due to changes in the wind field, caused by an eastward shift of the center of low pressure and got better results when correlating with the phases of the planetary wave-1 in the sea level pressure field.

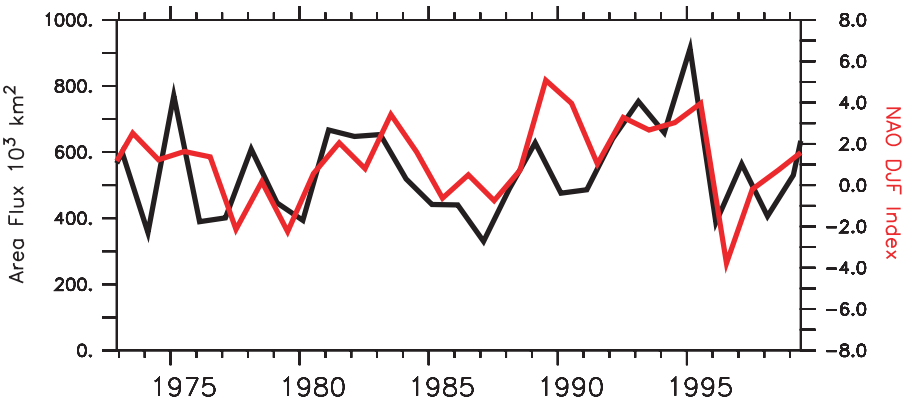

Figure 31 Fram Strait: absolute ice area flux (left axes) from reference simulation and winter NAO index (right axes) according to Kwok and Rothrock (1999) (Correlation r=0.63).

4.3 Arctic Freshwater Budget

4.3.1 Basins and Sections

The freshwater budget is established for the Arctic region which consists of several basins divided by sections (Fig. 32): the inner *Arctic* which is in contact with the Pacific Ocean through the *Bering Strait* on one side and with the *Nordic Seas* through the *Fram Strait* and the *Barent Sea* passage on the other side. Passing the *Canadian Archipelago* water can be exchanged with the *Baffin Bay* via *Lancaster Sound* and *Nares Strait.* The southern boundary of the *Nordic Seas* are given by *Denmark Strait* and the *Iceland-Norway* Section. Geographically, the Nordic Seas are separated from the North Atlantic by the sills in the Denmark Strait (˜600m) and the Iceland-Scotland-Ridge which is about 500m deep except for a narrow channel (˜800m) near the shelf in the east. In the west of Greenland, the *Davis Strait* is the only passage south of the *Baffin Bay*.

Figure 32 Arctic basins and sections as used for the freshwater budget. Subbasins (inner Arctic, Baffin and GIN) are colonized while purple lines indicate the sections enclosing the basins.

Since the Arctic freshwater export and exchange with the subpolar North Atlantic is in the main focus of this study, a separate budget for the inner Arctic will not be discussed here. The sea ice export is therefore treated as lateral freshwater transport equivalent with the oceanic transport.

4.3.2 Mean State

Simulation In the Arctic region, covering the basins within the arctic circle (inner Arctic, Baffin Bay and Nordic Seas/GIN), the mean freshwater balance for the REFERENCE run is shown in Fig. 33 schematically. Red numbers indicate surface fluxes (net precipitation, runoff, restoring; all fluxes are positive into the ocean) and the blue and purple figures denote lateral exchange through passages by ocean and sea ice. The mean spans the simulated time range from 1960 until 2000 at which these mean values depend on the choice of the reference salinity (stronger than the related anomalies do; c.f. Appendix A on page 151).

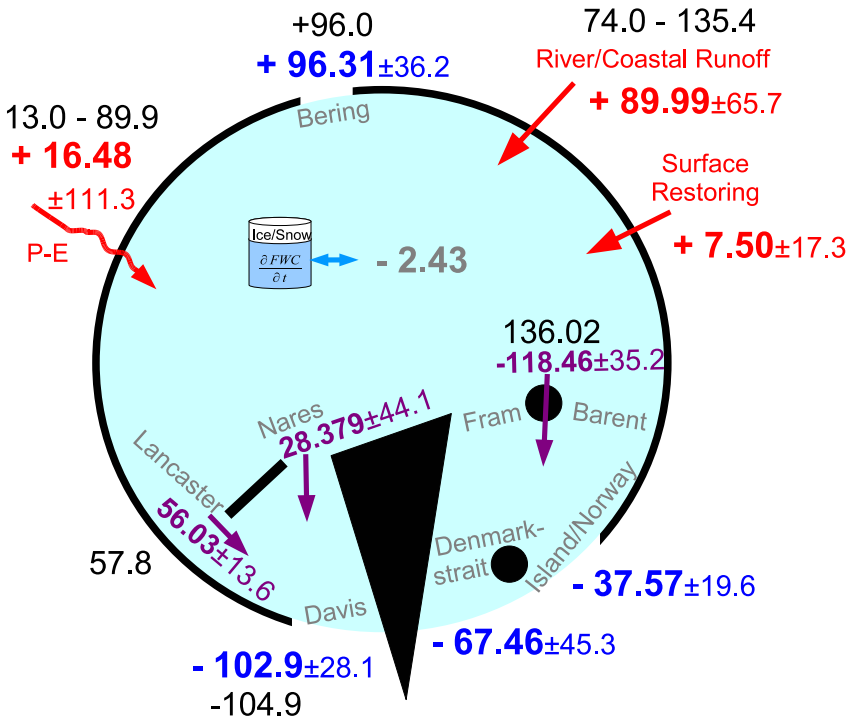

Figure 33 Schematic view on the Arctic basins with numbers from the mean freshwater budget (fluxes in mSv = $10^3 m^3/s$ ± standard deviation of the monthly time series) for the period 1960-2000 in the REFERENCE simulation. Figures denote net surface fluxes (red) into all sub-basins together, lateral import/export (blue) and lateral exchange within the basin (purple) as well as means and ranges of values found in literature (black; see text for further details.) .

At the surface, the largest freshwater input is provided by river and coastal runoff (89.99 ± 65.7 mSv or 79% of surface sum) whereas the net precipitation (precipitation minus open ocean evaporation) of about 16.48 ± 111.3 mSv contributes only for 14% to the mean though the monthly standard deviation is very large. The surface restoring adds only 7.5 ± 17.3 mSv (at open ocean as well as under ice) since the sea surface salinity in the Arctic basins tends a little bit to be too salty in comparison with Levitus.

The only lateral source of freshwater (liquid+ice/snow) in the Arctic is the Bering Strait inflow. The amount of 96.31 ± 36.2 mSv is in the order of magnitude of the runoffs. All other passage transports act as a sink of freshwater: west of Greenland, the Baffin Bay exports 102.9 ± 28.1 mSv freshwater through Davis Strait. In the east, nearly the same quantum (105.03±34.9 mSv) leaves the arctic circle at Denmark Strait and the Iceland-Norway passage together, whereas the latter one is an effective freshwater export due to a northward salt import by the NAC.

In the Nordic Seas by itself, the lateral imports of freshwater (118.46 ± 35.2 mSv) via Fram Strait and Barent Sea (salt transport to the north) are larger than the export in the south (105.03 mSv). Thus, the GIN Sea region is expected to gain freshwater. But this imbalance seems to depend on the time range for which the mean budget is established, as discussed later. A different picture draws the Baffin Bay, which looses freshwater (15.49 mSv) in the simulation.

$$\frac{\partial FWC}{\partial t} = \sum Surface + \sum Passages \tag{43}$$

$$\mathbf{3.43} \approx \quad \mathbf{113.97 - 111.62} \quad = 2.35$$

The complete mean freshwater budget for the ocean is shown by equation (43). The surface freshwater input (113.97 mSv) is nearly balanced by the lateral outflow (111.62 mSv) with a difference of 2.35 mSv, while the freshwater content of the ocean increases (3.43 mSv). This results in an imbalance of 1.08 mSv, which corresponds to less than 1% of the net surface freshwater flux. It may be accomplished by the weak deep 3D-restoring, which is not included in the balance due to diagnostic reasons.

Observations This freshwater budget fits well into what is known from observations. Serreze et al. (2006) composed different observational data sets with reanalysis data to get a complete freshwater balance for the Artic basins referenced to 34.8, which is only slightly different from the reference value used for the simulation (34.7). The range of freshwater fluxes at surface and at each passage (c.f. appendix B) is shown in Fig. 33 using black numbers (single values denote literature means). All simulated fluxes in REFERENCE lie in these ranges, even though some freshwater transports are very low, especially at Fram Strait and Barent Sea and at the surface.

For the two passages Tab. 2 compares model data (purple) with observations (black and green), separated in passages and ice/snow or liquid portions around Spitsbergen. While ice/snow transport at Fram Strait is about 73.0 mSv in both

[mSv]	Greenland-Norway	Fram	Barent
SUM	**118.46** *160* *116*	**98.86** *157* *99*	**19.60** *3* *17*
liqu	**39.66** *87* *43*	**26.09** *84* *32*	**13.57** *3* *17*
ice+ snow	**78.79** *73*	**72.77** *73*	**6.02** -

Table 2 REFERENCE: Freshwater transports at Fram Strait and Barent Sea in simulation (Purple) and observation as composed by Serreze et al. (2006)(black) and Aargaard and Carmack (1989) (green).

observation and simulation, only little is known about the measurable ice transport at Barent. The oceanic freshwater transport however, differs considerably. But the range of observational estimates is very broad. For the Fram Strait upper water outflow (76.1 mSv), Serreze et al. (2006) make use of the dataset by Meredith et al. (2001), which only exists for 2 years (1997,1998), whereas other studies suggest a conspicuously lower transport, e.g. Aargaard and Carmack (1989) with 31.71 mSv. Otherwise, an explanation for the smaller Fram Strait transport in the model may be too low salinities in the West Spitsbergen current (see Fig. 23) which transports salty water from the Atlantic northward. But one has to notice that the freshwater budget compiled by Serreze et al. (2006) includes an imbalance of 22 mSv and the range of observational estimates for passage transports are very large as it depends on the time range during which observations are undertaken. The uncertainties in observations are also discussed in the most recent study on the Arctic freshwater budget by Dickson et al. (2007), who found the range of total freshwater transport across Fram Strait (referenced to 34.8) between 125 mSv and 160 mSv (148 mSv using $S_0 = 35.2$), whereas the larger value is strongly based on estimates by Meredith et al. (2001) who used observations only for two years.

Farther south, Dickson et al. (2007) suggest an export of 202 mSv leaving the Nordic Seas which is nearly twice the transport in this study (105 mSv). They estimated this value as residual of their freshwater balance for the Nordic Seas relative to 35.2 with large contributions from the north (148 mSv compared to 118 mSv in the model) and by surface fluxes and runoffs (54 mSv vs. 7 mSv). Hence, four possible explanations can be considered: First, the model simulation

underestimates potentially the freshwater sources because there is no interannual variability neither in the river and coastal runoff nor in the Arctic precipitation fields. Second, the budget by Dickson et al. (2007) may provide too large surface fluxes since they used estimates by Serreze et al. (2006) which are based on ERA40 reanalysis data (see section 2.3.1.1 for a discussion of precipitation in reanalysis products). Third, the shortness of available data records compared to the time scale of transport variations might lead to a significant discrepancy from a long term mean. Finally forth, the balance of the Nordic Seas conducted by Dickson et al. (2007) is computed relative to an estimated mean salinity for the Atlantic inflow between Iceland and Norway which neglects interannual variations in the volume transport affecting the mean freshwater transport.

In the west of Greenland, there is a fairly good agreement of observations and simulated mean fluxes in this study: At Davis Strait, Cuny et al. (2005) suggest a freshwater transport of about 104.9 mSv, which is not far from the simulated 102.9 mSv. Further north, the Baffin Bay is fed by the Canadian Archipelago Throughflow at Nares Strait on one hand of about 28.38 mSv in simulation compared with observed 28.6 mSv, proposed by Münchow et al. (2006). On the other hand, the model resolution allows also the freshwater exchange through the Lancaster Sound of about 56.03 mSv, highly comparable with observational estimates of 57.8 mSv by Tang et al. (2004).

4.3.3 Temporal Variability

4.3.3.1 Nordic Seas (GIN)

As the Nordic Seas connect the subpolar north Atlantic with the fresh arctic, this is one of the most important regions for freshwater exchanges and is discussed therefore separately.

As can be seen in Fig.34a, the surface fluxes (red line) have only little influence on the interannual to decadal freshwater variability of the budget and can be neglected. Much more important is the lateral exchange (blue curve). The fresh water from the arctic, liquid and ice/snow, enters the Nordic Seas via Fram Strait (black curves in Fig.34b) with a strong interannual variability in the sea ice (dotted). Nearly 70% of the Fram Strait net freshwater input is transported farther south throughout the Denmark Strait (green), while 30% remains in the interior.

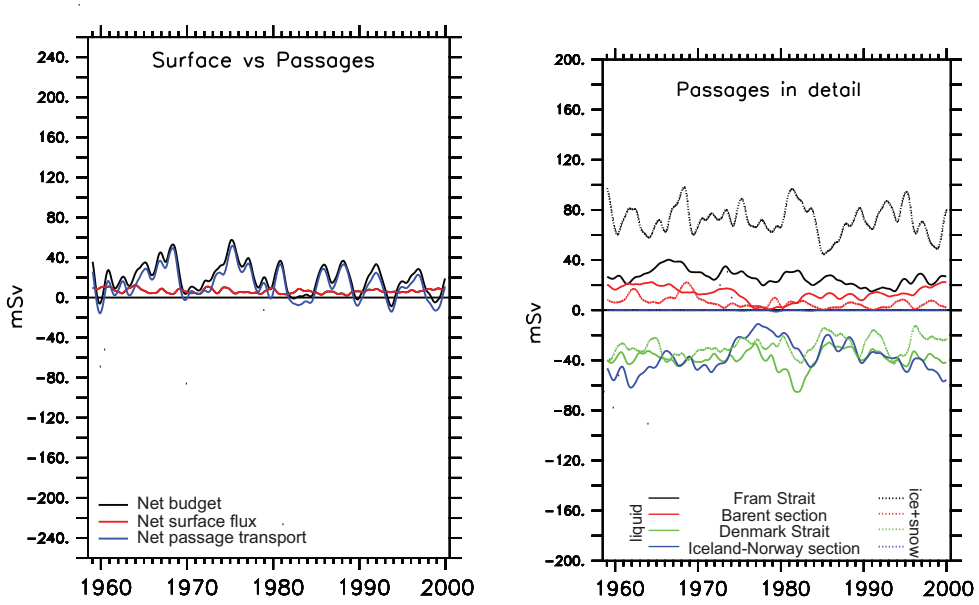

(a) (b)

Figure 34 Freshwater budget for the Nordic Seas (basin GIN) in experiment REFERENCE (**a**) Net flux anomalies (black) compared to component surface net flux (red) and lateral net transport across all sections (blue). (**b**) Freshwater transport (liquid and ice+snow) for each passage.

Another sink for freshwater besides Denmark Strait is the import of salty water that comes from the Iceland-Norway inflow, which provides a clear interdecadal variability and weaker variations on interannual timescales. The long-term variations in the southern salt import effect the Barent Sea transport (red curve) and are exported out of the Nordic Seas, while short-term anomalies seems to remain in the Nordic Seas basin.

In this context, the two freshening events by passage transports in the late 1960ies and mid-70ies (blue curve in Fig.34a) can be explained mainly by ice transport anomalies through Fram Strait (black dotted curve in Fig. 34b) and liquid inflow across the Iceland-Norway section (blue solid line in the same figure): The freshwater input is high in 1968, while the salt import decreases. In the mid 1970ies, Fram Strait FW import is slightly raised but the Iceland-Norway salt inflow is highly reduced and thus the Nordic Seas freshening is strong (black curve in Fig. 35). The very large liquid freshwater export at Denmark Strait 1982 is caused by both, strong sea ice import and the general basin freshening due to reduced salt

imports from south. The rapid reduction of simulated freshwater content after 1982 can be explained by the collapse of sea ice import through Fram Strait and the further decrease by the recreating salt inflow from the Atlantic.

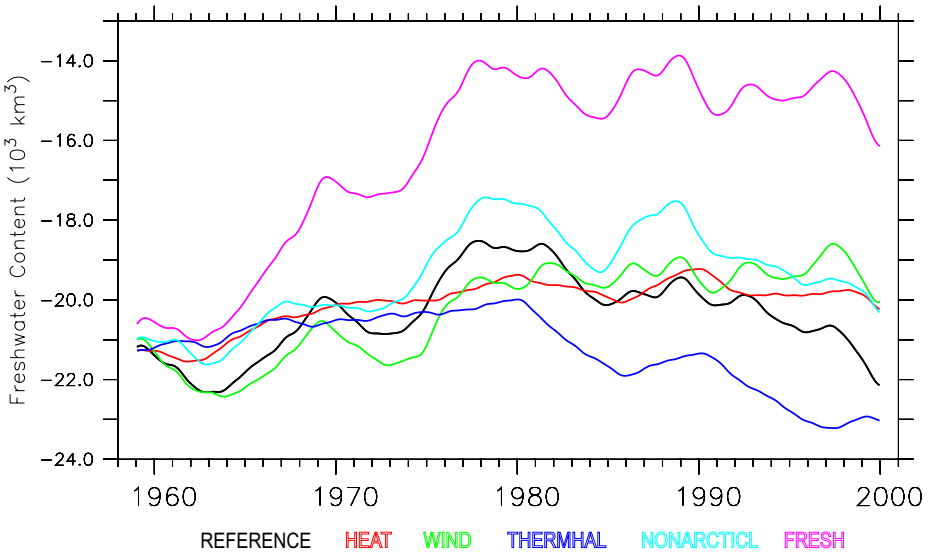

Figure 35 Simulated freshwater content in the Nordic Seas (basin GIN). The negative values results from the choice of the reference salinity S_0, which is lower than the mean salinity in the Nordic Seas. Positive (negative) variations mean freshening (salinification).

4.3.3.2 Arctic on the whole

As shown in section 4.3.2, the mean freshwater input into the north polar region is nearly balanced by the lateral export to the subpolar North Atlantic which is partly accomplished by the salt import. Nonetheless, the variability of these two components on interannual to decadal time scales is completely different. Fluctuations in the lateral transports act on a broad range (Fig. 36a) while the surface fluxes show only little variations (red line in Fig. 36b). The only long-term trend in the surface fluxes can be found in the restoring (blue line) which duplicates throughout the simulation period and indicate a slightly increasing surface salinity.

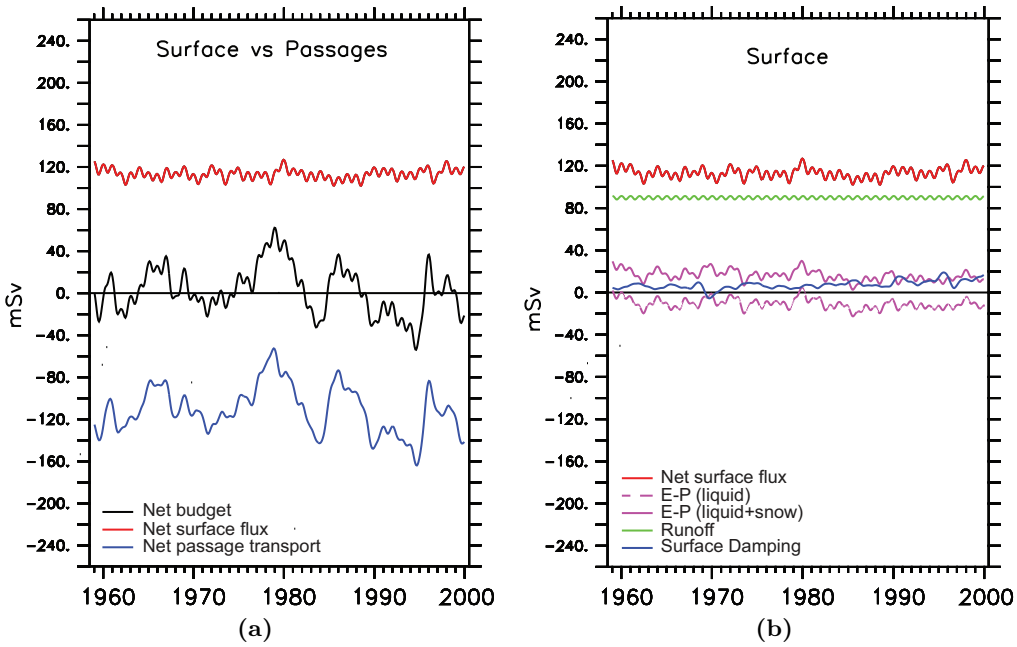

Figure 36 Arctic freshwater budget in REFERENCE: (**a**) surface flux (red), passage net transport (blue), basin net budget (black) (**b**) surface flux details: precipitation/evaporation with and without snow (purple), runoff (green), surface restoring (blue), net surface flux (red).

The net passage exchange variability in the northern basins (blue line in Fig. 36a) can be split into a liquid and a snow/ice portion. Fig. 37a shows that most of the variability is accomplished by the liquid freshwater exchange and less by the sea ice transport.

To identify the main contributions to the oceanic freshwater export variability, the lateral transport is split into its passage components. The liquid freshwater export across the Davis Strait (red) in the east of Greenland is the largest one and it seems to be anti correlated with the Denmark Strait (green) exports. But as it will be shown in the subpolar chapter (5.2.3.3 on page 88), the Davis Strait transport strongly depends on the gyre strength south of the passage and on an baroclinic effect on the strait due to freshwater anomalies in the West Greenland Current (WGC), originating from the Denmark Strait export.

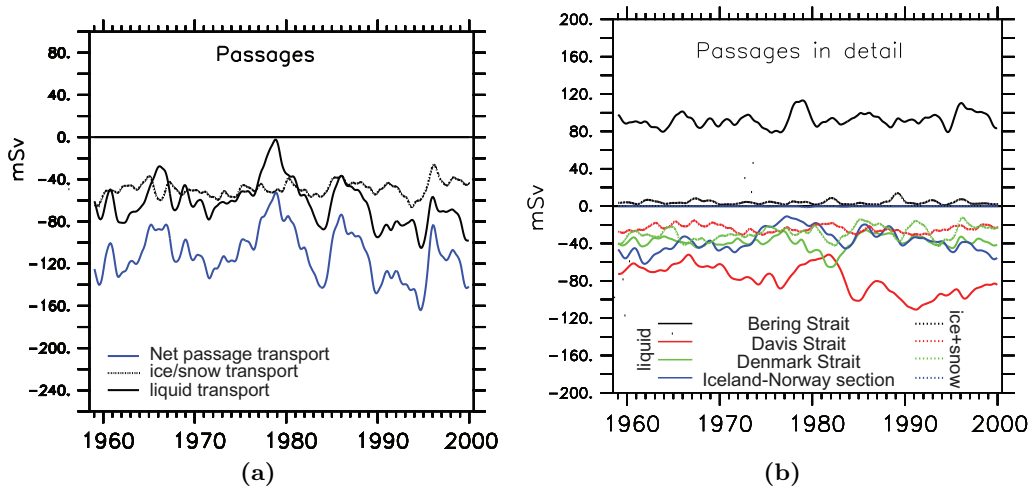

Figure 37 Arctic freshwater budget in REFERENCE: (**a**) Net passage transport across all sections (blue) compared to liquid (black solid) and ice/snow (black dotted) portions. (**b**) Passage transports in detail: liquid freshwater in the ocean (solid line) and freshwater by ice/snow transport (dotted). See labels in figure for colors indicating the section.

As a consequence, the variations in the net freshwater flux (black curve in Fig. 36a), making for the content changes in the north polar basins (Fig. 38) can be explained mainly by the variability of liquid freshwater transports at the southern boundary next to the Atlantic Ocean: The salt transport there decreases during the first half of the 1960ies and again after 1971 until 1974 and increases afterwards. As freshwater export anomalies at Denmark Strait and Davis Strait seems to compensate nearly each other on decadal timescales, the change in salinity import across the Iceland-Norway section can be identified as the main reason for longterm freshwater content changes (Fig. 38), which indicates a freshening until 1982 and a resalinification afterwards.

4.3.4 Sensitivity

To identify the forcing mechanisms that are responsible for the freshwater content variability in the Arctic basins (see Fig. 38), several sensitivity experiments have been analyzed and a budget has been established for each run.

At first it should be noted that all forcings do show a similar behavior in the first 20 years of model integration but a different trend since 1980. While the

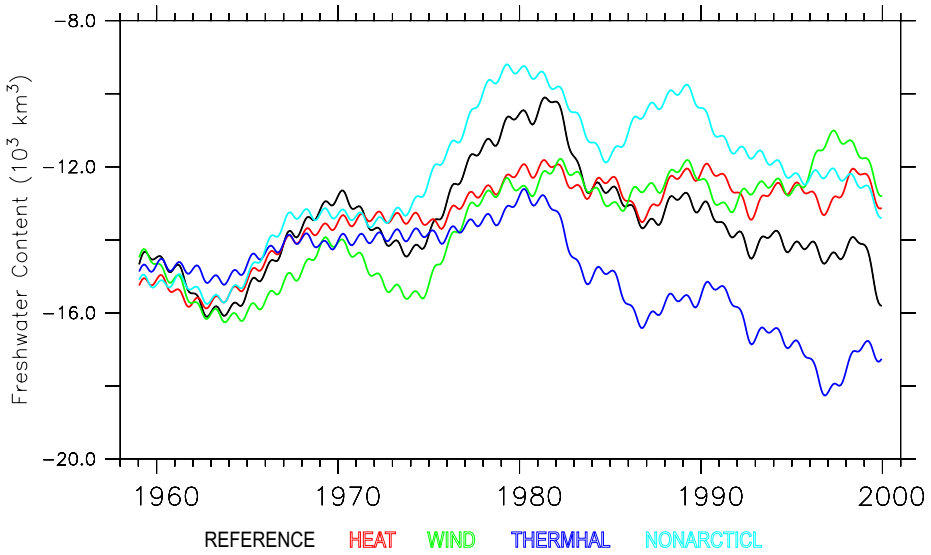

Figure 38 Arctic freshwater content ($10^3 km^3$) in the REFERENCE and the sensitivity experiments.

lowest freshwater content on one hand can be found in the thermohaline forced experiment THERMHAL a strong decreasing trend after 1980 seems to be responsible for a turnaround during that period in both the THERMHAL and the REFERENCE experiment. Contrary, the WIND experiment draws a complete different picture, where the interannual varying wind stress induces a permanent freshening.
The highest fresh water content on the other hand is reached, when there are climatological conditions in the Arctic region and interannual varying surface fluxes in the south (NONARCTIC). In this case, much of the interannual freshwater variability in the Nordic Seas (Fig. 35) can thus be explained rather by signals from the south of the arctic circle than by local processes. Concerning the REFERENCE experiment, the passage exchange at the southern sections in the NONARCTIC-experiment is indeed very similar, as will be shown beneath.

For the Arctic, the surface flux variability is negligible in aspects of freshwater in each experiment (Fig. 39). Therefore, the content variability is triggered by anomalies in the lateral exchange.

The accumulation of freshwater in the north polar basins in HEAT (Fig. 38) can be explained by a consecutive freshwater input (blue curve in the upper right panel of Fig. 39). The largest interannual anomaly in this experiment occurs in the mid-80s in the liquid Davis Strait export (red curve in Fig. 40), while the longterm variation can be traced to the change in salinity inflow at the

Iceland-Norway Passage (blue). All other transports only play a minor role in the temporal evolution of the freshwater budget (black curves in Fig. 39).

When interannual variations in the haline forcing fields are taken into account additionally (THERMHAL), the budget switches to a freshwater loss after 20 years. This is due to an increase of salt inflow through the Iceland-Norway passage and an accretion of the export at Davis Strait. This is consistent with a stronger gyre circulation within the Labrador Sea, as will be shown in the next chapter. The interannual variations, already seen in the HEAT-experiment, are amplified.

In both cases (heat and thermohaline), the ice export variability (Fig. 40, dotted lines) is negligible, as it strongly depends on the wind stress. And thus nearly the same sea ice export variability found in WIND is present in REFERENCE. The liquid Bering Strait inflow is likewise attributed to wind stress variations and the variability is in the same order of magnitude as at Davis or Denmark Strait.

In comparison with REFERENCE, most of the interannual to decadal variability in the passage exchange in Fig. 40 can be explained only by the dynamical effect of the interannual variable wind stress (WIND). And thus it is not surprising that almost the full variability of freshwater content in the Arctic region (Fig. 38) can be found again in the regional sensitivity experiment NONARCTIC, except for the freshening after 1985. This difference can be explained by the missing reduction of the wind-driven sea ice transport through Fram Strait and thus through Denmark Strait in the regional experiment during the late 1980s. Subsequently the Arctic basins are freshening.

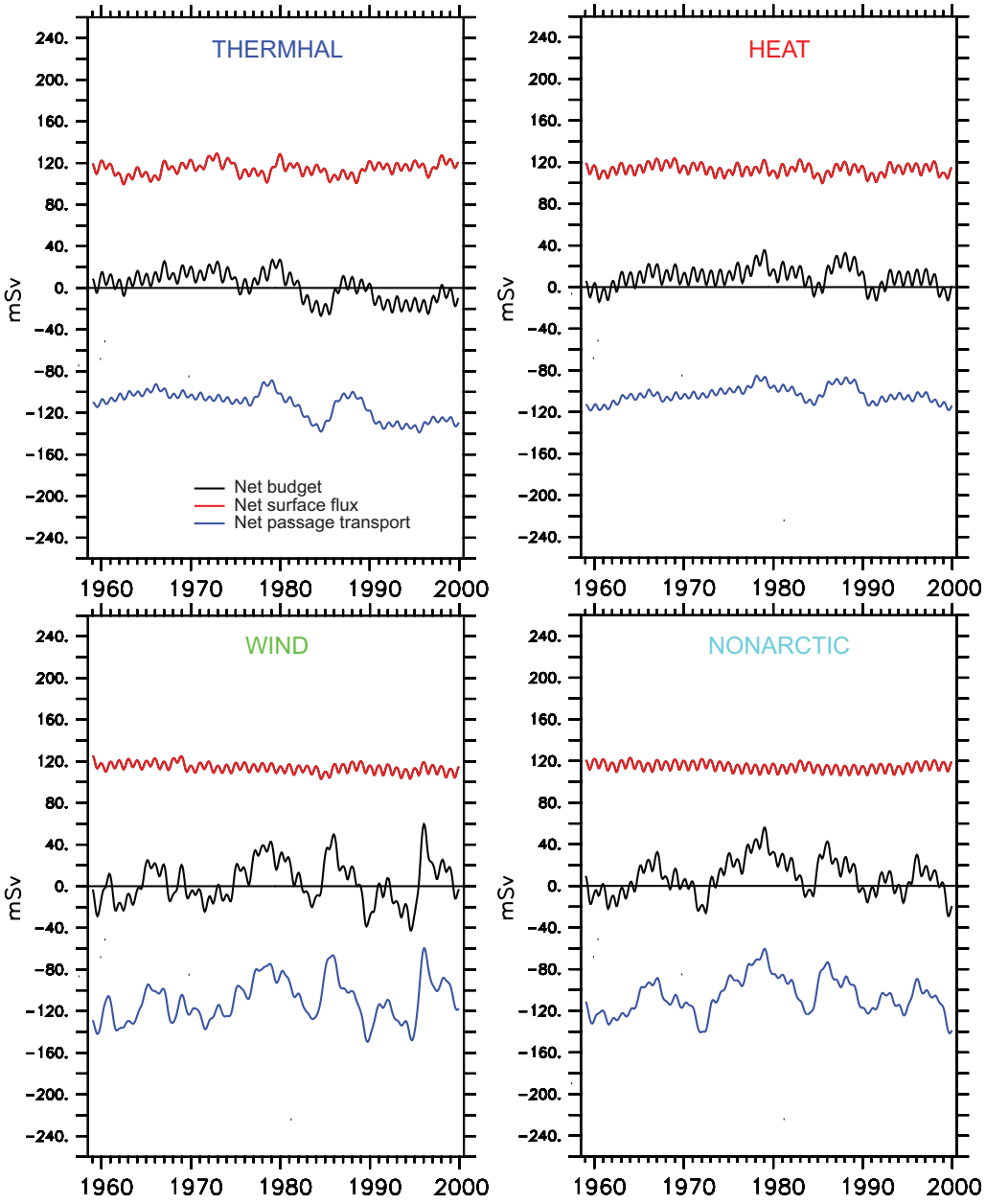

Figure 39 Sensitivity of Arctic freshwater budget: Net freshwater flux (black), surface flux(red) and net passage transports (blue) for the sensitivity experiments (THERMHAL, HEAT, WIND and NONARCTIC).

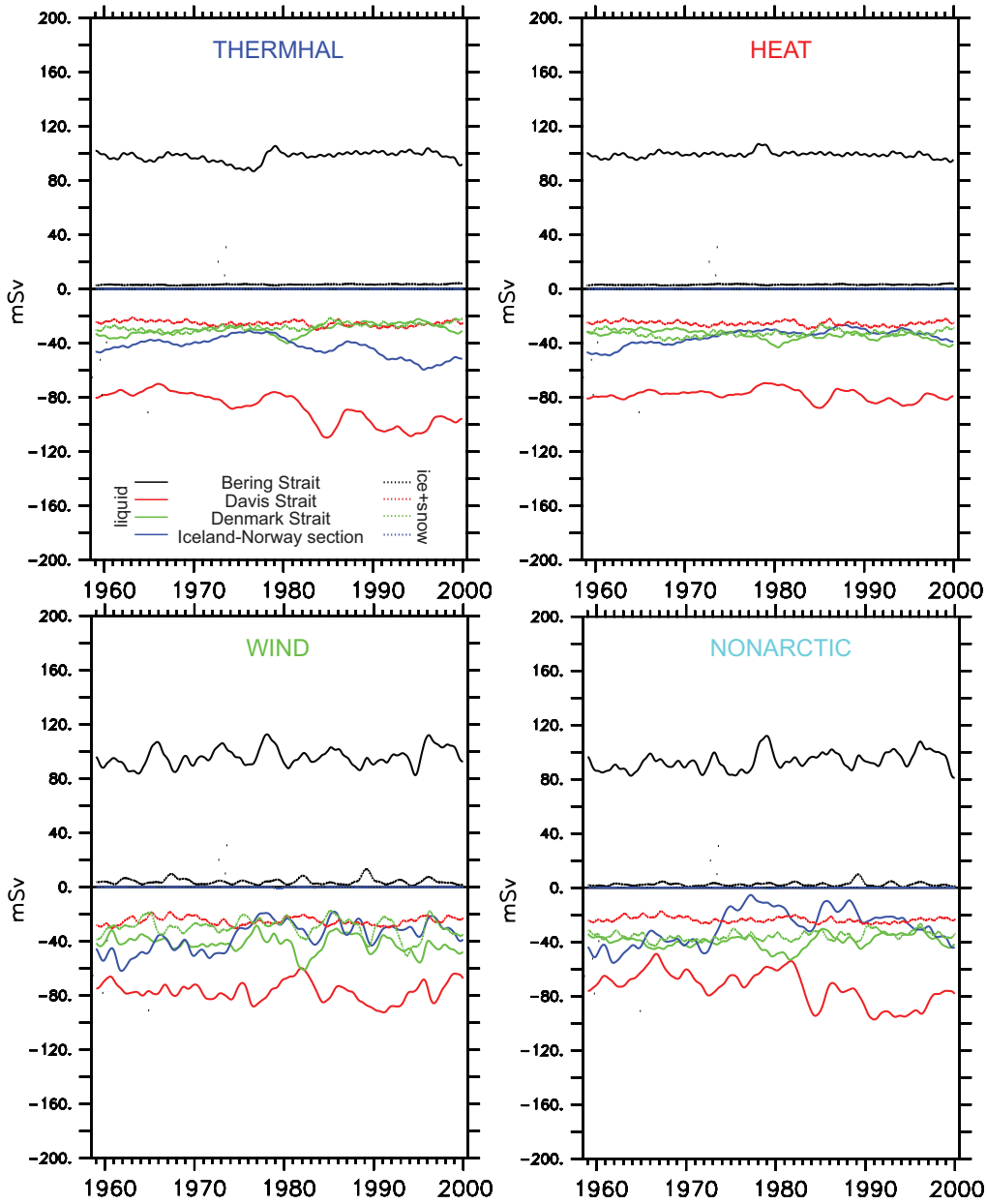

Figure 40 Sensitivity of Arctic passage freshwater transport across sections: liquid freshwater (solid) and ice/snow (dotted) for the sensitivity experiments (THERMHAL, HEAT, WIND and NONARCTIC).

5 Subpolar North Atlantic

The horizontal circulation in the North Atlantic ocean is shaped by the Subpolar Gyre. Besides the dense overflow crossing the sills from the Nordic Seas the deep convection within the cyclonic circulation is the second main source for the North Atlantic Deep Water. Similar to the Arctic, a freshwater budget is conducted for this region and a very similar gyre freshening is found in simulation as it is reported for observational estimates. In contrast to recent discussions, where surface fluxes and arctic freshwater extrusions are held responsible for the freshening, in this study the salt exchange with the subtropics in relation to the NAO is found as explanation. Additionally the deep salinity decrease in the Labrador Sea is shown to be highly correlated with the NAO.

5.1 Geographic and Hydrographic Conditions

The Subpolar North Atlantic (see Fig. 41) comprises the basins north of 47°N and south of the *Davis Strait*, *Denmark Strait* and the *Iceland-Faroe-Scotland Ridges*. The *Mid-Atlantic Ridge* and the *Reykjanes Ridge* separate the *Labrador Sea* and *New Foundland Basin* in the west and the *Irminger Sea* in the northwest from the *Iceland Basin* and the *West-European Basin* in the east.

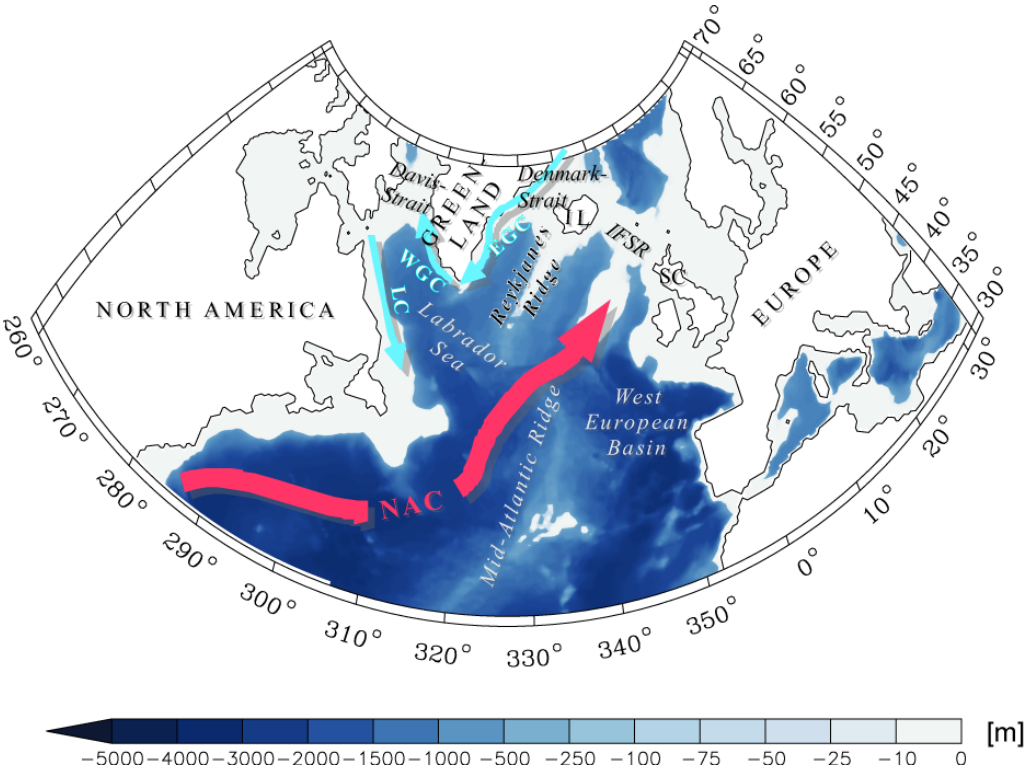

Figure 41 Bathymetry of the Subpolar North Atlantic with some main circulation features (**WGC** West Greenland Current, **EGC** East Greenland Current, **NAC** North Atlantic Current). **IFSR** denotes the Iceland-Faroe-Scotland Ridge.

The horizontal circulation is dominated by the cyclonic *Subpolar Gyre* (c.f. Fig. 42) with the *North Atlantic Current* (NAC) at the south eastern edge, the *East* and *West Greenland Currents* in the north and the *Labrador Current* in the west. The currents that form the gyre are forced by buoyancy contrasts in the ocean and the wind field above. Higher (lower) wind velocities for instant can redound to a stronger (weaker) wind stress curl and thus to intensified (reduced) ocean currents by an input of vorticity.

Subpolar Gyre Strength

The strength of the gyre can be defined as the maximum of the circular transport between the center of the gyre and the boundary and is thus a general expression for the intensity of the circulation velocities. In the model simulation it can be easily diagnosed using the barotropic stream function PSI, which is shown as longterm-mean in Fig. 42.

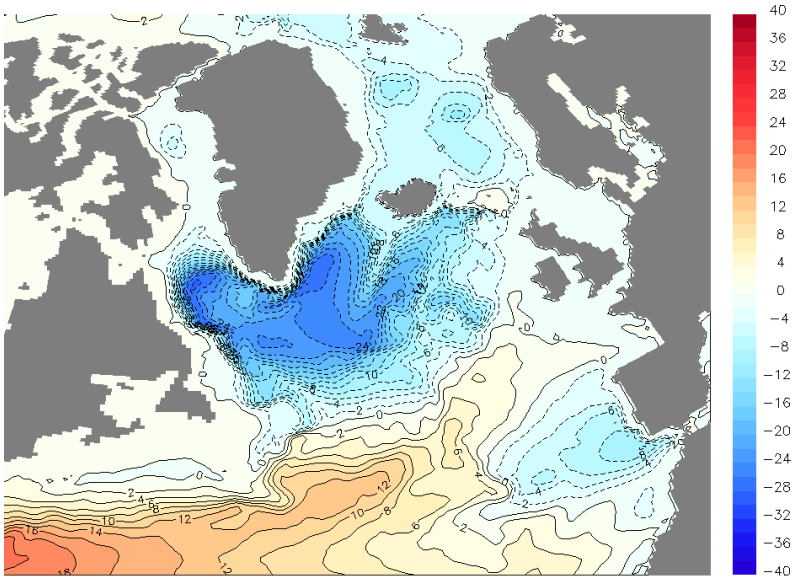

Figure 42 Mean barotropic stream function (Ψ) as filled contour lines (Sv) in experiment REFERENCE. Solid (dashed) contour lines indicate a clockwise (anti-clockwise) circulation.

The maximum cyclonic gyre transport in the central Labrador Sea is about 32 Sv in the simulation. This is at the lower bound of recent estimates for the volume transport range in the Labrador Current of 35-44Sv (Pickart et al., 2002; Dengler et al., 2006) but typical for low-resolution ocean models (Treguier et al., 2005). Several causes have been identified involving the representation of bathymetry, mesoscale eddies and Nordic Seas outflow (See Haine et al. (2008) for a detailed discussion). However, the accurate representation of phase and magnitude of the temporal variability is much more important than the mean transport.

Beside direct measurements of boundary currents, many efforts have been made to observe the variability of the gyre and its volume transport using satellite data.

Analyzing Empirical Orthogonal Functions of the Sea Level Anomaly, Häkkinen and Rhines (2004) defined a Subpolar Gyre index based on the Sea Surface Height (SSH) anomaly. The relation of the SSH index and the gyre transport has been approved for the high-resolution ocean model FLAME by Böning et al. (2006) and is also present in the low-resolution model used in this study (c.f. Fig. 69). Furthermore, they found evidence for a connection between such a SSH-based gyre index and the deep western outflow, which feeds the deeper limb of the meridional overturning cell.

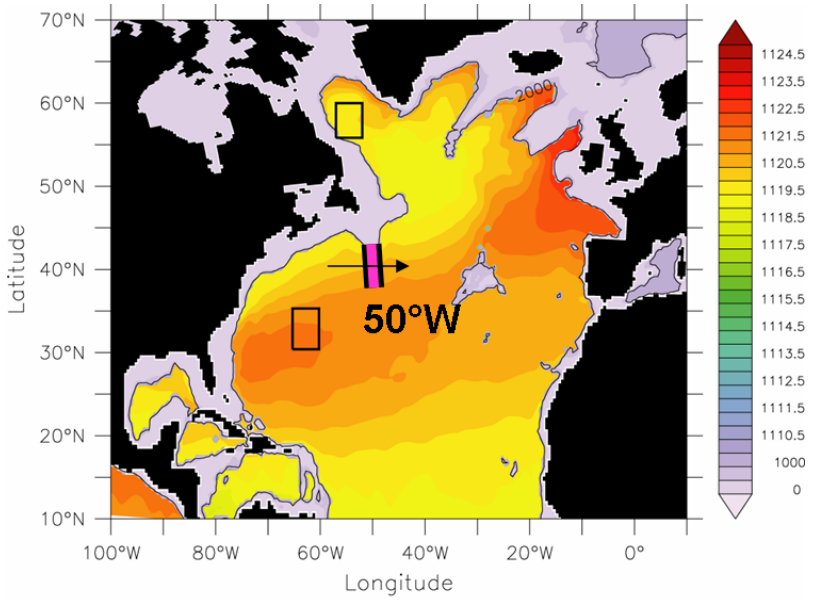

Figure 43 Simulated mean potential energy anomaly following Curry et al. (1998)($10^3 J/m^2$) with the 2000m isobath contoured. The black boxes indicate the areas of average which are taken for constructing the baroclinic transport index using the differences between those areas. The 50°W section is also shown as purple-black line.

Another index describing the subpolar circulation variability has been proposed by Curry and McCartney (2001) who expanded the Subpolar Gyre dynamics to the Subtropical Gyre. Their baroclinic transport index, based on the difference of potential energy anomalies for the upper 2000m and derived from observations in the Labrador Sea and near the Bermuda (see black boxes in Fig. 43) is an expression for the upper volume transport between the SPG and the STG, meaning the North Atlantic Current. The model used in this study simulates this index very well (Fig. 44) which indicates a reasonable representation of the dynamic variability in the North Atlantic. A comparison with the zonal transport across 50°W reveals that this index is capable to represent the volume transport in the NAC.

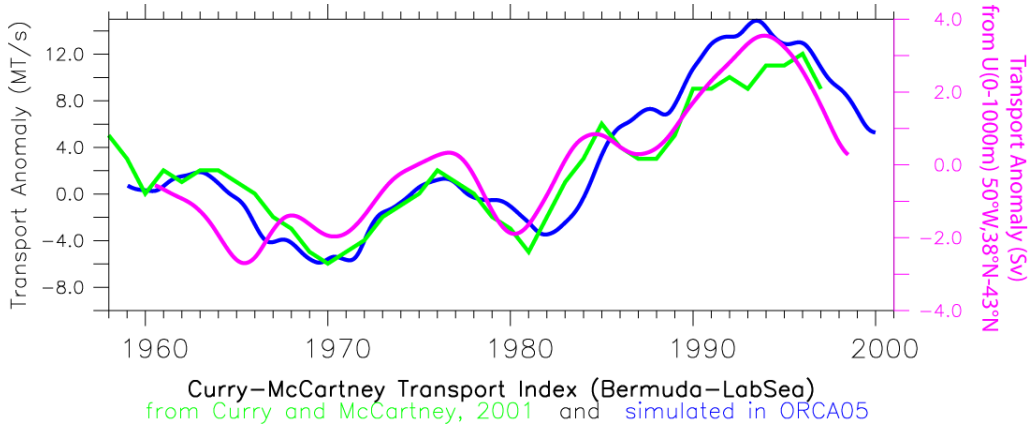

Figure 44 Baroclinic transport index using the transport anomaly ($MT/s \approx Sv$; left axis) as adopted from Curry and McCartney (2001, green curve) and applied to the simulated PEA (blue; c.f. Fig. 43). For comparison reasons also the simulated zonal transport (Sv) across 50°W, comprising the NAC, is shown (purple curve; right axis).

The importance of the Subpolar Gyre circulation does not only arise from the horizontal volume transport but mainly from the residence of the deep convection area within the gyre (see discussion in chapter 6) and its role for the interconnection of the cold and fresh north polar basin with the warm and salty subtropical waters in the south east. This is illustrated by the mean Sea Surface Temperature (SST) and the Sea Surface Salinity (SSS) in figure 45 which show northwestward gradients in the scope of the NAC and, in principle, meridional gradients farther east.

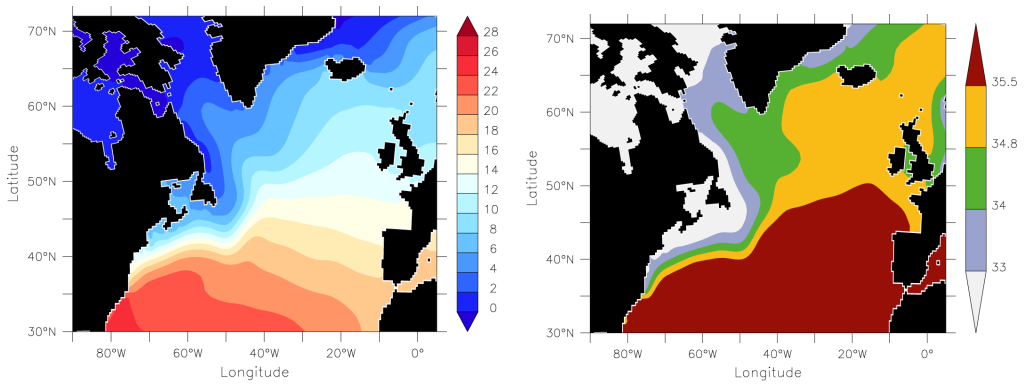

(a) **(b)**

Figure 45 Maps of the (**a**) mean sea surface temperature (°C) and (**b**) sea surface salinity in the subpolar and subtropical region from Levitus Climatology (Antonov et al. (1998); Boyer et al. (1998)).

5.2 Freshwater Budget

5.2.1 Basins and Sections

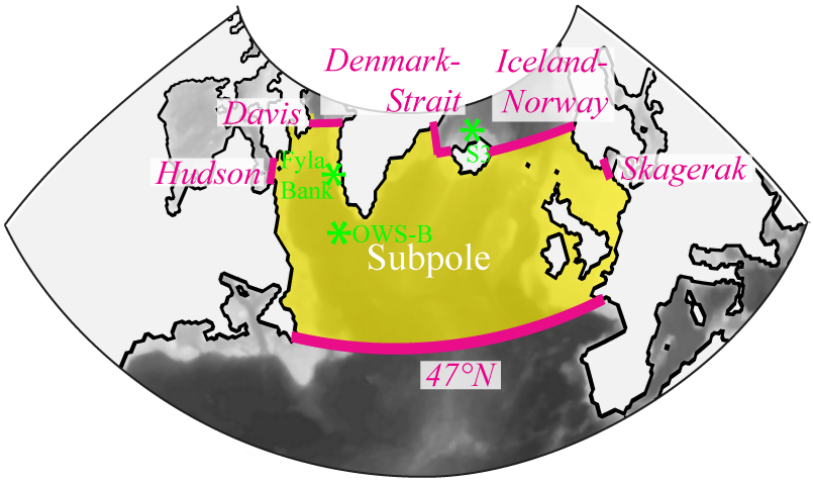

Figure 46 Subpolar basin with sections (purple lines) as used for the budget. Green stars indicate specific locations: S-3 in the Iceland Basin, Fyla Bank (FB) near the West Greenland Current and Ocean Weather Ship Bravo (OWS-B) in the central Labrador Sea.

The subpolar basin (see Fig. 46) encloses the basins between northern North America in the west, Europe in the East, the sills and ridges in the north (*Hudson, Davis, Denmark Strait, Iceland-Norway and Skagerrak*) and a zonal section in the south ($47°N$). Similar to the Arctic freshwater budget, fluxes and transports are defined as positive into the basin.

5.2.2 Mean Budget

The subpolar basin (Fig. 47) is supplied with freshwater from the north through Davis Strait ($103mSv$[1]), Denmark Strait ($67mSv$) and the Iceland-Norway section ($38mSv$), whereas the latter exports water with a higher mean salinity than the salinity of reference S_0 and thus appears as freshwater source for the subpolar basin. Thus, the northern sections provide a net freshwater input of $208mSv$. In contact with the Baltic Sea, the Skagerrak passage provides an additional freshwater source ($5mSv$), approximately three times less than the Hudson Passage

[1]Numbers for Arctic sections are taken from section 4.3.2 on page 63.

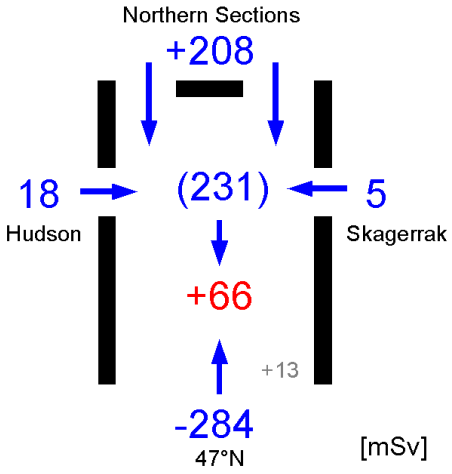

Figure 47 Schematic mean subpolar freshwater budget in experiment REFERENCE:. Blue numbers indicate lateral freshwater transport (liquid+ice/snow) and red for the net surface flux. Arrows are orientated positive into the basin (source).

($18mSv$) next to the Hudson Bay in the West.
At the southern section, the subpolar gyre looses a large amount of freshwater (-284.06 mSv) mainly due to the northward flow of saline water with the NAC..

The mean budget over 43 years then results in a freshwater content of about $108 \times 10^3 km^3$ and an imbalance of $13mSv$ which depends strongly on the period of averaging because the inter- and multi-decadal variability in the southern freshwater transport is very large.

5.2.3 Temporal Variability

5.2.3.1 Freshwater content change

Curry and Mauritzen (2005) as well as Peterson et al. (2006) combined hydrographic observations with ECMWF Reanalysis data (ERA40; Uppala et al. (2005)) to get a freshwater balance for the subpolar basin. They found a significant freshening from 1975 until 1990 with some indication of a reversal in the 1990ies. Remarkably, this is consistent with the freshening and resalinification on interdecadal timescales found in the simulation. The upper panel of figure 48 illustrates the good agreement of these two time series. The black curve shows the freshwater content varying with time in simulation, while the green curve with stars denote the observational estimates for each fifth year[2].

[2]The larger differences during the first 10 years of model integration may be a spin-up effect as the interannual experiments are restarted from 50year runs using climatological forcing fields.

The simulated freshwater content change is caused by freshwater flux anomalies which are shown in the lower panel as temporal derivative of the content change $\partial FWC/\partial t$ (grey curve). Positive flux anomalies (blue shade periods) make for an increase of subpolar freshwater content while negative anomalies (yellow shaded) make for a resalinification. This net flux anomaly shall be equal by definition to the sum of all transport anomalies crossing the sections as well as the net surface flux anomalies. Those are also shown in figure 48 for the surface (red), the net transport from north (green) and from the south (blue).

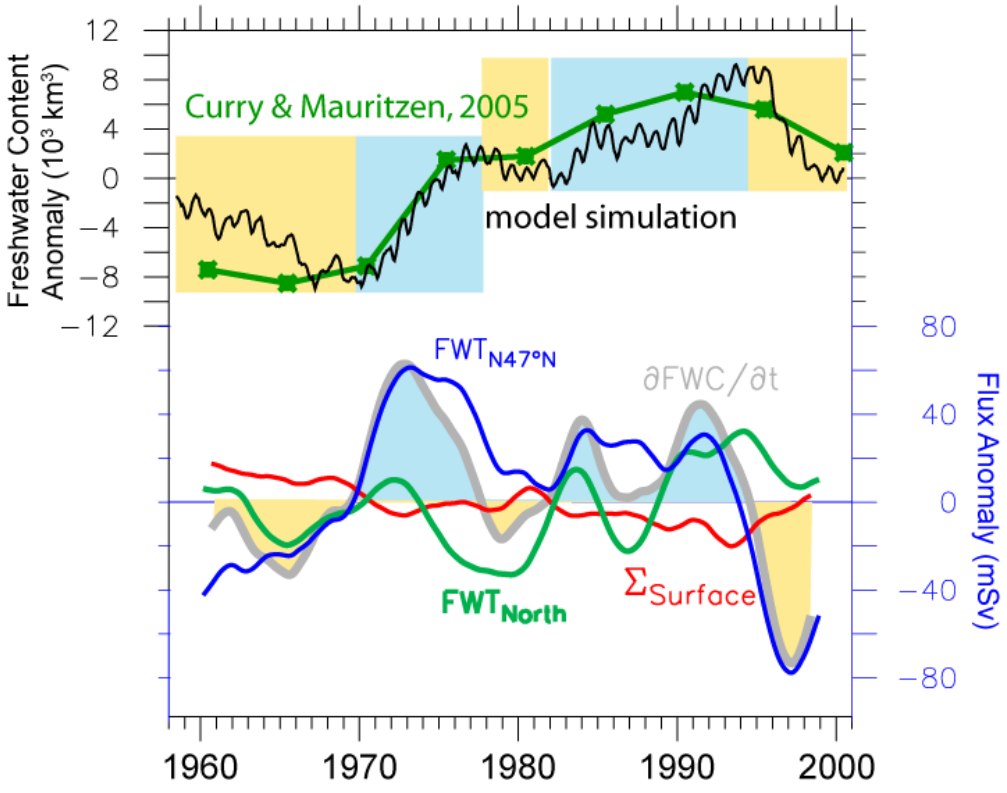

Figure 48 **Upper**: Time series of freshwater content anomalies from observation (green) conducted by Curry and Mauritzen (2005) for 5 year intervals and from simulation (black, smoothed by a running 25 month Hanning filter). **Lower**: freshwater flux anomalies from simulation: temporal derivative of freshwater content anomaly from the black curve above (lower grey), net freshwater transport from north (green) and south (blue), net surface flux (red). Time series are smoothed using a running 5 year Hanning box filter. Phases of freshening and salinification are shaded with blue and yellow respectively. Transports are supposed to be positive into the basin.

The surface flux variability is very small compared to the other components and exhibits a negative trend between the early 1960s and early 90s. But it only explains less than 1% of the net flux variability (c.f. Tab. 3).

Budget component	Explained variability
Net Surface Flux	<1%
Northern Sections	17%
Southern Sections	67%
SUM	100%
Residuum	>15%

Table 3 Uniquely explained variability of the freshwater content change using semi-partial correlations from a multiple regression analysis for the net flux anomaly and its three components from Fig. 48. SUM represents the algebraic sum of the lateral net transport and the net surface flux.

The net freshwater transport from the north provides a somewhat larger variability with a freshening during the late 60s and early 70s, the 80s again and finally since 1990 until the end of simulation. There seems to be also a trend of the same order of magnitude as in the surface flux but with the opposite sign. However, the freshwater anomaly originating from the Arctic explains only 17% of the whole freshwater content variability. And though it causes the freshening in the early 80s and solely around 1990 it is insufficient concerning the large freshening in the 70s.

The largest variability, especially on decadal and multi-decadal timescales, is caused by the freshwater exchange at the southern section, which explains 67% of the subpolar freshwater content variability. In the simulation it makes clearly for the intense freshening in the 70s and the resalinification in the 90s.

Since the sum of all three components (North+South+Surface) result in 100% of the explained subpolar content change anomaly, the remaining 15% can be related to joined effects, i.e. signals which are transferred quickly from one section (or the surface) to another section.

This is a surprising result, eminently since Curry and Mauritzen (2005); Peterson et al. (2006) made large efforts to explain the change of the subpolar freshwater content with strong surface flux anomalies and freshwater intrusions from the Arctic.

5.2.3.2 Surface fluxes

Some studies suggest a significant contribution to the subpolar freshwater content changes by net surface flux anomalies meaning precipitation minus evaporation (P-E), especially for the period 1970-1975 (Josey and Marsh, 2005; Boyer et al., 2007). Figure 49 shows a comparison of subpolar freshwater content changes based on World Ocean Data (e.g. Conkright et al., 2002) with surface net fluxes from NCEP/NCAR reanalysis (Kalnay et al., 1996). Boyer et al. (2007) inferred from a similar comparison the increase in the surface fluxes during the 1970s must have contributed significantly to the ocean freshening between 1968 and the late 70s. Although this P-E signal is also present in a second reanalysis product (ERA40; Uppala et al., 2005) as it is shown in figure 50 it does not appear in the model simulation in this study (labeled with CORE in the same figure). As it has been already discussed in section 2.3.1.1 there is an essential difference in the CORE forcing data and the reanalysis output: Any interannual variability before 1978 is neglected in the forcing due to uncertainties in the pre-satellite era as the authors of the reanalysis products, especially for NCEP/NCAR, advise caution with this period and recommend to validate precipitation anomalies by comparison with observations (Kalnay et al., 1996).

To verify if the model lacks an important signal rain gauge records from stations along the east coast of Canada provided by Environment Canada (2008), has been analyzed (51). Neither a single station nor the averaged time series (purple line) provide a anomalous drought in the 60s or a wet spell in the 70s. But there is a general good agreement between the averaged rain gauge records (Fig. Fig. 51) and all three precipitation products (NCEP/NCAR, ERA40 and CORE in Fig. 50) for the satellite era. Furthermore, COADS ship weather observations do not indicate a significant change of the precipitation during that time (K. Bumke, pers comm.). For the eastern North Atlantic a similar picture is drawn by Hoppe and Kiely (1999) for rain observations along the west coast of Ireland, who have not found any indications for an extraordinary increase in P throughout the 1970s.

However, the negligence of the supposed 70's surface signal in the model forcing data has no effect on the simulated freshwater content change. since the increase in subpolar freshwater content during the 70s is even so very close to the observational estimates by Curry and Mauritzen (2005).

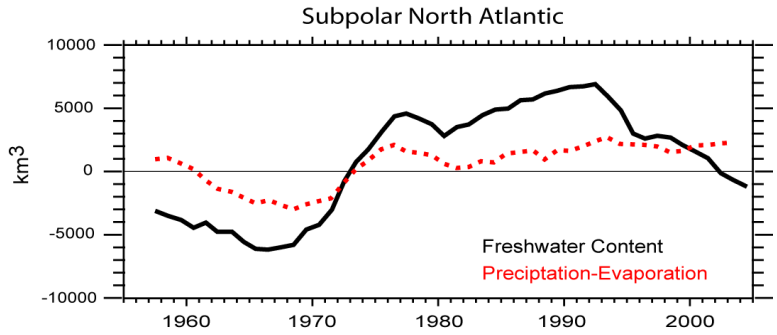

Figure 49 Subpolar freshwater content anomaly from Boyer et al. (2007) compared to the integrated surface net flux (red; precipitation minus evaporation from NCEP/NCAR reanalysis data).

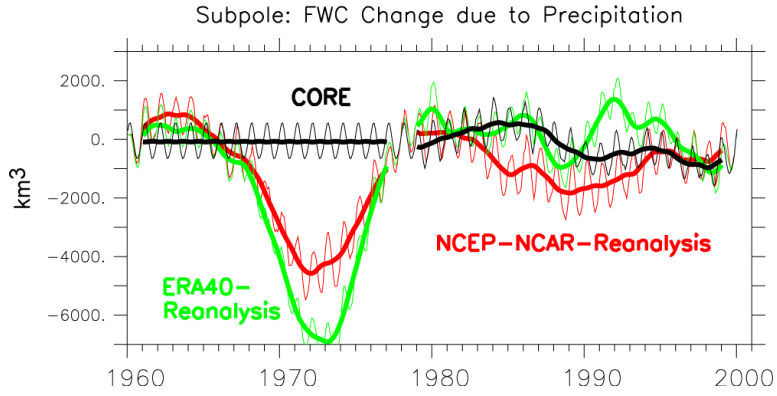

Figure 50 Anomalies of the integrated surface net flux over the subpolar basin based on different datasets (NCEP/NCAR: red; ERA40: green; CORE: black). Positive values denote a freshwater input into the ocean.

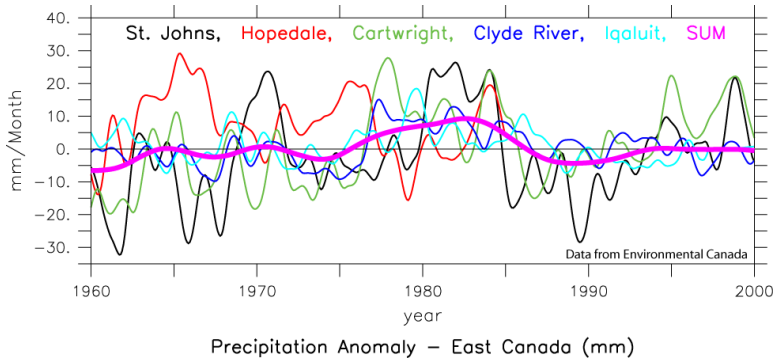

Figure 51 Time series of monthly rain gauge observations along the east coast of Canada (going from south to north: St. Johns, Hopedale, Cartwright, Clyde River and Iqaluit). The annual mean of all these stations i shown as thick magenta line (SUM).

5.2.3.3 Northern Sections

While the mean freshwater export through Davis Strait is similar to the observations, there are some differences on the eastern side of Greenland at the southern exit of the Nordic Seas, as already discussed for the Arctic freshwater budget. However, it has to be pointed out that the simulated Arctic freshwater export through the Fram Strait and the Canadian Archipelago of $5783 \pm 662\,km^3/yr$ is close to the assumed export of $\approx 5000\,km^3/yr$ originating from Aargaard and Carmack (1989) which has been also used in the study by Curry and Mauritzen, 2005 for their freshwater budget. Moreover, the main focus of this study is on the freshwater variability and thus the differences in the mean transports only play a minor part.

Davis Strait The freshwater transport across Davis Strait depends on one hand on the freshwater content in the Baffin Bay, which is supplied with freshwater coming through the Canadian Archipelago and with water of varying salinity from the West Greenland Current (Fig. 52b). On the other hand it depends on the strength of the Subpolar Gyre in the Labrador Sea (Fig. 52a): the stronger the gyre, the higher the (southward) transport. Besides the barotropic transport, the variations of the density gradient on the Davis Strait additionally implies a baroclinic velocity, causing larger (lesser) exports out of the Baffin Bay due to a

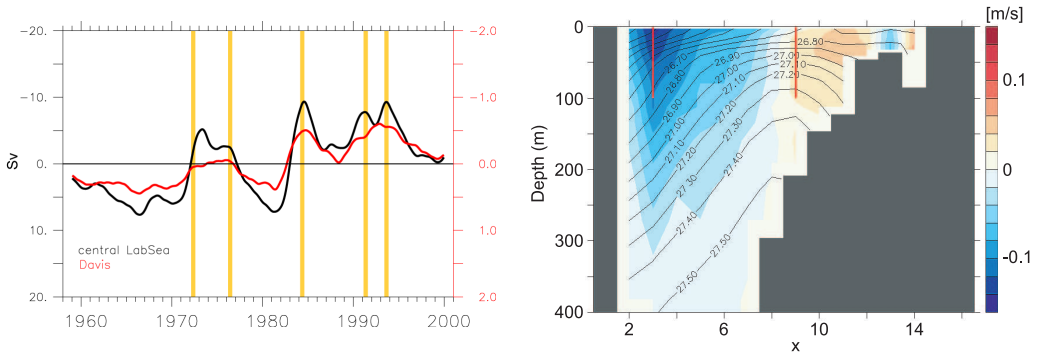

(a) (b)

Figure 52 Davis Strait in experiment THERMHAL(where local wind effects are excluded and thus reactions on remote changes in the Subpolar Gyre can be isolated. (**a**) Barotropic transport anomaly in the Labrador Sea (black; left axis) and at Davis Strait (red; right axis). Yellow lines mark years of increased salt import in the east. (**b**) Meridional mean velocity (shaded; positive velocities into the north; m/s.) and density $\sigma_0(kg/m^3)$ overlaid.

freshening (salinification) of the outflow or an increase (decrease) of salinity in the inflow (Fig. 53). Since the latter is connected to the Denmark Strait by the East and West Greenland Currents, this can also explain the moderate anti-correlation between the freshwater transports at these two passages (c.f. Fig. 37b). Overall, the Baffin Bay acts in this model study mainly as buffer for subpolar water masses.additionally modify the volume and thus the freshwater transport.

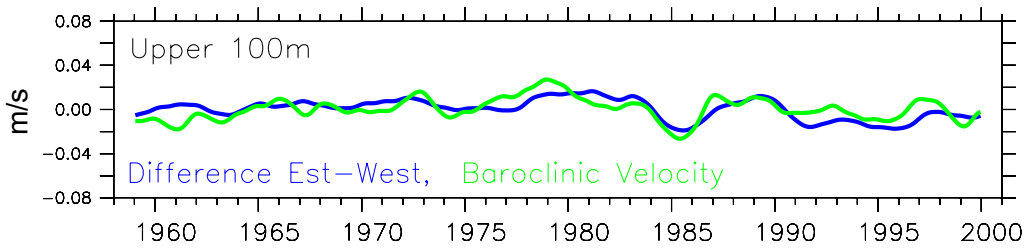

Figure 53 Difference of the meridional velocities (blue) at Davis Strait between the eastern inflow and western outflow in THERMHAL (locations are indicated by red lines in Fig. 52b) compared to the baroclinic induced velocity (green) in-between.

Great Salinity Anomalies A rapid freshening of the upper layer was observed in the arctic and subpolar region in the late 1960ies and throughout the 70ies, which is called the 'Great Salinity Anomaly' (GSA70) following Dickson et al. (1988). There have been a lot of reports on what the source was and how the anomaly was spreading (see the introduction for an overview). Since the 70s, there have been two other freshening events, called GSA80 and GSA90, as discussed by Belkin et al. (1998); Malmberg and Désert (1999); Blindheim et al. (2000); Belkin (2004).

For the first event (GSA70), the source was supposed to be located in the Fram Strait (Dickson et al., 1988; Aargaard and Carmack, 1989): In the late 1960ies there was an anomalous high export of sea ice from the Arctic, which raised the freshwater content in the upper layer of the Nordic Seas ($+2000\,km^3$ from observations; Dickson et al., 1988). This can be retrieved in the REFERENCE-run: From 1964 until 1968 the Fram Strait ice export increases and in 1969 is decreases abruptly (shown as equivalent freshwater flux in Fig. 54; blue solid curve) resulting in an freshwater surplus of $+2290\,km^3$ which is close to the observation.

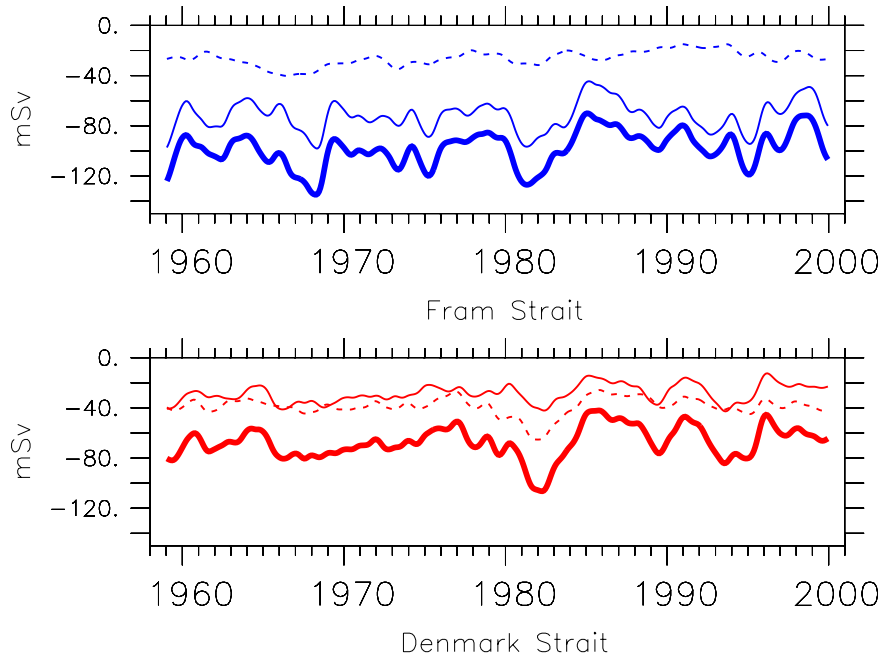

Figure 54 Simulation REFERENCE: Freshwater transport across Fram Strait (upper panel) and Denmark Strait (lower panel) for sea ice and snow (thin solid lines), liquid freshwater (dotted lines) and net transport (thick solid lines).

In the south of the Nordic Seas a freshening was then observed north of Iceland at station 'S-3' (green star in Fig. 46) as presented by Malmberg and Désert (1999). They found a significant jump in the mean states of temperature (≈ -2.5°C) and salinity (≈ -0.4) records before and after 1968 which is simulated very close to the observations (Fig. 55).

At Denmark Strait Aargaard and Carmack (1989) assumed, based on a model study investigating the mean ice balance, that most of the sea ice excess from the Fram Strait has been melt within the Nordic Seas resulting in an increase of freshwater in the East Greenland Current and thus expected to find the freshening signal further downstream following the advective hypothesis by Dickson et al. (1988). And effectively, in the West Greenland Current a shift in the salinity and temperature was found near station Fyla Bank one year later (Dickson et al., 1988; Ribergaard, 2004).

Though a similar freshening and cooling at Fyla Bank appears also in the simulation output (see Fig. 56), a clear advective signal cannot be found here because

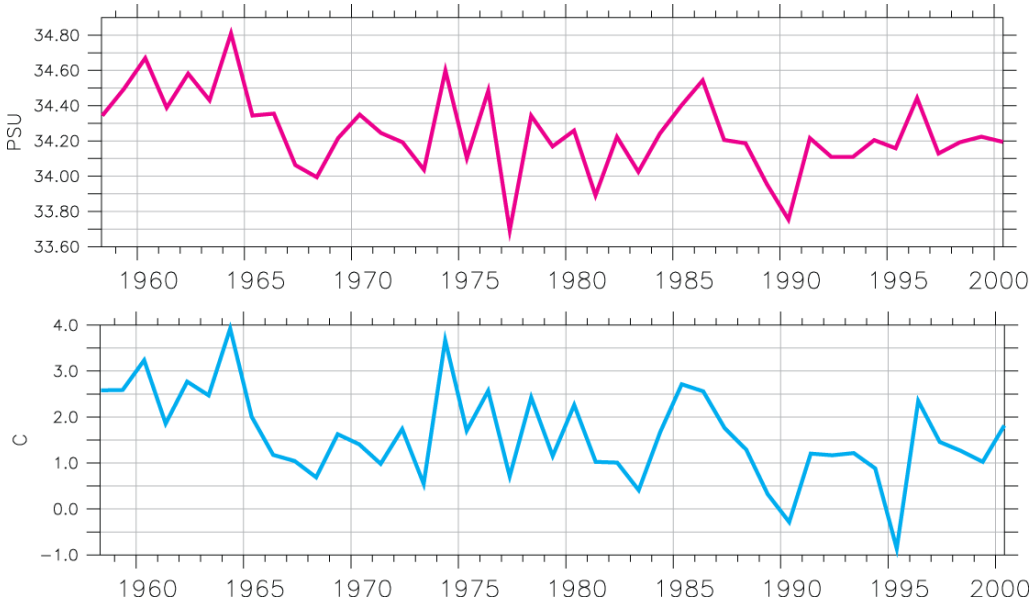

Figure 55 Time series of simulated near-surface salinity (upper panel) and temperature (in °C; lower panel) in experiment REFERENCE at station S-3 north of Iceland (see Fig. 46) according to Malmberg et al. (2001).

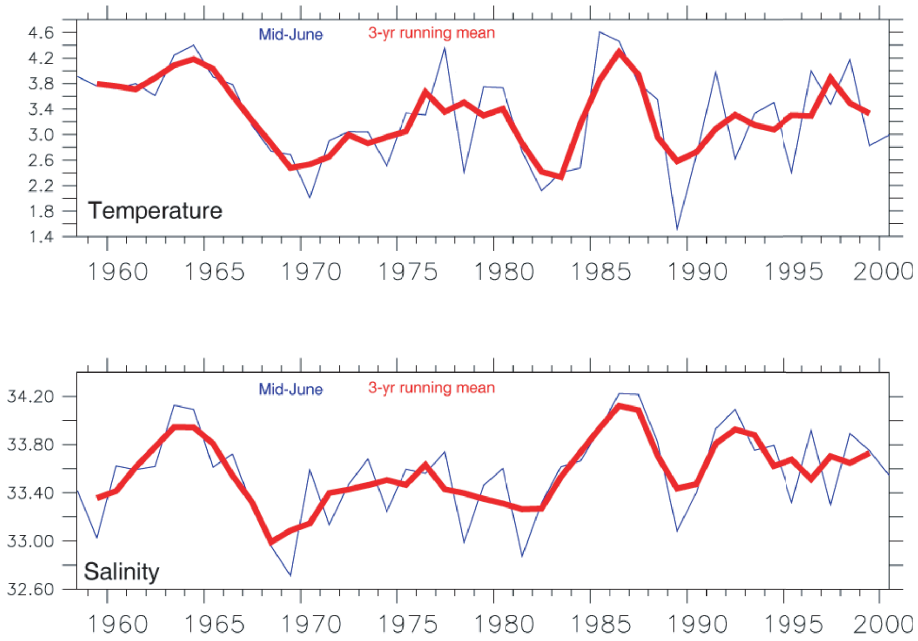

Figure 56 Time series of simulated (REFERENCE) upper layer temperature (°C, upper panel) and salinity (lower panel) during June (thin lines) in the northeast Labrador Sea near Fylla Bank (see Fig. 46) according to Ribergaard (2004). A running 3-year mean is shown additionally as thick red line.

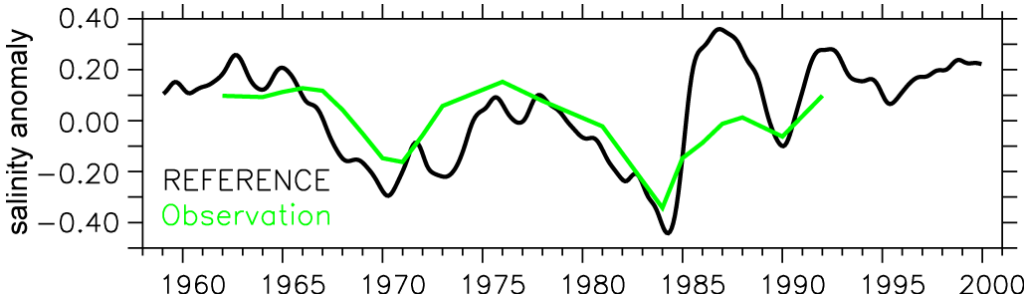

Figure 57 Central Labrador Sea: SSS anomaly in REFERENCE experiment and Observations (adapted from Lazier (1995); Belkin et al. (1998))

only a small part of the freshwater signal from the Fram Strait can pass the Denmark Strait where the liquid and sea ice freshwater transport (thin red curves) intensifies immediately in 1966 but only for one year ere it reduces slowly thereafter. This implies the possible existence of further freshening events similar to the traditional view on GSAs (c.f. Sundby and Drinkwater (2007)) but originating from the south which may have even a larger amplitude and thus a stronger impact on the subpolar upper layer salinity.

Subsequently, the freshening signal then has been recognized in the central Labrador Sea in the early 1970s where it has been under suspicion to have weakened the winterly Deep Convection (Lazier, 1980). Figure 57 shows the time series (green curve) of upper surface salinity (0-250m) in the central Labrador Sea (Ocean Weather Ship Bravo; OWS Bravo) according to Lazier (1995); Belkin et al. (1998). The simulation (black curve) provides a somewhat larger variability, especially in the late 1980s and early 1990s. But this might be an effect of the under-representation of mesoscale eddies which are capable to transport freshwater from the boundary currents into the interior, especially during phases of high level eddy kinetic energy (EKE) as discussed by Brandt et al. (2004)

The GSA70 then could be tracked further down stream to Flemish Cap where it was deflected towards the east. Though Dickson et al. (1988) proposed the arrival of the signal in the eastern basin in 1975 and back in the Nordic Seas during the early 1980ies, there is no incontrovertible evidence for this in observation. Even in the simulation it is nearly impossible to detect the GSA signal further on, since freshwater disturbances from the south can be larger:
Fig. 58 shows the change of the upper layer salinity content since 1968. In the upper left panel, the change of salinity content is shown for winter/spring 1970. The GSA70 signal is clearly located in the northern Labrador Sea (red circle), while also the Baffin Bay has freshened due to the low saline inflow through

Davis Strait. Afterwards, it spreads southward during 1971 and arrives off the coast, east of Flemish Cap in 1973. During that period, another freshwater signal, originating from the south has appeared in the NAC region (blue circle). Until 1975 the latter salinity anomaly has entered partly the Nordic Seas while the rest remains south of Iceland where it is merged together with the GSA70 signal.

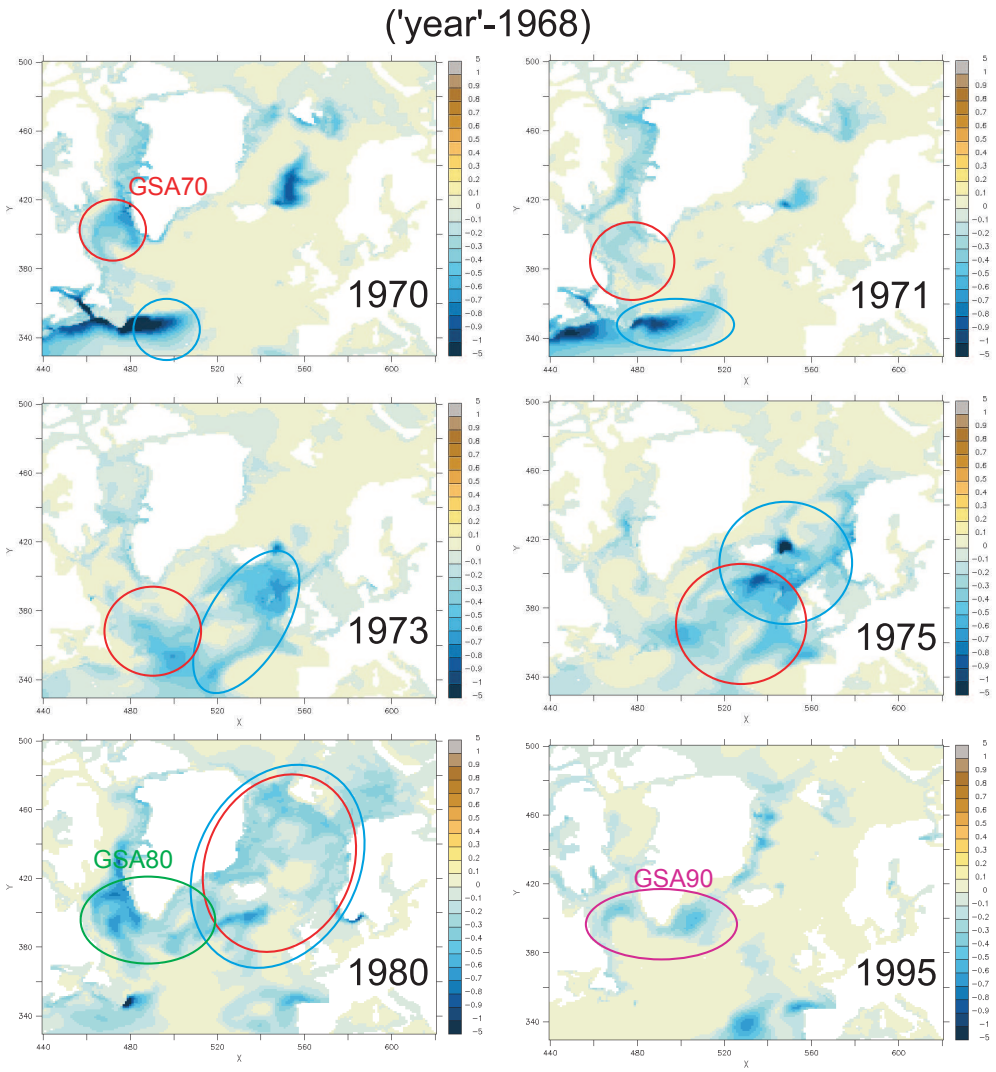

Figure 58 Difference of vertically integrated salinity content per model grid box (m) in the upper 500m between 1968 and several subsequent years (shown on the model grid). Blue (yellow) areas denote an increase (a reduction) of freshwater content. Colored circles indicate the loction of different freshening signals and their propagation throughout the years. The Great Salinity Anomalies (GSA) in the 70s (red circle), 80s (green) and 90s (purple) are labeled additionally.

The second GSA during the 1980s is assumed to be generated locally in the Labrador Sea (Belkin et al., 1998) or is advected there from the Davis Strait (Houghton and Visbeck, 2002). In the model simulation three different sources can be identified: First, the sea ice export through Fram Strait has increased with the beginning of the 1980s (c.f. section 4.2.3). Second, with the strengthened SPG during a fairly positive NAO phase, recirculating freshwater from the former GSA event reenters the Labrador Sea. Third, an extraordinary lack of salt import from the Atlantic resulting in a freshening signal, entrains into the upper layer and freshens further the Subpolar Gyre and the Nordic Seas. As a consequence the liquid freshwater transport at Denmark Strait increases and appears as the largest freshwater signal during the simulated period (Fig. 54).

The GSA90 signal is supposed to be released by a large amount of liquid freshwater imported from the Arctic at Fram Strait (Belkin, 2004). This cannot be supported by the model results in this study here, where the liquid freshwater transport across Fram Strait is the lowest throughout the simulation. However, the ice export at Fram is large again in 1995 and increases the ice (c.f. section 4.2.3) and liquid freshwater export at Denmark Strait superimposed by the water masses entrained in the Nordic Sea.

Summing up the GSAs, this model seems to simulate the observed indicators of a basin-wide freshening which occurs periodically in the subpolar North Atlantic. These have been commonly associated hitherto with freshwater intrusions originating from the Arctic region. Although, there are freshwater surges from the Arctic due to increased ice exports and liquid ocean transports, this simulation does not support the hypothesis of a purely advective signal coming from north but rather suggests a signal that propagates somewhere from the south affecting then the Nordic Seas and accordingly recirculates within the Subpolar Gyre.

5.2.3.4 Southern Section

The upper 700m in the western part of the zonal section at 47°N (Fig. 59) is dominated by lower salinities, the eastern part provides high salinities in the upper 1000m descending eastwards down to 2000m, affected by a generally northward transport with a thin layer of southward flowing fresher waters atop. The NAC with its core of high velocities towards the north connects these two salinity regimes.

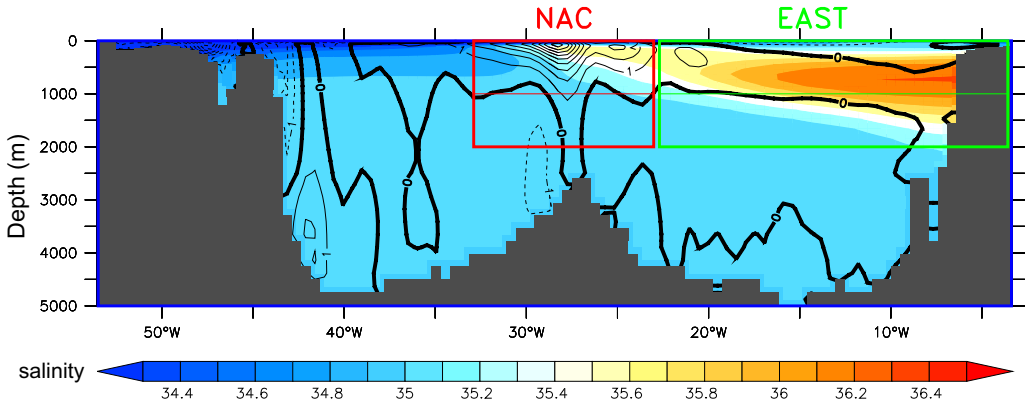

Figure 59 Section at 47°N: long-term mean salinity over depth (m; left axis) with averaged meridional velocity as overlaid contour lines (solid lines indicate a positive velocity towards the north).

To isolate the mechanisms that are responsible for the variations in the freshwater transport the section is first divided vertically into a surface and a mid-depth branch. As shown in Fig. 60 (the time series is 2-yr Hanning filtered to obtain interannual rather than seasonal variability), the zonally averaged northward transport is strong in the upper 1000 meters (negative values for northward salt-transport) and amounts twice ($40000m^3/s = 40mSv$) the southward flow (max $22mSv$), which has its largest deflection at about 1700m (positive values towards the south are caused by a mean salinity in this depth higher than the reference salinity S_0 and negative mean meridional velocities).

The vertically integrated southward transport anomaly in the deep (green curve in Fig. 61) then results in an ascent during the second half of the 1970ies, a rapid descent 1984-1986 and again an ascent in the late 80ies. There is no significant

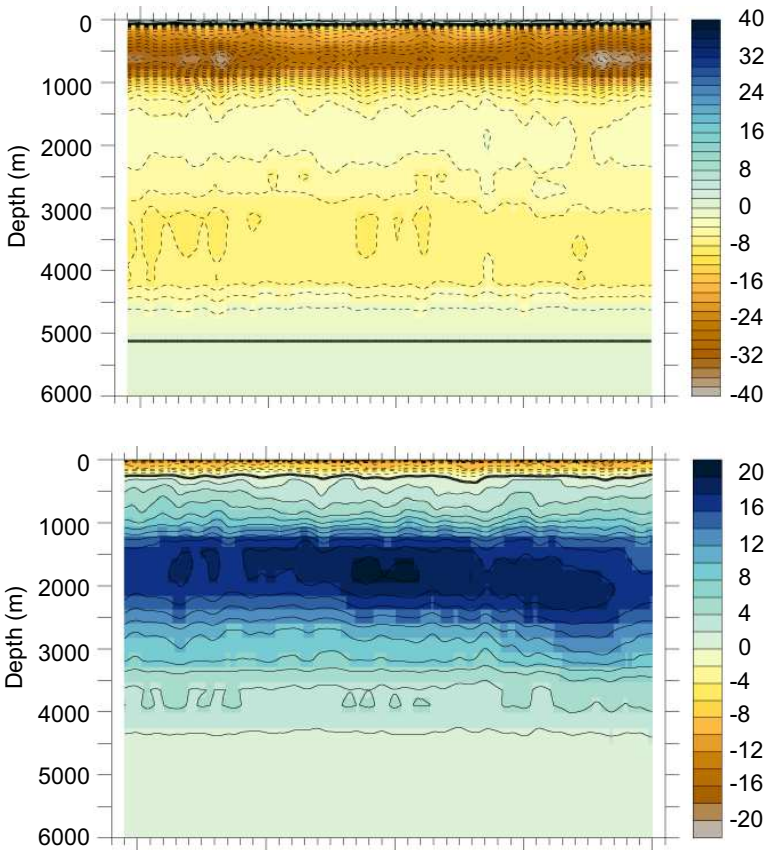

Figure 60 Hovmøller diagrams of meridional freshwater transport (in $mSv = 10^3 m^3 s^{-1}$; positive northward) across the section at 47°N confined to northward (upper panel) and southward (lower) velocities.

trend detectable in the depth. But in the upper 1000m (red curve) there is a clear interdecadal variability. The northward freshwater transport rises during the first half of the 1970ies and recovers until 1982. This is followed by a fast intensification of freshwater transport until 1987 and a general reduction during the next 10 years. Within the last 4 years it reaches again the longterm mean.

To locate now the freshwater signal in the vertical expansion the transport is integrated over the whole depth and is accumulated from west to east. Figure 62 clearly shows that the largest changes appear east of 30°W which comprises the NAC and the northern branch of the Subtropical Gyre further east.

Since the freshwater transport anomalies can be caused by changes in the velocity field as well as in the salinity, the transport east of 30°W is split into its components ($vS = v'\bar{S} + \bar{v}S'$). Figure 63a shows these components in comparison with

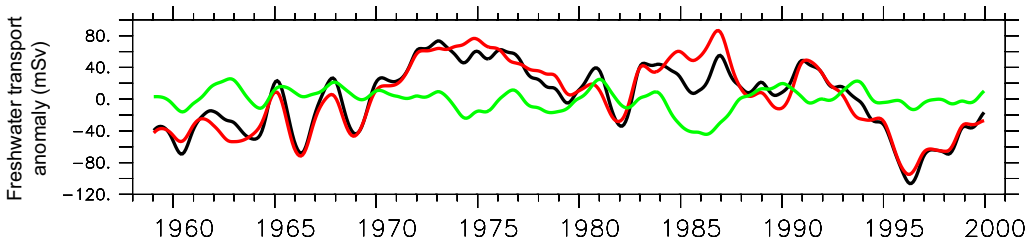

Figure 61 Time series of monthly freshwater transport anomalies (mSv) at 47°N in experiment REFERENCE for the total meridional exchange (black) and for upper/northward (red) and lower/southward (green) velocities only.

the net freshwater transport across the whole section 47°N (black) and for the subsection (blue). It is obvious that the latter accounts for most of the variability on interannual time scales and even longer. The red dotted curve representing the contribution by changes in the salinity ($\bar{v}S'$) accounts only for a small part of the freshening during the early 1970s and the resalinification in the 1990s while in the mid-80s there is a large effect due to changes in the salinity field. But the latter event is heavily reduced by a dynamic signal of opposite sign ($v'\bar{S}$; green dashed curve). Furthermore, the velocity changes are capable to explain the freshening in the 70s and the decrease of the freshwater transport in the 1990s. To isolate the impact of the NAC variability (volume transport and salinity) the eastern partial section is divided into further subsections: NAC and EAST (see boxes in Fig. 59).

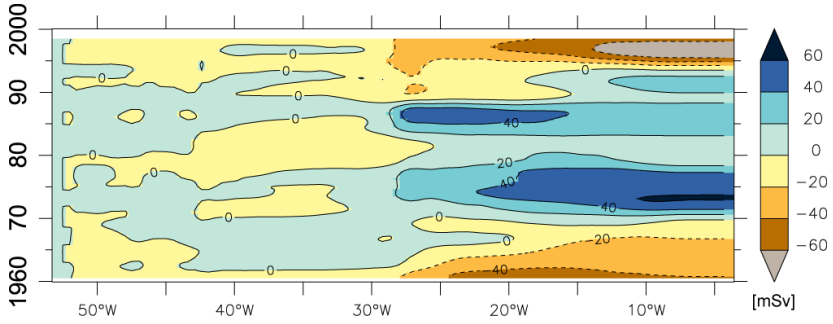

Figure 62 Hovmøller diagram of the vertically integrated and zonally accumulated freshwater transport (mSv) across section 47°N in the REFERENCE case.

In the figures 63 (b-c) the absolute freshwater transports are separated for each box similar to (a) but now only for the upper 1000m. Fig. 63b shows again the REFERENCE run with the freshwater transport from coast-to-coast (black), for

the region east of 25°W[3] as well as the NAC and EAST boxes. A remarkable result is, that the dependence on the velocity and salinity field can be assigned to different subsections:

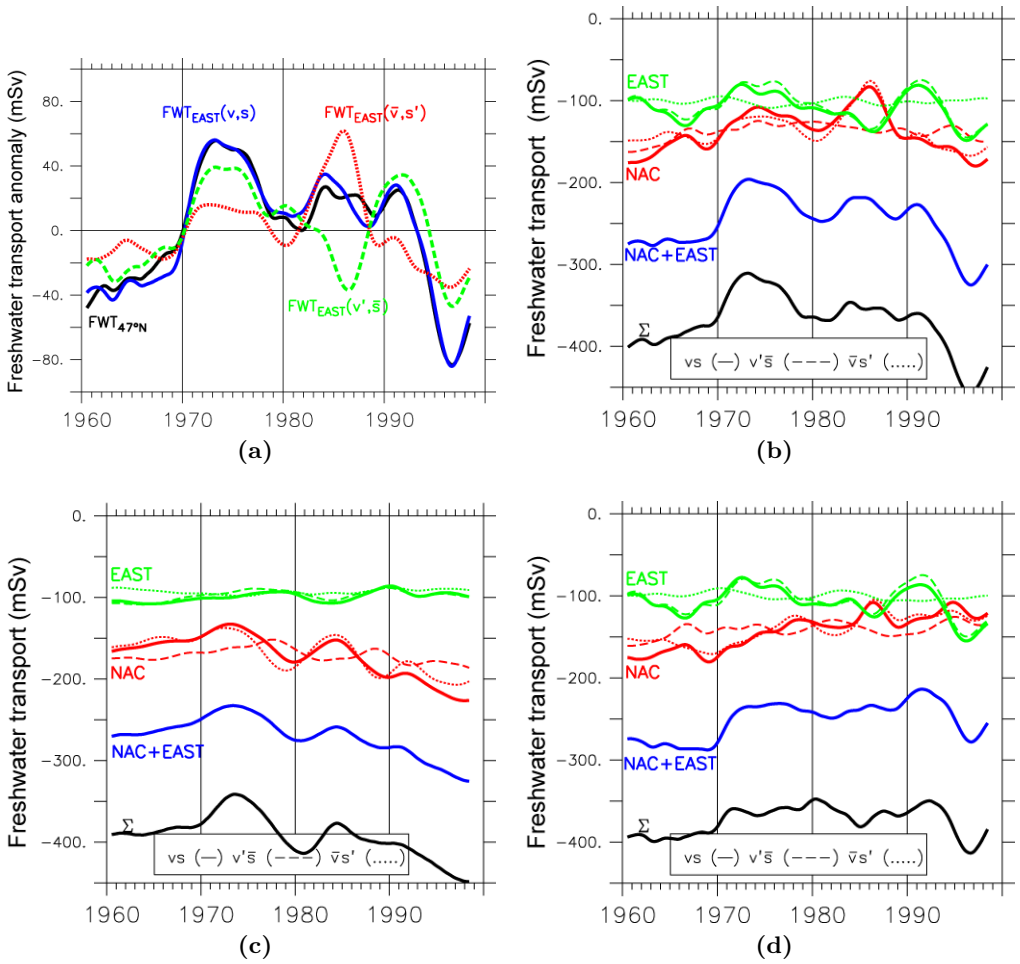

Figure 63 REFERENCE: Freshwater transport across 47°N (mSv). (**a**) Transport anomalies using the whole section (black) for integration in comparison with the subsection east of 30°W (blue). The latter is split into contributions by variations of both: velocity ($v'\bar{S}$; green dashed) and salinity ($\bar{v}S'$; red dotted). (**b-d**) Transport anomalies (solid) within the upper 1000m for the whole section (black) and for smaller subsections, according to the colored boxes in Fig. 59 for NAC (red), EAST (green) and both (NAC+EAST; blue) using different experiments: REFERENCE (b), THERMHAL (c) and WIND (d). The associated contributions by velocity (dashed) and salinity (dotted) changes are also shown for the two subsections.

[3]This differs slightly from the definitions before. 25°W has been chosen to get a better representation of the NAC dynamics.

The freshwater transport (vS, green solid) variability in EAST is mainly caused by anomalies in the meridional velocities ($v'\bar{S}$, green dashed) and not in the salinity field ($\bar{v}S'$, green dotted). This is different from and partly reversed in the NAC (red solid) where anomalies in S have a large influence ($\bar{v}S'$, red dotted) on intra decadal timescales and velocity variations (red dashed) induces freshwater transport anomalies on longer scales.

Since the mechanisms that are responsible for these dependencies on salinity and velocity are not clear, this diagnostic is repeated for the sensitivity experiments THERMHAL and WIND (see 63c,63d). Surprisingly, WIND, without any interannual varying thermohaline surface fluxes, results in very similar freshwater fluxes across the eastern subsection in comparison with the REFERENCE case. But a different picture is drawn by THERMHAL where long-term variations are mainly driven by salinity changes ($\bar{v}s'$) in the NAC and the freshwater export from the north in subsection WEST (the residual between the black and the blue curve).

As the wind has such a strong influence on the freshwater/salt exchange with the subtropical gyre one can expect a close relation to the North Atlantic Oscillation (NAO) which rules most of the North Atlantic ocean variability. And for the resalinification in the Nordic Seas during the 1990ies, such a connection has been already proposed by Hátún et al. (2005). They found an increase in the haline inflow into the Nordic Seas between 1993 and 1998 originating from the eastern subpolar basin. They where also able to relate this to the SSH-based Subpolar Gyre index by Häkkinen and Rhines (2004).

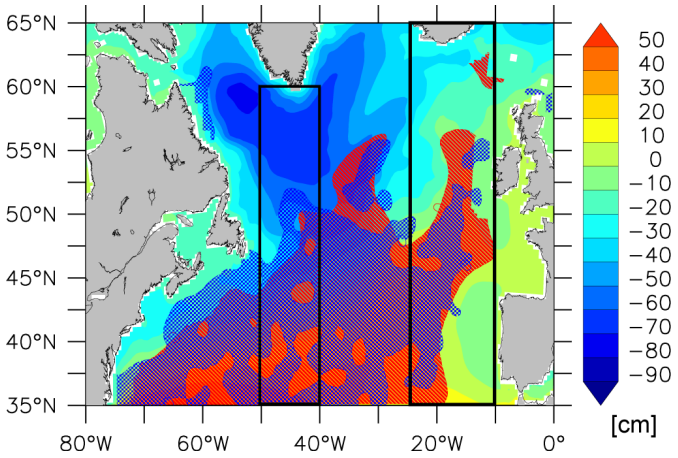

Figure 64 Shade of simulated mean sea surface height anomaly (cm; global mean removed) Pattern of negative SSH trend 1993-1998 from AVISO MSLA observations (blue hatched) and from simulation (red hatched) are overlaid.

According to the cyclonic (anti cyclonic) circulation, the Subpolar (Subtropical) Gyre is characterized by a low (high) SSH (shown in Fig. 64 as simulated mean SSH anomaly relative to the global average). For the period 1993-1998 a weakening of the Subpolar Gyre has been found accompanied by a positive SSH trend (Häkkinen and Rhines, 2004) while the Subtropical Gyre shows a negative SSH trend. There is a good agreement of the spatial trend distribution between observation (AVISO) and simulation (indicated by the blue and red patterns in Fig. 64). Also the meridional slope of the SSH trend (zonally averaged between 50°W and 40°W; see box in figure 64) is simulated very well (Fig. 65(a)).

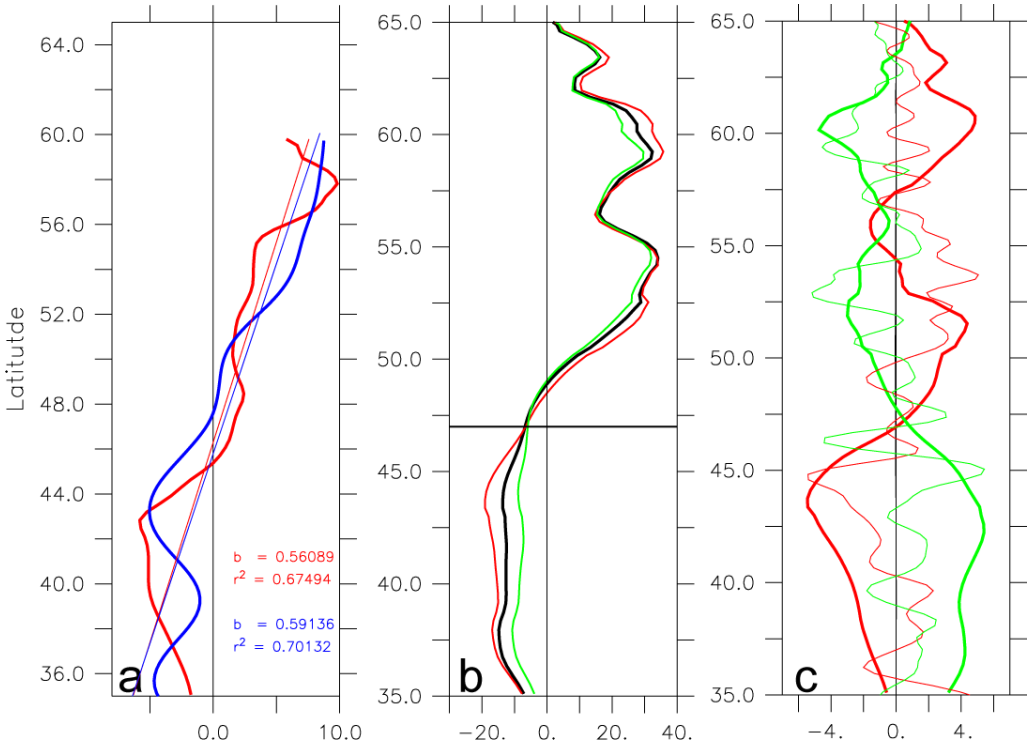

Figure 65 (**a**) Sea surface height (SSH) trend (mm/yr) in simulation (red) and AVISO observation (blue) for the period 1993-2000 zonally averaged between 50°W and 40°W (see left black box in Fig. 64). Meridional linear regression for both are also plotted (thin lines). The slope b and the coefficient of determination $r^2$are indicated respectively. (**b**) Mean zonal SSH gradient ($1 \times 10^{-8} m/m$) between 25°W and 10°W for the period 1993-2000 from simulation. The annual mean gradients for 1993 (red) and 1998 (green) are shown separately. (**c**) Annual mean zonal SSH gradient anomalies ($1 \times 10^{-8} m/m$) for 1993 (red) and 1998 (green) based on the (black) mean gradient from sub figure (b). Thick curves show model results compared to observations (thin curves).

However, more important than the meridional gradient is the zonal one in the east, which reflects changes in the meridional velocities. Figure 65(b) shows the SSH gradient between 25°W and 10°W (see right black box in Fig. 64) for the beginning and the end of the 1990s period. With the weakening of the NAO there is a flattening of the negative zonal gradients south of 47°N and a somewhat smaller change farther north.

A more detailed picture is drawn by the Figure 65(c) which illustrates the anomaly of the SSH gradients relative to the mean gradient (black curve in sub figure 65(b)). Thin curves are derived from AVISO-MSLA and differ from simulation especially in the subtropical and northern subpolar basin whereas the gradient anomaly across 47°N is very similar.

Since the SSH trends and gradients seem to be simulated in an acceptable manner, the velocity field from the model output can now be used to examine the dynamic mechanisms that govern the freshwater transport across the southern section.

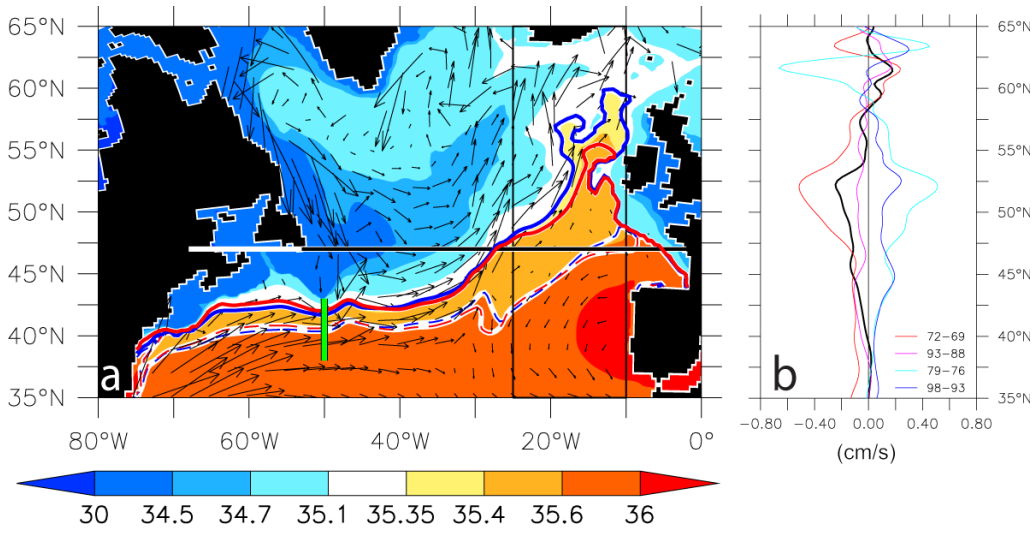

Figure 66 (**a**) Map of mean salinity and vectors of horizontal mean circulation (both vertically averaged over the upper 1000m). Contour lines indicate the 35.4 (solid) and 35.6 (dashed) isohaline for positive (red) and negative (blue) NAO phases. The zonal section at 47°N is also shown (black line). (**b**) Anomaly of the mean meridional velocity in the upper 1000m (cm/s), averaged zonally between 25°W and 10°W (see right black box in Fig. 64) for the simulated period 1958-2000 (black) and for periods of a strengthening (red and purple) and weakening (blue and light blue) NAO.

Figure 66(a) shows a map of simulated mean salinity in conjunction with the horizontal mean velocity as vector diagram overlaid, both averaged over the upper 1000m. The red and blue contour lines indicate the shift of the haline front between the Subtropical and Subpolar Gyre (35.4, solid; 35.6, dashed) under positive (red) and negative (blue) NAO conditions.

As the NAC near 47°N parallels the salt front, changes in the volume transport only have a minor effect on the freshwater transports. In contrast, in the east, where the flow parallels the meridional salinity gradient, the effect of dynamic changes is much larger though the mean velocities are very small compared to the ones governing the NAC.

The meridional velocity anomalies between 35°N and 65°N (averaged over the eastern box between 25°W and 10°W) are shown in figure 66(b) as temporal change throughout periods of increasing (left curves: red, purple) and decreasing (right curves: blue, light blue) NAO indices. The black curve indicates the velocity changes for the whole simulation period 1958-2000 reflecting the increasing NAO between the 1960s and the 1990s.

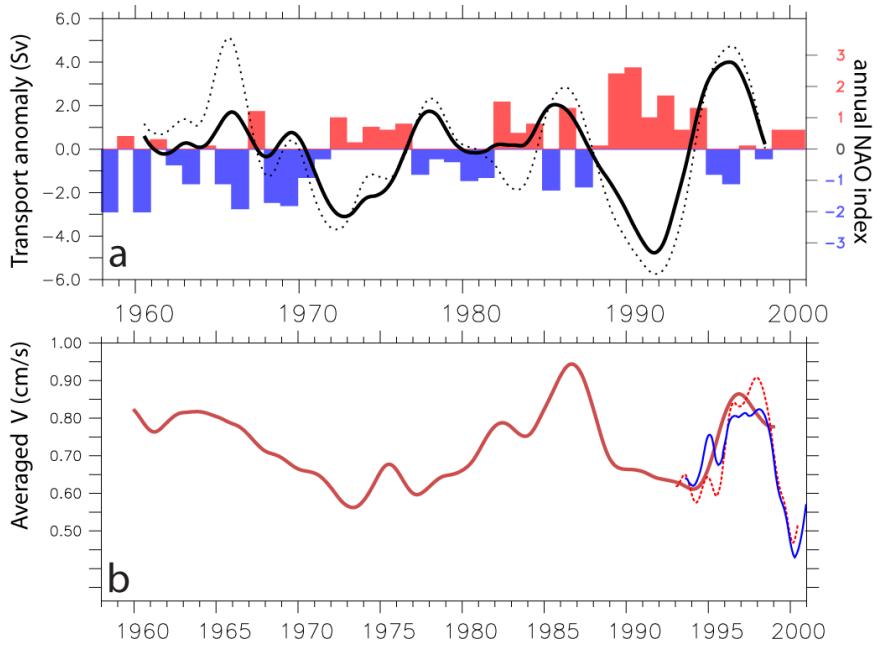

Figure 67 (**a**) Meridional Sverdrup Transport anomaly (Sv) across 47°N between 25°W and 10°W (thick solid) and the basin-wide section (thin dotted) resulting from the simulated wind stress curl. Additionally, the annual NAO index is shown as bar plot for positive (red) and negative (blue) phases. Time series are smoothed using a Hanning filter with a 5 year box. (**b**) Simulated meridional velocity (cm/s) across 47°N between 25°W and 10°W (red solid). Geostrophic velocities (upper 1000m) from Sea Surface Height gradients are also shown for simulation (red dotted) and AVISO observation (blue).

The strengthening of the westerlies during periods of increasing NAO induces an input of positive vorticity into the northern SPG and also negative vorticity in the mid-latitudes, especially at 47°N. This leads to a strengthening of both gyre circulations and to a horizontal circulation anomaly in-between, which has been discussed by Marshall et al. (2001) as 'Inter-Gyre-Gyre' in another context. The

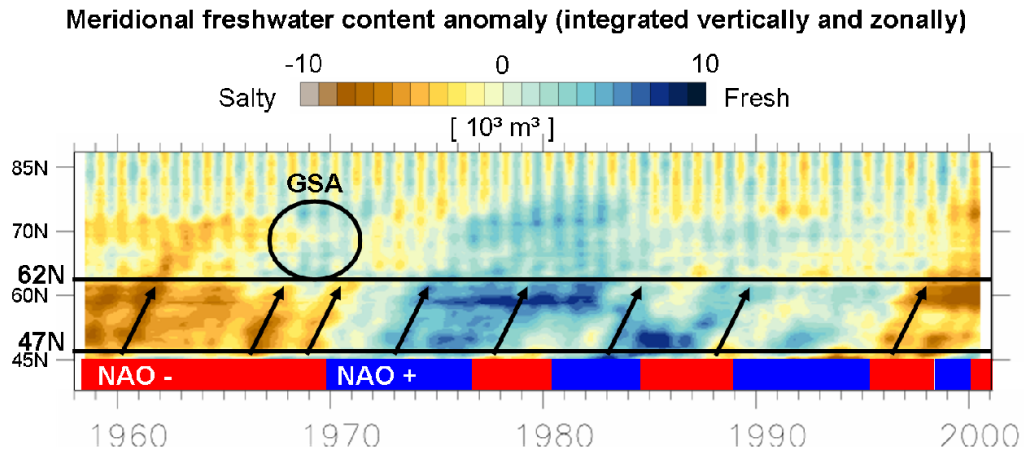

Figure 68 Hovmøller diagram of subpolar meridional FWC anomaly ($10^3 m^3$) from experiment REFERENCE. Blue (yellow) shaded regions indicate a freshening (salinification) related to the temporal mean. Black arrows indicate the northward propagation of anomaly signals between 47°N and 62°N. For comparison reasons the NAO (winter) index is shown at the lower end. The black circle denotes the freshening signal north of the sills associated with the GSA in the 70s.

resulting Sverdrup Transport anomaly across 47°N is shown in Fig. 67(a) for the basin wide transport (black curve) and the eastern subsection separately (black dotted curve) in comparison with the annual NAO index. There is a clear anti correlation with negative transport anomalies under strong NAO conditions and positive anomalies during weak NAO phases. This wind induced transport variability then leaves its fingerprint in the vertically (0-1000m) and zonally (eastern subsection) averaged meridional velocity across 47°N as shown in the lower sub figure Fig. 67(b). But also geostrophic velocity anomalies from local water mass redistributions (Bersch et al., 2007) as well as thermohaline driven changes in the MOC (e.g. deep convection and overflow) can affect this upper layer transport. Additionally, the velocity anomaly from geostrophic velocities derived from the model simulation (red dotted) and AVISO-MSLA (blue solid) data is shown which confirms the reliability of the model and the found mechanism.

Coming back to the question of signal dispersion and the spread of the freshwater transport anomalies, a Hovmøller diagram of the subpolar freshwater content anomaly for each latitude band (Fig. 68) makes it obvious that the large freshwater transport anomalies that enter the subpolar basin at 47°N clearly propagate northward (indicated by some arrows). The time scale for reaching the northern sections next to the arctic basins is about 1.5 years. There are also smaller freshening signals originating from the north and not from the south such as the GSA event in the late 60s and early 70s. But this signal has only a small impact on

the subpolar freshwater content between 47°N and ˜62°N.

This concept of a salty inflow within the upper 1000m depending on the NAO phase can explain at first the freshwater content in the upper ocean layer. To shed now some light into the deeper ocean and to elicit how the salt/freshwater signal is spread into lower ocean layers, the deep salinity near the Ocean Weather Ship (OWS) Bravo in the Labrador Sea is analyzed. Since it is located in the deeper part of the subpolar basin this is representative for the western deep subpolar basin at a glance.

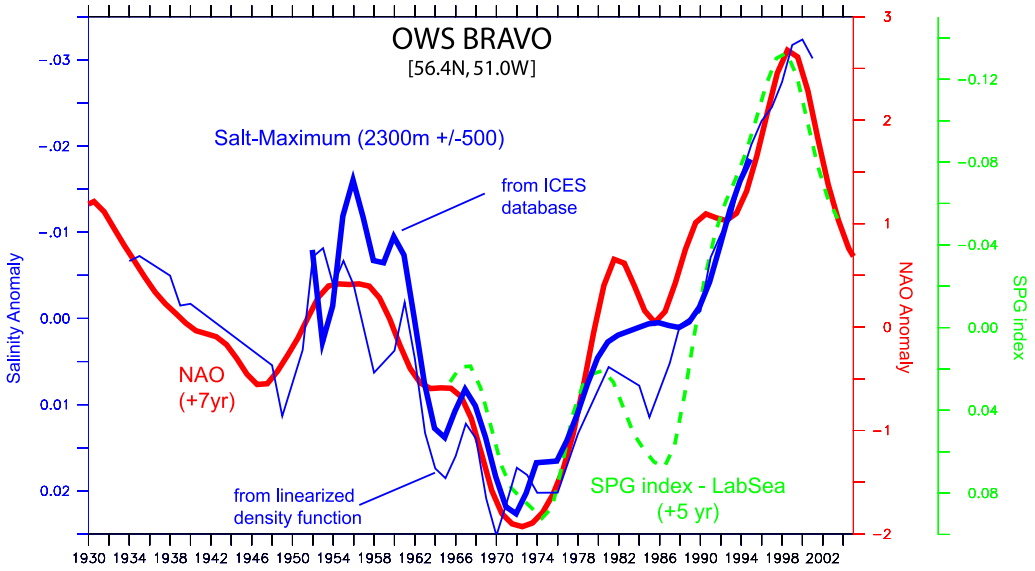

Figure 69 Time series of observed subpolar deep salinity anomalies (blue) taken next to station OWS-Bravo and averaged between 1800m and 2800m for two different data sets: from ICES (2007) (thick) and another derived from density time series as used by Latif et al. (2006). Additionally, the shifted (+7 years forward) NAO index (red) and a Subpolar Gyre index (m; green) from simulated SSH in the central Labrador Sea (shifted by +5 years) are shown.

Fig. 69 shows the salt maximum at $2300 \pm 500m$ depth (blue thick line), taken from the ocean database, which is provided by the International Council for the Exploration of the Sea ICES (2007). As there are large gaps in these records, especially in the mid-1980ies (see Fig. 6) an additional longer salinity time series (blue thin line) is derived from density and temperature data (as it is used for the LSW analysis by Latif et al. (2006)) taking a simplified density function into account which is based on the equation (A3.2) given by Gill (1982):

$$S = \frac{\sigma_{1500}}{(0.824493 - 4.09899 \times 10^{-3} * T + 7.6483 \times 10^{-5} * T^2 - 8.2467 \times 10^{-7} * T^3)}$$

Since there is a good accordance of in situ and derived salinity records, this authenticates the usability of the longer salinity time series.

As mentioned by Dickson et al. (2002) there was a continuous freshening of the deep subpolar gyre since 1970 until the end of the 20th century. But there was also a former increase in the deep salinity between 1954 and 1970. Assuming, this multi decadal variation is a delayed reaction on the salinity (or freshwater) conditions in the upper ocean, there must be a similar long-term signal as it is found for the NAO-related freshwater exchange at 47°N, which determines the subpolar freshwater content change in this study.

Observational data at OWS Bravo suggests indeed a relation between the interdecadal-to-multi decadal deep salinity change and the NAO winter index with a time lag of about 7 years between the leading NAO and the deep ocean reaction. It has to be noted that the local influence of the deep convection on the deep salinity is very small since the layer mainly below the Labrador Sea Water is investigated. Dickson et al. (2002) have compared different locations of source water masses that feed the deep Labrador Sea by entrainment, mixing and advection. The overall freshening they found is supported by this work which suggest a wide and deep freshwater content disturbance triggered by the NAO-related atmospheric wind stress forcing which has the capability to affect a broad range of water masses.

5.3 Implications for Heat Content Changes

The main focus of this study is the subpolar freshwater budget. However, Boyer et al. (2007) suggested a strong anti correlation between the freshwater and heat content change and therefore the simulated heat content anomaly is shown in Fig. 70 (grey dashed line) which confirms the anti correlation with the freshwater content anomaly (c.f. figure 48). Using observational data from the World Ocean Database and Surface fluxes from NCEP/NCAR reanalysis Boyer et al. (2007)

provided some possible explanations for the freshening of the subpolar gyre as they are discussed above but they could not explain the cooling.

In the model simulation t the subpolar heat content change can be explained neither by surface fluxes nor by the inflow of cold Arctic waters (Fig. 70). The heat content anomaly derived from the simulation output (black curve) provides a somewhat larger variability than in the case of Boyer et al. (2007) but it reveals the same characteristics and time scales of the cooling between 1970 and 1993. Though the meridional heat exchange with the Arctic basins (blue) reduces the subpolar heat content, the resulting heat content change however seems to be out of phase with the basin wide result. As already noticed by Boyer et al. (2007) the surface flux related heat content change (green) is not capable to explain the cooling since it acts in a contradictory manner.

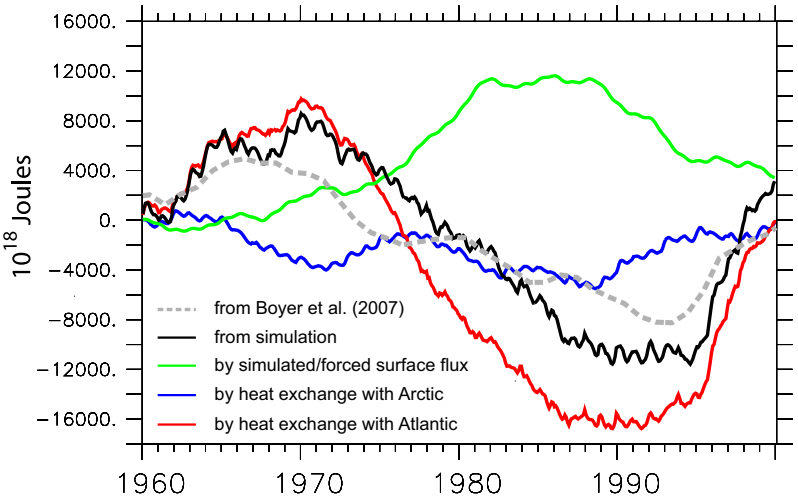

Figure 70 Heat content change ($10^{18}J$) in the Subpolar basin from Boyer et al. (2007)(grey) and from simulation (black) in comparison with accumulated net surface heat flux (green) and integrated net heat transports across the southern (red) and the northern (blue) section.

Similar to the discussion of the subpolar freshwater budget, where the exchange with the subtropics was found to be a crucial aspect, the variation of the meridional heat transport across 47°N (shown in Fig. 70 as red curve) is an important contributor to the subpolar heat content change. In contrast to the warming effect by surface fluxes, this study provides implication for the oceanic circulation leading to a cooling between 1970 and 1990.

6 Impact of Freshwater Fluxes on Deep water formation and Meridional Overturning

The Meridional Overturning Circulation (MOC) in the North Atlantic is a measure for the thermohaline deep water formation in the subpolar region. Warm and light surface waters are transported northward while cold and dense water feeds the deeper return flow. The water mass transformation in-between is accomplished mainly by deep convection and overflow.

The impact of changes in the North Atlantic freshwater budget as well as the effects of the different forcing components on these processes are investigated in the following chapter. It comes out, that, analyzing sensitivity experiments, the wind forcing is responsible for large interannual variations in the MOC as well as for multi-decadal fluctuations, while thermohaline fluxes cause long-term trends, apart from the convection which acts also on interannual scales. Furthermore a sensitivity experiment with additional freshwater input (FRESH) and another experiment using a regional mask for the interannual forcing (NONARCTIC) are discussed to explore the spatial impact.

6.1 Deep water formation

Since the Subpolar Gyre merges the salty, warm waters from the south with cold and fresh waters from north, this is the key region for the transformation of light surface waters into dense deep water. The two most important processes are the deep convection and the overflows, beside a general sinking by continuous buoyancy loss within the gyre. The first two processes are briefly introduced in the following sections.

6.1.1 Deep Convection

One of the most important regions for deep convection lies within the center of the gyre, in the Labrador Sea. Strong winterly heat fluxes (mainly caused by wind driven turbulent fluxes) cool the upper ocean layer and thus buoyancy is lost and surface waters can widely sink and feed deeper layers (Marshall and Schott, 1999). In the mid-abyssal layer, such newly formed Labrador Sea Water (LSW) is then carried out southward by the Deep Western Boundary Current (DWBC) or recirculates within the gyre.

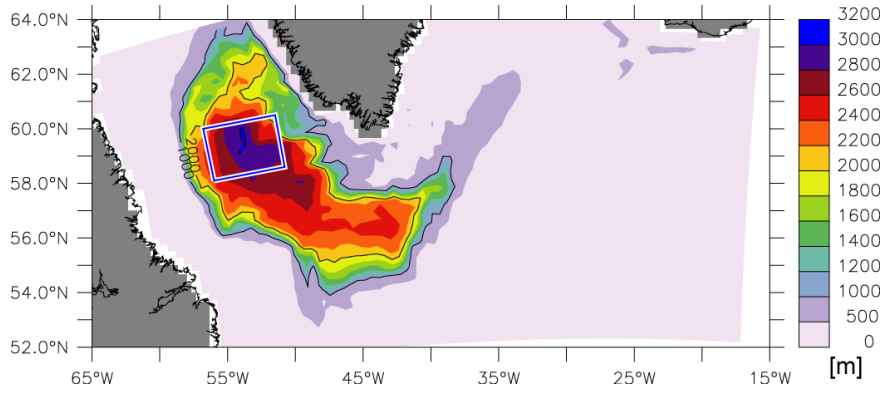

Figure 71 Map of all-winter mixed layer depth (MLD) maximum (m) in the REFERENCE experiment. Blue box indicate area of average for several diagnostic time series.

To quantify the convection activity the mean winter mixed layer depth (MLD) can be used: the deeper the mixed layer, the stronger the convection. In this study, it is defined as the depth where the density difference to the surface exceeds 0.01 kg/m^3. A map of the all-winter maximum MLD in the REFERENCE experiment is shown in Fig. 71. The deepest convection events reaches 300m in this

simulation which is somewhat deeper than what is assumed from observations of the LSW layer thickness (about 2400m). Beside the Labrador Sea, deep convection also occurs in the Irminger Sea southeast off the Greenland coast and is suspected to produce LSW as well (Pickart et al., 2003a,b; Falina et al., 2007). But this is reproduced only marginally by the simulation.

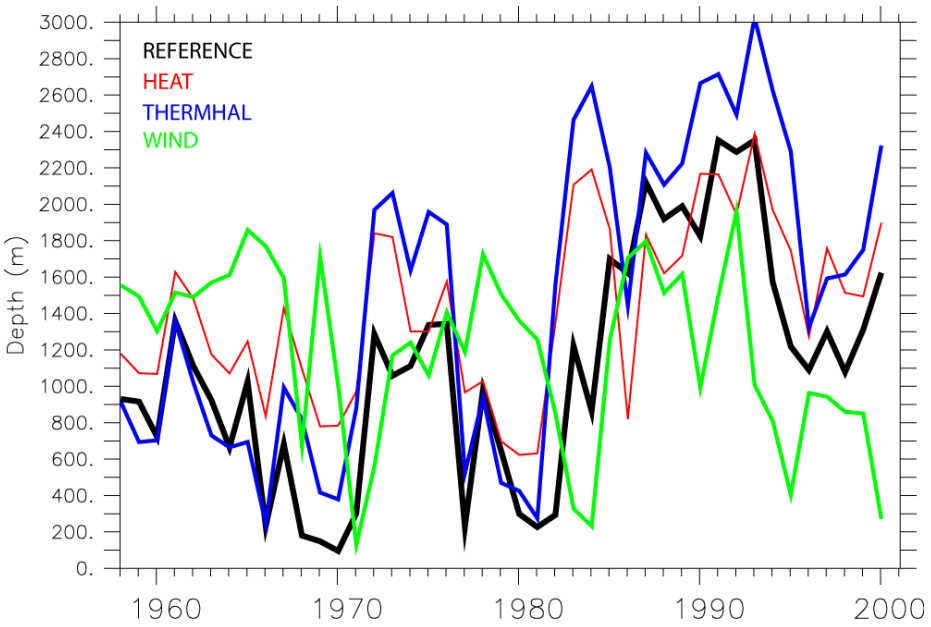

Figure 72 Time series of winterly MLD maximum in the central Labrador Sea (averaged over the blue box in Fig. 71) for the REFERENCE and most sensitivity experiments.

The time series of winterly MLD maxima in the central Labrador Sea (averaged over a distinct region) is shown in Fig. 72 (black for the experiment REFERENCE) which is in line with the observed Labrador Sea Water thickness and the relation to the NAO (c.f. Fig. 2). The interannual variability is associated with processes occurring in the presence of heat flux variations during NAO-high phases since the experiment REFERENCE provides nearly the same timing of deep convection events as in the sensitivity experiments HEAT and THERMHAL . Taking interannual haline fluxes into account increases the amplitude whilst the interannual wind stress variability (experiment WIND) leads instead to a reduction during NAO-high phases.

The deep convection is an important process for the oceanic heat transport. Surface water that looses buoyancy, gets denser which enhances the vertical mixing

locally makes room for new warm water to flow afterwards and to release heat further on. But the buoyancy loss during deep convection is not only a matter of temperature and heat fluxes but also of salinity. Freshwater intrusions can therefore weaken the convection and thus the transformation of surface waters into deep waters which is discussed in chapter 6.26.1 6.2 on the facing page.

6.1.2 Overflow

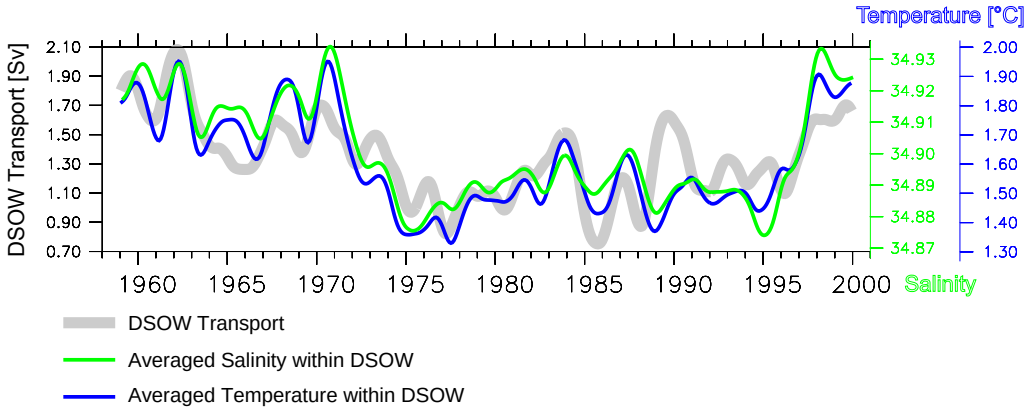

Figure 73 Time series of DSOW transport (grey), salinity (green; right axis in psu) and temperature (blue; rightmost axis in °C) right on the sill.

The overflow provides the densest water mass in the northern North Atlantic. Very cold and dense waters from the Arctic and from deep convection within the Nordic Seas fill up the basin and enter the subpolar gyre at the sills in the Denmark Strait and near the Faroe-Bank-Channel. South of the sills it spills down the topography feeding the subpolar abyssal layer and forms the deepest part of the Western Boundary Current. Several studies (e.g. Eden and Willebrand (2001); Beismann and Barnier (2004); Schweckendiek and Willebrand (2005)) demonstrated its immense impact on the deep return flow of the meridional overturning cell.

Concerning the source processes of the overflows, there is much less consensus. Some authors suggest the location of production within the Greenland Sea involving the convection activity in this region, while others push the idea forward that water masses from the nordic Iceland Sea play a major part. However, in each case the characteristics of the overflow depend strongly on the hydrographic

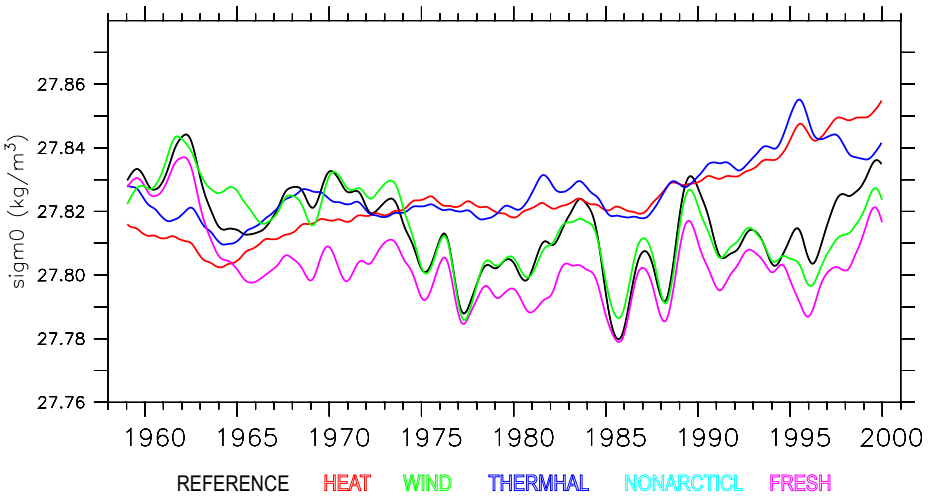

Figure 74 Denmark Strait Overflow Density (σ_0) for the REFERENCE case and various sensitivity experiments.

conditions in the Nordic Seas and thus on the Arctic (cold and fresh) and Atlantic (warm and haline) inflow. The dependence becomes obvious in the relation between the transport of Denmark Strait Overflow Water (DSOW; grey curve in Fig. 73) and the density on the sill (black curve in Fig. 74): When the density decreases (e.g. between 1970 and 1977), the transport declines (from 1.7Sv to 0.8Sv) and vice versa. From figure 73 it can be seen that the density fluctuations are governed by salt (green curve) and temperature (blue curve) variations simultaneously. . The comparison of the sensitivity experiments suggests that the DSOW density or transport variability on all time scales is mainly affected by the interannual wind variability (the REFERENCE case is very close to the WIND case in figure 74) while the thermohaline induced variations act on decadal time scales (red and blue in the same figure).

6.2 MOC reaction and sensitivity

The mean Meridional Overturning Circulation in the North Atlantic is shown in Fig. 75 as averaged overturning stream function from simulational data (REFERENCE experiment). Its largest transport is found near 40°N at about 700m depth, meaning there is a poleward mean volume transport of 12 Sv within the upper 700m and a compensating return flow in the deep.

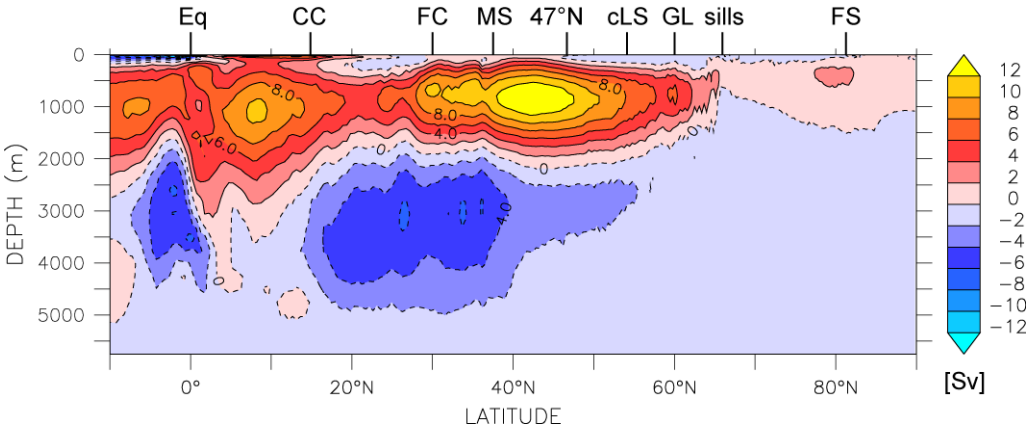

Figure 75 Simulated mean Meridional Overturning Circulation (MOC) in the northern Atlantic from experiment REFERENCE (Sv). Solid contour lines denote a clockwise circulation in the vertical plane. Acronyms at the upper end of the graph indicate specific locations: Equator (**Eq**), Caribbean Current (**CC**), Florida Current (**FC**), Mediterranean Sea (**MS**), zonal section at **47°N**, central Labrador Sea (**cLS**), southern tip of Greenland (**GL**), the northern **sills** and Fram Strait (**FS**).

The temporal variations of the meridional overturning in the North Atlantic can be split into two fractions. One driven by thermohaline processes and the other by wind (Biastoch et al., 2008). Fig. 76 shows these two parts as Hovmøller diagrams of the MOC maximum between 30°N and 70°N. The wind driven portion seems to depend mainly on the local wind stress, especially at 36°N. But it will be shown that there is also a thermohaline effect of the wind stress anomalies on the MOC in the North Atlantic. In the experiment with interannual varying thermohaline forcing the MOC anomalies have clearly their origin in the subpolar gyre (around 55°-57°N) propagating southward. The superposition of these two runs is shown in the lower left and agrees well with the MOC variability in the REFERENCE-run.

Thermohaline

HEAT is the simplest experiment of all; only interannual varying surface heat fluxes (sensible, latent and turbulent) are allowed in the forcing fields. The MOC maximum in Fig. 77 shows interannual fluctuations, which can be associated with the convection events in the Labrador Sea due to the timing. The mixed layer depth (MLD) in Fig. 72, as a quantity for the convection activity, deepens during high NAO phases and the subpolar gyre transport strengthens (shown as

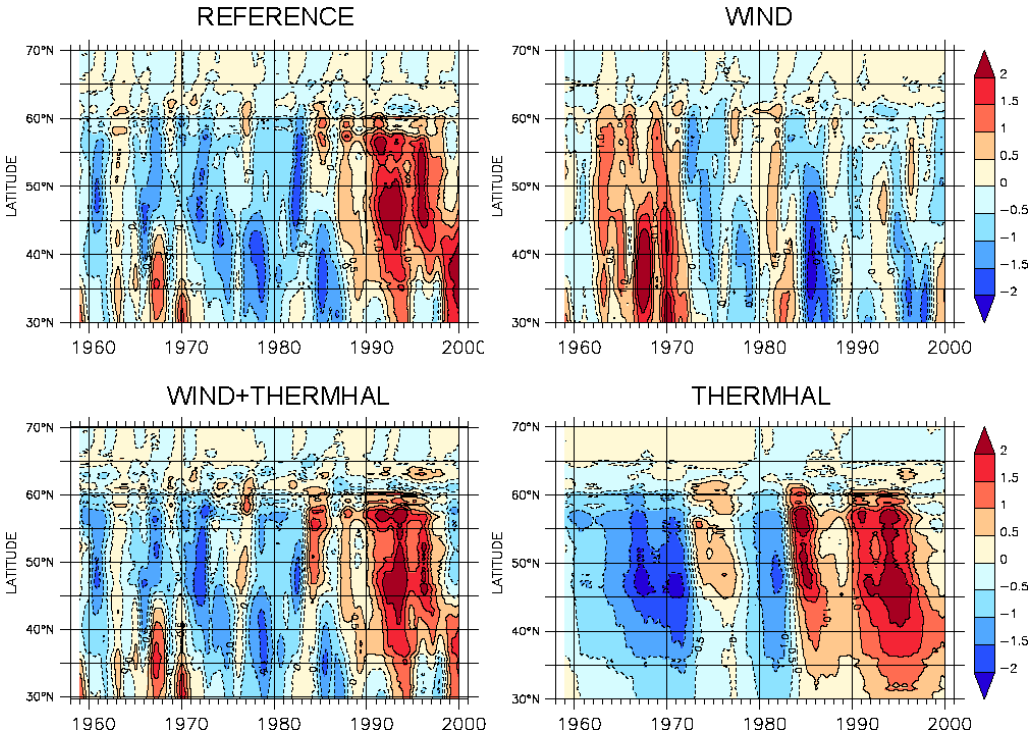

Figure 76 Hovmøller diagrams of local MOC maximum anomalies (Sv) between 30°N and 70°N for several experiments: REFERENCE (upper left), WIND (upper right), THERMHAL (lower right) and the sum of WIND and THERMHAL.

maximum barotropic stream function PSI in the Labrador Sea inFig. 78). As wind stress is kept climatological, this must be the result of geostrophic adjustment in the vicinity of newly formed dense water in the convection area. The MOC reacts within 1 year on the deep convection and increases as long as the convection activity is high. When the MLD is shallow then the MOC retards..

The impact of interannual heat flux variations on the freshwater budget can be assessed by comparing HEAT and THERMHAL. Fig. 79 shows higher sea surface salinities during NAO-high phases, which can be explained by a higher rate of evaporation: Especially before 1978, when the forcing data does not provide any interannual fluctuations in the precipitation field.. The higher salinities also have a feedback on convection: the mixed layer reaches deeper layers (see Fig. 72). Thus, the barotropic transport is stronger in the subpolar gyre (Fig. 78). As discussed before, this has a remarkable effect on the Davis Strait freshwater export (see section 5.2.3.3). In this experiment also the freshwater transport in the east of Greenland changes: In comparison with HEAT there is a reduction

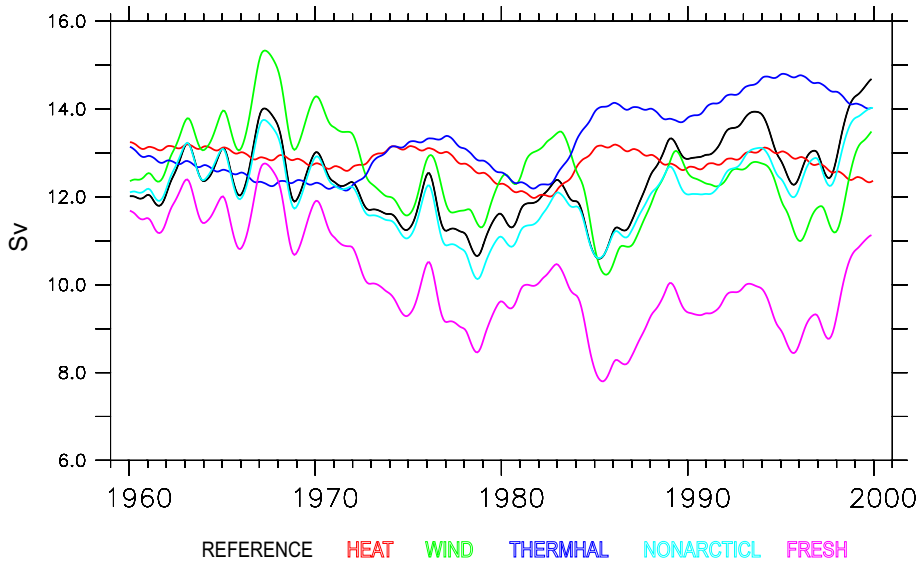

Figure 77 Time series of the MOC maximum (Sv) at 36°N for all experiments.

of salt export into the Nordic Seas and a lower freshwater import from the North via Denmark Strait. As the overflow density at Denmark Strait is nearly the same as in HEAT, the MOC intensification in THERMHAL must be caused by the extraordinary strong convection in the Labrador Sea.

Wind stress

Whereas interannual wind speed variability can enforce convection due to higher turbulent heat fluxes, the associated wind stress is capable to weaken the deep water formation by modifying the ocean circulation and thus changing the freshwater/salt imports from the north and the south. The experiment WIND makes use of interannual varying wind stress forcing fields while precipitation, evaporation and the radiative and turbulent heat fluxes are kept climatological. The most prominent feature in this case is the weakening MOC (Fig. 77). Even the NAO signature, seen in the thermohaline experiments as convective intensification, seems to vanish. As seen before, there is a strong local wind effect on the MOC at this location (36°N) but the longterm variability is caused by changes in convection intensity due to wind-driven changes in the ocean circulation an sea-ice drift in the Labrador Sea: Contrary to HEAT and THERMHAL the MLD shallows during +NAO phases instead of deepening. Even the barotropic gyre transport (Fig. 78) is the weakest in all experiments (Except for FRESH.

In this experiment the freshwater import (liquid and ice) into the Nordic Seas

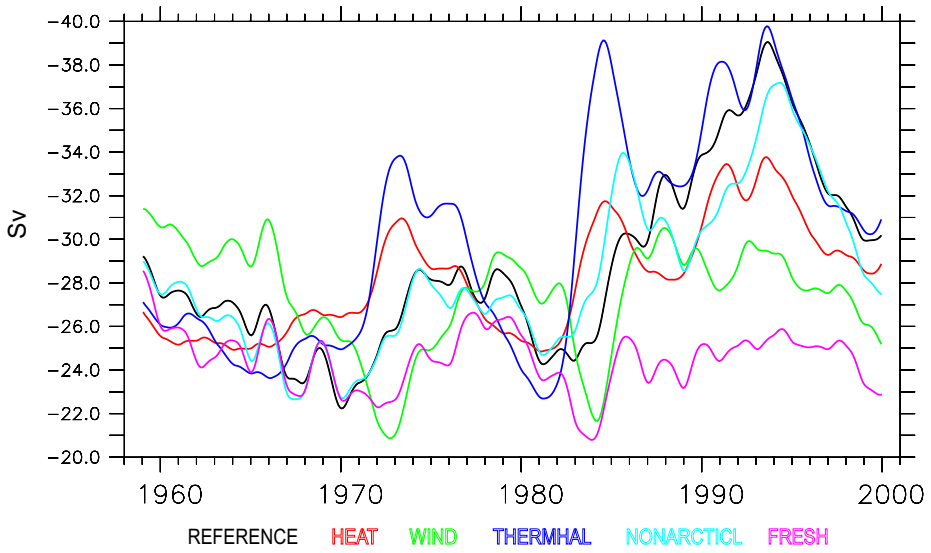

Figure 78 Time series of the horizontal barotropic stream function (Ψ, in Sv) in the Labrador Sea for all experiments. The negative values denote the cyclonic circulation of the Supolar Gyre.

strengthens during high NAO phases. One part remains in the Nordic Seas and enhances the freshwater content. The other part is exported by the East Greenland Current across Denmark Strait. Plenty of cold freshwater enters therefore the eastern Labrador Sea and partly reaches the Baffin Bay. The cold and fresh water south of the Davis Strait seems then to reduce surface heat fluxes and thus evaporation. More and more freshwater remains at the surface. Additionally, the north-north westerly winds during +NAO benefits the ice production in the central Labrador Sea, which suppresses any deep convection.

Thermohaline + Wind

The variability in the REFERENCE experiment can be understood as a superposition of both THERMHAL and WIND. This allows to separate processes and mechanisms associated with the thermohaline forcing from the dynamic effects due to wind stress changes. However, there are also joint effects: On the one hand, there are fluctuations in the surface heat flux which induce an interannual varying deep convection. This leads to differing deep water formation rates (LSW formation rate) and to variations in the vertical mixing. Due to convective changes in the density field, the horizontal transports in the subpolar gyre strengthen. On the other hand do wind stress anomalies in the arctic and subarctic region provide for freshwater export disruptions (liquid and ice) in the subpolar basin. In the

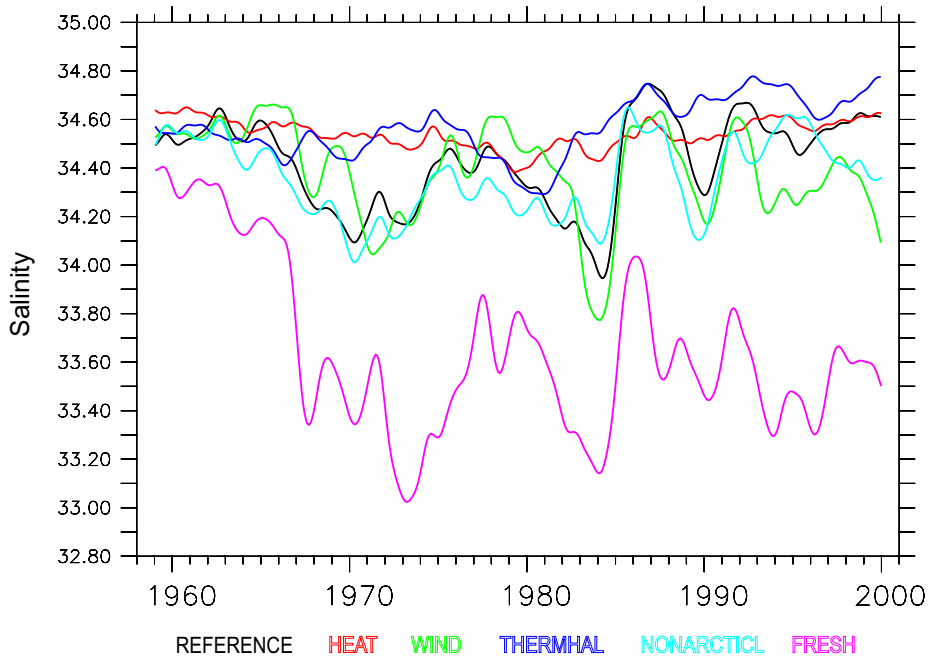

Figure 79 Time series of the sea surface salinity in the central Labrador Sea (see blue box in Fig. 71) for all experiments.

vicinity of too much freshwater at the surface, the buoyancy loss is then reduced and in the most extreme case, sea ice can spread over the central Labrador Sea under +NAO which would suppress any deep convection activity.

The Regional Experiment NONARCTIC

This regional sensitivity experiment (NONARCTIC) has been done to provide a basis for differentiating between signals from the south and the north namely the Arctic. North of the sills (Davis Strait, Denmark Strait and Iceland-Norway) all surface fluxes are kept climatological. One might expect this idealized simulation to show a slightly stronger mean MOC as freshwater disturbances from the north should not occur. But the MOC maximum in Fig. 77 draws a different picture, where the mean MOC is lower than in the REFERENCE case.

Although, the freshwater export variability through Fram Strait and Denmark Strait, concerning sea ice, is lower in this case, the net freshwater balance however is very similar to REFERENCE (see Fig. 39 and 40), even if the amplitude of the net Passage transport is somewhat smaller. Furthermore, even the mixed layer depth (MLD in figure 77) or the barotropic gyre strength (PSI in figure 78) are only little different from the reference experiment. This permits again the

conclusion that the interannual to decadal freshwater export variability from the arctic regions only play a minor role during the simulated time frame.

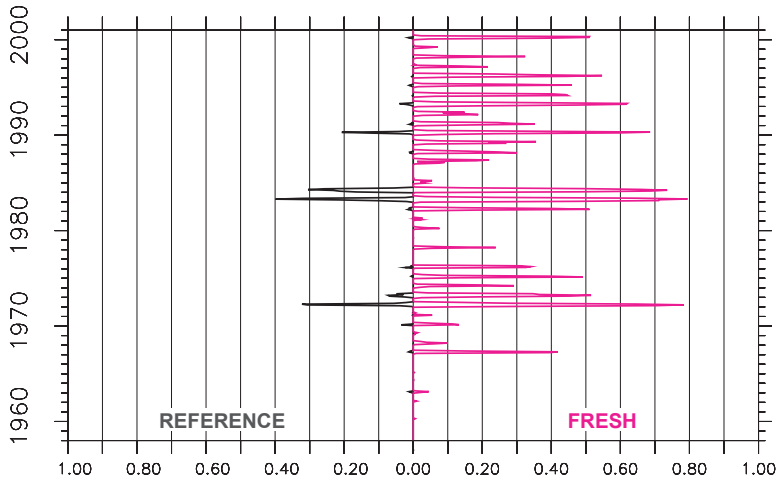

Figure 80 Winterly sea ice coverage in the central Labrador Sea in experiment REFERENCE and FRESH for the simulation period 1958-2000.

The Slowdown Experiment FRESH

The experiments discussed so far did not show any significant influence of the arctic freshwater export neither on the convection nor on the Atlantic MOC. To allow for releasing large amounts of freshwater, kept by the Greenland ice shield, which could intrude into the subpolar basin, hosing experiments has been done with several ocean models (ex. Gerdes et al. (2006)). Since the original CORE forcing data, as mentioned already in section 2.3.1.1, provides too much freshwater at the surface, a precipitation correction of about $80mSv$ in the northern (sub)polar region was applied. This is in the order of magnitude as used for the hosing experiments, where $0.1Sv$ is typically contributed around Greenland. The experiment FRESH makes use of this surface flux surplus.

The additional freshwater lowers the surface salinity in the Labrador Sea (purple curve in Fig. 79) and consequently the surface freshwater content rises dramatically during the first 10 years. Similar to WIND, this enhances ice production in the central Labrador Sea. Fig. 81a shows a map of the sea ice concentration in winter 1972 for the FRESH and the REFERENCE experiment, while the temporal evolution within the red box is plotted in Fig. 80. In the reference run, sea ice concentrations of more than 10% are unusual, whereas in FRESH it

exceeds 30% very often. Since the heat flux driven deep convection is delimited by the freezing point of water, below this point, there is no buoyancy loss due to heat loss anymore. Sea ice is produced instead and Labrador Sea water formation stops in FRESH within the first 3-4 years. (Fig. 81b and 72).

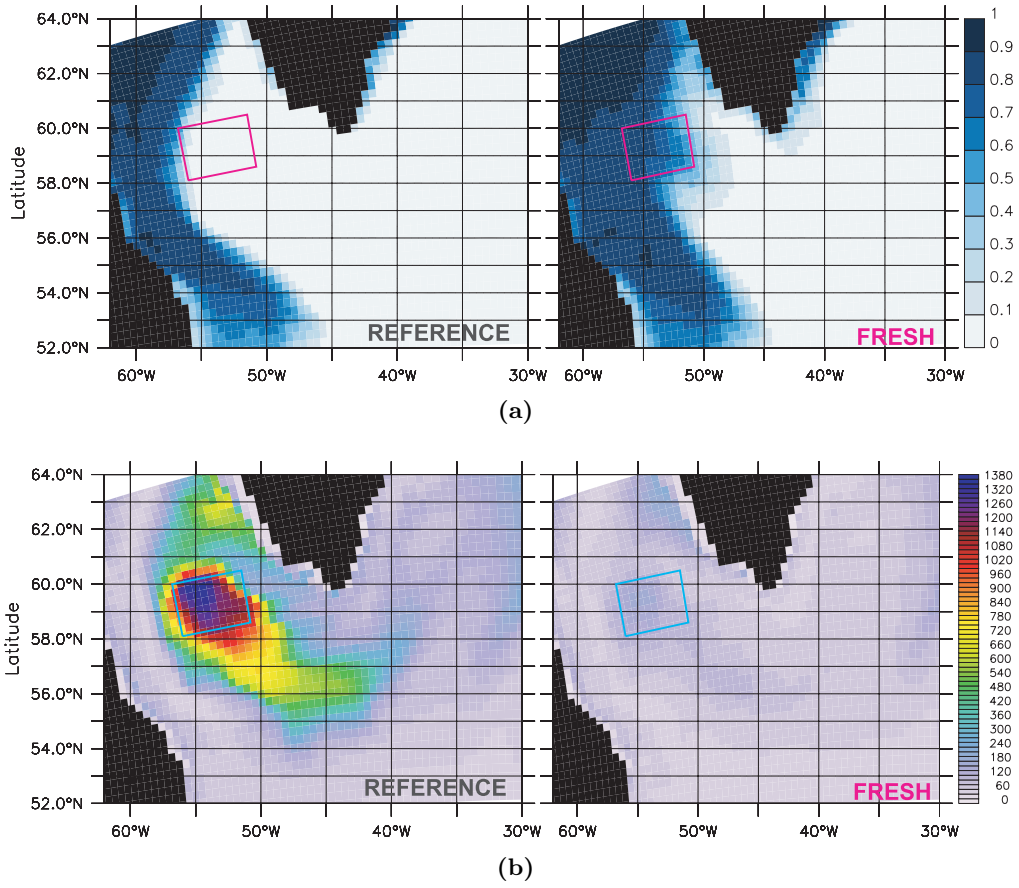

Figure 81 Simulated mean fields in the Labrador Sea for February 1972: (**a**) sea ice coverage for the REFERENCE case (left) and FRESH (right). (**b**) Map of mixed layer depth (same experiments as in (a)).

Since the Nordic Seas freshen excessively in FRESH (Fig. Fig. 35), also the Denmark Strait overflow density decreases (see figure 74) and the support for the deeper NADW reduces. Interestingly, it reaches similar low densities as in the REFERENCE .

The reaction of the Atlantic MOC maximum is shown in the upper panel of Fig. 82. There is a trend-like difference between FRESH and REFERENCE shown as linear regression with a slope of $62 mSv/yr$. This can be associated partially

with a reduced overflow (c.f. figure 74) while the difference (blue) between the detrended MOC (dashed green) and the reference MOC (solid black) represents the missing convective influence on the MOC. Its bandwidth of variability on interannual scales ($\approx 1.5Sv$) is very similar to the convective variations in HEAT and THERMHAL ($1-2Sv$). Thus, the additional freshwater induces a decline of the MOC, while the wind-driven interannual variability is preserved.

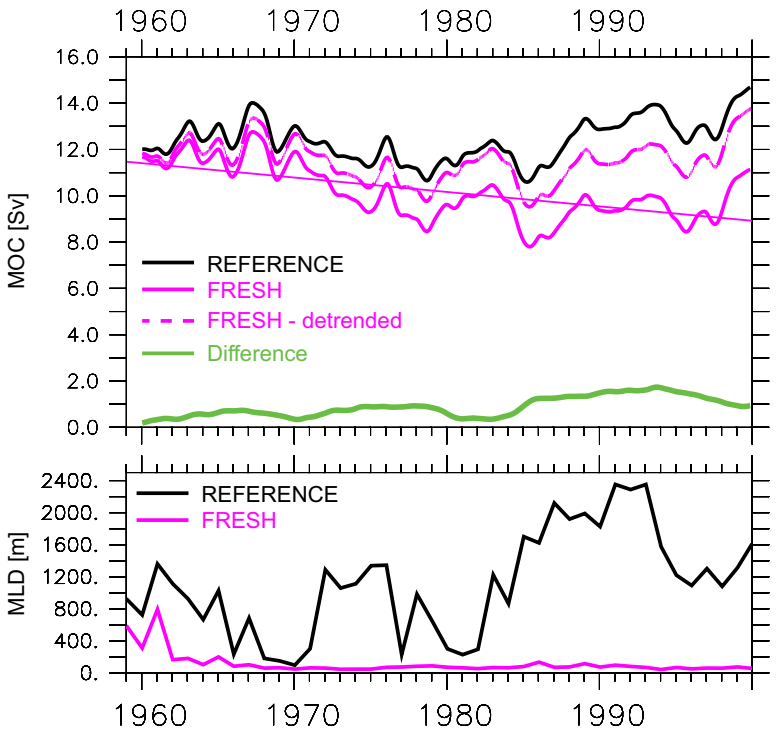

Figure 82 Time series of Atlantic MOC maximum at 36°N for the REFERENCE (black curve in the upper panel) and the FRESH (magenta) experiment. A linear trend (thin magenta line) is retrieved from the FRESH case and subtracted from the REFERENCE run resulting in a detrended MOC time series which can be understood as the remaining variability with the freshening effect (by the additional freshwater input in FRESH) removed (magenta dashed line). For the same two experiments, the winterly Labrador Sea MLD is shown in the lower panel (REFERENCE: black; FRESH: magenta). The disappearance of the deep convection in FRESH reverberates in the MOC where the difference (green, upper panel) between the detrended time series and the REFERENCE curve appears as the missing convection signal with typical decadal variation in phase with the NAO index.

7 Discussion and Conclusion

A freshwater budget for the Arctic and subpolar region has been established using a numerical ocean model, coupled with a sea ice model. In the following chapter, the results for the representation of sea ice and freshwater variability and the resulting freshwater transports and fluxes are summarized. Afterwards, the influence of the freshening on the deep water formation in the North Atlantic and its impact on the MOC is discussed. Finally a conclusion comprises the outcomes of this study.

7.1 Summary and Discussion

In this study, a freshwater budget for the northern North Atlantic and the Arctic has been established on the basis of numerical experiments with a global ocean-ice model forced by atmospheric conditions given by modified reanalysis products. Surprisingly, not the Arctic freshwater export was found to be the main contributor to subpolar freshwater content changes but the salinity exchange with the subtropical North Atlantic could explain most of the observed freshening. As driving mechanism for the exchange variability, the interannual wind stress variation in the westerlies has been identified.

a. Arctic sea ice

One part of the freshwater budget is the sea ice flux from the Arctic. Although the sea-ice simulation is based on a simple one-ice-category model, a comparison with observational data reveals a pretty good representation of the arctic mean ice extent as well as its seasonality and interannual variability. The ice coverage is discussed in terms of ice area which takes open ocean fractions, leads and polynias within the ice into account. The ice area simulated by the model concurs well with observations, which are retrieved from SSMI satellite data (GSFC, 2007) for the period 1978-2007. Even the long-term trend of the north polar ice area anomaly is present and very similar (observation: -53.0; simulation: -49.0$10^3 km^2/year$ for 1987-2000).
Since a weak relaxation of the water column towards the initial state is applied to the salinity and temperature in the arctic basins north of 67°N, the main hydrographic conditions like the arctic halocline remain close to observations over the course of the model integration. Mean ocean circulation as well as the mean sea ice drift in the Arctic (Beaufort Gyre and Transpolar Drift) are in accordance with observations, resulting in a realistic sea ice transport especially at Fram Strait with respect to drift velocity and volume flux. Observed sea ice area flux anomalies (Kwok and Rothrock, 1999), are also reproduced well, with a slight overestimation of the ice velocities in the early 1980ies and underestimation during the second half of the 80ies. Ice volume flux anomalies (Vinje, 2001), which represent the actual freshwater flux by sea ice much better, are reproduced likewise. Hence it can be assumed that the Artic ice transport and the associated freshwater export variability are simulated with sufficient realism to allow its use in the freshwater budget calculations.

b. Arctic freshwater budget

A comparison of the freshwater fluxes for each budget component with observational estimates (time mean and variability) reveals a good agreement, except for some differences in the liquid freshwater transport at Fram Strait using most recent measurements, while former estimates are closer to the simulated fluxes. In general, however, large uncertainties in these observations have to be accounted for, due to the relatively short time series. The difference in the freshwater formulation, namely different reference salinities, only play a minor part in this context.

In the nearly closed Arctic mean budget (less than 1% mismatch), the river and coastal runoffs (90 mSv) as well as the Bering Strait inflow (96 mSv) appear as the largest sources of freshwater. The export is distributed between Davis Strait (103 mSv) and across the Greenland-Scotland Ridge (105 mSv) in nearly equal shares. The budget thus reveals a near-balancing of the net surface flux, consisting of precipitation, evaporation and runoff, and the lateral exchange. This balancing is also found in the sensitivity experiments except for the FRESH run, where additional freshwater is put into the surface, leading to a drift in freshwater content no present in the other cases. The temporal evolution of the budget reveals a negligible net surface freshwater flux variability for all basins and experiments, compared to the much larger variations in the lateral fluxes.
The examination of interannual and interdecadal freshwater exchange variability reveals the wind stress as a main driver: The transport variability which appears in the sensitivity run WIND replicates the variability in the other experiments with interannual varying forcing, thus the freshwater transports are clearly related to the wind driven circulation, except for the Davis Strait where convection induced intensifications of the barotropic flow in the Labrador Sea additionally appears to affect the export.

c. Subpolar freshwater budget

The budget for the subpolar basin gives a similar picture. Though the net surface freshwater fluxes provide a contribution in the mean here, its variability has only a minor influence on the freshwater content change. This is in contrast to the inferences by Peterson et al. (2006) who suggested, using ERA-40 reanalysis products, the precipitation variability in the eastern basin to be a significant source for the SPG freshwater content changes. Apart from a possible contribution by a change

in the surface fluxes, Curry and Mauritzen (2005) advanced the hypothesis that large freshwater export anomalies from the north, e.g., those associated with the GSAs in the late 60s, 80s and 90s (Dickson et al., 1988), are a main source of the freshening between 1970 and 1995. In contrast, this study suggests an alternative explanation for the freshwater content changes: the simulated freshwater content variation, which fits the observational estimates by Curry and Mauritzen (2005) and Peterson et al. (2006) both regarding the amplitude and the timing, is determined primarily by freshwater flux variations in the south. First, as revealed by the regional experiment NONARCTIC without any interannual variability in the forcing fields north of 67°N, there is nearly the same freshwater content evolution as in the REFERENCE run. Second, the freshwater content variability in the Subpolar Gyre domain is to a large degree given by freshwater flux changes at the southern boundary (47°N) of this domain; more specifically the contribution from the south is much larger than the contribution from the north.

While observational estimates of freshwater flux changes across open ocean sections are not available, some consistency checks have been applied, e.g., to the magnitude of the northern source. In particular, the question of a possible underrepresentation of nordic freshwater intrusions can be alleviated by the apparently realistic simulation of the magnitude of GSA events, especially the one in the 1970s: the GSA70 is assumed to be generated by an increase in the sea ice export through the Fram Strait (Dickson et al., 1988); in REFERENCE the observed ice export, especially through Fram Strait, is captured quite realistically. The simulation allows to track the ensuing GSA throughout the Subpolar Gyre: while the shift in surface salinity north of Iceland (station S-3; Malmberg et al. (2001)) and in the West Greenland Current near Fylla Bank in the north eastern Labrador Sea appears reproduced in the simulation, it provides only limited evidence for a coherent advective signal beyond Denmark Strait; especially its appearance in the eastern basin and suspected return into the Nordic Seas cannot be identified clearly, reminiscent of the difficulties in the study by Dickson et al. (1988): the simulation suggests that the main reason for the GSA-signal to become blurred is that this nordic signal coincided with the appearance of low salinities in the NAC system coming from further south during that period.

The next GSA event during the 1980ies was discussed by Belkin et al. (1998) who located the origin of the freshening within the Labrador Sea. In the simulation it appears as recirculated freshwater within the SPG accompanied by an all-time maximum export of liquid freshwater through the Denmark Strait. Part of it ap-

pears to be caused by a decreased inflow of saline Atlantic water into the Nordic Seas in previous years, followed by an increase of the ice export at Fram Strait. The resulting increase of the freshwater content in the Nordic Seas is followed by a large freshwater export, an observational confirmation for such a signal at Denmark Strait is however lacking.
Another freshwater source for the GSA80 may be provided by the Davis Strait, as suggested by Houghton and Visbeck (2002), who analyzed observational records throughout the Labrador Sea. In the simulation, the increased freshwater transport at Davis is mainly caused by a preceeding freshening of the Baffin Bay due to a slight increase of liquid freshwater import through Nares Strait on one hand and an import of low saline waters by the WGC on the other hand. A concomitant strengthening of the SPG in the Labrador Sea during a strong positive NAO phase then contributes to the export of this freshwater, and subsequent negative salinity anomalies in the Labrador Sea.

For the third GSA during the 1990ies, Belkin (2004) proposed an increase of the freshwater export at Fram Strait again, now mainly involving the liquid freshwater. The simulation also reveals an increase in the freshwater flux, however mainly in the ice fraction. While the simulated ice volume flux anomalies at Fram Strait appear close to observations, especially in the 1990ies, the causes for the difference in the liquid freshwater transport remain unclear.

The most significant finding of the present study is that a much larger freshwater signal than the GSA events occurs at the southern boundary of the subpolar basin: the integration of the freshwater flux anomalies at that section (47°N) contributes the bulk of the freshwater content changes in the Subpolar Gyre. Hátún et al. (2005) already suggested a NAO-related mechanism in the eastern Subpolar Gyre to explain the inflow of anomalously saline waters into the Nordic Sea during the mid-1990ies. The present study extends and generalizes this idea to explain also the freshwater flux anomalies during former NAO phases: Under positive NAO conditions, the increased westerlies change the wind stress curl in such a way that there is a generation of positive vorticity in the northern Subpolar Gyre and negative vorticity in the inter-gyre regime between the SPG an the Subtropical Gyre. Thus both gyres strengthen and a southward velocity anomaly establishes in the West European Basin. The relevance of this wind stress curl driven mechanism is corroborated by a sensitivity experiment with wind stress as the only forcing component providing interannual variability: Is shows that the eastern freshwater flux variability depends on velocity variations. Owing to

this, the northward flow of saline waters is retarded, giving rise to a freshwater anomaly propagating northward, especially at depths of 500-1000m, i.e. in a layer, comprising subpolar mode waters and the upper part of Mediterranean Water. Simultaneously there is some weak increase in the freshwater import from the Nordic Seas into the Subpolar basin. The surplus of freshwater recirculates within the gyre to be eventually mixed down by winter convection, ultimately feeding the LSW layer. This deep water mass is able to partly leave the subpolar basin via the Deep Western Boundary Current which strengthen actually during positive NAO phases (Böning et al. (2006)) but it is by far not enough to remove the large positive freshwater anomaly in the SPG.
Under weak NAO conditions, the saline inflow is reestablished and enters the Subpolar Gyre via the NAC system (NAC core and east of it). This is supported by recent observational studies by Lozier and Stewart, (in press), who discuss the relation of Mediterranean Water inflow into the Subpolar Gyre in relation to the phase of the NAO index, and by Holliday et al. (2008) who found a signal of resalinification after 1990 propagating north along the European continental slope.

d. Deep water formation

The freshening of the Subpolar Gyre has a clear, but minor effect on the deep water formation. The deep convection in the Labrador Sea, as source for the upper NADW, is mainly governed by local surface fluxes; freshwater fluxes can increase or decrease the mixing depth for several hundreds of meters, which is shown by the MLD difference between the two sensitivity experiments HEAT and THERMHAL. A reduced Sea Surface Salinity (SSS) due to advective signals furthermore reduces the MLD in the early 1970ies, 1980ies and 1990ies. The freshening 1982-1984 clearly stands out here, because the lowest SSS during the simulated time frame is reached (similar to observations by Belkin et al. (1998)), which constricts the deep convection in such a way that the MLD only extends to mid-depths, although the NAO related heat flux cooling is strong. Without such a freshening a specific MLD peak appears in the early 1980s, e.g. in THERMHAL. It has to be noted, however, that the reduced convection in this case cannot be attributed only to GSA events originating from further north, because the southern freshwater exchange with the Subtropical Gyre and the local wind stress, acting on the ocean circulation and sea ice drift in the Labrador Sea, also play a significant role (not analyzed further in the present study).

The SPG freshening also affects the lower NADW, which is mainly fed by the dense overflow waters from the sills between the Subpolar basin and the Nordic Seas: The transport of the Denmark Strait Overflow Water (DSOW) is highly correlated with the deepest density on the sill. In the model simulation here, the density decreases between 1970 and 1985 due to a freshening which, because of the climatological relaxation conditions applied to the ocean north of the sills, has to be attributed to a freshening of the inflow of Atlantic Waters. These findings are in accordance with observations by Dickson et al. (2002), who reported on a similar reduction of the DSOW salinity from 34.93 to 34.87 in this period.

The freshening of the DSOW was invoked by Dickson et al. (2002) to explain the negative salinity trend in the abyssal Labrador Sea. Such a signal is also present in the REFERENCE run, shown there to be linked to the NAO-related freshwater flux variability at 47°N. Obviously, part of the freshwater imported within the upper 500m crosses the sills to enter the Nordic Seas, subsequently affecting the source waters of the overflows. With the overflows the salinity signal arrives in the deep western Subpolar Gyre after about 7 years, as suggested by the time lag between the NAO index and the evolution of the deep salinity, as demonstrated by observational data at Ocean Weather Ship Bravo in the southern Labrador Sea.

e. Meridional Overturning Circulation

As the freshwater content change in the SPG affects the deep water formation, this has also implications for the Atlantic MOC. Biastoch et al. (2008) show that the atmospherically forced variability of the Meridional Overturning Circulation (MOC) can be split into two parts: a wind-driven component contributing mainly to interannual variations and a thermohaline part accounting for longer-term changes.
Accordingly, the MOC in the sensitivity experiment HEAT, which includes interannual forcing variability only for heat fluxes, provides fluctuations on decadal time scales of about $\pm 1 - 2Sv$. This MOC variability can be attributed to the anomalies in the deep water formation by Labrador Sea Deep Convection, which are mainly associated with variability in winter cooling related to the NAO. When interannual variations in the surface freshwater fluxes are taken into account additionally (THERMHAL), the amplitude of decadal fluctuations in the MOC during deep convection phases increases ($\pm 2Sv$). The intensity of convection during

high NAO phases increases in this case because of higher SSS. In particular, the progressive intensification of the MOC between 1988 and 1995 appears related to continuous production of new LSW on a high level during this phase which, in this experiment, is stronger than in the companion case with climatological freshwater flux (HEAT). (Note that in this respect THERMHAL also differs from several previous model studies, which typically used a relatively strong restoring of SSS towards climatology.)

In contrast to the intra- and inter-decadal MOC variability due to thermohaline forcing anomalies, the wind field changes in WIND set up fluctuations on shorter timescales, as discussed by Biastoch et al. (2008, submitted). Apart from local effects of meridional Ekman transport variability, there is also a less obvious role of the wind stress through an indirect effect on the thermohaline processes in the subpolar region. During positive NAO phases, when the wind stress strengthens, deep convection is retarded due to fresher surface conditions (higher wind driven freshwater imports from north and south) and a larger ice extent due to the fact that the wind stress causes the sea ice to drift further offshore. As a result, less deep water is formed in the Labrador Sea and the barotropic gyre circulation weakens.

In the overflow water, the deep density at the Denmark Strait sill provides also a large interannual variability as well as a variation on inter- to multi-decadal timescales. The former is caused by local wind effects on the Strait while the latter is induced by a gradual freshening of the source water masses in the Arctic and subpolar region between 1970 and 1995. As already discussed above for the 47° section, this salinity decrease is mainly caused by the wind driven salt (or freshwater) exchange between the SPG and the STG.

The MOC variability in experiment REFERENCE can thus be understood as a composite of the sensitivity runs THERMHAL and WIND. The heat flux driven deep convection in the Labrador Sea is the main cause of decadal-to-interdecadal changes, while the wind stress variability mainly accounts for interannual variations in the MOC. Additionally, there is a decadal undulation in the overturning which can be attributed to the effect of wind-driven circulation changes on deep water formation, i.e., the effect of varying freshwater exchange between the Subtropical and the Subpolar Gyre : a decrease of salinities, for example, can weaken the winterly convection activity, which in turn results in a retarded LSW production and a less dense DSOW, combining to a reduced MOC.

How additional input of freshwater could weaken the MOC was examined by

the FRESH experiment. Similar to other 'hosing' experiments, which simulate melting multi-year sea ice and glaciers on land for climate warming scenarios, an auxiliary freshwater contribution (0.08 Sv north of 40°N) is put into the surface layer. The resulting fresher surface conditions suppress the deep convection and, in turn, support rising of sea ice production in the central Lab Sea within the first 3-4 years. The sea ice cap from then on effectively prevents deep convection, even during strong NAO phases, and lead to a MOC reduction of up to 1 Sv within the first 5 years. The additional freshwater recirculates within the upper layer of the gyre and enters the Nordic Seas, adding to the surface freshening which is occurring there. As the source water masses of the overflow water get freshened and lighter, the overflow density also reduces, additionally retarding the MOC by $\sim$ 3Sv after 10-12 years.

It has to be emphasized again that the freshwater-related variability exposed by the present set of experiments is mainly of a dynamical origin: Wind stress variability governs the water mass exchange between the Subtropical and Subpolar Gyre and thus accounts for variations in the poleward salt transport in the upper layer. The wind fluctuations also drive the Arctic sea ice export variability and thus the smaller freshwater intrusions from the north. The wind stress is therefore the most important trigger for freshwater variability in the SPG on a broad range of time scales.

7.2 Conclusion

In this study, causes and implications of the observed multi-decadal changes of the freshwater content in the subpolar North Atlantic are investigated. For this purpose the components of the freshwater budget are examined using simulational data generated with a global ocean model. It has a horizontal resolution of about 36km at 60°N and is coupled with a viscous-plastic sea-ice model. At the surface, fluxes for heat, freshwater and wind stress are prescribed by the CORE forcing formulation for the period 1958-2000. Beside a reference (hindcasting) run with most realistic forcing conditions, i.e. all components are varying interannually, several sensitivity experiments have been conducted with different combinations of climatological and interannually varying forcing fields. The model output allows investigations of the relative role of three components that can change the freshwater content in the subpolar basin: the net surface freshwater flux, the exchange of freshwater with the Nordic Seas and the exchange of freshwater with the Subtropical Gyre (STG).

In summary, this model study suggests a new and alternative explanation for the observed freshwater content changes in the northern North Atlantic, where the primary source is attributed to the wind-driven variability of the salt exchange between the Subpolar Gyre (SPG) and the STG. Series of sensitivity experiments reveal that the change of salty inflow by the North Atlantic Current (NAC) and in the eastern basin account for the largest freshwater signals, while subarctic freshwater export variations only play a secondary role. It also suggests that the major freshwater signals in the various parts of the northern North Atlantic, i.e. the surface layers, the deep salinity trends at Ocean Weather Ship Bravo, and at least part of the salinity decline of the overflow, can all be traced to this main mechanism, triggered by the long-term variability of the mid-latitude westerlies associated with the NAO.

Despite the magnitude of the freshening during the 1970-1990, its effect on the Meridional Overturning Circulation (MOC) was only about 1Sv at 36°N. This mainly results from a slight weakening of the deep water formation: first, Labrador Sea Deep Convection, which is mainly driven by winterly surface heat flux cooling, is reduced in the presence of fresher surface conditions. Successively, the overflow density, foremost of Denmark Strait Overflow Water (DSOW), decreases as the Nordic Seas freshens due to a reduced salt inflow, thus leading to a reduced outflow of dense DSOW.

Because of the time lag of O(7 years) between the NAO-related northward influx of freshwater/salt from the STG, the freshening of the Nordic Seas, and thus, of the overflows, there appears some potential for a predictability of part of (multi-)decadal MOC changes. Specifically, the currently observed "reversal" of the freshening trend between the 1960s and 1990s in the eastern North Atlantic (Holliday et al., 2008) will in the next years contribute to a salinifcation in the Nordic Seas and, in turn, of the overflows; these changes can thus be expected to represent a factor which contribute to an increase in the MOC. It has to be noted though that this factor is secondary in importance to the local buoyancy fluxes in the Labrador Sea. The potential gain in MOC predictability thus needs to be investigated further.

Bibliography

Aargaard, K. and Carmack, E. C. (1989). The Role of the Sea Ice and other Fresh-Water in the Arctic Circulation. *Journal of Geophysical Research-Oceans*, 94(C10):14485–14498. 6, 44, 66, 88, 89, 90

Aargaard, K., Fahrbach, E., Meincke, J., and Swift, J. H. (1991). Saline Outflow From The Arctic-Ocean - Its Contribution To The Deep Waters Of The Greenland, Norwegian, And Iceland Seas. *Journal of Geophysical Research-Oceans*, 96(C11):20433–20441. 3

Adcroft, A., Hill, C., and Marshall, J. (1997). Representation of topography by shaved cells in a height coordinate ocean model. *Monthly Weather Review*, 125(9):2293–2315. 15

Antonov, J., Levitus, S., Boyer, T., Conkright, M., O'Brien, T., and Stephens, C. (1998). *World Ocean Atlas 1998 Vol. 1: Temperature of the Atlantic Ocean.* U.S. Government Printing Office, Washington, D.C. 32, 81

Arakawa, A. and Lamb, V. (1977). Computational Design of the Basic Dynamical Processes of the UCLA General Circulation Model. *Methods in Computational Physics*, 17:174–267. 14, 18

Arctic Climatology Project (1997). Environmental Working Group joint U.S.-Russian atlas of the Arctic Ocean - winter period. In Timokhov, L. and F. Tanis. Ann Arbor, M., editors, *Environmental Research Institute of Michigan in association with the National Snow and Ice Data Center. CD-ROM.* Environmental Research Institute of Michigan in association with the National Snow and Ice Data Center. CD-ROM. 32

Arctic Climatology Project (1998). Environmental Working Group joint U.S.-Russian atlas of the Arctic Ocean - summer period. In Timokhov, L. and F. Tanis. Ann Arbor, M., editors, *Environmental Research Institute of Michigan in association with the National Snow and Ice Data Center. CD-ROM.* Environmental Research Institute of Michigan in association with the National Snow and Ice Data Center. CD-ROM. 32

Avsic, T., Karstensen, J., Send, U., and Fischer, J. (2006). Interannual variability of newly formed Labrador Sea Water from 1994 to 2005. *Geophysical Research Letters*, 33(21):L21S02. 3

Barnier, B., Madec, G., Penduff, T., Molines, J.-M., Treguier, A.-M., Le Sommer, J., Beckmann, A., Biastoch, A., Böning, C., Dengg, J., Derval, C., Durand, E., Gulev, S., Remy, E., Talandier, C., Theetten, S., Maltrud, M., McClean, J., and De Cuevas, B. (2006). Impact of partial steps and momentum advection schemes in a global ocean circulation model at eddy-permitting resolution. *Ocean Dynamics*, 56(5):543–567. 15

Baumgartner, A. and Reichel, E. (1975). *The world water balance*. Elsevier. 35

Beckmann, A. and Birnbaum, G. (2001). Coupled Sea Ice-ocean Models. In Steele, J. H., editor, *Encyclopedia of Ocean Sciences*, pages 560–570. Academic Press, Oxford. 26

Beismann, J.-O. and Barnier, B. (2004). Variability of the meridional overturning circulation of the North Atlantic: sensitivity to overflows of dense water masses. *Ocean Dynamics*, 54(1):92–106. 110

Belkin, I. M. (2004). Propagation of the "Great Salinity Anomaly" of the 1990s around the northern North Atlantic. *Geophysical Research Letters*, 31(8):L08306. 4, 6, 8, 9, 89, 94, 125

Belkin, I. M., Levitus, S., Antonov, J., and Malmberg, S. A. (1998). "Great Salinity Anomalies" in the North Atlantic. *Progress In Oceanography*, 41(1):1–68. 4, 6, 9, 89, 92, 94, 124, 126

Bersch, M., Yashayaev, I., and Koltermann, K. (2007). Recent changes of the thermohaline circulation in the subpolar North Atlantic. *Ocean Dynamics*, 57(3):223–235. 103

Biastoch, A., Böning, C. W., Getzlaff, J., Molines, J.-M., and Madec, G. (2008). Causes of interannual-decadal variability in the meridional overturning circulation of the mid-latitude North Atlantic Ocean. submitted to Journal of Climate. 112, 127, 128

Bindoff, N., Willebrand, J., Artale, V., Cazenave, A., Gregory, J., Gulev, S., Hanawa, K., Le Quéré, C., Levitus, S., Nojiri, Y., Shum, C., Talley, L., and Unnikrishnan, A. (2007). Observations: Oceanic Climate Change and Sea Level. In Solomon, S., Qin, D., Manning, M., Chen, Z., Marquis, M., Averyt, K., Tignor, M., and Miller, H., editors, *Climate Change 2007: The Physical Science Basis. Contribution of Working Group I to the Fourth Assessment Report of the Intergovernmental Panel on Climate Change*. Cambridge University Press,. 2

Blindheim, J., Borovkov, V., Hansen, B., Malmberg, S.-A., Turrell, W., and Osterhus, S. (2000). Upper layer cooling and freshening in the Norwegian Sea in relation to atmospheric forcing. *Deep Sea Research Part I: Oceanographic Research Papers*, 47(4):655–680. 4, 89

Blindheim, J. and Østerhus, S. (2005). *The Nordic Seas: An Integrated Perspective*, volume 158 of *AGU Monograph 158*, chapter The Nordic Seas, main oceanographic features, pages 11–38. American Geophysical Union, Washington DC. 56

Böning, C. W., Scheinert, M., Dengg, J., Biastoch, A., and Funk, A. (2006). Decadal variability of subpolar gyre transport and its reverberation in the North Atlantic overturning. *Geophysical Research Letters*, 33(21):L21S01. 80, 126

Boyer, T., Levitus, S., Antonov, J., Conkright, M., O'Brien, T., and Stephens, C. (1998). *World Ocean Atlas 1998 Vol. 4: Salinity of the Atlantic Ocean*. U.S. Government Printing Office, Washington, D.C. 32, 37, 81

Boyer, T., Levitus, S., Antonov, J., Locarnini, R., Mishonov, A., Garcia, H., and Josey, S. A. (2007). Changes in freshwater content in the north atlantic ocean 1955-2006. *Geophysical Research Letters*, 34(16):L16603. 44, 86, 87, 105, 106

Brandt, P., Schott, F., Funk, A., and Martins, C. (2004). Seasonal to interannual variability of the eddy field in the Labrador Sea from satellite altimetry. *Journal of Geophysical Research-Oceans*, 109(C2). 92

Brewer, P., Broecker, W., Jenkins, W., Rhines, P., Rooth, C., Swift, J., Takahashi, T., and Willimas, R. (1983). A Climatic Freshening of the Deep Atlantic North of 50° N over the Past 20 Year. *Science*, 222(4629):1237–1239. 4, 6

Brodeau, L. and Barnier, B. (2006). DRAKKAR Forcing set 3. in prep. 35

Carmack, E. (1990). *Polar oceanography. Part A: physical science.*, chapter Large-

Scale Physical Oceanography of the Polar Oceans. Academic Press, San Diego, CA. 3

Cavalieri, D. (2002). A link between Fram Strait sea ice export and atmospheric planetary wave phase. *Geophysical Research Letters*, 29(12). 62

Chen, M., Xie, P., Janowiak, J., and Arkin, P. (2002). Global land precipitation: A 50-yr monthly analysis based on gauge observations. *Journal of Hydrometeorology*, 3(3):249–266. 33

Cohen, J., Cohen, P., West, S. G., and Aiken, L. S. (2003). *Applied Multiple Regression/Correlation Analysis for the Behavioral Sciences*. Lawrence Erlbaum Associates, 3rd edition. 49

Conkright, M., Antonov, J., Baranova, O., Boyer, T., Garcia, H., Gelfeld, R., Johnson, D., Locarnini, R., Murphy, P., O'Brien, T., et al. (2002). World Ocean Database 2001, Volume 1: Introduction. *NOAA Atlas NESDIS*, 42. 32, 86

Cox, M. (1987). Isopycnal diffusion in a z-coordinate ocean model. *Ocean Modelling*, 74:1–5. 16

Cuny, J., Rhines, P. B., and Kwok, R. (2005). Davis Strait volume, freshwater and heat fluxes. *Deep-Sea Research Part I-Oceanographic Research Papers*, 52(3):519–542. 47, 67

Curry, R. and Mauritzen, C. (2005). Dilution of the northern North Atlantic Ocean in recent decades. *Science*, 308(5729):1772–1774. 8, 10, 83, 84, 85, 86, 88, 124

Curry, R. G. and McCartney, M. S. (2001). Ocean gyre circulation change associated with the north atlantic oscillation. *Journal Of Physical Oceanography*, 31:3374–3400. 80, 81

Curry, R. G., McCartney, M. S., and Joyce, T. M. (1998). Oceanic transport of subpolar climate signals to mid-depth subtropical waters. *Nature*, 391(6667):575–577. 3, 4, 80

Dai, A. G. and Trenberth, K. E. (2002). Estimates of freshwater discharge from continents: Latitudinal and seasonal variations. *Journal of Hydrometeorology*, 3(6):660–687. 35, 36

Dell'Aquila, A., Lucarini, V., Ruti, P., and Calmanti, S. (2005). Hayashi spectra of the northern hemisphere mid-latitude atmospheric variability in the NCEP-NCAR and ECMWF reanalyses. *Climate Dynamics*, 25(6):639–652. 34

Dengler, M., Fischer, J., Schott, F. A., and Zantopp, R. (2006). Deep labrador current and its variability in 1996-2005. *Geophysical Research Letters*, 33(21):L21S06. 79

Dickson, A. R., Meincke, J., Malmberg, S.-A., and Lee, A. J. (1988). The "Great Salinity Anomaly" in the Northern North Atlantic 1968-1982. *Progress in Oceanography*, 20:103–151. 4, 6, 7, 8, 9, 61, 89, 90, 92, 124

Dickson, B., Yashayaev, I., Meincke, J., Turrell, B., Dye, S., and Holfort, J. (2002). Rapid freshening of the deep North Atlantic Ocean over the past four decades. *Nature*, 416(6883):832–837. 4, 7, 9, 105, 127

Dickson, R., Rudels, B., Dye, S., Karcher, M., Meincke, J., and Yashayaev, I. (2007). Current estimates of freshwater flux through Arctic and subarctic seas. *Progress in Oceanography*, 73(3-4):210–230. 44, 56, 66, 67, 151

Eden, C. and Willebrand, J. (2001). Mechnism of Interannual to Decadal Variability of the North Atlantic Circulation. *Journal Of Climate*, 14:2266–2280. 110

Efthymiadis, D., New, M., and Washington, R. (2005). On the reconstruction of seasonal oceanic precipitation in the presatellite era. *Journal of Geophysical Research, Atmosphere*, 110(D6). 33, 34

Eldevik, T., Straneo, F., Sandø, A., and Furevik, T. (2005). *The Nordic Seas: An integrated perspective*, volume 158 of *AGU Monograph 158*, chapter Pathways and export of Greenland Sea Water, pages 89–104. American Geophysical Union, Washington DC. 56

Environment Canada (2008). Climate data online. National Climate Data and Information Archive. 86

ETOPO5 (1988). Data Announcement 88-MGG-02, Digital relief of the Surface of the Earth. NOAA. http://www.ngdc.noaa.gov/mgg/global/. National Geophysical Data Center, Boulder, Colorado. 15

Falina, A., Sarafanov, A., and Sokov, A. (2007). Variability and renewal of Labrador Sea Water in the Irminger Basin in 1991-2004. *Journal Of Geophysical Research-Oceans*, 112(C1):C01006. 3, 109

Fichefet, T. and Morales Maqueda, M. (1997). Sensitivity of a global sea ice model to the treatment of ice thermodynamics and dynamics. *Journal of Geophysical Research*, 102(C6):12,609–12,646. 14, 17, 19, 24, 26

Ganachaud, A. and Wunsch, C. (2000). Improved Estimates of global ocean circulation, heat transport and mixing from hydrographic data. *Nature*, 408:453–457. 2

Ganachaud, A. and Wunsch, C. (2003). Large-scale ocean heat and freshwater transports during the World Ocean Circulation Experiment. *Journal Of Climate*, 16(4):696–705. 2

Gent, P. and McWilliams, J. (1990). Isopygnal Mixing in ocean circulation models. *Journal of Physical Oceanography*, 20:150–155. 16

Gerdes, R., Hurka, J., Karcher, M., Kauker, F., and Koeberle, C. (2005). Simulated history of convection in the Greenland and Labrador seas, 1948-2001. In *The Nordic Seas: an integrated perspective: oceanography, climatology, biogeochemistry, and modeling*, volume vol. 158 of *Geophysical monograph (Geophys. monogr.)*, pages 221–238. American Geophysical Union, Washington, DC. 9, 10

Gerdes, R., Hurlin, W., and Griffies, S. M. (2006). Sensitivity of a global ocean model to increased run-off from Greenland. *Ocean Modelling*, 12(3-4):416–435. 10, 117

Gill, A. E. (1982). *Atmosphere-Ocean Dynamics,*. Academic Press, New York. 104

Goosse, H., Campin, J.-M., Deleersnijder, E., Fichefet, T., Mathieu, P.-P., Maqueda, M. A. M., and Tartinville, B. (1999). Description of the CLIO model version 3.0. Technical report, Institut d'Astronomie et de Géophysique Georges Lemaître, Belgique. 17, 22

GRDC (2004a). Global Runoff Data Center: Comparisons of GRDC freshwater flux estimate with literature. 35

GRDC (2004b). Global Runoff Data Center, Long Term Mean Annual Freshwater Surface Water Fluxes into the World Oceans: Runoff Estimates. 35

GSFC (2007). Goddard Space Flight Center (GSFC) Sea Ice Extent from Satellite (SSMI) using the NASA Team Algorithm. http://nsidc.org/data/smnr_ssmi_ancillary/area_extent.html. 58, 59, 60, 122

Haak, H., Jungclaus, J., Mikolajewicz, U., and Latif, M. (2003). Formation and propagation of great salinity anomalies. *Geophysical Research Letters*, 30(9):1473. 10

Haine, T., Boening, C., Brandt, P., Fischer, J., Funk, A., Kieke, D., Kvaleberg, E., Rhein, M., and Visbeck, M. (2008). *Arctic-subarctic Ocean Fluxes: Defining the Role of the Northern Seas in Climate*, chapter (27) North Atlantic Deep Water transformation in the Labrador Sea, recirculation through the subpolar gyre, and discharge to the Subtropics., pages 653–701. Springer. 3, 79

Häkkinen, S. (1993). An Arctic Source For The Great Salinity Anomaly - A Simulation Of The Arctic Ice-Ocean System For 1955-1975. *Journal Of Geophysical Research-Oceans*, 98(C9):16397–16410. 6

Häkkinen, S. (1999). A simulation of thermohaline effects of a great salinity anomaly. *Journal of Climate*, 12(6):1781–1795. 10

Häkkinen, S. (2002a). Freshening of the Labrador Sea surface waters in the 1990s: Another great salinity anomaly? *Geophysical Research Letters*, 29(24):2232. 7

Häkkinen, S. (2002b). Surface salinity variability in the northern North Atlantic during recent decades. *Journal of Geophysical Research-Oceans*, 107(C12):8003. 7

Häkkinen, S. and Proshutinsky, A. (2004). Freshwater content variability in the Arctic Ocean. *Journal of Geophysical Research*, 109(C03051):1–17. 55

Häkkinen, S. and Rhines, P. B. (2004). Decline of Subpolar North Atlantic Circulation During the 1990s. *Science*, 304:555–559. 8, 80, 99, 100

Hansen, B. and Osterhus, S. (2000). North Atlantic-Nordic Seas exchanges. *Progress In Oceanography*, 45(2):109–208. 2

Hátún, H., Sandø, A., Drange, H., Hansen, B., and Valdimarsson, H. (2005). Influence of the Atlantic subpolar gyre on the thermohaline circulation. *Science*, 309(5742):1841–1844. 8, 9, 99, 125

Hernandez, A., Kelly, G., and Uppala, S. (2004). The tovs/atovs observing system in era-40. *ERA -40 Project Report Series*, 16. 33

Hibler, W. (1979). A Dynamic Thermodynamic Sea Ice Model. *Journal of Physical Oceanography*, 9:815–846. 25, 26, 27, 28

Hibler, W. (1980). *Dynamics of Snow and Ice Masses*, chapter Sea ice growth, drift and decay, pages 141–209. Academic Press. 26

Hibler, W. and Walsh, J. (1980). On Modeling Seasonal and Interannual Fluctuations of Arctic Sea Ice. *Journal of Physical Oceanography*, 12(12):1514–1523. 27, 28

Holfort, J., Hansen, E., Østerhus, S., Dye, S., Jonsson, S., Meincke, J., Mortensen, J., and Meredith, M. (2008). *Arctic-subarctic Ocean Fluxes: Defining the Role of the Northern Seas in Climate*, chapter (11) Freshwater Fluxes East of Greenland, pages 653–701. Springer. 44

Holliday, N. P., Hughes, S. L., Bacon, S., Beszczynska-Moeller, A., Hansen, B., Lavin, A., Loeng, H., Mork, K. A., Osterhus, S., Sherwin, T., and Walczowski, W. (2008). Reversal of the 1960s to 1990s freshening trend in the northeast North Atlantic and Nordic Seas. *Geophysical Research Letters*, 35(3). 9, 126, 131

Hoppe, H. and Kiely, G. (1999). Precipitation over Ireland - Observed change since 1940. *Physics and Chemistry of the Earth Part B-Hydrology Oceans and Atmosphere*, 24(1-2):91–96. 86

Houghton, R. W. and Visbeck, M. H. (2002). Quasi-decadal salinity fluctuations in the Labrador Sea. *Journal Of Physical Oceanography*, 32(2):687–701. 6, 9, 94, 125

Hourdin, F. and Armengaud, A. (1999). The use of finite-volume methods for atmospheric advection of trace species. Part I: Test of various formulations in a general circulation model. *Monthly Weather Review*, 127(5):822–837. 16

Howell, D. C. (1992). *Statistical Methods for Psychology*. Duxburry Press, 3rd edition. 49

Huesmann, A. and Hitchman, M. (2003). The 1978 shift in the NCEP reanalysis stratospheric quasi-biennial oscillation. *Geophysical Research Letters*, 30(2). 33, 34

Hurrell, J. W. (1995). Decadal Trends In The North-Atlantic Oscillation - Regional Temperatures And Precipitation. *Science*, 269(5224):676–679. 3, 4

ICES (2007). International Council for the Exploration of the Sea: Oceanographic Database and Services. http://www.ices.dk/ocean/. 8, 104

IHO (1953). Limits of oceans and seas, special publication 23. published by the International Hydrographic Organization. 52

Johnson, H. L. and Marshall, D. P. (2002). Localization of aprupt change in the North Atlantic thermohaline circulation. *Geophysical Research Letters*, 29(10):7.1–7.4. 2, 9

Jonsson, S. and Valdimarsson, H. (2004). A new path for the Denmark strait

overflow water from the Iceland Sea to Denmark Strait. *Geophysical Research Letters*, 31(3):L03305. 2, 3, 56

Josey, S. A. and Marsh, R. (2005). Surface freshwater flux variability and recent freshening of the North Atlantic in the eastern subpolar gyre. *Journal of Geophysical Research-Oceans*, 110(C5):C05008. 7, 8, 86

Jungclaus, J. H., Haak, H., Esch, M., Roeckner, E., and Marotzke, J. (2006). Will Greenland melting halt the thermohaline circulation? *Geophysical Research Letters*, 33(17):L17708. 10

Kalnay, E., Kanamitsu, M., Kistler, R., Collins, W., Deaven, D., Gandin, L., Iredell, M., Saha, S., White, G., Woollen, J., et al. (1996). The NCEP/NCAR 40-Year Reanalysis Project. *Bulletin of the American Meteorological Society*, 77(3):437–471. 33, 34, 35, 86

Kantha, L. H. and Clayson, C. A. (2000). *Numerical Models of Oceans and Oceanic Processes*, volume 66 of *International Geophysics Series*. Academic Press. 32

Kara, A. B., Rochford, P. A., and Hurlburt, H. E. (2000). Efficient and Accurate Bulk Parameterizations of Air-Sea Fluxes for Use in General Circulation Models. *Journal of Atmospheric and Oceanic Technology*, 17(10):1421–1438. 32

Karcher, M., Gerdes, R., Kauker, F., Koberle, C., and Yashayaev, I. (2005). Arctic Ocean change heralds North Atlantic freshening. *Geophysical Research Letters*, 32(21):L21606. 6

Käse, R. H. and Oschlies, A. (2000). Flow through Denmark Strait. *Journal Of Geophysical Research-Oceans*, 105(C12):28527–28546. 3

Kieke, D., Rhein, M., Stramma, L., Smethie, W. M., LeBel, D. A., and Zenk, W. (2006). Changes in the CFC inventories and formation rates of Upper Labrador Sea Water, 1997-2001. *JPO*, 36(1):64–86. 3

Killworth, P. D. (1983). Deep Convection In The World Ocean. *Reviews Of Geophysics*, 21(1):1–26. 3

Kwok, R. and Rothrock, D. A. (1999). Variability of Fram Strait ice flux and North Atlantic Oscillation. *Journal of Geophysical Research-Oceans*, 104(C10):23615–23615. 60, 61, 62, 122

Large, W. and Yeager, S. (2004). Diurnal to decadal global forcing for ocean and sea-ice models: the data sets and flux climatologies. Technical Note TN-

460+STR, NCAR, P.O. Box 3000 Boulder, Colorado 80307. 5, 6, 32, 33, 34, 35, 38

Latif, M., Böning, C., Willebrand, J., Biastoch, A., Dengg, J., Keenlyside, N., Schweckendiek, U., and Madec, G. (2006). Is the Thermohaline Circulation Changing? *Journal of Climate*, 19(18):4631–4637. 3, 4, 104

Lazar, A. (1997). *La branche froide de la circulation thermohaline: sensibilité à la diffusion turbulente dans un modèle de circulation générale idéalisée*. Thèse, l'Université Pierre et Marie Curie, Paris, France. 16

Lazier, J. (1995). *Natural Climate Variability on Decade-to-Century Time Scales*, chapter (3) The salinity decrease in the Labrador Sea over the past thirty years, pages 295–305. National Academy Press. 92

Lazier, J., Hendry, R., Clarke, A., Yashayaev, I., and Rhines, P. (2002). Convection and restratification in the Labrador Sea, 1990-2000. *Deep-Sea Research Part I-Oceanographic Research Papers*, 49(10):1819–1835. 9

Lazier, J. R. (1980). Oceanographic conditions at ocean weather ship Bravo, 1964-1974. *Atmos.-Ocean.*, 18:227–238. 3, 4, 9, 92

Lippsett, L. (2005). Is global warming cahnging the Arctic? *Oceanus Magazin*, 44(3):24–35. 16, 53, 56

Lozier, M. and Stewart, N. M. (in press). On the temporally-varying northward penetration of mediterranean overflow waters and eastward penetration of labrador sea waters. 126

Macrander, A. (2004). *Variability and prcesses of the Denmark Strait overflow*. PhD thesis, University of Kiel. 3

Macrander, A., Send, U., Valdimarsson, H., Jonsson, S., and Kase, R. H. (2005). Interannual changes in the overflow from the nordic seas into the atlantic ocean through denmark strait. *Geophysical Research Letters*, 32(6):L06606. 2

Madec, G. (2007). NEMO, the ocean engine. Notes de l'IPSL B102T15-E5, Université P. et M. Currie, 4 place Jissieu, Paris cedex 5. En préparation. 14, 15

Madec, G., Delecluse, P., Imbard, M., and Levy, C. (1998). OPA 8.1 Ocean General Circulation Model. Reference manual, Institut Pierre Simon Laplace (LODYC). 14, 16

Madec, G. and Imbard, M. (1996). A global ocean mesh to overcome the North Pole singularity. *Climate Dynamics*, 12(6):381–388. 14

Malmberg, S.-A. and Désert, J. (1999). Hydrographic conditions in North Icelandic waters and annual air temperature in Iceland. ICES Council Meeting 1999 L:14. 89, 90

Malmberg, S.-A., Mortensen, J., and Jónsson, S. (2001). Oceanic fluxes in Icelandic waters. In *ICES Annual Science Conference*, number ICES CM 2001/W:08. 91, 124

Mariotti, A. and Arkin, P. (2007). The north atlantic oscillation and oceanic precipitation variability. *Climate Dynamics*, 28(1):35–51. 33

Marshall, J., Johnson, H., and Goodman, J. (2001). A study of the interaction of the North Atlantic oscillation with ocean circulation. *Journal Of Climate*, 14(7):1399–1421. 3, 102

Marshall, J. and Schott, F. (1999). Open-Ocean Convection: Observations, Theory, and Models. *Reviews of Geophysics*, 37(1):1–64. 3, 108

Martin, T. and Gerdes, R. (2006). Sea ice drift variability in AOMIP models and observations. draft. 54

Mauritzen, C. and Häkkinen, S. (1997). Influence of sea ice on the thermohaline circulation in the Arctic-North Atlantic Ocean. *Geophysical Research Letters*, 24(24):3257–3260. 10

McBean, G., Alekseev, G., Chen, D., Førland, E., Fyfe, J., Groisman, P. Y., King, Roger Melling, H., Vose, R., and Whitfield, P. H. (2005). *Arctic Climate Impact Assessment - Scientific Report*, chapter Arctic Climate: Past and Present, pages 21–60. Cambridge University Press. 16, 27, 52, 55

McCartney, M. S. and Talley, L. D. (1984). Warm-To-Cold Water Conversion In The Northern North-Atlantic Ocean. *Journal Of Physical Oceanography*, 14(5):922–935. 3

McPhee, M. G. (1992). Turbulent Heat-Flux In The Upper Ocean Under Sea Ice. *Journal Of Geophysical Research-Oceans*, 97(C4):5365–5379. 30

McPhee, M. G., Maykut, G. A., and Morison, J. H. (1987). Dynamics And Thermodynamics Of The Ice Upper Ocean System In The Marginal Ice-Zone Of The Greenland Sea. *Journal Of Geophysical Research-Oceans*, 92(C7):7017–7031. 29, 30

Meier, W., Stroeve, J., and Fetterer, F. (2007). Whither Arctic sea ice? A clear signal of decline regionally, seasonally and extending beyond the satellite record. *Annals of Glaciology*, 46:428–434. 60

Mellor, G. L. and Kantha, L. (1989). An ice-ocean coupled model. *Journal of Geophysical Research-Oceans*, 94(C8):10937–10954. 19

Meredith, M., Heywood, K., Dennis, P., Goldson, L., White, R., Fahrbach, E., Schauer, U., and Osterhus, S. (2001). Freshwater fluxes through the western Fram Strait. *Geophysical Research Letters*, 28(8):1615–1618. 66

Molines, J., B., B., Penduff, T., Brodeau, L., Treguier, A., Theetten, S., and Madec, G. (2006). Definition of the interannual experiment ORCA025-G70, 1958-2004. Report LEGI-DRA-2-11-2006i, LEGI. 35

Mysak, L. A. (2001). Oceanography - Patterns of Arctic circulation. *Science*, 293(5533):1269–1270. 55

Münchow, A., Melling, H., and Falkner, K. K. (2006). An Observational Estimate of Volume and Freshwater Flux Leaving the Arctic Ocean through Nares Strait. submitted to J. Phys. Oceanogr.; revised. 67

NSIDC (2007). Arctic Sea Ice Shatters All Previous Record Lows. Press Release. 60

Orsi, A., Johnson, G., and Bullister, J. (1999). Circulation, mixing, and production of Antarctic Bottom Water. *Progress in Oceanography*, 43(1):55–109. 3

Overland, J. and Pease, C. (1988). Modeling ice dynamics of coastal seas. *Journal of Geophysical Research*, 93(C12):15619–15637. 26, 27, 28

Peterson, B. J., McClelland, J., Curry, R., Holmes, R. M., Walsh, J. E., and Aagaard, K. (2006). Trajectory shifts in the Arctic and subarctic freshwater cycle. *Science*, 313(5790):1061–1066. 8, 83, 85, 123, 124

Peterson, T. and Vose, R. (1997). An overview of the global historical climatology network temperature database. *Bulletin of the American Meteorological Society*, 78(12):2837–2849. 33

Pickart, R. S., Spall, M. A., Ribergaard, M. H., Moore, G. W. K., and Milliff, R. F. (2003a). Deep convection in the Irminger Sea forced by the Greenland tip jet. *Nature*, 424(6945):152–156. 3, 109

Pickart, R. S., Straneo, F., and Moore, G. (2003b). Is Labrador Sea Water formed in the Irminger basin? *Deep-Sea Research I*, 50:23–52. 3, 109

Pickart, R. S., Torres, D. J., and Clarke, R. A. (2002). Hydrography of the labrador sea during active convection. *Journal Of Physical Oceanography*, 32:428–457. 79

Poccard, I., Janicot, S., and Camberlin, P. (2000). Comparison of rainfall structures between NCEP/NCAR reanalyses and observed data over tropical Africa. *Climate Dynamics*, 16(12):897–915. 34

Proshutinsky, A., Bourke, R. H., and McLaughlin, F. A. (2002). The role of the Beaufort Gyre in Arctic climate variability: Seasonal to decadal climate scales. *Geophysical Research Letters*, 29(23):2100. 55

Proshutinsky, A. Y. and Johnson, M. (2001). Two regimes of the Arctic's circulation from ocean models with ice and contaminants. *Marine Pollution Bulletin*, 43(1-6):61–70. 54

Quadfasel, D., Gascard, J. C., and Koltermann, K. P. (1987). Large-Scale Oceanography In Fram Strait During The 1984 Marginal Ice-Zone Experiment. *Journal Of Geophysical Research-Oceans*, 92(C7):6719–6728. 3

Read, J. F. and Gould, W. J. (1992). Cooling and freshening of the subpolar North Atlantic Ocean since the 1960s. *Nature*, 360:55–57. 4, 7

Reverdin, G., Durand, F., Mortensen, J., Schott, F., Valdimarsson, H., and Zenk, W. (2002). Recent changes in the surface salinity of the North Atlantic subpolar gyre. *Journal Of Geophysical Research-Oceans*, 107(C12):8010. 7

Rhein, M., Fischer, J., Smethie, W. M., Smythe-Wright, D., Weiss, R. F., Mertens, C., Min, D.-H., Fleischmann, U., and Putzka, A. (2002). Labrador Sea Water: Pathways, CFC Inventory, and Formation Rates. *Journal of Physical Oceanography*, 32(2):648–665. 3

Ribergaard, M. H. (2004). *On the coupling between hydrography and larval transport in Southwest Greenland waters*. Ph.d, Univeristy of Copenhagen. 90, 91

Rigor, I. G., Wallace, J. M., and Colony, R. L. (2002). Response of sea ice to the Arctic oscillation. *Journal Of Climate*, 15(18):2648–2663. 55

Rudels, B. (1993). *Flow and creep in the solar system observations, modeling, and theory*, chapter High latitude convection., pages –. Kluwer Academic Publishers, Dordrecht; Boston. 3

Schmittner, A., Latif, M., and Schneider, B. (2005). Model projections of the North Atlantic thermohaline circulation for the 21st century assessed by observations. *Geophysical Research Letters*, 32(23):L23710. 10

Schweckendiek, U. and Willebrand, J. (2005). Mechanisms affecting the overturning response in global warming simulations. *Journal Of Climate*, 18(23):4925–4936. 10, 110

Semtner, A. J. (1976). Model for thermodynamic growth of sea ice in numerical investigations of climate. *Journal of Physical Oceanography*, 6(3):379–389. 19, 22

Serreze, M. and Hurst, C. (2000). Representation of mean Arctic precipitation from NCEP-NCAR and ERA reanalyses. *Journal of Climate*, 13(1):182–201. 34

Serreze, M. C., Barrett, A. P., Slater, A. G., Woodgate, R. A., Aagaard, K., Lammers, R. B., Steele, M., Moritz, R., Meredith, M., and Lee, C. M. (2006). The large-scale freshwater cycle of the Arctic. *Journal Of Geophysical Research-Oceans*, 111(C11):C11010. 44, 65, 66, 67, 151, 153

Serreze, M. C., Holland, M. M., and Stroeve, J. (2007). Perspectives on the Arctic's Shrinking Sea-Ice Cover. *Science*, 315(5818):1533–1536. 60

Steele, M., Morley, R., and Ermold, W. (2001). PHC: A Global Ocean Hydrography with a High-Quality Arctic Ocean. *Journal of Climate*, 14(9):2079–2087. 32

Steele, M., Zhang, J., and Ermold, W. (2004). The beaufort gyre: Models, observations & truth. Presentation at 7th AOMIP workshop, GFDL, Princton, NJ. 55

Steele, M., Zhang, J., Rothrock, D., and Stern, H. (1997). The force balance of sea ice in a numerical model of the Arctic Ocean. *Journal of Geophysical Research*, 102(21):061–21. 26, 27, 28

Stouffer, R. J., Yin, J., Gregory, J. M., Dixon, K. W., Spelman, M. J., Hurlin, W., Weaver, A. J., Eby, M., Flato, G. M., Hasumi, H., Hu, A., Jungclaus, J. H., Kamenkovich, I. V., Levermann, A., Montoya, M., Murakami, S., Nawrath, S., Oka, A., Peltier, W. R., Robitaille, D. Y., Sokolov, A., Vettoretti, G., and Weber, S. L. (2006). Investigating the causes of the response of the thermohaline circulation to past and future climate changes. *Journal Of Climate*, 19(8):1365–1387. 10

Stroeve, J., Holland, M., Meier, W., Scambos, T., and Serreze, M. (2007). Arctic sea ice decline: Faster than forecast. *Geophysical Research Letters*, 34. 60

Sundby, S. and Drinkwater, K. (2007). On the mechanisms behind salinity anomaly signals of the northern North Atlantic. *Progress In Oceanography*, 73(2):190–202. 9, 92

Talley, L. D. (1996). North Atlantic circulation and variability, reviewed for the CNLS conference. *Physica D*, 98(2-4):625–646. 2

Talley, L. D. and McCartney, M. S. (1982). Distribution And Circulation Of Labrador Sea-Water. *Journal Of Physical Oceanography*, 12(11):1189–1205. 3

Tang, C. C. L., Ross, C. K., Yao, T., Petrie, B., DeTracey, B. M., and Dunlap, E. (2004). The circulation, water masses and sea-ice of Baffin Bay. *Progress in Oceanography*, 63(4):183–228. 67

Tartinville, B., Campin, J., Fichefet, T., and Goosse, H. (2001). Realistic representation of the surface freshwater flux in an ice-ocean general circulation model. *Ocean Modelling*, 3(1):95–108. 30

The Lab Sea Group (1998). The Labrador Sea Deep Convection Experiment. *Bulletin of the American Meteorological Society*, 79(10):2033–2058. 3

Treguier, A. M., Theetten, S., Chassignet, E. P., Penduff, T., Smith, R., Talley, L., Beismann, J. O., and Boning, C. (2005). The north atlantic subpolar gyre in four high-resolution models. *Journal of Physical Oceanography*, 35(5):757–774. See also Corrigendum (Jul 2005). 79

Trenberth, K. E. and Caron, J. M. (2001). Estimates of meridional atmosphere and ocean heat transports. *Journal Of Climate*, 14(16):3433–3443. 2

Trenberth, K. E. and Solomon, A. (1994). The Global Heat-Balance - Heat Transports In The Atmosphere And Ocean. *Climate Dynamics*, 10(3):107–134. 2

Tully, J. and Barber, F. (1960). An estuarine analogy in the sub-Arctic Pacific Ocean. *J. Fish. Res. Bd. Canada*, 17:91–112. 44

Uppala, S., Kallberg, P., Simmons, A., Andrae, U., da Costa Bechtold, V., Fiorino, M., Gibson, J., Haseler, J., Hernandez, A., Kelly, G., Li, X., Onogi, K., Saarinen, S., Sokka, N., Allan, R., Andersson, E., Arpe, K., Balmaseda, M., Beljaars, A., van de Berg, L., Bidlot, J., Bormann, N., Caires, S., Chevallier, F., Dethof, A., Dragosavac, M., Fisher, M., Fuentes, M., Hagemann, S., Holm, E., Hoskins, B., Isaksen, L., Janssen, P., Jenne, R., McNally, A., Mahfouf, J.-F., Morcrette, J.-J., Rayner, N., Saunders, R., Simon, P., Sterl, A., Trenberth, K., Untch, A., Vasiljevic, D., Viterbo, P., and Woollen, J. (2005). The ERA-40 re-analysis. *Quart. J. Roy. Meteor. Soc.*, 131:2961–3012. 7, 33, 34, 35, 83, 86

Vinje, T. (2001). Fram strait ice fluxes and atmospheric circulation: 1950-2000. *Journal of Climate*, 14(16):3508–3517. 61, 122

Whitehead, J. A. (1998). Topographic control of oceanic flows in deep passages and straits. *Reviews Of Geophysics*, 36(3):423–440. 3

Wijffels, S. E., Schmitt, R. W., Bryden, H. L., and Stigebrandt, A. (1992). Transport of Freshwater by the Oceans. *Journal of Physical Oceanography*, 22(2):155–162. 4, 6, 44

Worthington, L. V. (1976). *On the North Atlantic circulation*. Johns Hopkins University Press, Baltimore. 3

Xie, P. and Arkin, P. (1996). Analyses of global monthly precipitation using gauge observations, satellite estimates, and numerical model predictions. *Journal of Climate*, 9(4):840–858. 34

Xie, P. and Arkin, P. (1997). Global precipitation: A 17-year monthly analysis based on gauge observations, satellite estimates, and numerical model outputs. *Bulletin of the American Meteorological Society*, 78(11):2539–2558. 34

Appendix

A Reference Salinity

The following examples illustrate the dependence of freshwater computation on the chosen reference salinityS_0.

In this study, a reference salinity of 34.7 is used while others, e.g. Serreze et al. (2006), use 34.8 or even 35.2 (Dickson et al., 2007). The freshwater content and the net transport into the basin are computed for the subpolar basin (as described in this study) using the REFERENCE experiment.

The differences of the mean freshwater content (FWC) as well as the mean transport (FWT) are large for different reference salinities (see Tab. A-1 and Fig. A-1). But compared to their standard deviation, the differences of the anomalies are very small (see Tab. A-2). This is also true for the transport across one single section, the Fram Strait (Tab. A-3).

salinity	34.7	34.8	35.2
content $[10^{12}m^3]$	-108.5 ± 4.7	-67.1 ± 4.7	96.0 ± 4.6
net transport [mSv]	109.7 ± 102.1	106.5 ± 101.8	93.85 ± 100.5

Table A-1 Mean freshwater content and transport for the Subpolar basin (1958-2000). The standard deviation is also given for each.number.

Mean difference of monthly anomalies	(34.7) − (34.8)	(34.7) − (35.2)
content $[m^3]$	3.18×10^6	2.8×10^6
net transport $[mSv]$	0.003	0.012

Table A-2 Mean difference of monthly freshwater content and transport anomalies between different reference salinity cases.

freshwater transport [mSv]	34.7	34.8	35.2
Mean	-26.09	-32.23	-56.46
Standard. deviation	±11.42	±12.27	±19.61
Mean difference of anomalies[1]	0	7×10^{-7}	7×10^{-7}

Table A-3 Mean freshwater transport and mean difference of monthly anomalies for the Fram Strait section. Values are given in mSv.

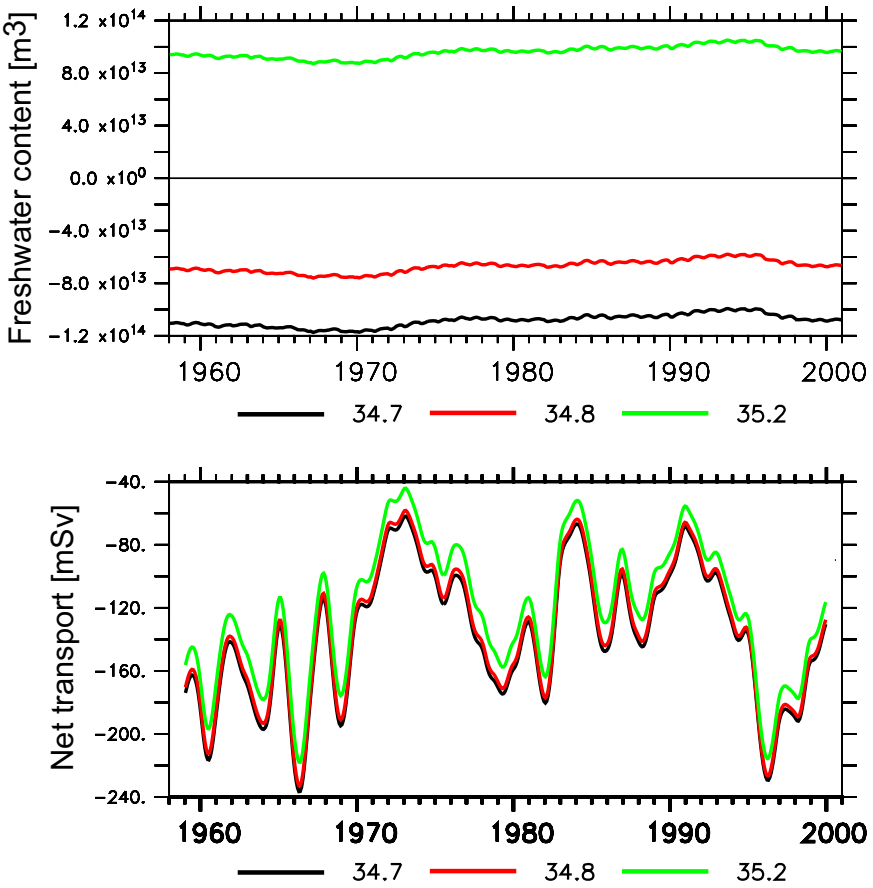

Figure A-1 Absolute freshwater content (upper panel ;m^3) and absolute transport (lower panel; mSv) for the Subpolar basin using different values for the reference salinity S_0 :34.7 (black), 34.8 (red) and 35.2 (green).

B Observed Freshwater Transports

The following tabular shows the freshwater transports taken from Serreze et al. (2006) and the translation into mSv ($1km^3/yr \approx 10^9 m3/yr = 31.71 m^3/s$) as used in section 4.3.2.

Term	km^3/yr	$mSv = 10^3 m^3/s$
Fram Strait upper water outflow	+2400	+76
West Spitsbergen Current (Atlantic inflow)	+760	+24
Fram Strait deep outflow	-500	-16
Fram Strait liquid freshwater outflow	**+2660**	**+84**
Fram Strait ice outflow	**+2300**	**73**
Norwegian Coastal Current	-250	-8
Barents Sea Branch (Atlantic inflow)	+340	11
Barent Sea liquid outflow	**+90**	**3**

Table B-1 Freshwater transports from Serreze et al. (2006) (positive values denote a southward freshwater transport out of the Arctic).

C Freshwater Budgets

The complete freshwater budgets are shown in the following for the basins **SUBPOLE** (Subpolar North Atlantic), **ARCTIC** (all arctic basins), **inner ARCTIC**, **GIN** (Nordic Seas) and **BAFFIN** (Baffin Bay) for each experiment separately (REFERENCE, HEAT, THERMHAL, WIND and NONARCTIC)

Each plane consists of time series for the following freshwater fluxes/transports (in Sv) and content (in km^3):

Upper left *Basin-wide net surface flux compared to net passage transport*

net budget (black), net surface flux into the basin (red), and net passage transport into the basin (blue)

Upper right Surface fluxes by components

net surface flux (red), liquid precipitation E-P (magenta, dashed), total precipitation (magenta, solid), river and coastal runoff (green) and surface restoring (blue). All positive into the basin.

Lower left Net passage transport by liquid ocean and by sea ice

net transport (blue), ice+snow transport (black, dotted), ocean transport (black, solid)

Lower right Passage transports by sections

liquid ocean transport (solid) and ice+snow transport (dotted). Colors indicate different sections for different basins (see legend within the plot).

Middle left Absolute freshwater content

C.1 SUBPOLE

REFERENCE

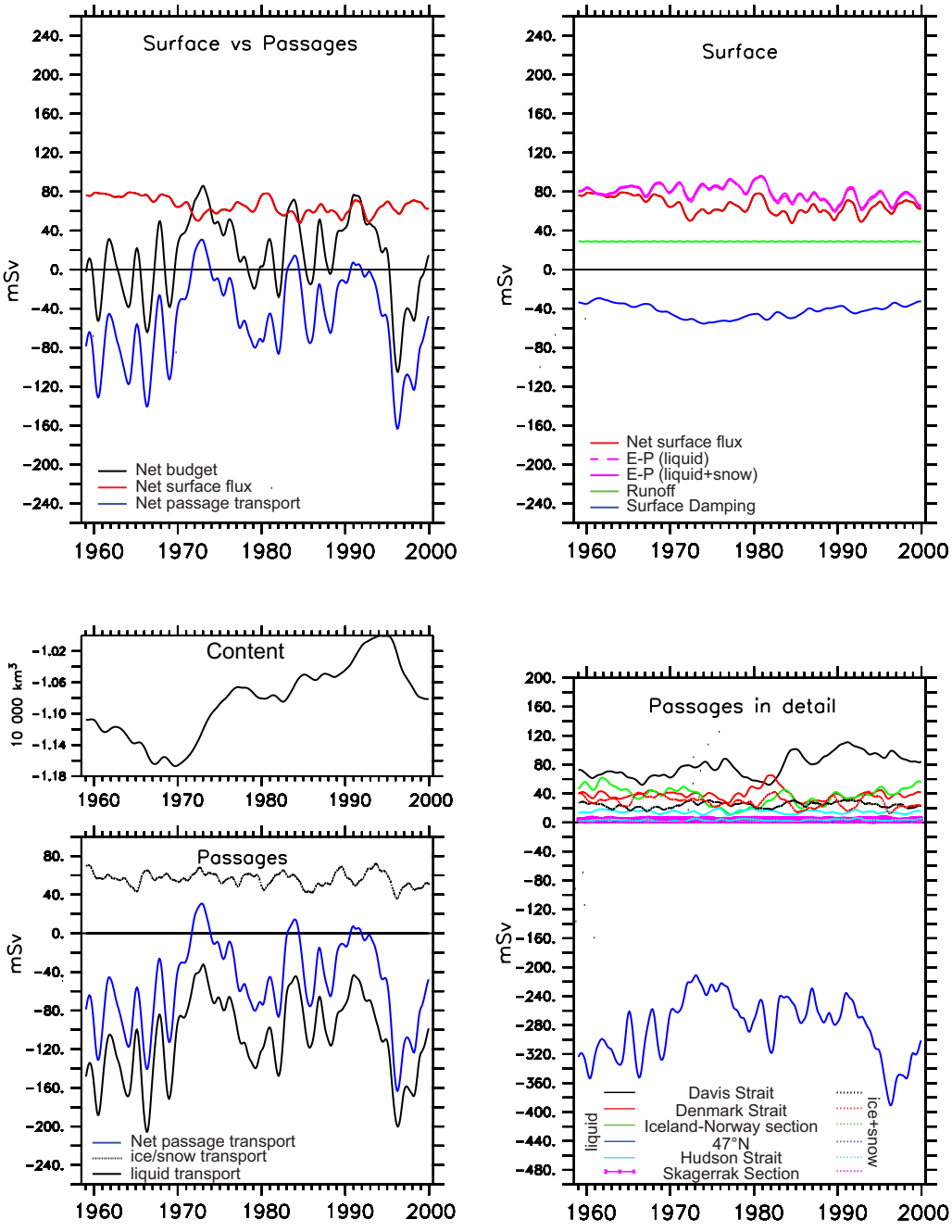

HEAT

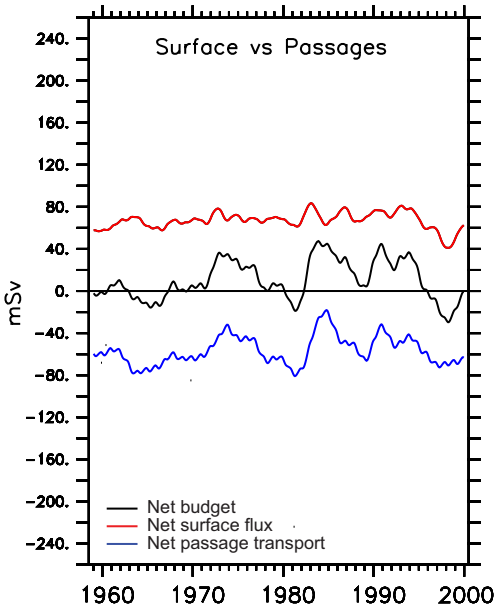
Surface vs Passages
mSv
240.
200.
160.
120.
80.
40.
0.
-40.
-80.
-120.
-160.
-200.
-240.
1960
1970
1980
1990
2000
Net budget
Net surface flux
Net passage transport

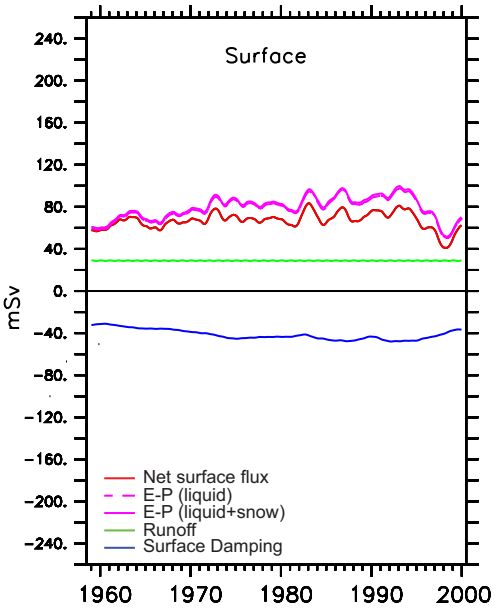
Surface
mSv
240.
200.
160.
120.
80.
40.
0.
-40.
-80.
-120.
-160.
-200.
-240.
1960
1970
1980
1990
2000
Net surface flux
E-P (liquid)
E-P (liquid+snow)
Runoff
Surface Damping

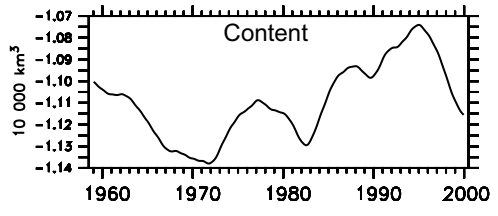
Content
10 000 km³
-1.07
-1.08
-1.09
-1.10
-1.11
-1.12
-1.13
-1.14
1960
1970
1980
1990
2000

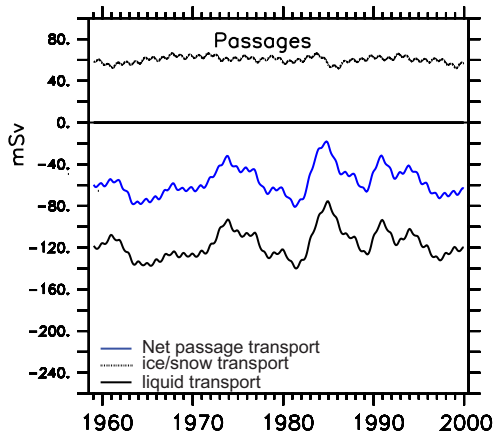
Passages
mSv
80.
40.
0.
-40.
-80.
-120.
-160.
-200.
-240.
1960
1970
1980
1990
2000
Net passage transport
ice/snow transport
liquid transport

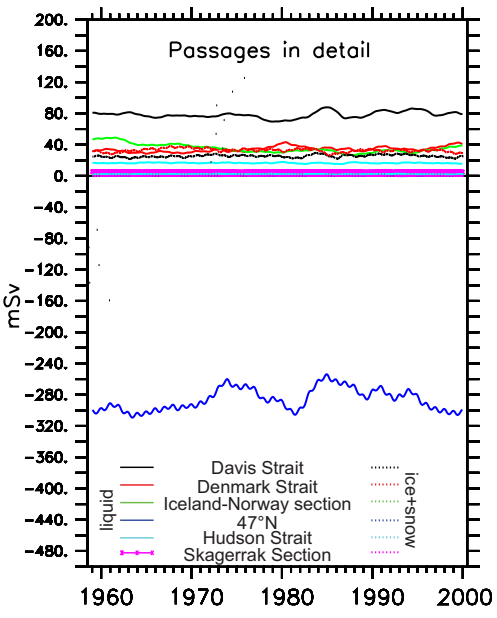
Passages in detail
mSv
200.
160.
120.
80.
40.
0.
-40.
-80.
-120.
-160.
-200.
-240.
-280.
-320.
-360.
-400.
-440.
-480.
1960
1970
1980
1990
2000
liquid
Davis Strait
Denmark Strait
Iceland-Norway section
47°N
Hudson Strait
Skagerrak Section
ice+snow

THERMHAL

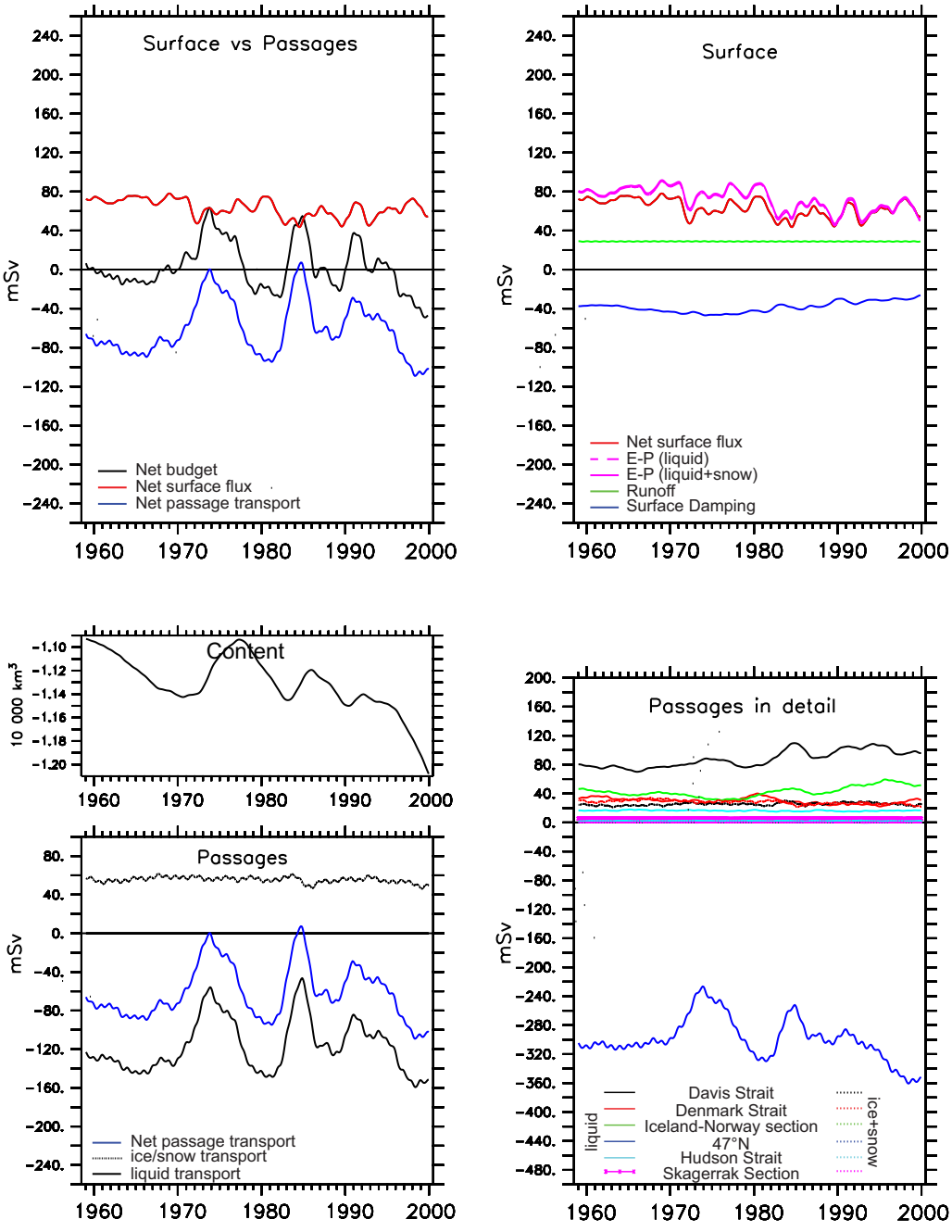
Surface vs Passages
mSv
Net budget
Net surface flux
Net passage transport
Surface
Net surface flux
E-P (liquid)
E-P (liquid+snow)
Runoff
Surface Damping
Content
10 000 km³
Passages
Net passage transport
ice/snow transport
liquid transport
Passages in detail
liquid
ice+snow
Davis Strait
Denmark Strait
Iceland-Norway section
47°N
Hudson Strait
Skagerrak Section
1960
1970
1980
1990
2000

WIND

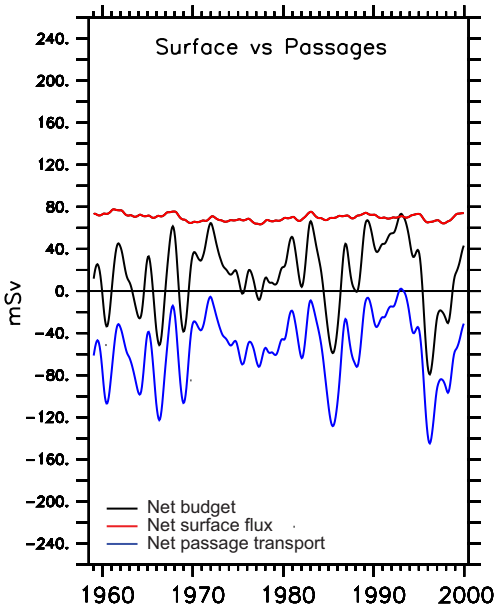
Surface vs Passages
mSv
Net budget
Net surface flux
Net passage transport

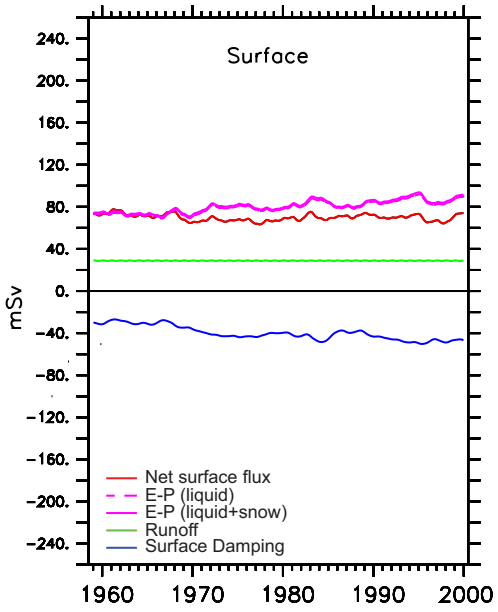
Surface
mSv
Net surface flux
E-P (liquid)
E-P (liquid+snow)
Runoff
Surface Damping

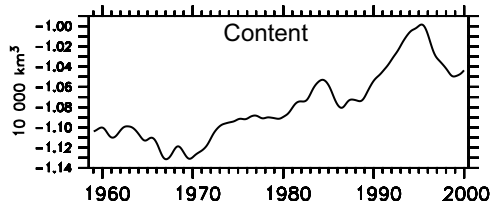
Content
10 000 km³

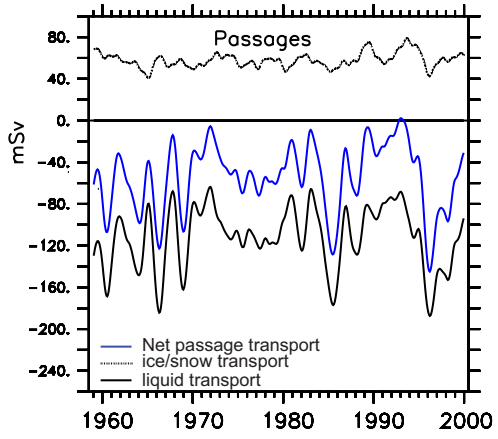
Passages
mSv
Net passage transport
ice/snow transport
liquid transport

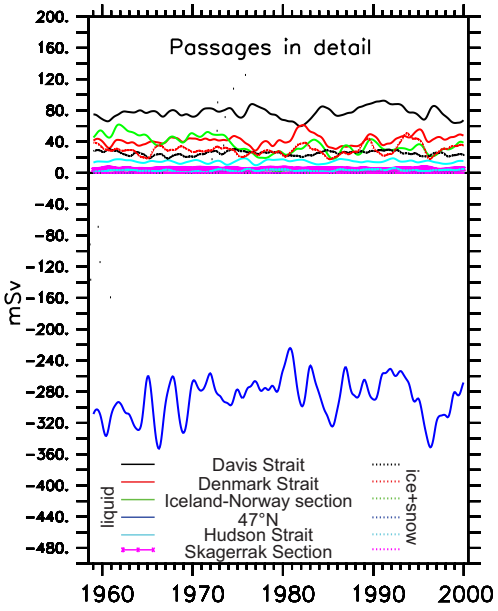
Passages in detail
mSv
liquid
ice+snow
Davis Strait
Denmark Strait
Iceland-Norway section
47°N
Hudson Strait
Skagerrak Section

NONARCTIC

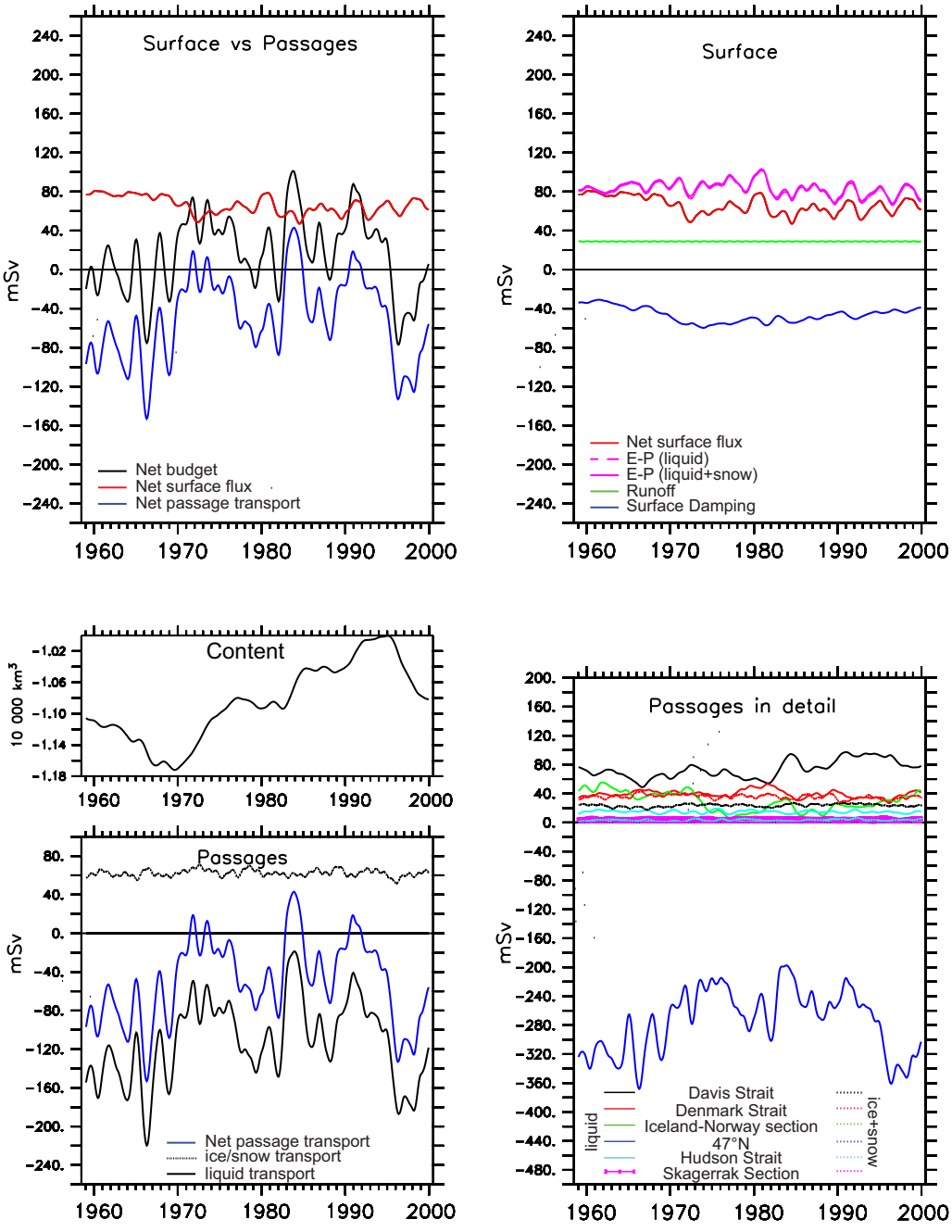
Surface vs Passages
mSv
Net budget
Net surface flux
Net passage transport
Surface
Net surface flux
E-P (liquid)
E-P (liquid+snow)
Runoff
Surface Damping
Content
10 000 km³
Passages
Net passage transport
ice/snow transport
liquid transport
Passages in detail
Davis Strait
Denmark Strait
Iceland-Norway section
47°N
Hudson Strait
Skagerrak Section
liquid
ice+snow
1960
1970
1980
1990
2000

C.2 ARCTIC

REFERENCE

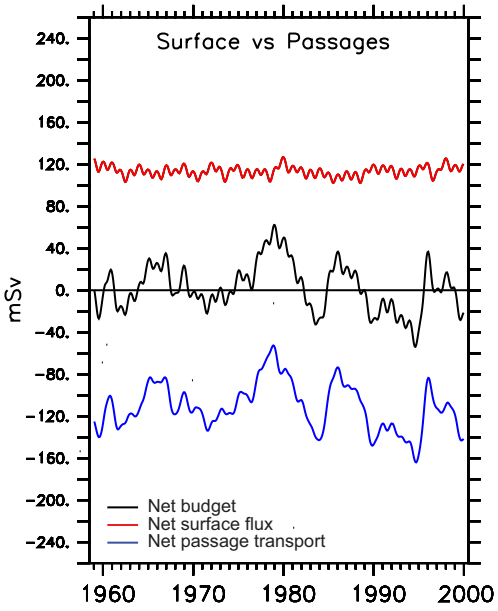

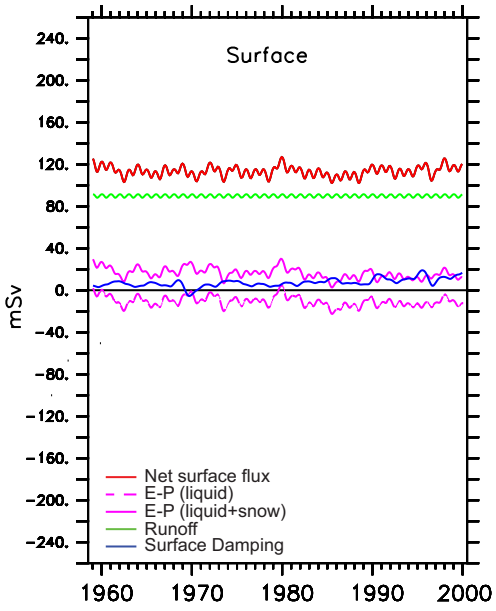

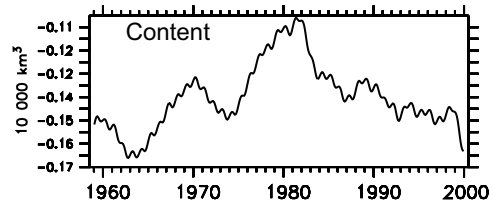

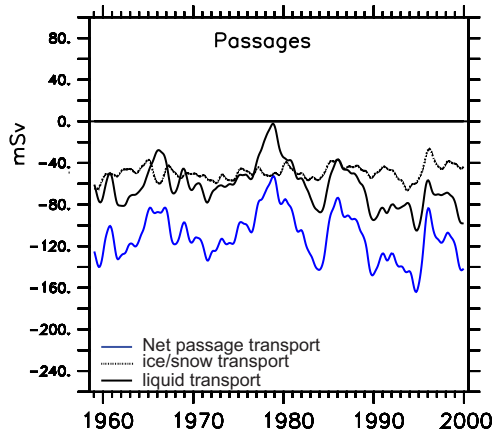

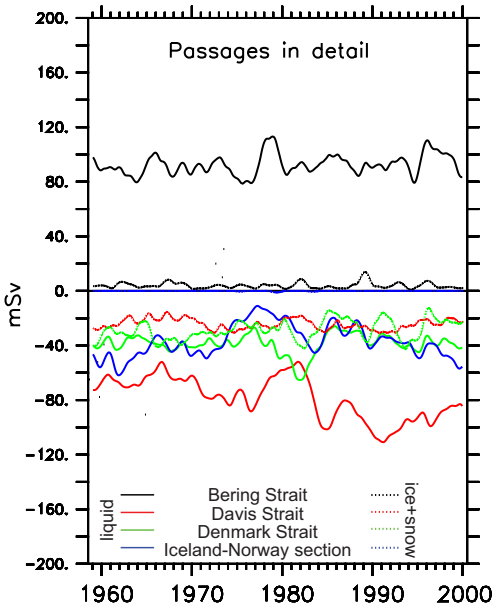

HEAT

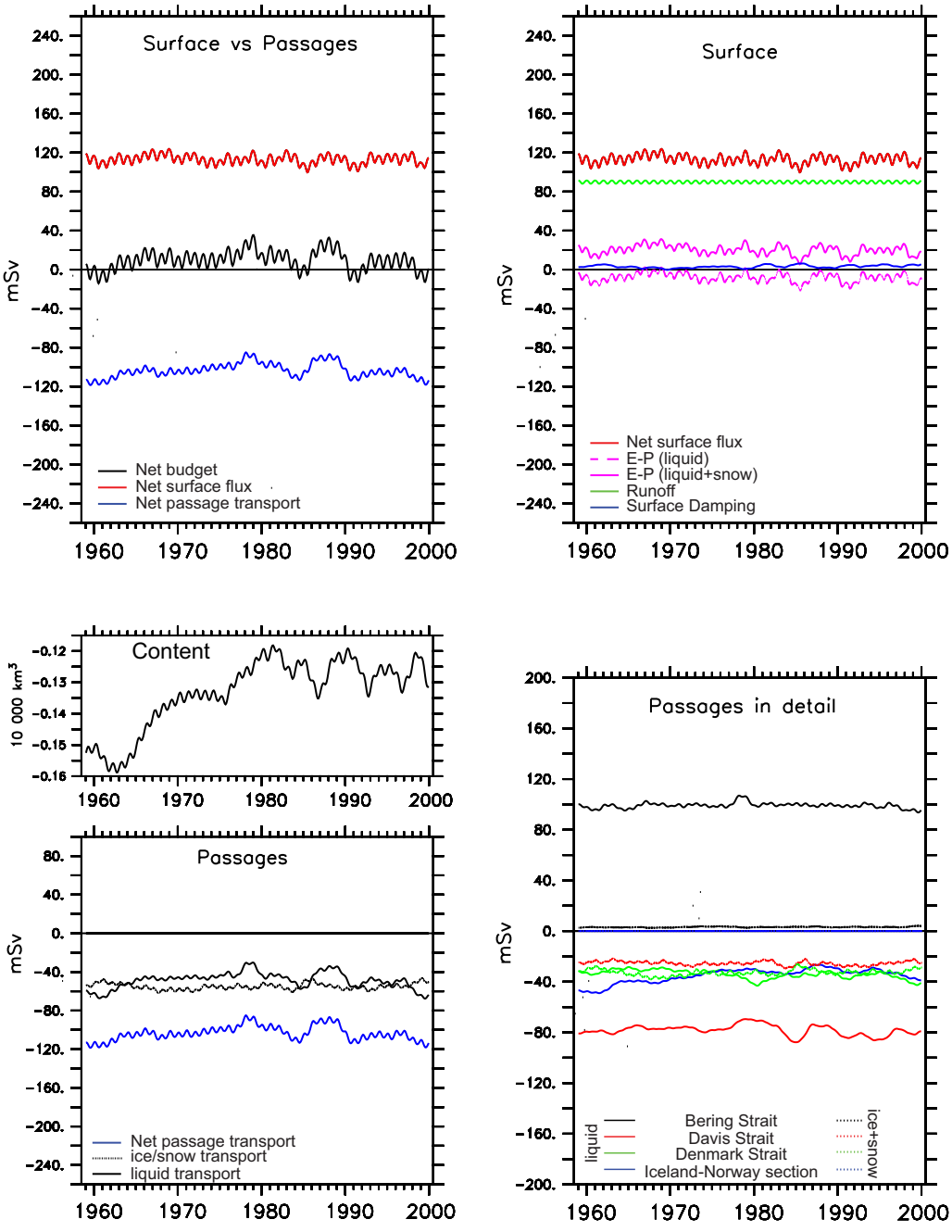
Surface vs Passages
mSv
Net budget
Net surface flux
Net passage transport
Surface
Net surface flux
E-P (liquid)
E-P (liquid+snow)
Runoff
Surface Damping
Content
10 000 km³
Passages
Net passage transport
ice/snow transport
liquid transport
Passages in detail
liquid
ice+snow
Bering Strait
Davis Strait
Denmark Strait
Iceland-Norway section
1960
1970
1980
1990
2000

THERMHAL

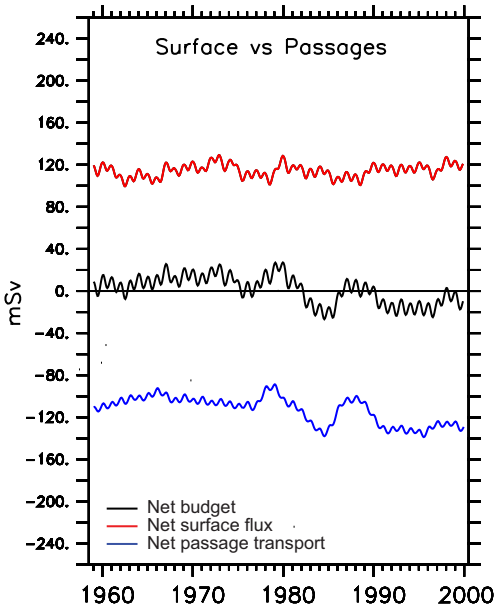
Surface vs Passages
mSv
240.
200.
160.
120.
80.
40.
0.
-40.
-80.
-120.
-160.
-200.
-240.
1960
1970
1980
1990
2000
Net budget
Net surface flux
Net passage transport

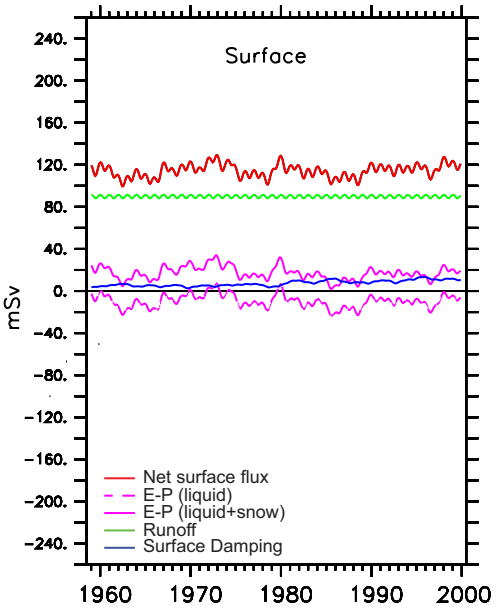
Surface
mSv
240.
200.
160.
120.
80.
40.
0.
-40.
-80.
-120.
-160.
-200.
-240.
1960
1970
1980
1990
2000
Net surface flux
E-P (liquid)
E-P (liquid+snow)
Runoff
Surface Damping

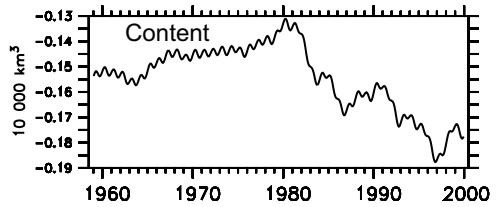
Content
10 000 km³
-0.13
-0.14
-0.15
-0.16
-0.17
-0.18
-0.19
1960
1970
1980
1990
2000

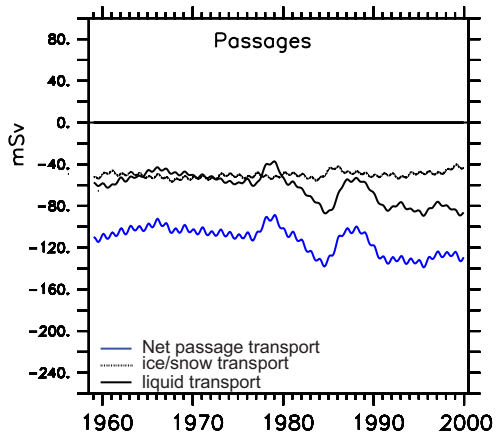
Passages
mSv
80.
40.
0.
-40.
-80.
-120.
-160.
-200.
-240.
1960
1970
1980
1990
2000
Net passage transport
ice/snow transport
liquid transport

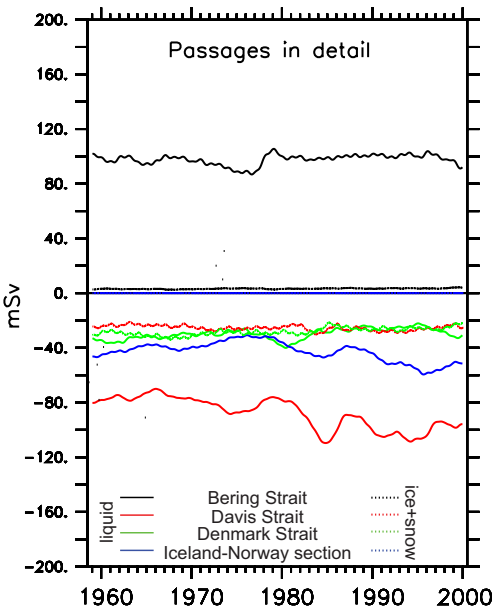
Passages in detail
mSv
200.
160.
120.
80.
40.
0.
-40.
-80.
-120.
-160.
-200.
1960
1970
1980
1990
2000
liquid
Bering Strait
Davis Strait
Denmark Strait
Iceland-Norway section
ice+snow

WIND

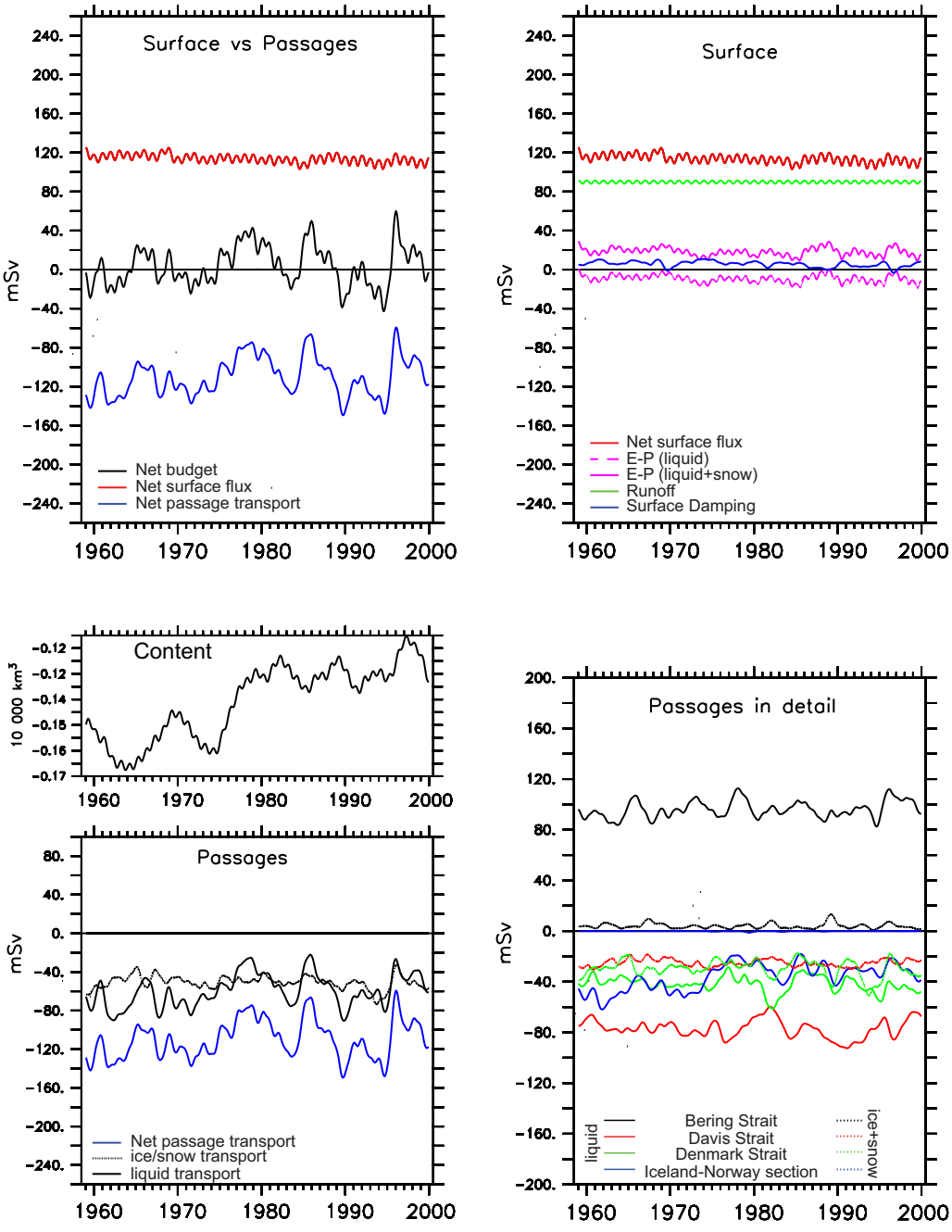
Surface vs Passages
mSv
Net budget
Net surface flux
Net passage transport
Surface
Net surface flux
E-P (liquid)
E-P (liquid+snow)
Runoff
Surface Damping
Content
10 000 km³
Passages
Net passage transport
ice/snow transport
liquid transport
Passages in detail
liquid
ice+snow
Bering Strait
Davis Strait
Denmark Strait
Iceland-Norway section
1960
1970
1980
1990
2000

NONARCTIC

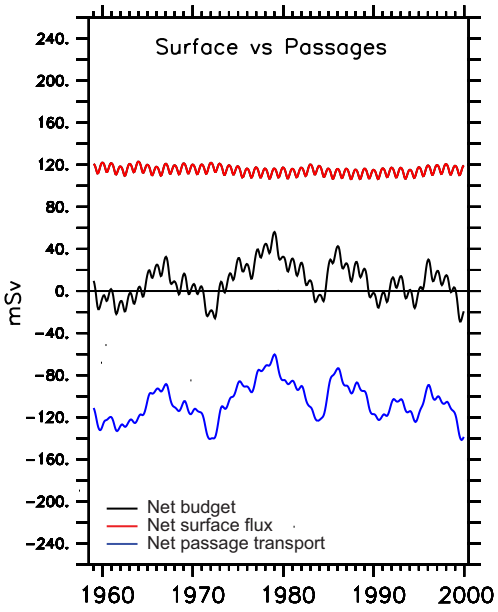
Surface vs Passages
mSv
240.
200.
160.
120.
80.
40.
0.
-40.
-80.
-120.
-160.
-200.
-240.
1960
1970
1980
1990
2000
Net budget
Net surface flux
Net passage transport

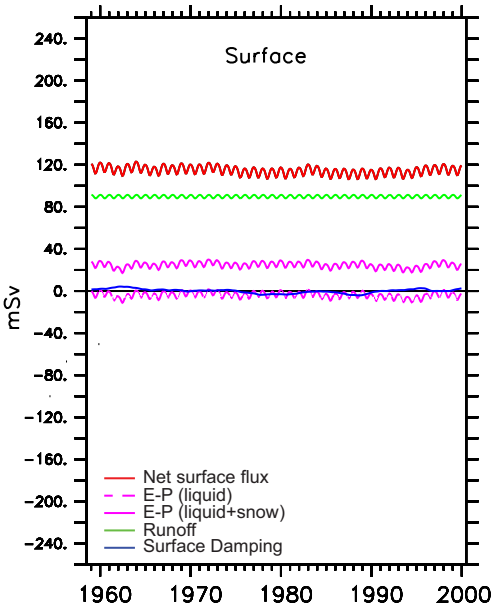
Surface
mSv
240.
200.
160.
120.
80.
40.
0.
-40.
-80.
-120.
-160.
-200.
-240.
1960
1970
1980
1990
2000
Net surface flux
E-P (liquid)
E-P (liquid+snow)
Runoff
Surface Damping

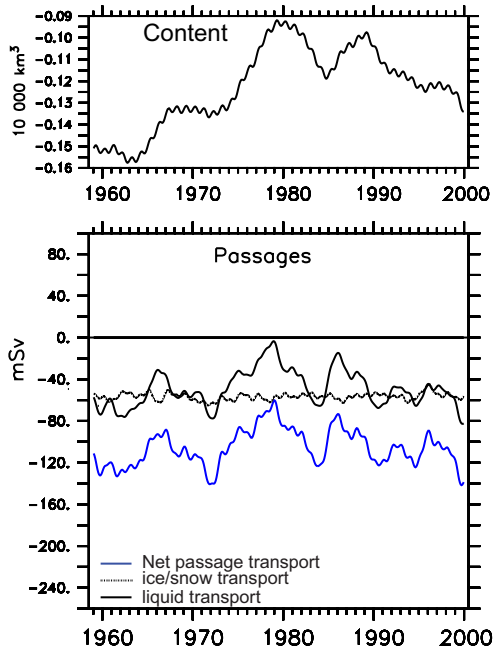
Content
10 000 km³
-0.09
-0.10
-0.11
-0.12
-0.13
-0.14
-0.15
-0.16
1960
1970
1980
1990
2000
Passages
mSv
80.
40.
0.
-40.
-80.
-120.
-160.
-200.
-240.
1960
1970
1980
1990
2000
Net passage transport
ice/snow transport
liquid transport

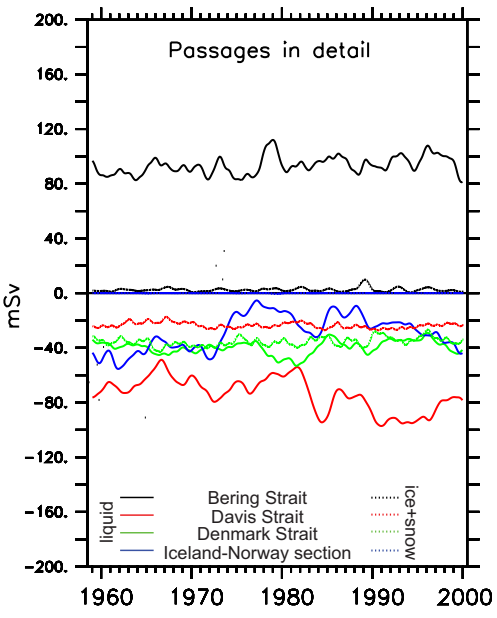
Passages in detail
mSv
200.
160.
120.
80.
40.
0.
-40.
-80.
-120.
-160.
-200.
1960
1970
1980
1990
2000
liquid
Bering Strait
Davis Strait
Denmark Strait
Iceland-Norway section
ice+snow

C.3 inner ARCTIC

REFERENCE

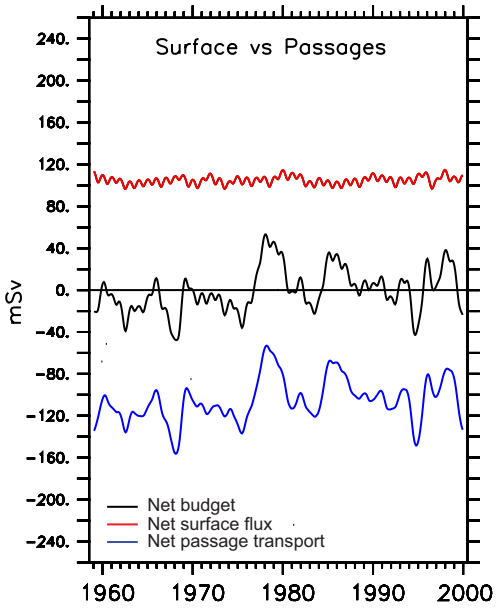

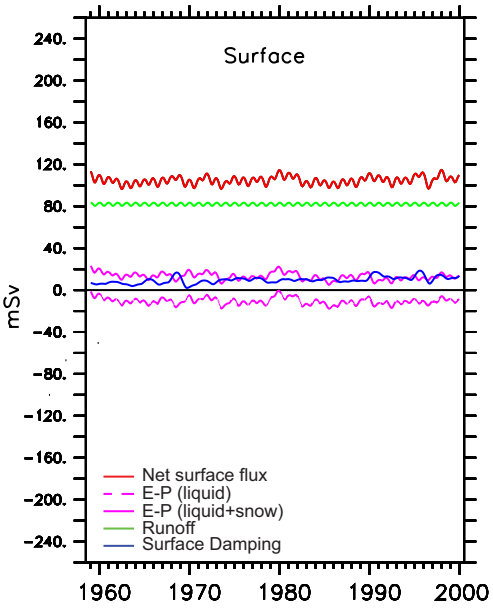

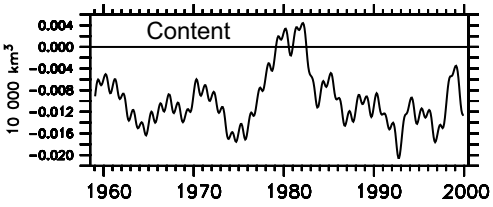

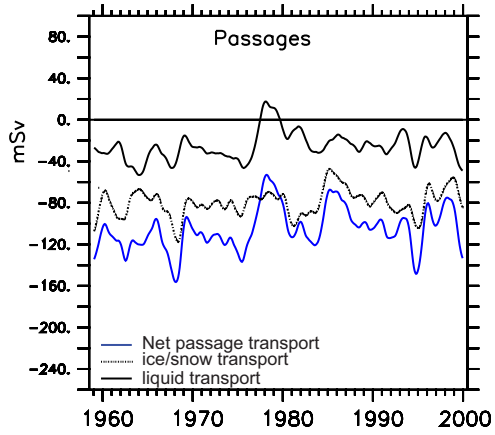

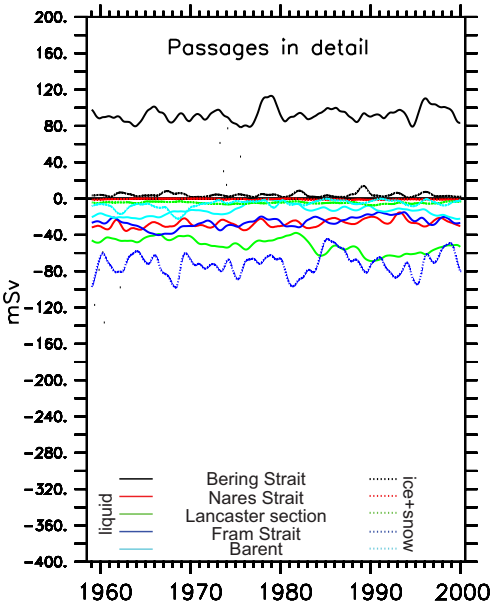

HEAT

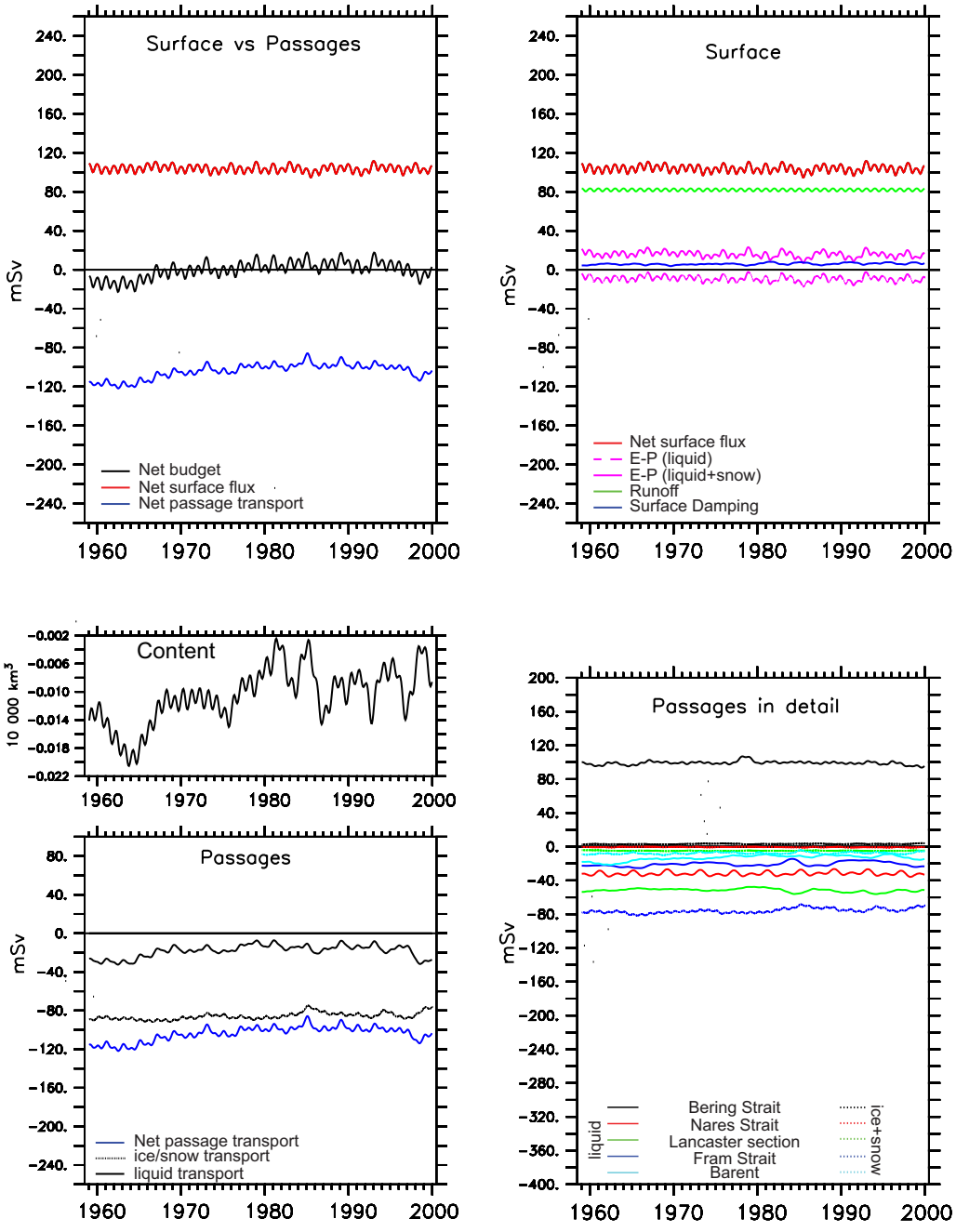
Surface vs Passages
mSv
Net budget
Net surface flux
Net passage transport
Surface
Net surface flux
E-P (liquid)
E-P (liquid+snow)
Runoff
Surface Damping
Content
10 000 km³
Passages
Net passage transport
ice/snow transport
liquid transport
Passages in detail
liquid
Bering Strait
Nares Strait
Lancaster section
Fram Strait
Barent
ice+snow
1960
1970
1980
1990
2000

THERMHAL

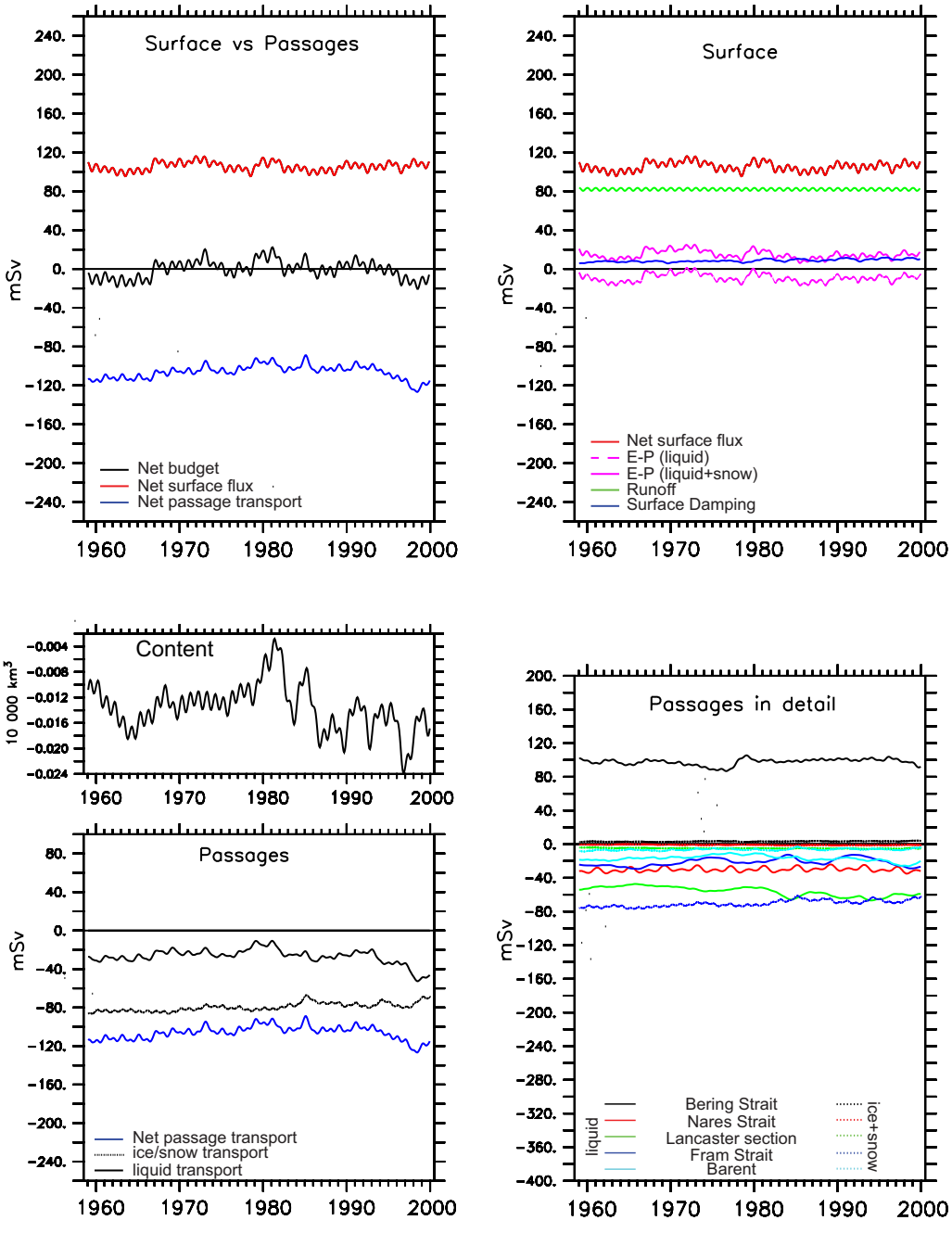
Surface vs Passages
mSv
Net budget
Net surface flux
Net passage transport
Surface
Net surface flux
E-P (liquid)
E-P (liquid+snow)
Runoff
Surface Damping
Content
10 000 km³
Passages
Net passage transport
ice/snow transport
liquid transport
Passages in detail
liquid
ice+snow
Bering Strait
Nares Strait
Lancaster section
Fram Strait
Barent
1960
1970
1980
1990
2000

WIND

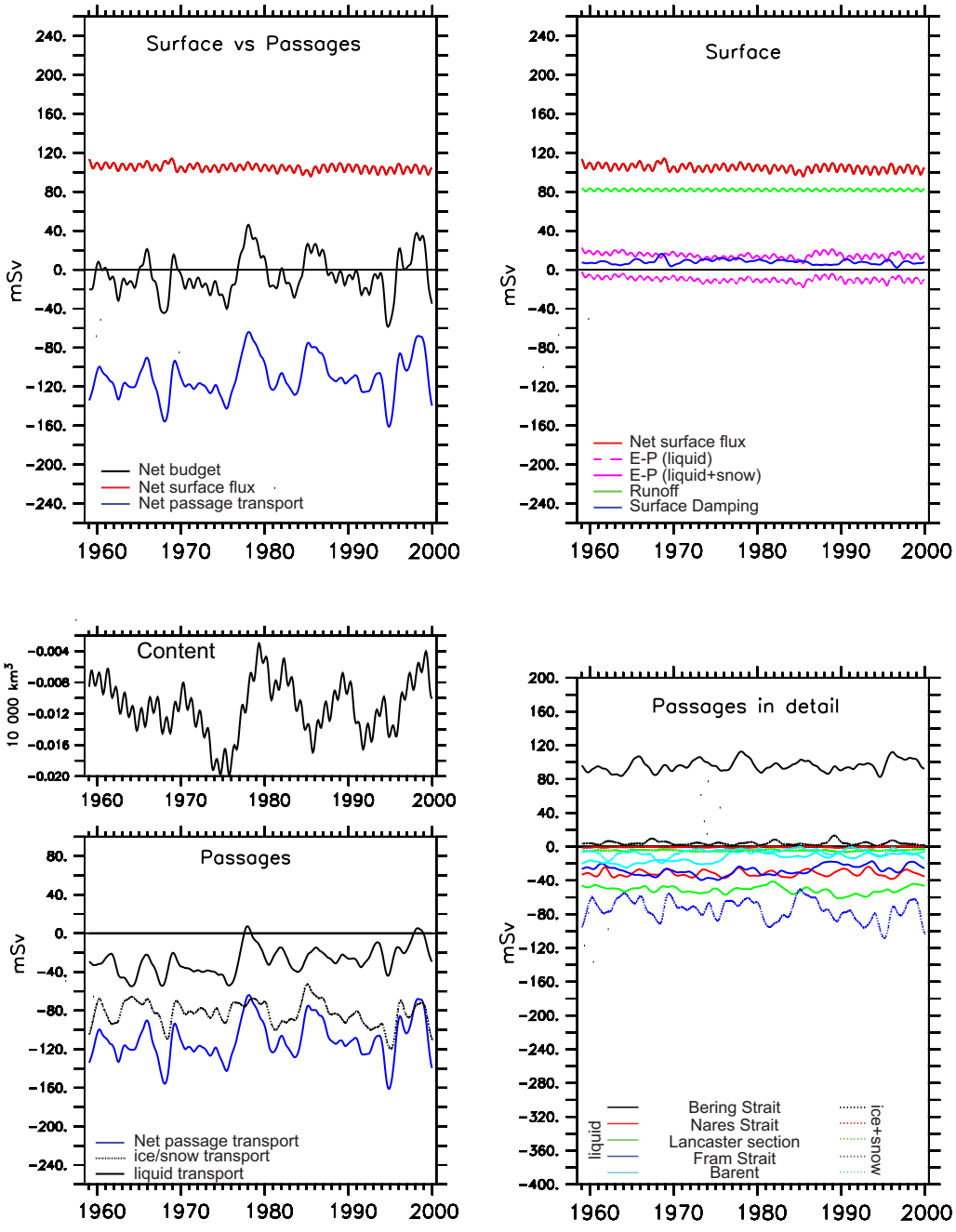
Surface vs Passages
mSv
Net budget
Net surface flux
Net passage transport
Surface
Net surface flux
E-P (liquid)
E-P (liquid+snow)
Runoff
Surface Damping
Content
10 000 km³
Passages
Net passage transport
ice/snow transport
liquid transport
Passages in detail
liquid
Bering Strait
Nares Strait
Lancaster section
Fram Strait
Barent
ice+snow
1960
1970
1980
1990
2000

NONARCTIC

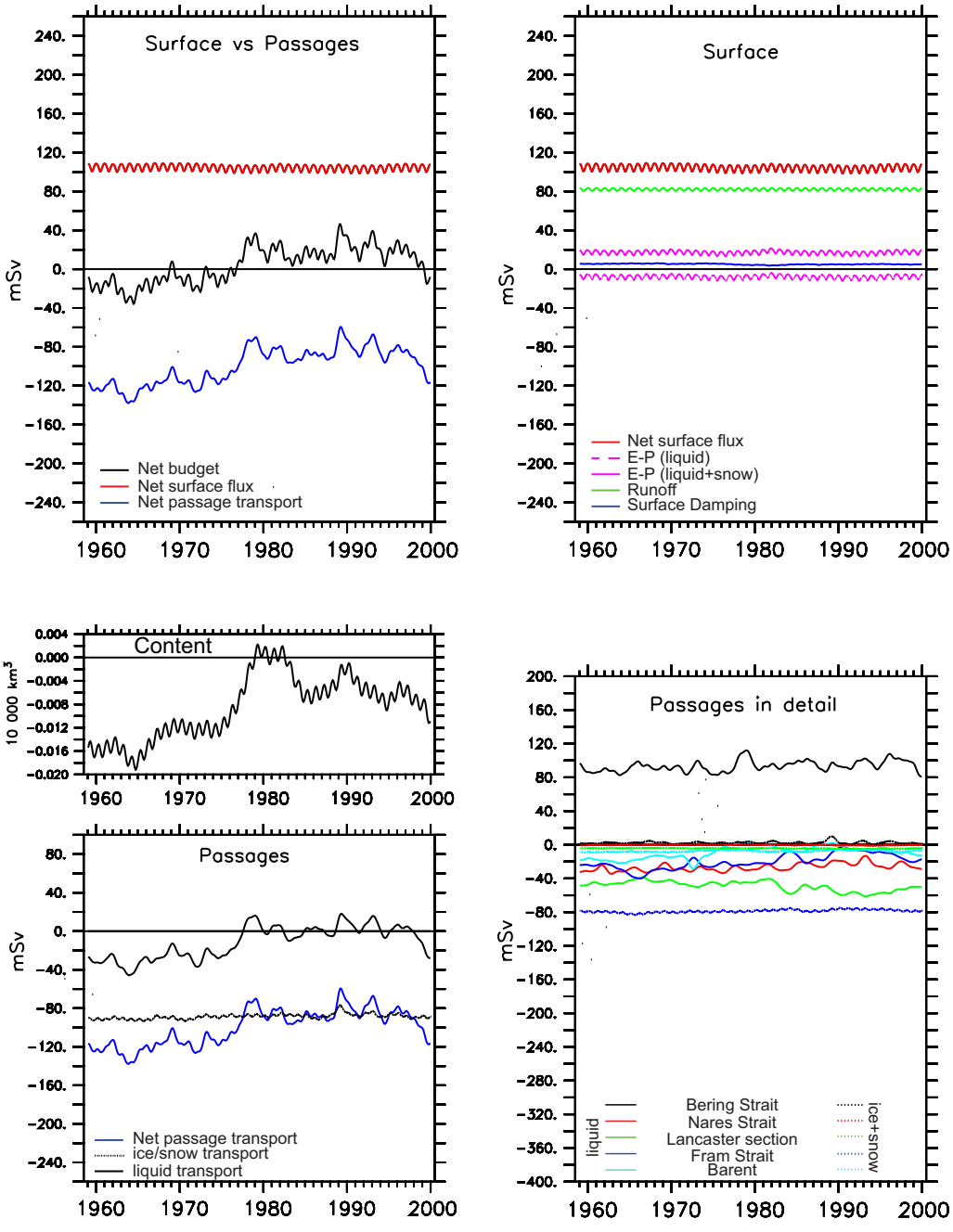
Surface vs Passages
mSv
Net budget
Net surface flux
Net passage transport
Surface
Net surface flux
E-P (liquid)
E-P (liquid+snow)
Runoff
Surface Damping
Content
10 000 km³
Passages
Net passage transport
ice/snow transport
liquid transport
Passages in detail
liquid
ice+snow
Bering Strait
Nares Strait
Lancaster section
Fram Strait
Barent
1960
1970
1980
1990
2000

C.4 NORDIC SEAS / GIN

REFERENCE

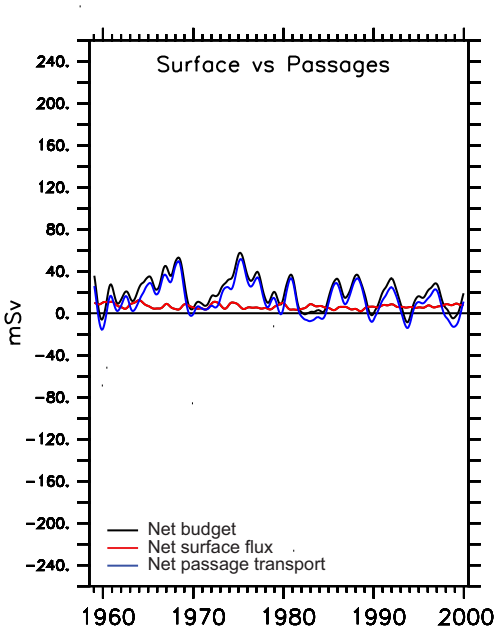

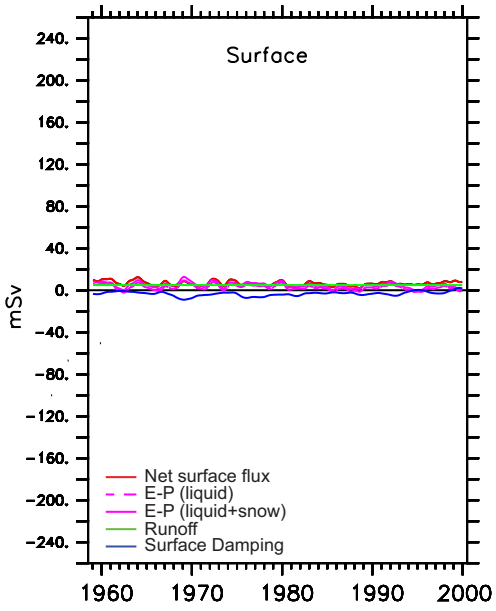

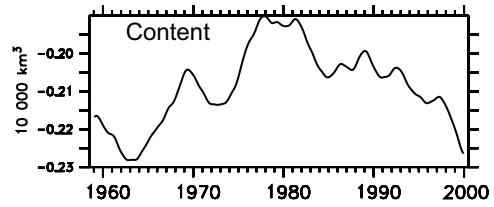

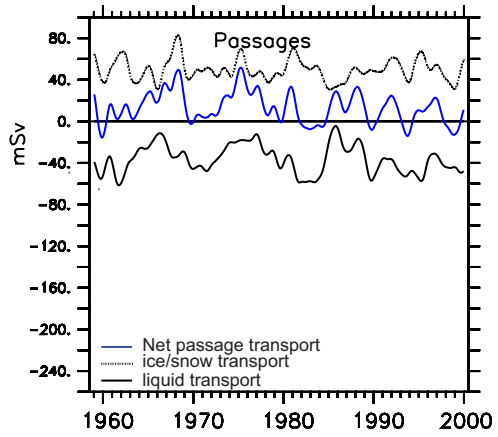

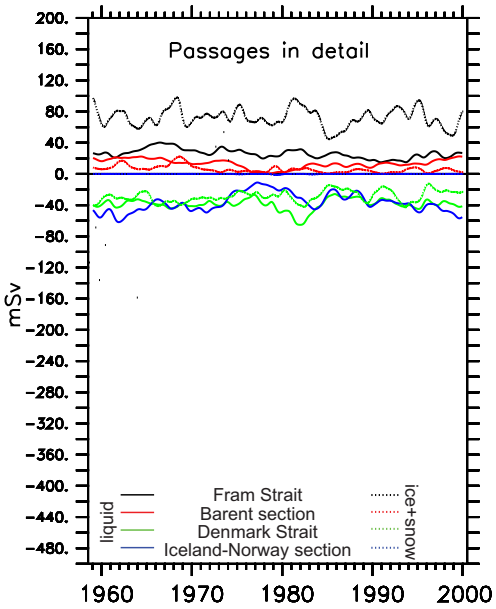

HEAT

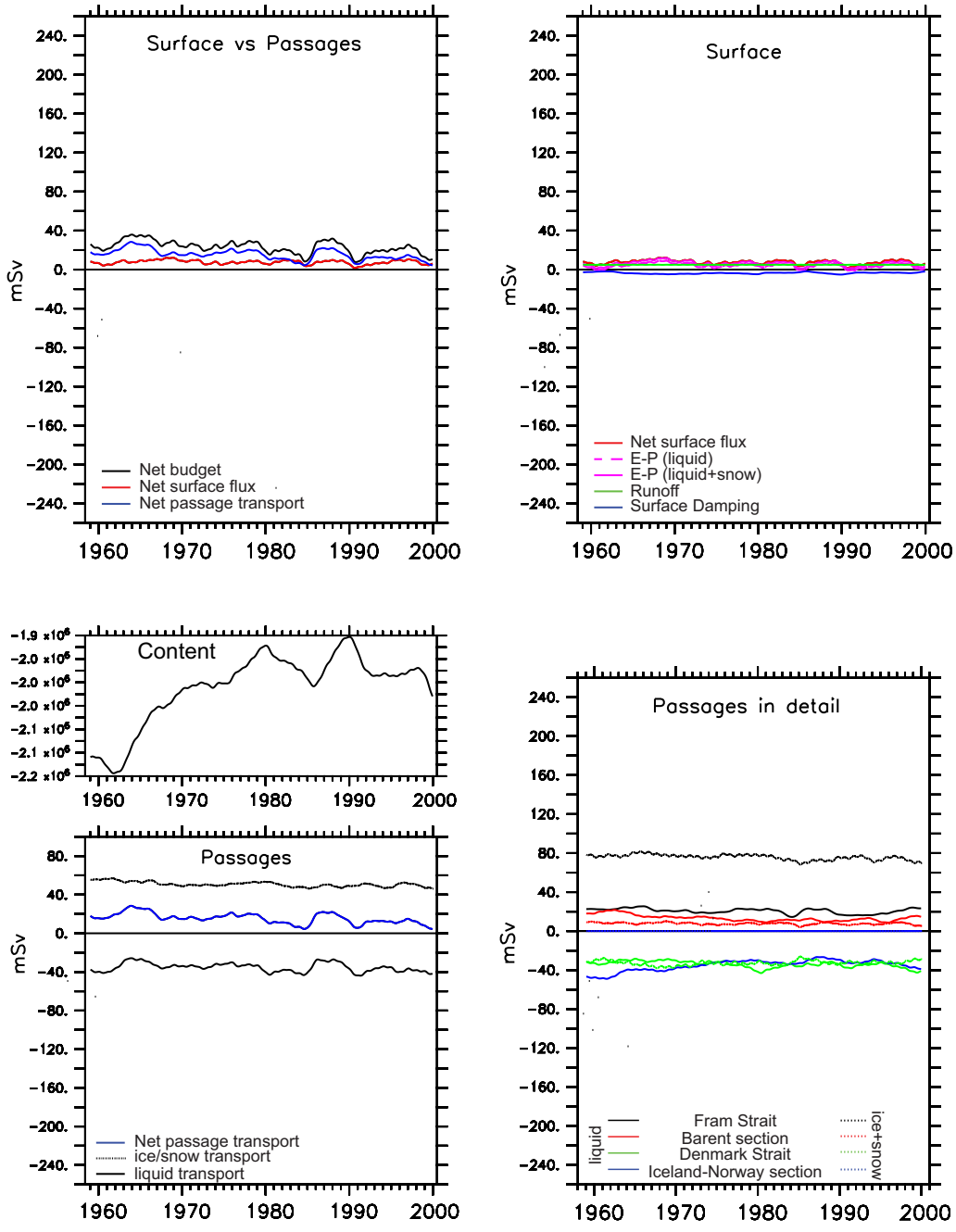
Surface vs Passages
mSv
Net budget
Net surface flux
Net passage transport
Surface
Net surface flux
E-P (liquid)
E-P (liquid+snow)
Runoff
Surface Damping
Content
Passages
Net passage transport
ice/snow transport
liquid transport
Passages in detail
liquid
ice+snow
Fram Strait
Barent section
Denmark Strait
Iceland-Norway section
1960
1970
1980
1990
2000

THERMHAL

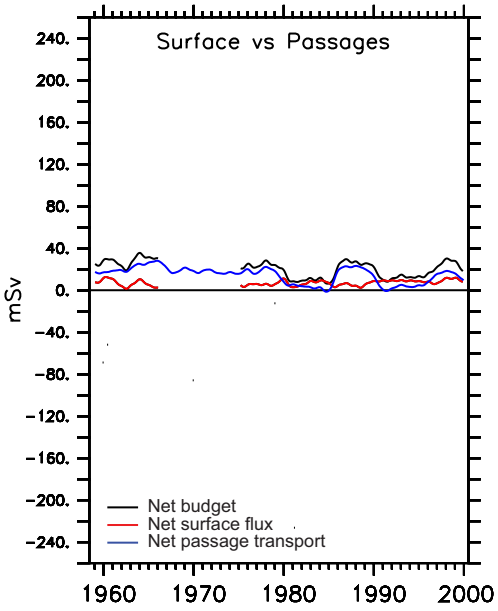
Surface vs Passages
mSv
Net budget
Net surface flux
Net passage transport

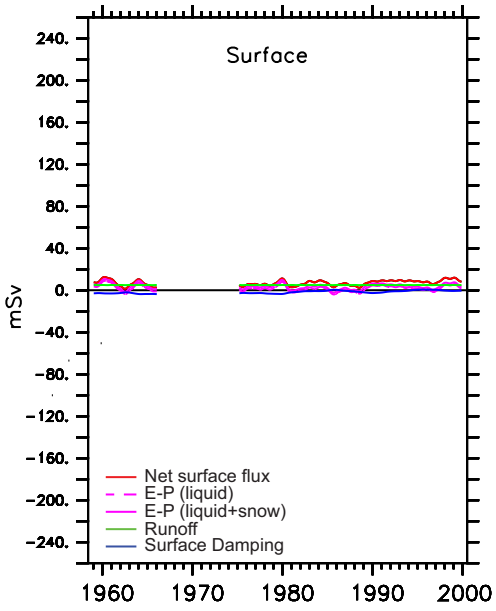
Surface
mSv
Net surface flux
E-P (liquid)
E-P (liquid+snow)
Runoff
Surface Damping

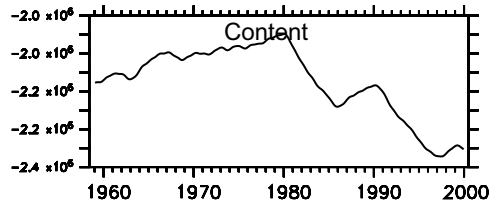
Content

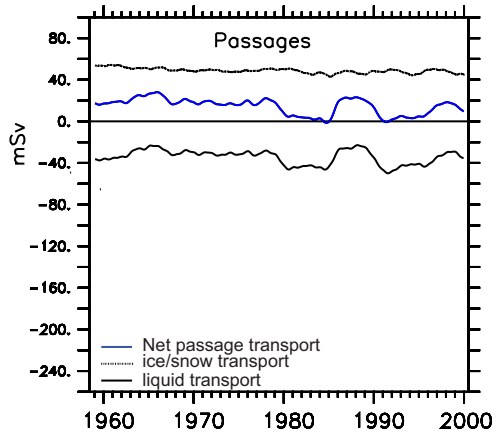
Passages
mSv
Net passage transport
ice/snow transport
liquid transport

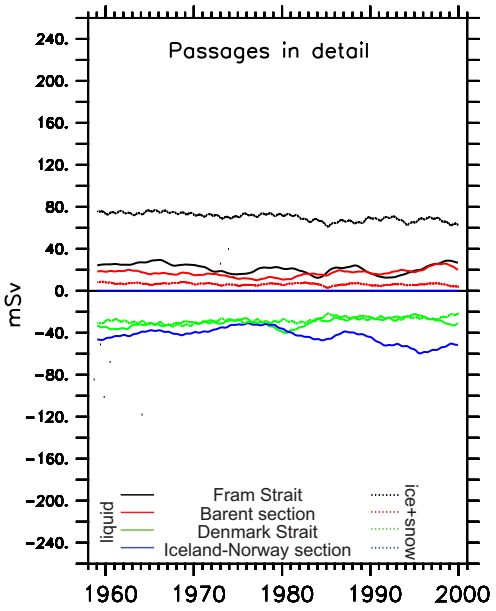
Passages in detail
mSv
liquid
Fram Strait
Barent section
Denmark Strait
Iceland-Norway section
ice+snow

WIND

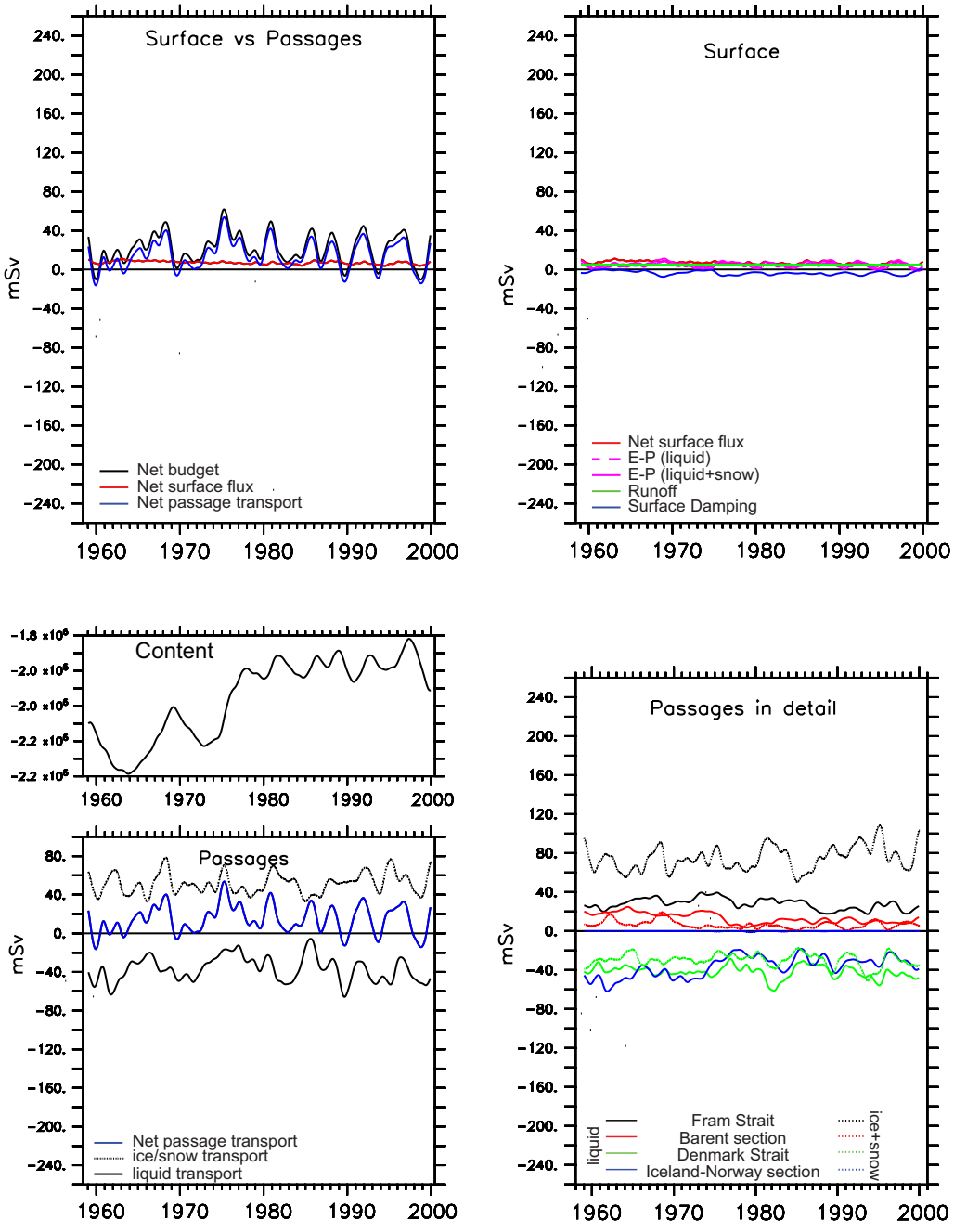
Surface vs Passages
mSv
Net budget
Net surface flux
Net passage transport
Surface
Net surface flux
E-P (liquid)
E-P (liquid+snow)
Runoff
Surface Damping
Content
Passages
Net passage transport
ice/snow transport
liquid transport
Passages in detail
liquid
ice+snow
Fram Strait
Barent section
Denmark Strait
Iceland-Norway section
1960
1970
1980
1990
2000

NONARCTIC

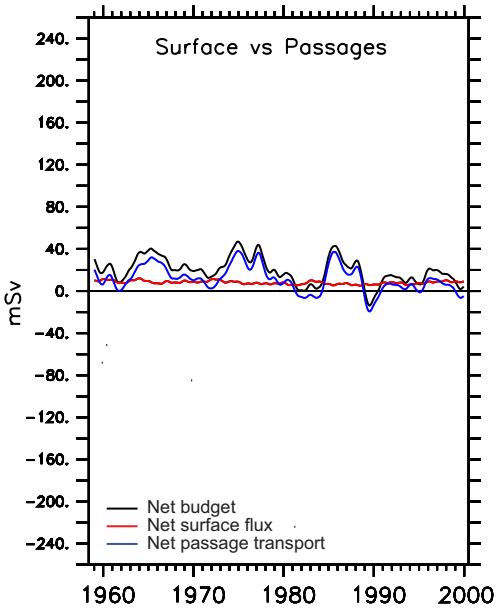
Surface vs Passages
mSv
Net budget
Net surface flux
Net passage transport

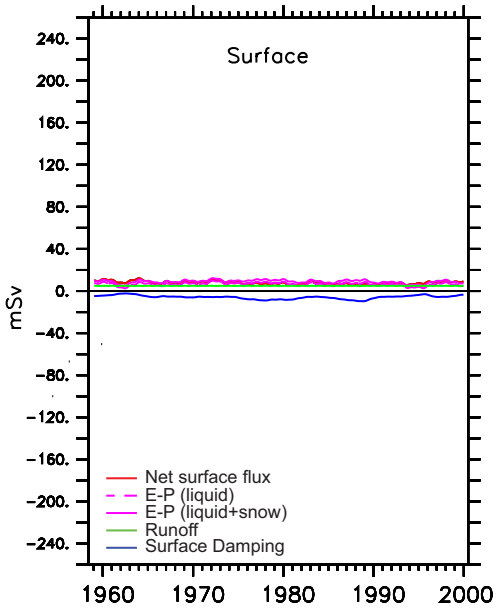
Surface
mSv
Net surface flux
E-P (liquid)
E-P (liquid+snow)
Runoff
Surface Damping

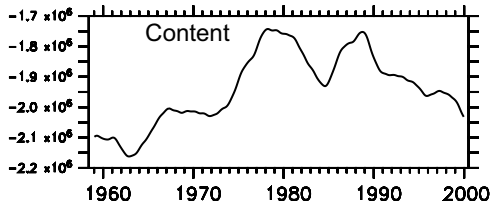
Content

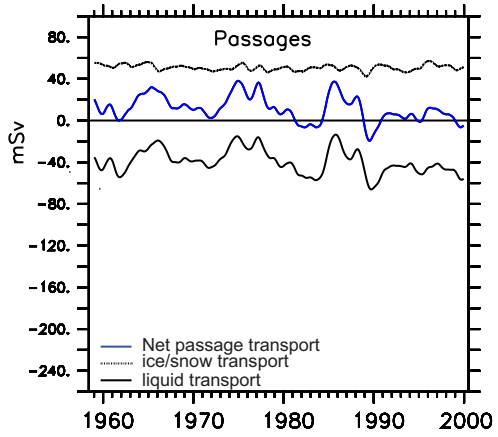
Passages
mSv
Net passage transport
ice/snow transport
liquid transport

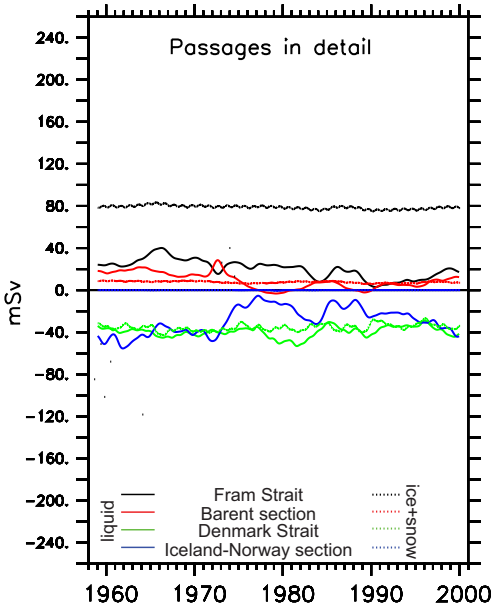
Passages in detail
mSv
liquid
Fram Strait
Barent section
Denmark Strait
Iceland-Norway section
ice+snow

C.5 BAFFIN BAY

REFERENCE

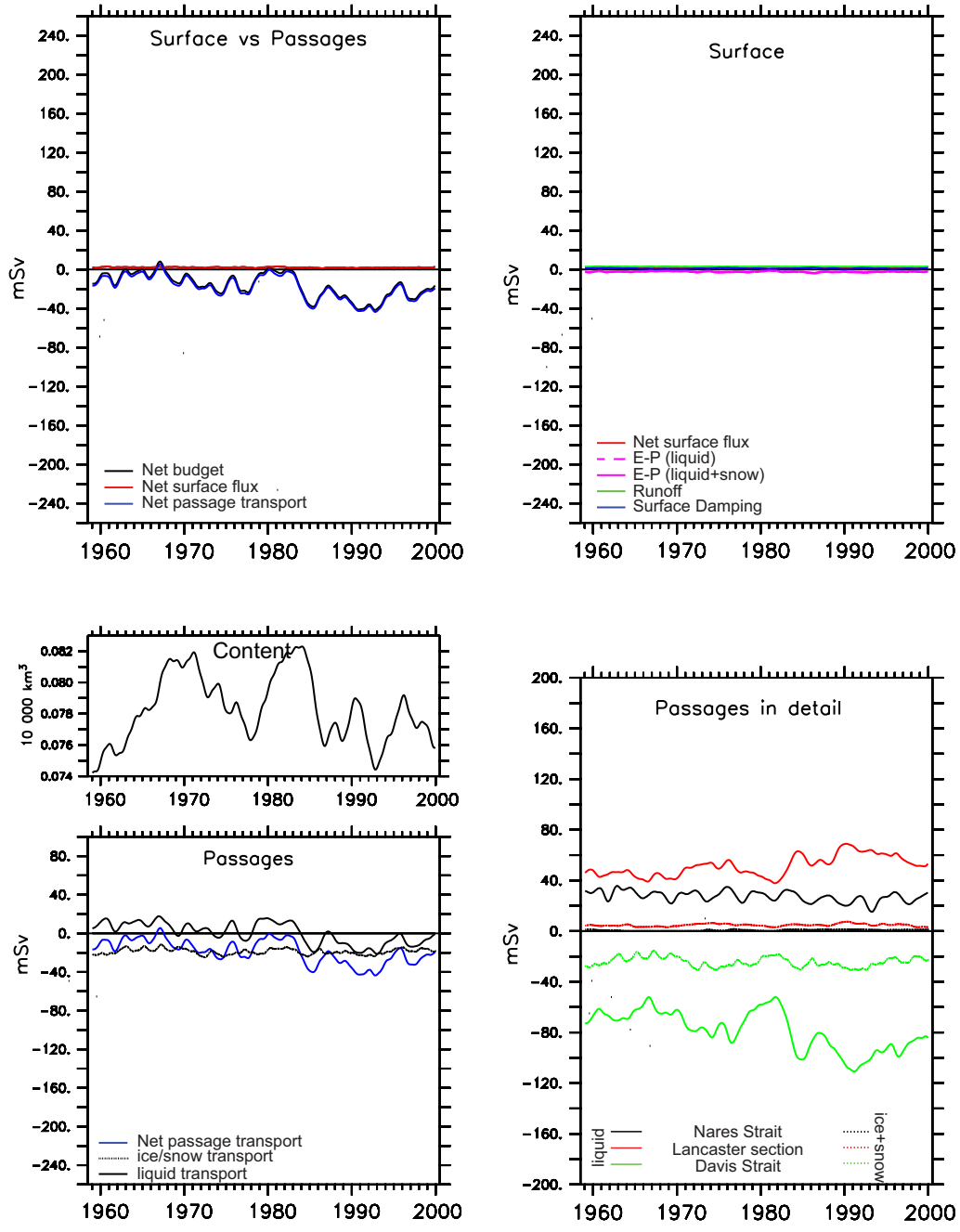

HEAT

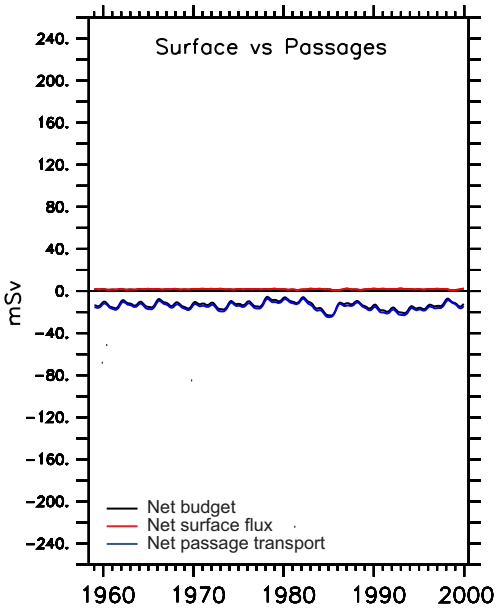
Surface vs Passages
mSv
Net budget
Net surface flux
Net passage transport

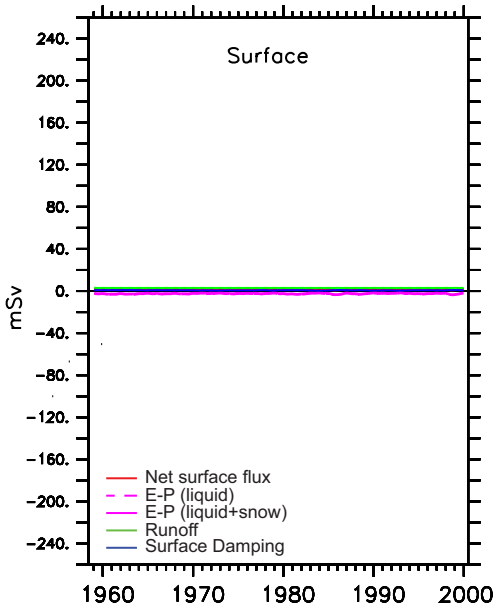
Surface
mSv
Net surface flux
E-P (liquid)
E-P (liquid+snow)
Runoff
Surface Damping

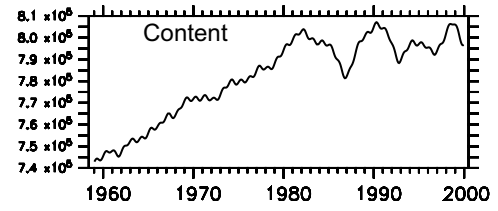
Content

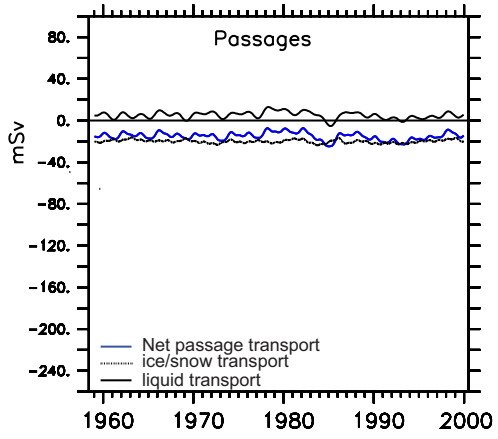
Passages
mSv
Net passage transport
ice/snow transport
liquid transport

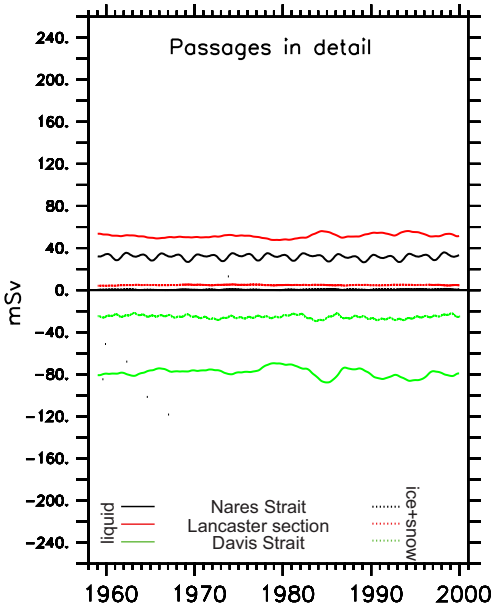
Passages in detail
mSv
liquid
Nares Strait
Lancaster section
Davis Strait
ice+snow

THERMHAL

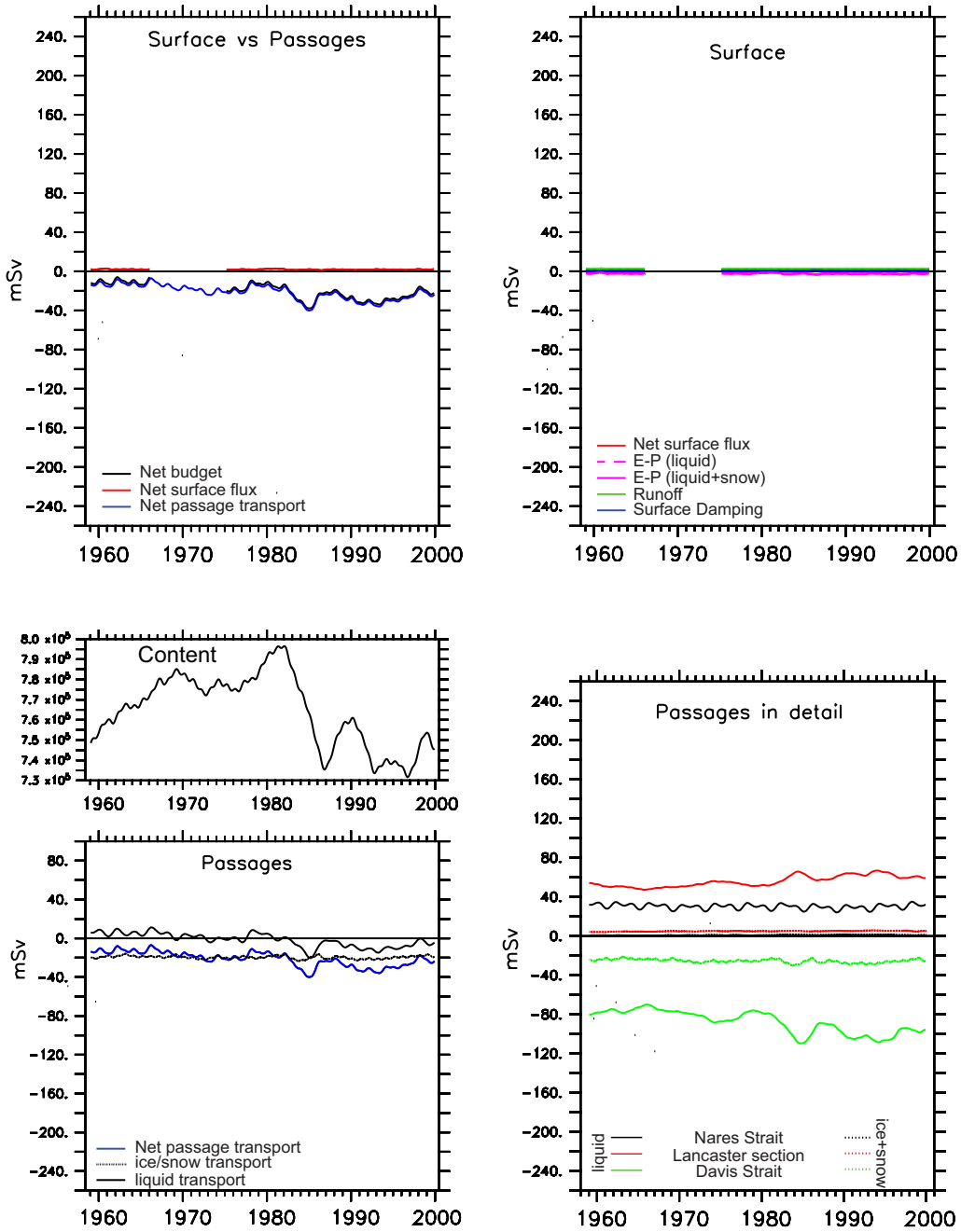
Surface vs Passages
mSv
Net budget
Net surface flux
Net passage transport
Surface
Net surface flux
E-P (liquid)
E-P (liquid+snow)
Runoff
Surface Damping
Content
Passages
Net passage transport
ice/snow transport
liquid transport
Passages in detail
liquid
ice+snow
Nares Strait
Lancaster section
Davis Strait
1960
1970
1980
1990
2000

WIND

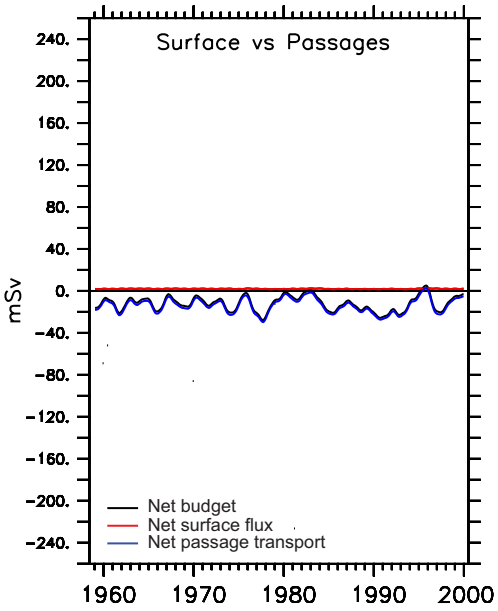
Surface vs Passages
mSv
Net budget
Net surface flux
Net passage transport
1960
1970
1980
1990
2000

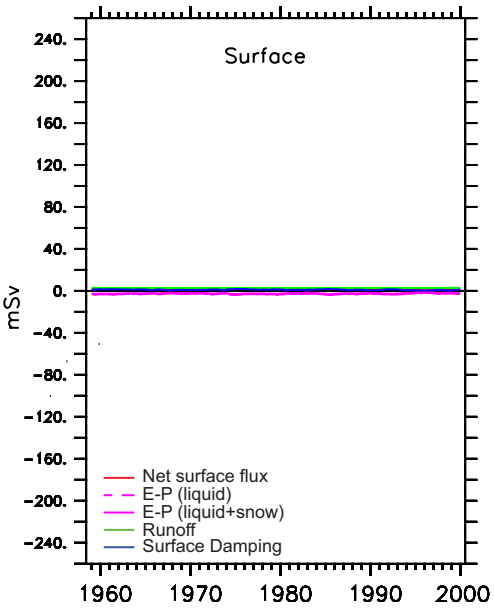
Surface
mSv
Net surface flux
E-P (liquid)
E-P (liquid+snow)
Runoff
Surface Damping
1960
1970
1980
1990
2000

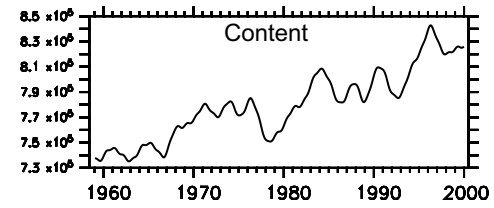
Content
1960
1970
1980
1990
2000

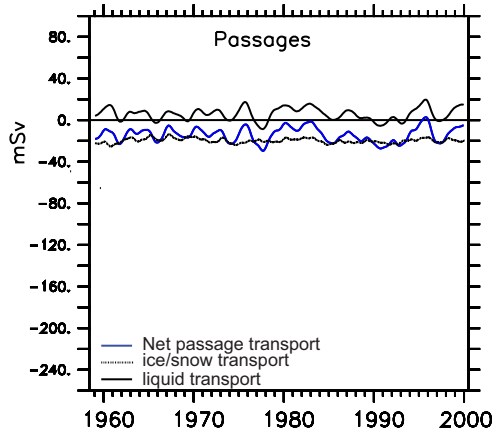
Passages
mSv
Net passage transport
ice/snow transport
liquid transport
1960
1970
1980
1990
2000

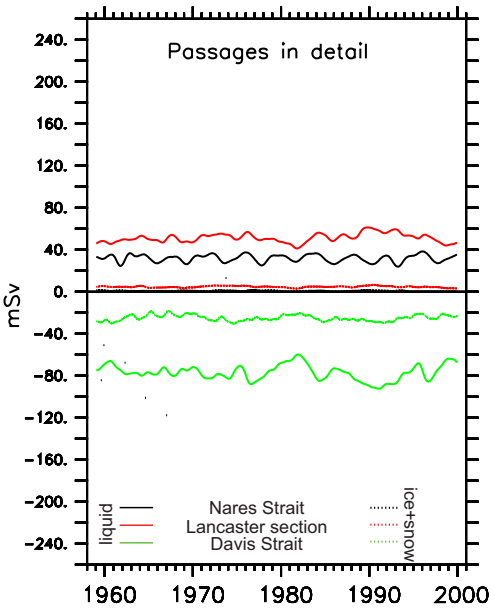
Passages in detail
mSv
liquid
Nares Strait
Lancaster section
Davis Strait
ice+snow
1960
1970
1980
1990
2000

NONARCTIC

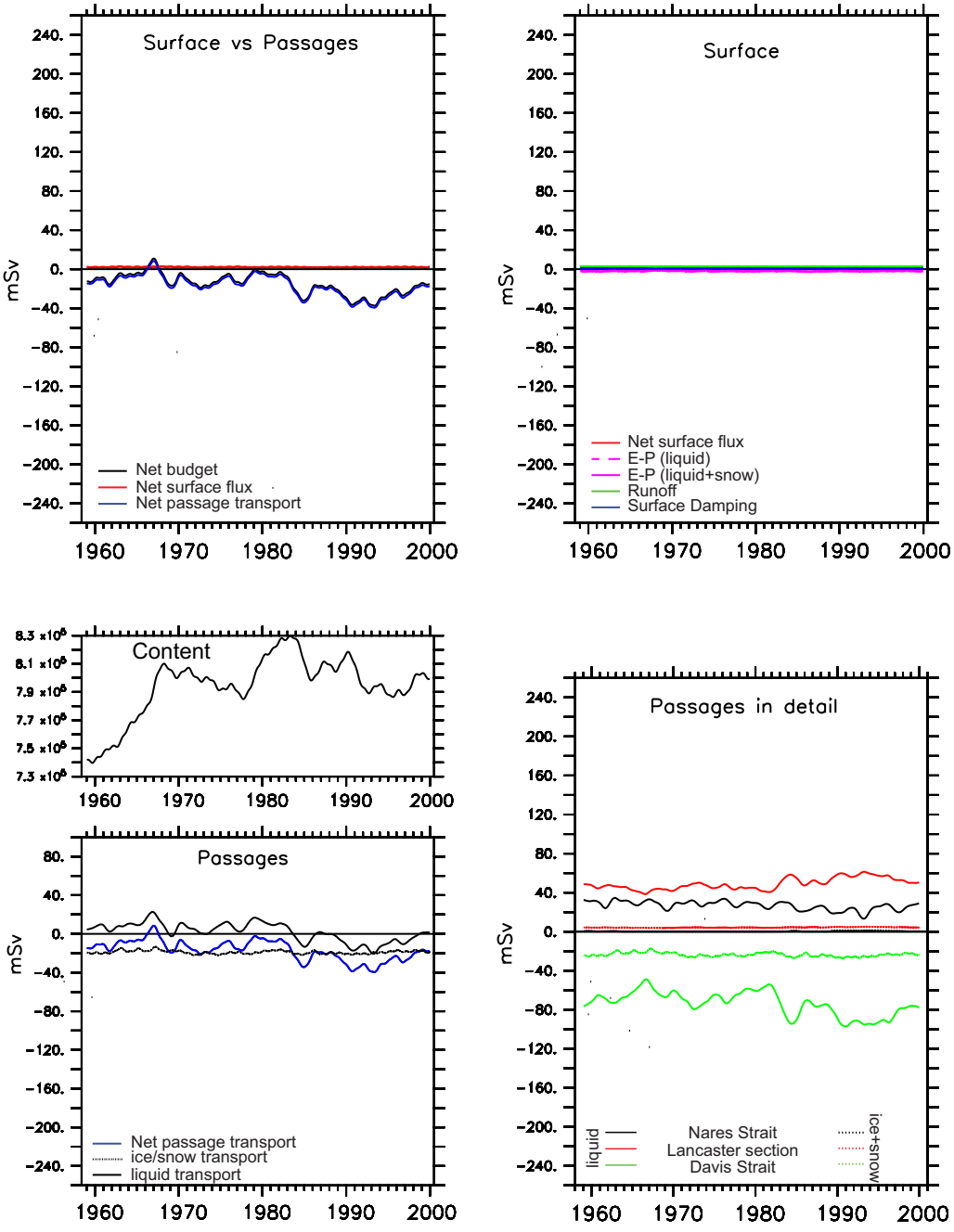
Surface vs Passages
mSv
Net budget
Net surface flux
Net passage transport
Surface
Net surface flux
E-P (liquid)
E-P (liquid+snow)
Runoff
Surface Damping
Content
Passages
Net passage transport
ice/snow transport
liquid transport
Passages in detail
liquid
ice+snow
Nares Strait
Lancaster section
Davis Strait
1960
1970
1980
1990
2000

D Nomenclature

$\rho_c = \{\rho_s, \rho_i\}$, $\rho_{ice} = 900kg/m^3$, $\rho_{snow} = 330kg/m^3$	Density of snow/ice
$c_p = c_{pi} = c_{ps} = 1093Jkg^{-1}K^{-1}$	specific heat for ice/snow
$T_c = \{T_0, T_1, T_2\}$	internal temperature (snow/ice)
$h_e = \frac{k_s k_i}{k_s + k_i}\left(\frac{h_s}{k_i} + \frac{h_i}{k_i}\right)$	effective thickness for heat conduction
$h_c = \{h_I, h_S\}$	average ice/snow layer thickness per grid cell
e	base of the natural logarithm function
ϵ	threshold thickness
$k_c = \{(k_i = 20344W/mK), (k_s = 0.21W/mK)\}$	thermal conductivity for ice/snow
F_{sw}	net short wave radiation (incl. albedo)
h_{su}	constant thickness of surface layer (evolution is negligible, but stabilizes coupled models)
$i_0 = 0.18(1 - c_{ld}) + 0.35c_{ld}$	albedo effect ($i_0 = 0$ for snow)
c_{ld}	fractional cloud amount
ϵ_{su}	emissivity of surface layer (snow OR ice)
σ_{SB}	Stefan-Boltzmann constant
T_{su}	surface Temperature
F_{cb}	conductive heatflux within bottom ice layer
F_w	heat flux from the ocean
L_i	volumetric heat of fusion (liquid sea water→sea ice)
α_{su}	surface albedo
β_{si}	compaction of the soaked snow ($\beta_{si} = 1$)

ρ_0	density of sea water
$\Gamma[x] = \begin{cases} 0 & \text{for } x \leq 0 \\ 1 & \text{for } x > 0 \end{cases}$	Heaviside function
m_{si}	mass of snow and ice per unit area
$\vec{u}_i$	ice velocity
$\vec{\tau_{ai}}$	forces from air per unit area
$\vec{\tau_{wi}}$	forces from water per unit area
η	sea surface elevation
σ	2-dimensional stress tensor
$\mu = \frac{\zeta}{e_c^2}$	non-linear bulk viscosity
e_c	eccentricity of elliptical stress tensor curve [ecc]
$\zeta = \frac{P}{2\Delta}$	non linear shear viscosity
P	ice strength (Rheology)
$\underline{\dot{T}}(\dot{\epsilon})$	trace of stress rate tensor
$\underline{I}$	2 dimensional unity tensor
$\Delta = \max\{\dot{\epsilon_0}, f(\dot{\epsilon}, e_c)\}$	maximum function of 'creep limit' $\dot{\epsilon_0}$[creep1] or f.
P^*	first bulk-rheology parameter (empirical) [P*]
C	second bulk-rheology parameter (empirical) [c_rhg]
h_i	ice thickness
γ	leads closure rate [exld]
A_{max}	maximum lead fraction
Ψ	transport Field
$Q_s = \rho_s c_{ps} \int_0^{h_s} T_s(z)dz$	sensible heat content of snow
$Q_i = \rho_i c_{pi} \int_0^{h_i} T_i(z)dz$	sensible heat content of ice
Q_l	latent turbulent heat flux
Q_I	solar insolation
$cdmp2D$	damping coefficients (2D) [days]
$\rho_{water} = 1000kg/m^3$	density of pure water
S_{init}	initial sea surface salinity
SSS	sea surface salinity
$\gamma_{Bottom}, \gamma_{Surface}$	reciprocal damping timescales at the Bottom and Surface [1/s]
z	depth of T-grid point level
h_{trans}	transition depth, in which the surface damping time scale reduces with depth to 1/e of its value.
$\Lambda_v = 2. \times 10^6$	latent heat of vaporisation $[J/kg]$

$\rho_a = 1.22$	near surface air density $[kg/m^3]$
$c_p = 1000.5$	specific heat of the air $[J/kg/K]$
Θ_{10}	potential air temperature

Danksagung

Mein besonderer Dank gilt meinem Doktorvater, Herrn Prof. Dr. Claus W. Böning, der mit zahlreichen Fragen und Anregungen mich und diese Arbeit zu lenken und leiten wusste.

Vielen Dank an die Mitarbeiter der Abteilung Theorie und Modellierung am Kieler Leibniz Institut für Meereswissenschaften, die mir stets mit Rat und Hilfe zu Seite standen.
Besonders möchte ich mich bei Dr. Arne Biastoch für die intensiven Diskussionen und technischen Hilfestellungen zur Bewältigung dieser Arbeit bedanken.

Ein ganz herzlicher Dank geht an Dr. Sabine Hüttl für die langjährige Zimmerpartnerschaft. Deine gute Laune und die gemeinsamen Musikeinlagen haben mir über so manche Durststrecke hinweg geholfen.

Bei Prof. Dr. Aike Beckmann möchte ich mich für meinen Gastaufenthalt in Helsinki bedanken, bei dem ich Gelegnheit hatte, etwas über Eismodellierung zu lernen.

Die freundlichen Worte und wertvollen Ratschläge von Herrn Prof. Dr. Fritz Schott haben mir nicht nur während meines Studiums geholfen, sondern werden mich auch weiterhin leiten. Vielen Dank für die unschätzbaren Erfahrungen, die ich dank Ihnen machen durfte.

Schließlich möchte ich mich bei meiner Familie bedanken, dass sie mir die Freiheit gibt, meinen Weg zu gehen.

Und all diejenigen, die ihr hier nicht genannt, seid euch meines Dankes gewiss, dass ihr mir den Rücken freigehalten, mich zum Lachen und Nachdenken gebracht habt, dass ihr mich unterstüzt und vor Schäden bewahrt habt, Danke.

Erklärung

Hiermit erkläre ich, dass ich die vorliegende Dissertation, abgesehen durch die Beratung meiner akademischen Lehrer, selbstständig verfasst habe und keine weiteren Quellen und Hilfsmittel, als die hier angegebenen verwendet habe.

Diese Arbeit hat weder ganz, noch in Teilen, bereits an anderer Stelle einer Prüfungskommission zur Erlangung des Doktorgrades vorgelegen.

Ich erkläre, dass die vorliegende Arbeit gemäß der Grundsätze zur Sicherung guter wissenschaftlicher Praxis der Deutschen Forschungsgemeinschaft erstellt wurde.

Kiel, den 27. Mai 2008

Markus Scheinert